ENVIRONMENTAL FATIGUE OF POLYMERS - A FRACTURE MECHANICS APPROACH

by

Hany Mohamed Abd El-Hakeem

A thesis submitted for the degree of
Doctor of Philosophy of the University of London
and for the
Diploma of Imperial College

May 1975

Department of Mechanical Engineering
Imperial College of Science and Technology
London SW7 2BX

ABSTRACT

The present study demonstrates the success of fracture mechanics principles in characterising the growth behaviour of environmental fatigue cracks and crazes in thermoplastics.

A comprehensive experimental study has been made of the environmental dynamic fatigue crack propagation in conditioned nylon 66 in different environments (air at 50% RH, distilled water and diluted sulphuric acid) and high density polyethylene (HDPE) in both air and Adinol. The effects of the environment, test frequency, range and level of loading on the rate of cyclic crack propagation ($\dot{a}_N$) have been discussed and investigated. An empirical model for predicting $\dot{a}_N$ and based on the stress intensity factor (K) has been proposed. The model correlates $\dot{a}_N$ with a parameter ψ ($\psi = f(K,R)$). A unique relationship has been obtained when the experimental data were represented on an $\dot{a}_N/\psi$ basis in any particular environment and at any test frequency. The proposed model provides a unifying pattern for most of the previous laws used in predicting the cyclic growth rates in polymeric materials; moreover, it can easily be expressed in energy terms and in terms of the condition of the cyclic plastic zone ahead of the crack tip (size and displacement).

Also, the study of cyclic crack growth of low density polyethylene (LDPE) in methanol has shown that the linear superposition model (previously suggested for metals) is applicable in this case when allowances are made for the rate sensitivity of the material.

Environmental fatigue studies using a rotating bending test have been conducted on HDPE in both air and Adinol, and PMMA in air and methanol. The initial notch depth has an obvious effect on the results (represented on a K/N basis) and this has been justified to some extent by analytical treatment and by the expected increase in temperature as the initial notch depth decreases. The environmental effect on the fatigue life has also been discussed in both cases.

For a better understanding of the mechanism of dynamic failure in the PMMA/methanol system, and to simulate the rotating bend test geometry, the study has been extended to static fatigue failure in this system for the particular geometry of round notched bars. The criterion of void coalescence within the crazes grown under these conditions has

been studied in detail and a qualitative description of the failure process has been given. The craze growth behaviour has also been analysed and the analytically predicted rates of growth have shown good agreement with the measured values.

ACKNOWLEDGEMENTS

The author is pleased to express his sincere gratitude to several members of the Mechanical Engineering Department at Imperial College for their advice and co-operation during the course of his study. In particular, he is indebted to Dr L.E. Culver for his support, encouragement and enthusiastic supervision during the present study and Dr G.P. Marshall for his helpful and invaluable suggestions.

Special thanks are due to Professor J.G. Williams for his stimulating encouragement and for financial support during a period of the study. Mr E.L. Zichy of ICI is also thanked for his valuable discussions and for providing the nylon material for the fatigue tests. The author also wishes to thank Mr L.H. Coutts and Mr P.D. Ewing of the Polymer Engineering Group for their assistance on the technical aspects of the experimental work, and also Miss E.A. Quin for the typing of this thesis.

Finally, the author is indebted to his wife, without whose sacrifices it would have been impossible to accomplish this work.

CONTENTS

Page

NOTATION*

a	:	characteristic length of a crack
a_o	:	initial crack length
$\dot{a}$	:	crack speed
$\dot{a}_N$	:	cyclic rate of crack growth
A	:	average voiding area in a craze or parameter depending on material properties and test conditions
B, B', B''	:	parameters depending on material properties and test conditions
c	:	finite effect correction factor in round notched bars
$\overline{c}$	:	parameter varies with a/R_o in round notched bars
C	:	parameter depending on material properties and test conditions
d	:	diameter at notched section of a round bar
d_o	:	characteristic diameter of crack tip
D	:	outer diameter of a round bar
E	:	Young's modulus
E^*	:	complex modulus
E'	:	storage modulus
E''	:	loss modulus
E_o	:	0.1 min value of $E(t)$ or unit time value of $E(t)$
f	:	frequency
$f(\ )$	:	function of $(\ )$
F	:	finite effects correction factor
G	:	strain energy release rate
G_c	:	critical strain energy release rate
h	:	channel height
J	:	Rice's contour integral

---

* This list does not include the symbols used in the Appendices. These are defined as they appear.

k : numerical factor

K : stress intensity factor

K_o : initial stress intensity factor

K_a : stress intensity factor amplitude

K_c : critical value of stress intensity factor

K_{IC} : critical value of stress intensity factor for mode I stress environment in crack plane

K_e : equivalent stress intensity factor

K_m : mean stress intensity factor in cyclic loading or stress intensity factor at craze initiation

K_n : elastic stress concentration factor or stress intensity factor controlling value of craze growth behaviour in SEN specimens

K_{ISCC} : threshold value of K for mode I stress environment in crack plane, in stress corrosion cracking

K_{th} : threshold value of ΔK

K_{ath_1} : threshold value of K_a at $R = -1$

K_{th_o} : threshold value of ΔK at $R = 0$

ℓ : specimen length

ℓ' : effective specimen length

ℓ_o : average distance between the sites of inhomogeneities in a polymer

L : parameter depending on material properties and test conditions

m : parameter depending on material properties and test conditions

M : bending moment

$\overline{M}_n$: the number - average molecular weight

$\overline{M}_w$: the weight - average molecular weight

n : parameter depending on material properties and test conditions

N : number of cycles

N_f, N_t : number of cycles to failure

N_i : number of cycles for initiation period

N_p : number of cycles for crack propagation period

P : applied load or pressure

Q : hysteresis energy per cycle

r_p : plastic zone radius at crack tip

r_{pc} : cyclic plastic zone radius at crack tip

R : ratio of minimum to maximum stress in a cycle

R_o : outer radius of a round bar

S or σ : stress

S_a or σ_a : stress amplitude

S_m : mean stress

S_u : ultimate tensile stress

S_y or σ_y : yield stress

t : specimen thickness or time

T_g : glass transition temperature

U : crack opening displacement

U^* : dimensionless COD

U_a : displacement at crack tip

U_b : displacement at craze tip

U_c : critical value of U

v : void contents in a craze

V : velocity

w : specimen width

W : strain energy density

W_d : dissipated energy density per cycle

x : craze length

$\dot{x}_f$: final craze speed

Y : finite effects correction factor

α : parameter depending on material properties and test conditions

β : parameter depending on material properties and test conditions

γ : parameter depending on material properties and test conditions

δ : phase angle between stress and strain

δ_a : height of the deformed section at crack tip

δ_b : height of the deformed section at craze tip

Δ : plastic zone size or range of

ε : strain

ε_o : strain limiting value in a craze

ε_c : critical strain

ε_F : true strain at fracture in tension

ε_p : plastic strain

ε_y : uniaxial yield strain

η : viscosity

λ : parameter equal to $K_{max}^2 - K_{min}^2$

μ : elastic shear modulus = $E/2(1 + \nu)$

ν : Poisson's ratio

ξ : parameter characterising the stress condition: $\xi = (3 - 4\nu)$ for plane strain and $\xi = (3 - \nu)/(1 + \nu)$ for plane stress

ρ : characteristic radius of crack tip or density

σ_o : 0.1 min value of $\sigma(t)$ or unit time value of $\sigma(t)$

σ_c : craze stress

σ_F : true fracture stress in tension

σ_m : mean stress over crack area

σ_n : nominal stress at crack tip

τ	:	time of one cycle = $1/f$ or rate of energy available from the stress field
ω	:	radial frequency

ABBREVIATIONS

COD	:	crack opening displacement
ESC	:	environmental stress cracking
HDPE	:	high density polyethylene
LDPE	:	low density polyethylene
LEFM	:	linear elastic fracture mechanics
MFI	:	melt flow index
N66	:	nylon 66
PC	:	polycarbonate
PE	:	polyethylene
PMMA	:	polymethylmethacrylate
PVC	:	polyvinyl chloride
SCC	:	stress corrosion cracking
SEN	:	single edge notch

INTRODUCTION

Since plastics have been recognised as structural materials, they are now being used by design and materials engineers in many applications where they can suitably replace metals and other conventional materials. As most of the widely used engineering materials have been developed over many years, their characteristics and properties are now widely known. Plastics, on the other hand, are comparatively new, and studies of their mechanical behaviour have recently been stimulated by their uses in new fields of application. Further exploitation of plastics in the engineering field necessitates better and more comprehensive understanding of their responses to various types of loading under different service conditions, since many engineering applications require the material to be able to sustain considerable loads, often for long times, which might vary in nature.

If lessons are to be learned from experience in the applications of metals, one of the most critical areas for determining the service behaviour under load is the study of environmental failures by cracking under both dynamic and static loading conditions (termed, respectively, corrosion fatigue and stress corrosion cracking). In the case of metals, such environmental failures represent a major problem and are the cause of much concern to materials engineers and designers. There is a large body of knowledge for metals in this field, but unfortunately in the case of polymers, while some information is available for the environmental behaviour of these materials under constant loads, very little is known about the nature of fracture when they are subjected to environmental attack under dynamic loads.

At the moment, therefore, it was felt that an attempt should be made to study the environmental fatigue behaviour of these polymeric materials. Established techniques already exist for the study of metals, and those in use for related problems in polymers are capable of extension into this field.

However, before the environmental fatigue problem of polymers can be treated, a brief survey is necessary to throw some light on the general aspects of the problem and the contributions of different techniques, with particular reference to the important role recently played by fracture mechanics in characterising the problem. Moreover, it is

necessary to discuss the particular structure and viscoelastic nature of the polymeric materials and their effects on the environmental fatigue failure phenomena.

CHAPTER ONE

FATIGUE FAILURE PHENOMENON AND THE ROLE OF FRACTURE MECHANICS

1.1 Definition

Fatigue can be defined in general terms (Gotham, 1969) as "a progressive weakening of a test piece or component with increasing time under load, such that loads which would be supported satisfactorily at short times produce failure at long times". This broad definition applies to all types of loading and environment. The term fatigue may be subdivided into two main classes - static fatigue and dynamic fatigue - in order to differentiate between the behaviour of materials subjected to continuous and cyclic loading. However, for metals the term fatigue is generally restricted to failure as a result of cyclic loading.

1.2 Historical Survey of the Fatigue Problem

That metals might break under the repeated application of a stress insufficient to cause failure on the first application was first realised towards the middle of the nineteenth century, mainly as a result of experience in railway engineering, for example (Rankine, 1843). The first comprehensive investigation of the fatigue of metals was carried out by Wöhler between 1858 and 1870; he designed a rotating bending machine which forms the basis of design for the most widely used type of fatigue machines now in operation. From his tests under various stress conditions on wrought iron and steel he deduced two fundamental results: (a) fatigue failure can occur below the elastic limit, and (b) there is a limiting range of stress below which fatigue failure will not occur. The first attempt to relate fatigue failure with the occurrence of plastic deformation was made by Bauschinger (1886). He observed that the limit of proportionality in a static test could be changed by the application of a fluctuating stress reaching a stable value after a few reversals. At the end of the nineteenth century, the first microscopic observations of deformation caused by fluctuating stresses were made by Ewing and Humfrey (1903). They demonstrated that fatigue cracking was associated with slip lines, and this represented a

big step forward towards an understanding of fatigue behaviour.

The first observations of fatigue in corrosive environments rather than air were reported by Haigh (1917), who noted the effect of sea water on steel cables. However, no concentrated effort to identify and characterise the problem was made until a comprehensive series of investigations were carried out by McAdam and his co-workers in the USA from 1926 to 1941. During the same period, Gough and his co-workers (Gough, 1932) in England also contributed a great deal to the existing literature on the subject. McAdam's (1926) first observations of corrosion fatigue (a term which may be defined as the combined action of an aggressive environment and a cyclic stress leading to premature failure of metals by cracking) resulted from a study of thermal effects on the fatigue behaviour of various ferrous alloys. In his attempt to increase the rate of heat removed from fatigued specimens, he surrounded them with water and noted that although only slight corrosion occurred, the fatigue life was considerably reduced. A "corrosion fatigue limit" rather than the normal endurance limit was found, this limit being much lower than that observed under atmospheric conditions.

The majority of the observed fatigue failures are corrosion fatigue failures, since only in an absolute vacuum could "pure" fatigue occur. For example, it has been shown for many metals that air contributes strongly to increases in fatigue crack propagation rates. In general, corrosion fatigue is a process quite distinct from stress corrosion cracking (SCC), which results from a steady stress acting in a corrosive environment. SCC is suffered only by alloys in specific environments, while all metals which are susceptible to corrosion are susceptible to corrosion fatigue in any aggressive environment.

1.3 A Brief Survey of the Laws Describing Fatigue Behaviour

1.3.1 Laws concerned with the total fatigue life

One of the earliest of the empirical laws correlating the stress amplitude (S_a), with the number of cycles to failure (N_f) was that by Basquin (1910). His law fitted the data well under the condition of stress amplitudes being small enough for macroscopic behaviour to be entirely elastic, but large enough to cause failure in the steepest-falling region of the (S-log N) curve. The Basquin relation was:

$$S_a^{\,m} N_f = \text{constant} \tag{1.1}$$

where m is constant in the range 8 to 20.

A more recent modified form by Ham (1966) was of the form:

$$S_a (2N_f)^m = \sigma_F \tag{1.2}$$

where m in this case is in the range of 0.05 to 0.12 and σ_F is the true stress of fracture in tension.

The Goodman representation of the effect of mean stress on fatigue life is one of the most popular of the empirical fatigue laws, used as a guide for design, amongst engineers. However, the original law has been modified to the relation shown below:

$$S_a \leqslant \left[1 - \frac{S_m}{S_u}\right] S \tag{1.3}$$

where S_a is the alternating stress amplitude superimposed on a mean stress S_m to give a guaranteed life time of at least N_f, S is the alternating stress with zero mean stress to give failure after N_f cycles and S_u the ultimate tensile stress.

A more conservative criterion was given by Soderberg as:

$$S_a \leqslant \left[1 - \frac{S_m}{S_y}\right] S \tag{1.4}$$

where S_y is the yield stress.

The simplest basis of predicting the fatigue life under varying stresses from the S-N curve is by means of the linear cumulative damage law first suggested by Palmgren and restated by Miner (1945). The assumption was that the application of n_i cycles at a stress S_i for

which the average number of cycles to failure is N_i causes an amount of fatigue damage n_i/N_i and failure will occur when:

$$\sum_i \frac{n_i}{N_i} = 1 \qquad (1.5)$$

There are many criticisms of Miner's hypothesis as a design criterion. Many experiments designed to provide cross-checks failed to prove or disprove this hypothesis because of the extensive scatter shown by the experimental results. However, a conservative design could be produced using correct forms of data by using Miner's Law.

Up to this point, consideration has only been given to fatigue situations characterised by the stress amplitude. In cases characterised by constant strain amplitude, the Manson (1965)-Coffin (1962) relation is applicable where the plastic component of the alternating strain is appreciable and known (for large cyclic strains the elastic strain will be negligible). In terms of plastic strain amplitude ($\pm \Delta\varepsilon_p/2$) the relation is:

$$\Delta\varepsilon_p \, (2N_f)^m = \varepsilon_F \qquad (1.6)$$

where m is in the range 0.5 to 0.7 and ε_F is the true strain at fracture in tension. Equation (1.6) implies that the resistance of a material to alternating plastic strain is dependent on its ductility and equation (1.2) implies that the resistance of a material to alternating elastic strain depends primarily on its strength. The resistance to total strain is thus mainly dependent on ductility at high stress at which plastic strain predominates and on strength at low stress when elastic strain predominates.

1.3.2 Laws concerned with fatigue crack propagation

The total fatigue life can be divided into two stages: (1) crack initiation period, and (2) crack propagation period (Forsythe, 1961). In stage (1) slip band cracks are formed in metals by the growth of

intrusions on planes closely aligned to the maximum shear stress direction, and may propagate apparently by the same mechanism for an appreciable proportion of the life. The transition to stage (2) growth usually occurs when a crack meets a slip obstacle such as a grain boundary. The main controlling parameter for growth in the second stage is the maximum principal tensile stress and it is during this stage that striations or "beach markings" may occur. The transition from stage (1) "microscopic" to stage (2) "macroscopic" depends entirely on the microstructure of the material, the loading conditions and the environmental characteristics.

In high cycle fatigue and/or the absence of stress raisers, the crack nucleation stage may constitute the major part of the total fatigue life. On the other hand, in low cycle fatigue and/or the presence of severe stress concentrations the reverse will be true.

The problem of fatigue crack propagation is difficult to solve theoretically, but a simplified treatment has been attempted by Head (1953) and it is considered the first crack propagation law. Head based his analyses on Orowan's (1939) theory of strain-hardening which takes place at the crack tip. He treated the problem of a crack in an infinite sheet subjected to a uniform stress perpendicular to the crack and deduced that the rate of crack propagation would be given by:

$$\frac{da}{dN} = \frac{a^{3/2}}{\Delta^{1/2}} f(\sigma) \qquad (1.7)$$

where a is half the crack length, σ is the range of the applied stress and Δ is the size of the plastic zone ahead of the crack tip (presumed constant dueing crack propagation).

Frost and Dugdale (1958) presented a new approach to crack propagation. Noting that the plastic zone size increased with increasing crack length, they concluded that:

$$\frac{da}{dN} = \frac{\sigma^3 a}{C} \qquad (1.8)$$

where C is a parameter depending on material properties and frequency.

About the same time McEvily and Illg (1958) modified a method of analysis presuming that the crack tip in a material has a characteristic radius (ρ) which allows computation of the stress at the crack tip (σ_o) by using elastic stress concentration factor (K_n) (i.e. $\sigma_o = K_n \sigma_{net}$ where σ_{net} is the net stress at the cracked section). They concluded that the crack extension rate will be a function of σ_o, i.e.,

$$\frac{da}{dN} = f(K_n \sigma_{net}) \tag{1.9}$$

For the specific configuration of an infinite sheet mentioned above

$$\frac{da}{dN} = f\left(\sigma\left[1 + 2\left(\frac{a}{\rho}\right)^{\frac{1}{2}}\right]\right) \tag{1.10}$$

where $\sigma_{net} = \sigma$ and $K_n = 1 + 2(a/\rho)^{\frac{1}{2}}$.

McEvily and Illg obtained empirically the form of the function in equation (1.9) as:

$$\log \frac{da}{dN} = 0.00509 K_n \sigma_{net} - 5.472 - \frac{34}{K_n \sigma_{net} - 34} \tag{1.11}$$

It should be noted that equations (1.9) and (1.11) are not restricted to special configurations as was the case in equations (1.7) and (1.8).

Independent of McEvily and Illg, Paris (1957) proposed a crack propagation theory based on Irwin's (1957a) stress intensity factor (K) (see Appendix A) which reflects the effect of external load and configuration on the intensity of the stress field around a crack tip. The local stress field distribution is not affected by changes in the overall configuration. Therefore, it was reasonable to consider K as the controlling parameter of crack extension, i.e.,

$$\frac{da}{dN} = f\ (K) \qquad (1.12)$$

In the case of an infinite plate where $K = \sigma(\pi a)^{\frac{1}{2}}$ the Paris law could be expressed as:

$$\frac{da}{dN} = f\left(\sigma(\pi a)^{\frac{1}{2}}\right) \qquad (1.13)$$

Somewhat later, Liu (1963) restated the Frost and Dugdale analysis using the concept of total hysteresis energy absorption to failure at the crack tip, giving:

$$\frac{da}{dN} = C\ \sigma^2\ a \qquad (1.14)$$

Paris and Erdogan (1963) proved that the Paris law (equation (1.12)) is equivalent to the McEvily and Illg law (equation (1.9)) for all specimen configurations.

In recent years a concentrated effort has been made to examine the actual rate of crack propagation in various materials using the concepts of fracture mechanics, which have proved to be very good tools for dealing with such problems. However, the initial introduction of fracture mechanics to the analysis of cyclic crack propagation is attributed to Paris (1957).

1.4 Fracture Mechanics and Fatigue Behaviour

Fracture mechanics is the science of studying the fracture behaviour of a material using a continuum approach. Its main task is to learn enough about crack propagation and the stress conditions which result in cracking to prevent, or at least to predict, the growth of cracks from inherent flaws. The scientific study of fracture began with Griffith's (1921) work on cracks in brittle solids (glass, in his case) and its extension by Orowan (1949) to metals and other ductile materials. More recently, these ideas (largely as a result of Irwin's (1948) work) have further developed into the science of fracture

mechanics. The fracture of materials must ultimately be expressed in terms of their atomic or microscopic constitution. The work of this thesis is only on the macroscopic aspect of fracture mechanics which uses concepts drawn from continuum mechanics.

Excellent comprehensive surveys of fracture mechanics concepts already exist elsewhere, for example, Hayes (1970). However, a brief review of these concepts and a short summary of the derivations of parameters which are used in the theoretical and empirical analyses of fatigue failure problems are given in Appendix A. During the present work only the final expressions or results will be used.

1.4.1 The use of fracture mechanics in dynamic fatigue

Linear elastic fracture mechanics concepts (LEFM) have been successfully used in describing the fracture behaviour under monotonically increasing loads (e.g. Anon., 1965), therefore, it was logical for these concepts to be extended to the study of slow crack growth (subcritical growth) in both static and dynamic loading conditions. Paris proposed that crack propagation rates were a function of Irwin's stress intensity factor K (or the strain energy release rate G (see Appendix A)). He concluded that K should be related to the cyclic rate of crack propagation ($da/dN = \dot{a}_N$) by some unique function (equation (1.12)). More specifically, Paris (1963), according to experimental results on an aluminium alloy, expressed $\dot{a}_N$ in terms of the range of the stress intensity factor ΔK ($=K_{max} - K_{min}$) by the relation:

$$\dot{a}_N = A\ (\Delta K)^m \qquad (1.15)$$

where A is a parameter depending on material properties and test conditions and m is a numerical constant that has been found to take values between 2 and 9, but it usually lies close to 4. However, the value of m may change considerably according to variations of environmental conditions, rate of loading (test frequency) or the range of applied stress. Moreover, if test results cover a wide range of ΔK, a single value of m is insufficient. Barsom's (1971) results on steel demonstrates that a logarithmic plot of $\dot{a}_N$ against ΔK yields

three distinct regions of varying slope m. In regions 1 and 3 $\dot{a}_N$ was strongly stress intensity dependent while in region 2 the crack rate of cyclic growth was less sensitive to ΔK and this region is the one which was usually represented by the power law of equation (1.15). The general pattern of three-region representation was also applicable to high strength aluminium, magnesium and titanium alloys exposed to aggressive environments (Speidel et al, 1971).

1.4.2 The effect of mean stress on crack propagation

Since the formulation of equation (1.15) a vast quantity of experimental data of crack propagation was correlated with the stress intensity factor and it has been recognised that the simple correlation of equation (1.15) did not yield an accurate representation of the data obtained from experiments conducted at different values of mean stress (Frost, 1966; Frost and Greenan, 1970). There is, as yet, no generally accepted approach that deals with the influence of the mean stress on $\dot{a}_N$. However, there are certain trends associated with mean stress effects, for example, for a given crack growth rate there is usually a decrease in the allowable amplitude as the mean stress increases (Forman et al, 1967).

The following is a survey of the existing expressions which attempt to deal with the effect of mean stress.

Forman et al (1967) proposed a relation which includes the effect of mean stress as well as the fast crack propagation as K_{max} approaches the critical value of the stress intensity factor, K_{IC}, thus:

$$\dot{a}_N = \frac{A\ (\Delta K)^m}{(1 - R)\ K_{IC} - \Delta K} \qquad (1.16)$$

where R is the ratio of minimum to maximum stress in a fatigue cycle. Forman's relation has been examined by several investigators and it fitted the crack growth data well (e.g. Hudson (1969) on high strength aluminium alloys; Crooker and Lange (1968) on high strength steel). Some modifications have been proposed for Forman's relation to represent the results better, for example, Pearson (1968) suggested the form of:

$$\dot{a}_N = \frac{A\, K_{IC}\, (\Delta K)^m}{((1 - R)\, K_{IC} - \Delta K)^{\frac{1}{2}}} \qquad (1.17)$$

for thick specimens of aluminium alloys of high and low fracture toughness.

Erdogan and Ratwani (1970) proposed a modification of Forman's formula to take into account a threshold value of ΔK (K_{th}) at which the fatigue crack propagation is practically zero:

$$\dot{a}_N = \frac{A\, (\frac{2}{1 - R})\, (\Delta K - K_{th})^m}{K_c - (\frac{2}{1 - R})\, \Delta K} \qquad (1.18)$$

They applied this modified formula (equation (1.18)) as well as Forman's formula (equation (1.16)) to the results of fatigue crack propagation in plates and shells of aluminium alloy. Both equations (1.16) and (1.18) seemed to be very satisfactory. However, the experimental results were far from the threshold value, so the advantage of applying equation (1.18) rather than equation (1.16) in the region of very slow fatigue crack growth rate did not appear.

Cherepanov and Halmanov (1972) obtained a theoretical expression for fatigue crack growth rate, based on dimensional analysis, in the form:

$$\dot{a}_N = \beta \left(\frac{K_{max}^2 - K_{min}^2}{K_c^2} + ln \left(\frac{K_c^2 - K_{max}^2}{K_c^2 - K_{min}^2} \right) \right) \qquad (1.19)$$

where β depends on material properties σ_y, E and K_c and must be determined experimentally. They showed that their formula is in good agreement with Forman's formula and represented the experimental data from steel and aluminium alloys with reasonable accuracy.

Erdogan (1968) suggested a crack growth model taking into account the effect of the plastic zone size which could be represented in terms of K_{max} reached in a load cycle; his proposed formula was:

$$\dot{a}_N = A\ (\Delta K)^m\ (K_{max})^n \qquad (1.20)$$

Erdogan's formula has been applied successfully to both metals and polymers (Mukherjee, 1973). However, some shortcomings were noted when it was applied to high strength aluminium alloys at high rates of fatigue crack growth (Hudson, 1969).

Another empirical formula has been proposed by Klesnil and Lukas (1972) of the form:

$$\dot{a}_N = A\left[K_a^{\beta}\ (\frac{2}{1-R})^{\gamma\beta} - K_{ath_1}^{\beta(1-\alpha)}\ K_a^{\beta\alpha}\ (\frac{2}{1-R})^{\alpha\beta\gamma}\right] \qquad (1.21)$$

where α, β and γ are material constants; K_a is the amplitude of the stress intensity factor and K_{ath_1} is the value of K_a at $R = -1$ where the fatigue crack propagation is practically zero. They successfully applied their formula to fatigue crack propagation data for steels.

1.4.3 COD and cyclic plastic zone size as governing parameters for crack propagation

Modelling the cyclic crack growth, as shown in the preceding section, as $\dot{a}_N$ dependence on the stress intensity factor and ratio R did not throw much light on the nature of the mechanism responsible for crack growth. However, few attempts have been made to relate $\dot{a}_N$ to rational physical parameters representing the condition prevailing at the crack tip, such as COD or cyclic plastic zone size.

A recent paper by Donahue et al (1972) has dealt with the bluntening and resharpening process at the crack tip; in their approach they assumed that the advance per cycle is proportional to the crack opening displacement range (ΔU) which in turn depends upon K^2 (equation (A.19) in Appendix A); moreover, they considered the threshold value of COD and this led to the following expression:

$$\dot{a}_N = \frac{4A}{\pi\ \sigma_y\ E}\left[(\Delta K)^2\ (\frac{1+R}{1-R}) - K_{th_o}{}^2\right] \qquad (1.22)$$

where K_{th_o} is the value of ΔK at $R = 0$ where the fatigue crack propagation is practically zero.

McEvily et al (1973) demonstrated that the previous expression overestimated the effect of the mean stress when it was compared with the experimental results. For better prediction of the behaviour they suggested the following modification:

$$\dot{a}_N = \frac{4A}{\pi \sigma_y E} \left[\Delta K - K_{th_o} \left(\frac{1-R}{1+R}\right)^{\frac{1}{2}}\right]^2 \left(\frac{1+R}{1-R}\right) \qquad (1.23)$$

The empirical form proposed by McEvily and Wei (1971) was based on equation (1.22), for the condition of $R = 0$, and the Goodman diagram for fatigue crack growth rates, which is equivalent to the original Goodman diagram. Their expression was:

$$\dot{a}_N = \frac{4A}{\pi \sigma_y E} \left\{\left[\frac{\Delta K}{1 - \left(\frac{R}{1-R}\right) \frac{\Delta K}{K_c}}\right]^2 - K_{th}^2\right\} \qquad (1.24)$$

where $$K_{th} = K_{th_o} \Big/ \left[1 + \left(\frac{R}{1-R}\right) \frac{K_{th_o}}{K_c}\right]$$

Recently, Arad et al (1972c) proposed a formula of the form:

$$\dot{a}_N = A \lambda^m = A \left((\Delta K)^2 \frac{1+R}{1-R}\right)^m \qquad (1.25)$$

where $\lambda = (K_{max}^2 - K_{min}^2) = 2 \Delta K K_m \alpha \Delta (COD)$. They successfully applied this formula to cracks growing in polymers. This equation is similar to equation (1.22) when K_{th_o} is neglected and the term between the brackets is raised to the power m.

Johnson and Paris (1968) showed that the radius of the cyclic plastic zone at the crack tip for the general case of plane stress is:

$$r_{pc} = \frac{1}{2\pi}\left(\frac{\Delta K}{2\sigma_y}\right)^2 \qquad (1.26)$$

For tests conducted at different ratios R the effect is only an origin shift to the minimum value of K and in successive cycles r_{pc} is again governed by ΔK only. Considering the similarity of the laws representing the plastic zone size and the crack opening displacement - both U and r_p being proportional to K^2 (equations (A.9), (A.10) and (A.18) in Appendix A) - it may be said that crack growth equations based on the COD parameter (e.g. equations (1.22) and (1.25)) are at the same time relating the crack propagation to the crack tip plastic deformation.

1.4.4 The effects of environment on fatigue crack propagation

It has been recognised that the fatigue failure process could be enhanced by the presence of an aggressive environment. McEvily and Wei (1971) have shown that the environmental effect on fatigue crack growth of metals may be characterised in three general patterns of behaviour as shown in Figure 1.

Type A behaviour represents the material/environment systems where the environmental effect results from both actions of fatigue and corrosion, this is typically the behaviour of the aluminium/water system. The environment reduces the apparent threshold for crack growth and increases the rate of crack growth at any given K level; as K approaches K_{IC} the environmental influence diminishes as a result of the limiting nature of the transport process or due to other mechanical/chemical interactions. Type B behaviour is typical of hydrogen/steel systems. The environmental effect is quite strong above some apparent threshold K_{ISCC} * and is negligible below this level. A broad range of material/environment systems exhibit behaviour that falls between these two extremes (type C), with type A behaviour at K levels below the apparent threshold K level and type B behaviour above this

---

* K_{ISCC} is the stress corrosion cracking stress intensity threshold for a particular material/environment system under constant loading conditions.

threshold.

However, the influence of an aggressive environment may be seen through its effect on the constants given in the predictive equations of the previous two sections without considering the details of the effect of the environment upon the mechanism of growth. For example, a corrosive environment causes A to increase and K_{th_o} to decrease in equations (1.22) and (1.24) (McEvily and Wei, 1971). Another aspect of the environmental effect is the frequency dependence of the rate of crack propagation. Experimental evidence has shown that while there was no intrinsic frequency effect for most high strength metals over a very wide range of test frequency, a frequency dependence has been observed when tests were conducted in aggressive environments (e.g. Feeney et al, 1970; Wei and Landes, 1969; Wei, 1970).

Other interesting predictive approaches are those which have been based upon a liner superposition of stress corrosion effects upon the mechanical fatigue process. The expression given by Wei and Landes (1969) is an example of this type of approach. They have suggested that the rate of crack growth in a corrosive environment is considered to be the algebraic sum of the rate of growth in an inert environment and that of an environmental component computed from sustained load crack growth data obtained in the same aggressive environment and the load profile of the fatigue cycle. Viz:

$$\left(\frac{da}{dN}\right)_{\substack{(corrosion\\ fatigue)}} = \left(\frac{da}{dN}\right)_{(environment)} + \left(\frac{da}{dN}\right)_{\substack{(fatigue\ in\ inert\\ environment)}} \qquad (1.27)$$

This approach is applicable in type B behaviour (Figure 1) since below K_{ISCC} there is no environmental effect.

The superposition model proposed by Gerberich et al (1971) is essentially the same as the earlier model of Wei and Landes (1969). The only difference is that the SCC component ($(da/dN)_{(environment)}$ in equation (1.27)) was calculated in the Wei and Landes model by integrating the SCC growth rate over a single fatigue cycle using a step-wise procedure involving numerical or graphical solutions. Gerberich et al utilised the mean value theorem to assess the average stress intensity in any one cycle and took known relationships between

SCC growth rate (da/dt) and stress intensity (K) to determine an analytical function for the corrosion fatigue rate.

Another proof of the validity of applying fracture mechanics in stress corrosion and corrosion fatigue problems was given by Tyzack (1971). He introduced the concept of chemical work of fracture ($2\gamma_c$), defined as the chemical work of dissolution done by advancing the crack by unit area; it is therefore analogous to surface energy in Griffith's treatment of fracture. Then he examined his new concept in stress corrosion problems and extended it to the problem of corrosion fatigue.

Tyzack suggested that LEFM and COD concepts could be applied in both stress corrosion and corrosion fatigue. In stress corrosion in metals the subcritical crack growth occurs by a chemical process: local anodic dissolution at the crack tip, associated in some way with the localised yielding in the crack vicinity. In corrosion fatigue, failure occurs due to combined chemical and mechanical effects.

From the foregoing discussion it is evident that the concepts of LEFM have played a major role in characterising the process of crack propagation in both static and dynamic conditions. By contrast, comparatively little effort has been devoted to the analysis of the crack growth initiation process (e.g. Jack and Price's (1970) results on mild steel). However, a detailed discussion of the initiation process is out of the scope of the present work.

CHAPTER TWO

ENVIRONMENTAL FATIGUE FAILURE OF THERMOPLASTICS AND THEIR STRUCTURAL PROPERTIES

It is intended in this chapter to discuss the effects of the structure and viscoelastic behaviour of polymeric materials on the fatigue failure phenomenon in its general terms (as defined in Chapter One). Particular reference will be made to the materials used in the present investigation (nylon, polyethylene and PMMA) and environmental effects on the failure process. Moreover, a review of the current knowledge on these subjects which are of direct relevance to the work presented in this thesis is included in this chapter.

2.1 Viscoelastic Behaviour and Structural Aspects

One of the main features that differentiates polymers from metals is the time-dependence of their mechanical behaviour in many service environments. This behaviour, termed viscoelasticity, manifests itself in different ways; stress relaxation under constant deformation, creep under constant load, dependence of stress on strain rate in monotonic loading and damping in dynamic loading are all viscoelastic phenomena.

The term "viscoelasticity" describes behaviour which combines liquid-like and solid-like characteristics. The linearity of a viscoelastic system implies that its solid-like part is linearly elastic (obeys Hooke's law) and that its liquid-like part is linearly viscous (obeys Newton's law). Thus, linear viscoelastic behaviour implies that in a given experiment the ratio of stress to strain is a function of time or frequency alone and not of stress magnitude (Ferry, 1970). Polymeric materials exhibit linear viscoelastic behaviour at infinitesimal strains, while their behaviour deviates from linearity at finite strains; the distinction between the two regimes varies greatly from one material to another and its definition depends on the degree of required precision. In linearly viscoelastic materials it is sufficient to describe the mechanical behaviour by one parameter, such as the creep compliance or the relaxation modulus, as a function of time or frequency and any other parameter can be obtained by applying the

theory of linear viscoselasticity (Ferry, 1970).

2.1.1 Structural aspects of polymers

Polymers are composed of long flexible thread-like molecules in which the atoms are bonded together by strong co-valent bonds. The thread-like molecule has an average volume much greater than the atomic dimensions. In some polymers, the monomer units of which the chain back-bone is constructed may carry side groups. In others, random cross-linking may occur between the thread-like molecules, and according to the amount of cross-linking introduced a wide variety of properties may be obtained. The thread-like molecule is always changing its contour according to its thermal energy. Under the effect of stress new configurations are obtained; the response to the stress is rapid on a local scale while the long-range response is slow.

a) Amorphous polymers: Amorphous polymers are those which possess no intrinsic microstructure on a scale higher than the molecular. The main feature that distinguishes different amorphous polymers is the glass transition temperature (T_g). Every polymeric system has its characteristic T_g, below which the long range readjustments are severely restricted while there is still a wide range of response rates to external stress due to rearrangements on a more local scale. Above T_g these materials become rubbery, i.e. their Young's modulus falls rapidly with rising temperature to a value typical of a rubber and rubber-like elasticity is observed. This transition is called the glass-rubber transition. PMMA is a typical example of an amorphous thermoplastic of high molecular weight which is below its T_g at room temperature.

b) Semicrystalline polymers: Many of the commercially useful thermoplastics are semicrystalline. Full crystallisation is never obtained when crystallising the polymer from its molten state because of the low mobility of the molecules to form crystallites in the viscous polymer melt. Crystallites start to grow from different points when cooling down the melt and they tend to accept the higher molecular weight, more perfect chains and to reject the lower molecular weight, less perfect ones (Keith, 1964).

The crystallites grow in all directions from the centre of nucleation in the form of flat lamellae, or sometimes spiral lamellae - "fibrils" - to form the spherulites which have the spherical organisation. Each spherulite grows rapidly until spherulites fill all the space. Subsequently, branching of lamellae continues within the spherulite using up the material not crystallised initially. The molecules within the crystallised lamellae are folded back and forth through the thickness of the lamella with their axes normal to the lamellar surface. The crystallisation process is greatly affected by the degree of under-cooling of the polymer melt. When under-cooling is large many nuclei form causing the spherulites to be smaller and causing less rejection of low molecular weight and defective chains from the early growing lamellae. Finally, the growth rates will be high enough to prohibit the high molecular weight chains from disentangling themselves from the melt, and some chains tend to have their two ends embedded in different crystals forming intercrystalline links (Keith and Padden, 1959). These links may extend between crystallites in the same spherulite as well as crystallites in different spherulites. A significant number of the other chain ends are embedded in the intercrystalline material (Vadimsky et al, 1969). However, for any semicrystalline polymer there is a particular degree of under-cooling at which the rate of crystallisation is a maximum.

The previously mentioned construction of spherulites containing intercrystalline material and crystallites connected by inter-crystalline links suggests that internal stresses must exist in and between spherulites. This is supported by the observation of small cracks at the boundaries of spherulites and along their radii in unstressed polymers (Padden and Keith, 1959).

Polyethylene and nylon are typical examples of semicrystalline polymers. Polyethylene is an example of a material that crystallises so rapidly over a broad temperature range that it cannot be quenched to a fully amorphous state. The non-crystalline part of polyethylene is rubber-like at room temperature, being below its T_g. Low density polyethylenes (LDPE) show a T_g of about $-100^{o}C$ while in high density polyethylenes (HDPE) it is very

difficult to sense. LDPE ($\rho \simeq 0.92$ gm/cm^3) is highly branched due to side reactions in the polymerisation and has an extremely large spread of molecular weight ($\overline{M}_w/\overline{M}_n \simeq 50$) and these materials are usually 40 to 60% crystalline. HDPE ($\rho \simeq 0.95$ gm/cm^3) has very little chain branching and a smaller range of molecular weight ($\overline{M}_w/\overline{M}_n$ = 10-20) and these materials are usually 60 to 80% crystalline.

Nylons are different from polyethylenes in that the degree of crystallinity of a given nylon can be controlled over a wide range, and the noncrystalline part exhibits a T_g that lies between room temperature and the melting temperature (for nylon 66 its α transition occurs at 67°C (Weyland et al, 1970)). Nylons have a very narrow range of molecular weight (e.g. for nylon 66, $\overline{M}_w/\overline{M}_n \simeq 1.85$ (Burke and Orofino, 1969)).

2.1.2 Time, frequency and temperature effects

Owing to the previously mentioned structure of polymeric materials, different kinds of mobilities and rearrangements of the molecules can be obtained. These include long range aspects of the mobility which permit configurational rearrangements of the chain back-bones, and the more local aspects of the motion of the side groups or even much more specific local motion such as the rotation of the terminal groups. In the semi-crystalline polymer, motions within the crystal lattice may develop some sort of chain rotational oscillations (Wada, 1966) and outside the lattice the lamellae may slide with respect to each other, as well as the short-range configurational mobilities in the amorphous part.

Under conditions of stress and strain the type of molecular response depends primarily on polymer structure, temperature of the experiment and the test time or frequency. Thus, the stress-strain ratio, within the limits of linearity, is a function of these variables. The theory of linear viscoelasticity correlates this ratio with the previously mentioned three factors (time, frequency and temperature) (Ferry, 1970).

Under the effect of sinusoidally oscillating stress, the stress and strain are not in phase (because of viscoelastic behaviour). Some of the energy input is stored and recovered in each cycle and some is

dissipated as heat, so the modulus E is defined as a complex sum of a storage component (E') and a loss component (E'') and is given as E^*; hence:

$$E^* = E' + i E'' \tag{2.1}$$

and

$$E''/E' = \tan \delta \tag{2.2}$$

where δ is the phase angle between stress and strain. *Tan* δ is referred to as the loss tangent; its value is proportional to the ratio of energy dissipated to energy stored per quarter cycle. The dissipated energy density per cycle (W_d) (Ferry, 1970) is given by:

$$W_d = \frac{\pi E''}{|E^*|^2} \sigma_a^2 \tag{2.3}$$

and the rate of energy dissipated per unit volume of the material ($\dot{W}_d$) is:

$$\dot{W}_d = \frac{\omega}{2} \frac{E''}{|E^*|^2} \sigma_a^2 \tag{2.4}$$

where ω is the radial frequency = $2\pi f$ where f is the frequency. The rise in temperature depends on the rate of dissipated energy and on the heat capacity of the system. However, the temperature may reach a steady state value, for continuous sinusoidal deformation, depending on the rate of heat loss to the surroundings.

Since both the relaxation modulus $E(t)$ in a relaxation experiment and the storage modulus $E'(\omega)$ are measures of stored elastic energy, thus qualitatively $E(t)$ is equivalent to $E'(\omega)$ at $t = 1/\omega$. In particular, when $E(t)$ changes slowly with time $E(t) \simeq E'(1/t)$. With respect to the loss modulus E'' and the loss tangent *tan* δ they are expected to reach some peak over the whole range of frequency. At very high frequencies the molecular adjustments (even the short range adjustments) cannot take place and dissipate energy within the period of deformation.

At very low frequencies there is enough time for molecular rearrangements to take place at the same rate as the stress variations. At intermediate stages some of the energy is recovered and some is dissipated as heat depending on the type of molecular adjustments within the period of deformation. In practice, more than one maximum will appear over the whole range of frequency due to the different types of molecular mobilities associated with a particular range of frequency.

The effect of increasing the test temperature is to increase the free volume which gives the molecules more freedom in mobility and greater ability to readjust their configurations. This effect is nearly equivalent to shifting the viscoelastic function to higher frequencies or lower times (Ferry, 1970). Therefore, E'' or $tan\ \delta$ as a function of temperature at constant test frequency will show more than one maximum over the range of temperature and increasing the frequency is roughly equivalent to shifting the function towards higher temperatures. However, the maxima in $tan\ \delta$ and E'' may not coincide.

Each of these peaks over the temperature range is associated with a particular type of mechanism of mobility and rearrangement of the molecules. These mechanisms are referred to as α, β, γ, δ, etc., the one at highest temperature is usually designated as α, the following one β and so on. In amorphous polymers the peak α occurs around the T_g and is associated with the transition from a glass-like to a rubber-like condition. In semicrystalline polymers the α mechanism cannot be attributed to the amorphous part only and may be associated with crystallite melting (e.g. polyethylene), and the β mechanism in this case occurs around the T_g.

2.1.3 The viscoelastic behaviour of PMMA, polyethylene and nylon 66

PMMA is an amorphous polymer below its T_g at room temperature ($T_g \simeq 100^{\circ}C$ for PMMA); it is thus to be expected that its viscoelastic functions are affected by the secondary mechanisms in tests conducted at room temperature. Koppelmann (1958) has shown the effect of frequency on $tan\ \delta$ for PMMA near $25^{\circ}C$. As shown in Figure 2a, the loss tangent has a broad maximum at approximately 8 Hz. This maximum is expected to be due to the β mechanism as the temperature is below T_g. In tests conducted at constant frequency (1 Hz) and at different temperatures, as shown in Figure 2b, (Nielsen, 1962) the effect of both α and β mechanisms

clearly gives two maxima in the loss tangent at 130°C and 40°C respectively.

Polyethylene is a semicrystalline polymer above its T_g and crystallises over a broad temperature range, so that it melts also over a broad temperature range. The effect of temperature on one of its viscoelastic functions (E'') is shown in Figure 3, (Takayanagi, 1967). Two maxima are obtained at 90°C and -120°C and may be attributed to α and β mechanisms respectively. Here, the α transition cannot be attributed to the cessation of long range configurational rearrangements in the amorphous region; it is almost certainly of a rather different nature and due to the rearrangements in the amorphous region brought about by the crystalline melting process which is known to set in at about 50°C. The β mechanism in this case occurs at around the T_g.

Nylon 66 is a semicrystalline polymer above its T_g at room temperature. Nylons are very hygroscopic and this factor should be considered when representing the viscoelastic functions. The variations of $tan\ \delta$ with temperature for nylon 66 with a water content about 0.2% and 0.1% is shown in Figure 4a (Starkweather, 1973). The figure shows three maxima α, β and γ at 55, -80 and -140°C respectively for 0.2% nylon. In the case of dry slowly cooled nylon 66 (0.1% water content), there was no β mechanism and the γ maximum is slightly shifted towards higher temperatures, Figure 4a. However, increasing the water content of a slow cooled nylon allows the β peak to appear and shifts it gradually to lower temperatures as the water content increases. Since crystallites start to melt at a temperature much higher than 50°C, the α mechanism is associated with the motion of long range chain segments in the amorphous part near the T_g.

The α, β and γ peaks all shift to lower temperatures as the water content is increased (Figure 4b). The height of the β peak first increases and then decreases as the water content is increased. The mechanism for this may be the onset of water motion from one sorption site to another, a process which depends on the presence of both occupied and unoccupied sites, thus the amount of motion would be greatest at an intermediate water content (Starkweather, 1973).

2.2 Static Fatigue Failure in Polymers

The problem of static fatigue failure in polymers may be divided into two parts according to whether it is a failure by direct cracking

or first by crazing and then by subsequent crack growth through the craze. Failure by cracking can be identified by defining the crack as a flaw in which two new surfaces are created, these surfaces not being bridged by the polymer.

On the other hand, crazing is a familiar phenomenon associated with amorphous glassy polymers. The term crazing is applied to a network of small defects which have the appearance of being very small cracks. Crazes are usually planar and highly reflective like true cracks grown under unidirectional tensile stress in transparent bodies. A brief survey of crazing in glassy polymers with particular reference to craze structure and the role of the environment is included in Appendix B.

2.2.1 Fracture mechanics and kinetics of crazes under constant loads

The principals of fracture mechanics have met with great success in describing craze initiation and propagation in glassy polymers. Marshall et al (1970) have proposed a model based on the COD approach in conjunction with simple flow analysis to describe the movement of the liquid within the craze in PMMA single edge notched specimens (SEN) in methanol. It was found that both the initiation and growth chracteristics of the craze are controlled by the initial stress intensity factor K_o (using the original crack length, since the crack is stationary while the craze is growing).

Two important values of K_o emerged. The first was K_m, below which no craze growth would occur and its value is independent of specimen thickness. The second value, K_n, was found to control the craze growth pattern. For $K_m < K_o < K_n$ craze growth rates decelerated with time and fracture never occurred. For $K_o > K_n$ craze growth rates decelerated until a certain value of craze speed was reached, $\dot{x}_f$, and the craze continued to grow with this final speed. $\dot{x}_f$ was found to be a function of K_o and both K_n and $\dot{x}_f$ were found to depend on the specimen thickness.

The craze growth was explained to follow one of two distinct patterns. The first was termed "end flow"; the environment flows only through the crack tip into the craze for tests in the range $K_m < K_o < K_n$. That type of flow always led to eventual craze arrest. The second was termed "side flow" in which all the flow was through the sides of the craze (as in the case where craze growth was with constant speed $\dot{x}_f$).

The model proposed yielded a relation for craze growth for tests in the range of $K_m < K_o < K_n$, given as:

$$x = constant\ (K_o - K_m)\ t^{\frac{1}{2}} \tag{2.5}$$

where x is the craze length and t is the time. For crazes growing with constant speed $\dot{x}_f$, the relation is:

$$\dot{x}_f = constant\ \left\{(K_o - K_m)^2 - (K_n - K_m)^2\right\} \tag{2.6}$$

Williams and Marshall (1975) have further developed the previous model by considering approximate power laws of time dependence of the viscoelastic parameters (the modulus E and the yield stress σ_y). They assumed that:

$$\sigma_y(t) = \sigma_o\ t^{-m} \text{ and } E(t) = E_o\ t^{-n} \tag{2.7}$$

where σ_o and E_o are the unit time values and m and n are constants. Furthermore, they assumed that craze growth is either relaxation controlled or flow controlled. For relaxation controlled crazes, their model and calculations yielded the following expression:

$$x \ \alpha \ K_o^{\,2}\ t^{2m} \tag{2.8}$$

For flow controlled crazes in the case of $K_m < K_o < K_n$, the craze length was expressed as:

$$x \ \alpha \ K_o\ t^{\frac{1}{2} + \frac{m+n}{2}} \tag{2.9}$$

and for the flow controlled side flow condition the final craze speed was given as:

$$\dot{x} \quad \alpha \quad K_o^2 \, t^{(m+n)} \tag{2.10}$$

Williams and Marshall went on to use their model in calculating the average void spacing distance in the craze (ℓ_o). The calculated value was 250 Å, a figure which agrees with Kambour's and Holik's (1969a) direct observations.

Another type of notch which has practical importance is the surface notch. Tests on surface notched specimens of PMMA in methanol (Parvin, 1972) showed that the controlling parameters of craze growth are K_m, K_n and K_o as in the case of SEN specimens.

A study of the growth of cracks in PMMA/methanol crazes in SEN specimens has been made by Graham et al (1972). They used a high-power optical microscope to observe craze growth rates and the point of crack initiation and subsequent propagation under constant load conditions. It was found that the initial crack remained stationary for approximately 90% of the total testing time while the craze had grown a considerable distance, depending on the K_o level. Using Dugdale's model and finite width corre c tions for the specimen configuration, they were able to compute the true energy of fracture. It was found that the energy absorbed per unit area during the craze growth process and subsequent to initial loading, which is necessary to produce fracture, is approximately the same as for fracture in air. The mechanism which was implied is that if the initial loading in the liquid environment does not produce fracture immediately then this energy is dissipated at the start of the softening process by the formation of a new craze structure. If a softened craze structure is established, then the same amount of work must be expended to rupture the softened craze so as to cause fracture in air.

From the preceding section it is clear that fracture mechanics concepts have been very successful in dealing with the kinetics of environmental crazes in glassy polymers, particularly PMMA.

2.2.2 Stress cracking in polymers

Stress cracking is the long term brittle failure of a material under tensile stress appreciably below the limits of its short time strength. Stress cracking in polymers takes the form of stable crack propagation (a stable crack is one which can be stopped by load reversals) which gradually accelerates with time. This type of stable propagation is typical of viscoelastic materials and stems from the rate sensitivity of the modulus. There have been a number of attempts to develop theoretical models for this type of viscoelastic cracking. These theories were based on the principles of fracture mechanics and energy balance concepts, in conjunction with the viscoelastic properties of the materials assuming linear viscoelasticity (except at the crack tip). A good review of these theories was given by Knauss (1972). For example, Wnuk and Knauss (1970) derived an expression for the fracture initiation time of a penny-shaped crack in a viscoelastic solid. Knauss (1970) predicted the crack growth following initiation in a centrally cracked large sheet. However, the main feature of the existing theories of crack growth is that the deformed material near the crack tip is replaced by a very idealised model and the solutions of the time dependent crack size are given numerically. In some cases in which the solution was given analytically it was restricted to very idealised conditions such as those of the Maxwell model material (Wnuk and Knauss, 1970).

In a new theory developed recently by Schapery (1973) most of the limitations noted in the previous theories were removed. Although the continuum was assumed to be linearly viscoelastic, the nature of the deformed material at the crack tip, in which the eventual failure occurs (the "failure zone"), is quite arbitrary and could include a material which is highly nonlinear, rate dependent and even discontinuous. This implies that the theory should be valid for many different materials including polymers exhibiting crazing at the crack tip. The theory gives analytical solutions for crack initiation time and instantaneous velocity, both in terms of the opening-mode stress intensity factor, K_I. The application of the theory was very successful in unfilled and filled polymeric materials under constant and variable loading.

The shortage of accurate knowledge of the viscoelastic functions and the structural behaviour of many of the polymeric materials has limited the evaluation of the success of the theoretical analysis in representing

the experimental results.

Once again, fracture mechanics has proved to be successful not only in theoretical derivations but also in experimental studies of stress cracking in polymers. Marshall et al (1969a) studied crack growth in PMMA in air under constant loading conditions. They showed that a unique relationship exists between the fracture mechanics parameter, K_c, and the crack speed $\dot{a}$ irrespective of specimen configuration. K_c was found to rise steadily as the crack velocity comes up to the instability point. Williams (1972) performed an approximate viscoelastic analysis for crack growth in PMMA, and showed that the crack grows under a constant value of G_c when it runs below its initiation speed while it grows under constant COD if it runs above its initiation speed. He considered in his analysis the sensitivity of the modulus and the yield stress to the strain rate at the crack tip.

Another useful application of fracture mechanics was in the case of crystal polystyrene. Marshall et al (1973) have shown that the notching technique is very important and that it is the cause of the fluctuations in the reported values of K_c (evaluated at crack instability) quoted from different sources. They attributed this to the presence of craze bunches at the crack tip and showed that high frequency fatigue notching has produced pure cracks which resulted in lowering the level of K_c versus stable crack speed and K_c at instability.

One of the characteristics of crystalline polymers is that the departure from linear viscoelasticity appears at very small strains (Ferry, 1970). Even so, the parameter K has proved to be a sensitive measure of stress cracking resistance. Marshall et al (1972) produced a relation between K_c and the crack speed for HDPE similar to that for PMMA and polystyrene and showed that the values obtained were independent of the specimen geometry.

2.2.3 Environmental stress cracking (ESC)

The problem of ESC in crystalline polymers has been reported in the literature (e.g. polyethylene stress cracking in fuming nitric acid (Hinton and Keller, 1969) and the stress cracking of polyamides (nylons) in metal salts (Dunn and Sansom, 1969)). However, the example which is extensively studied but still poorly understood is the ESC of polyolefins (particularly polyethylene) in the presence of detergents and organic

liquids. This is largely because polyethylenes have been widely used as an insulation and coating for undersea telephone cables and for underground pipe work. A survey of the published work on this problem was given by Howard (1964).

There have been several experimental studies of the kinetics of the ESC problem. However, to the author's knowledge, the only theoretical study is that by Williams and Marshall (1975). They assumed that E and σ_y could be approximated by equation (2.7) and that crack growth is either relaxation or flow controlled as in the case of environmental craze growth. For relaxation controlled fracture the criterion would be constant COD (U_c) (Williams, 1972). The expressions they obtained for $\dot{a}$ in relaxation and flow controlled conditions were given respectively as:

$$\dot{a} \alpha K^{2\left(\frac{1-m+n}{m+n}\right)} / U_c^{\left(\frac{1-2m}{m+n}\right)} \qquad (2.11)$$

and

$$\dot{a} \alpha K^2 \qquad (2.12)$$

where K is the current value of the stress intensity factor and $\dot{a}$ in equation (2.12) depends on specimen thickness.

Williams and Marshall have shown the agreement between their theory and the experimental data both for polymers (PMMA, polyethylene and polystyrene) and inorganic glass.

a) Environmental stress cracking of polyethylene (PE): The initiation of ESC in PE is, as in other cases, at inherent flaws or inhomogeneities at the surface, and cracking tends to be between spherulites and along spherulitic radii (Isaksen et al, 1963) where internal stresses exist (see Section 2.1.1(b)). Also cracking occurs in the disordered zone where the folded chains undergo reorganisation into extended chains between crystallites. The mechanism of ESC in polyethylenes is not yet precisely known (Kambour, 1972). However, there may be two mechanisms operating, since anhydrous detergents and small molecule organic liquids are more effective cracking agents for low molecular weight resins, but water solutions of detergents are more effective for high molecular

weight resins (Pelagatti and Baretta, 1959). For high molecular weight resins Isaksen et al (1963) suggested that an absorption mechanism may operate. The detergent molecules are absorbed on the surfaces formed in the reorganisation regions at the end of the intercrystalline links and exert an internal or spreading pressure on this already weakened structure. The structure is then no longer strong enough to carry the stress and failure occurs in the intercrystalline links.

The previous studies of PE have shown several parameters which affect the resistance to cracking; such as the degree of crystallinity, the molecular weight and the temperature. It was impossible to be certain that the effect of crystallinity is independent of the effect of molecular weight (Landes, 1960).

However, it has been observed that evaluating resistance to ESC depends very much on the test method used. The results of constant strain and constant stress tests often are contradictory and data are very hard to reproduce.

Recently, the application of fracture mechanics to the problem of ESC of PE has shown the possibility of performing reproducible tests by measuring the stress intensity factor. Marshall et al (1969b) tested two grades of LDPE (MFI 20 and 7) in two different environments (methanol and ethanol), using SEN specimens under constant loading conditions. A unique relationship between K_c and the crack speed was obtained independent of specimen thickness or lengthy pre-soaking in the environment. The stable crack speed rose steadily with increasing K_c. They also evaluated the strain rate effects and found good correlation between the theoretical and experimental results. Similar results were also obtained for high and medium density polyethylenes tested in detergents (Marshall et al, 1972; Sullivan, 1972).

All the above tests suggest the use of K_c of notched specimens as the controlling parameter in ESC of PE rather than the critical stress or strain of unnotched specimens where the discrepancy is introduced by materials having different degrees of surface finish.

b) Environmental stress cracking of nylons: The organic acids like the phenols can cause stress cracking of nylons. These acids can

dissolve nylons and the dissolution process involves the replacement of the interchain hydrogen bonds by the solvent hydrogen bonds. This process has a plasticising effect since it lowers the T_g and melting points and causes what is known as "solvent stress cracking".

Metal salts dissolved either in water or in organic media can also act as stress cracking agents (Dunn and Sansom, 1969). Increasing temperature, moisture content of the nylon, concentration of the cracking agent and level of stress caused more rapid crack initiation and failure of the specimen. Cracking may be attributed to increasing stresses and lowering of the modulus caused by the localised swelling and plasticisation.

However, there have been no studies of ESC of nylons from the mechanical point of view as in the case of polyethylenes.

2.3 Dynamic Fatigue Failure of Polymers

The use of plastics as structureal materials is increasing rapidly and they are now frequently used by engineering designers to replace metals wherever appropriate. Plastics have favourable properties such as the high strength to weight ratio, good damping properties and excellent electrical resistance. Now the applications in which plastics may suffer dynamic fatigue failure are becoming quite common as these materials are used for gears, dampers, load bearings, etc.

There are as yet no extensive studies of the dynamic fatigue properties of polymeric materials and most of the reported studies have dealt with conventional techniques such as those yielding S–N diagrams. A few have focussed on the two observed modes of failure (ductile due to thermal softening and brittle due to incremental crack propagation). More recently, fracture mechanics concepts have been introduced into the problem of dynamic fatigue of polymers and a few attempts have been made to test their applicability.

Because of the sensitivity of the polymeric materials to temperature and frequency a careful choice of the dynamic test variables should be made. These include frequency, environmental conditions, the mode of deformation (e.g. flexural or uniaxial), type of loading (e.g. continuous or discontinuous), the level of the applied mean stress and the cyclic wave form (e.g. sinusoidal, triangular or square).

2.3.1 Failure by cyclic thermal softening

This type of failure occurs because thermoplastics have a high damping capacity (as a result of internal frictional movements between the molecules) and low thermal conductivity. Riddel et al (1966) have studied the thermal softening failures using the reversed bending test on cantilever specimens. They carried out their tests on different polymeric materials including PMMA, PE and nylon 6 at a frequency of 30 Hz and plotted the normal S-N curves. The failure temperatures were found to be generally around the T_g of the polymer corresponding roughly to the α transition. In some materials a fatigue limit was reached and it has been noticed that the temperature rise eventually stabilised at a low level. The fatigue limit was affected by different parameters, for example, it was higher, the lower the frequency of testing, the smaller the thickness of the specimen and the higher the crystallinity of the material. In some other cases a fatigue limit was not observed and the material continued to fail by thermal softening for the lowest stress applied (e.g. nylon 6).

Opp et al (1969) developed a model for polymers based on the concept of hysteresis energy per cycle Q (Feltner and Morrow, 1959), which states that QN_f = constant. They assumed that Q is constant through the whole test (this is not true because of the strong dependence of the loss modulus (equation (2.3)) on temperature rise during the test). Their low-cycle fatigue results for a number of polymers have shown "melt failures" at high strain levels and failure by crack propagation at low strain levels. Their developed theory predicts these phenomena as well as the effects of other parameters such as specimen dimensions, ambient temperature, level of strain and cyclic wave form.

However, in a recent study by Constable et al (1970a), they showed qualitatively how the failure by cyclic thermal softening can be related to the loss compliance or modulus, specimen geometry, frequency and the magnitude of cyclic load. They carried out their tests on PMMA and PVC in flexure and rotating bending cyclic loading. In the case of PMMA, increasing the frequency or ambient temperature for the same specimen geometry changed the mode of failure from entirely cracking to entirely thermal softening. The effect of increasing the ambient temperature by small amounts or increasing the specimen diameter was to cause thermal failures at lower stress for the same number of cycles. Tests on PVC

showed that failure occurred entirely by cracking for the whole range of frequency (25 to 67 Hz) and at an ambient temperature of 20°C although the simplified theory (no heat transfer from the specimen) predicted entirely thermal softening failure.

However, there is some evidence that thermal softening may occur even in the case of failure by crack propagation. Regel et al (1973) in their tests on nylon 6 and polyvinylalcohol precracked specimens loaded at a frequency of 16 to 200 Hz, found a rise in temperature of up to 70°C at the crack tip while the temperature of the specimen at a distance from the crack tip remained close to ambient. When air was blown onto the crack tip, the crack growth rate decreased.

2.3.2 Failure by cyclic crack propagation

In some cases success has been achieved by the application of the empirical laws of metals in the dynamic fatigue or polymers. For example, Tomkins and Biggs (1969) found that the Coffin-Manson law (equation (1.6)) was obeyed by nylon 66 while it was not successful in the case of Araldite. They also applied Miner's linear cumulative damage law (equation (1.5)) to nylon 66. The linear damage law fitted the data for cycling at decreasing strain amplitude, while cycling at increasing strain amplitude resulted in greater damage than predicted by equation (1.5).

According to the fact that inherent flaws exist in thermoplastics (inclusion of foreign particles or gas bubbles during processing, irregularities in the molecular structure and scratches during machining and handling) and these flaws act as stress raisers, therefore, cyclic fatigue cracks start to grow from these sites with relatively low initiation periods (McEvily et al, 1963). It is more logical to induce initial cracks of known sizes and study their propagation behaviour rather than depending on undetermined flaws in the material. Attempts have been made to apply fracture mechanics concepts in such a study and met with great success.

Andrews and Walker (1971) studied the crack propagation of a range of LDPE, their study was based upon the work of Rivlin and Thomas (1953) for rubber which was in turn based upon Griffith's work. Their results on cyclic tensile fatigue at constant strain amplitude and $R = 0$, using SEN specimens, were expressed in the form:

$$\frac{da}{dN} = B\,(\tau)^n \qquad (2.13)$$

where B and n are constants and τ is the fracture mechanics parameter (the rate of energy available from the stress field with respect to the crack length). τ for an edge crack in a semi-infinite sheet under uniform tensile stress acting normal to the crack axis was expressed in the form:

$$\tau = k\,a\,W \qquad (2.14)$$

where k is a numerical constant which varies with the value of W (it was found to vary between π and 1) and W is the input energy density.

Andrews and Walker observed two distinct regions of crack growth in the materials studied, with different values of the constants B and n linked by a transition zone in which the crack propagation with constant or decreasing velocity as ΔK increases. They attributed this to the change from brittle to ductile fracture.

The use of equations (2.13) and (2.14) was thought to be more suitable than the use of classical fracture mechanics, since most polymeric solids exhibit finite elastic deformation, non-Hookean behaviour and time dependent properties, and deviation from linear viscoelasticity appears at small strains for crystalline polymers.

a) Fracture mechanics and the factors influencing cyclic crack growth: It has been previously shown (Section 2.2) that the parameters of the classical fracture mechanics, such as G and K, are successful in describing the behaviour of cracks and crazes in static fatigue of polymers and it will be shown below that they are also successful in dealing with the dynamic fatigue problem in these materials.

The demonstration of Paris and Sih (1965) that LEFM could be used in the case of brittle fracture in linear viscoelastic plastics if allowance is made for the time-rate dependence of the stress intensity factor and the observations of McEvily et al (1963) that

the fatigue crack growth in some polymers (e.g. PC and PE) has much in common with that in metals, led to the study of the relation between $\dot{a}_N$ and ΔK.

The experimental studies of Watts and Burns (1967) on PMMA, Borduas et al (1968) on PMMA and Mukherjee et al (1969) on PMMA and PC suggest the validity of the Paris law (equation (1.15)) for these materials and that the crack growth rate is independent of specimen thickness and loading history.

Similar studies have been done by Hertzberg et al (1970,1973). They examined the fatigue crack propagation behaviour of a very wide range of engineering plastics including nylon 66, LDPE and PMMA. They carried out their tests on tensile SEN specimens and all tests were performed between 0.33 and 20 Hz. In all cases $\dot{a}_N$ was found to be a power function of ΔK (equation (1.15)). Great differences in $\dot{a}_N$ for a given ΔK were observed for different polymeric materials differing only moderately in modulus E at room temperature, while metals exhibit comparable $\dot{a}_N$ for a given ΔK when normalised with respect to E (Pearson, 1966). The behaviour of polymers is much more complicated than that of metals and necessitates a full understanding of the role of the molecular motions and energy dissipation processes as related to their chemistry and structure. Hertzberg et al suggested that the behaviour of polymers could be generally correlated with their damping properties. Increasing the mechanical losses by damping increases the resistance to cyclic crack propagation. However, there is a role still played by E in the crack propagation resistance; for example, both nylon 66 and LDPE have high damping while LDPE has much less resistance to cyclic crack growth than nylon 66. This is apparently due to the much lower E of LDPE.

Hertzberg et al (1973) demonstrated the difficulty of predicting the effect of frequency (ω) on $\dot{a}_N$ since frequency changes could produce various material responses. Increasing ω may increase or decrease E'', $\tan\delta$, E and σ_y. Thus, the net result may be an increase or decrease in the dynamic fatigue resistance depending on the share of each of these parameters (the effect of frequency will be discussed in detail in Chapter Three). This shows that the effect of frequency in polymeric materials is extremely complex.

Arad et al (1971,1972a,b,c,1973a) studied the cyclic crack growth in centrally notched plates of different thermoplastics (PMMA, PC and nylon 66). They studied the effect of ΔK, K_m, orientation, wave form and frequency (f). Arad et al proposed the formula of equation (1.25) to correlate $\dot{a}_N$ with ΔK and K_m, and at the same time with COD and the plastic zone size at the crack tip (see page 29). Equation (1.25) represented the experimental data of the tested polymers well except in the case of PC: when $\dot{K}$ (= $\Delta K f/2$) exceeded 4000 lbf/in$^{3/2}$s, the effect of K_m became negligible in comparison to ΔK and $\dot{a}_N$ could be represented by the Paris law (equation (1.15)).

The effect of molecular orientation in the extrusion direction in nylon 66 extruded sheets was found to cause a decrease in $\dot{a}_N$ when cracks propagated perpendicular to the extrusion direction compared to cracks propagating parallel to it. Also, in their study of PC at a frequency of 0.1 Hz they found that $\dot{a}_N$ was slightly higher under sinusoidal than under triangular loading. Such an effect was attributed to an increase in hold time under higher loading.

Arad et al conducted their tests at three frequencies (0.1, 5 and 20 Hz), and found in all cases that $\dot{a}_N$ decreases as the frequency increases except in PC, when $\dot{K}$ > 4000 lbf/in$^{3/2}$s, an increase in the frequency led to an increase in $\dot{a}_N$. They argued that the increase in crack speed (or rate of applied load) causes a rise in K_{IC} in the stable growth region which results in smaller $\dot{a}_N$ under higher frequency. They also discussed the effect of frequency on the yield stress and the plastic zone size ahead of the crack tip and the effect of increasing or decreasing W_d (equation (2.3)) as the frequency increases or decreases. They attributed the behaviour of PC to its particular viscoelastic properties.

In 1973 Mukherjee showed that the effect of ΔK, the level of ΔK and the frequency or temperature on the cyclic crack growth could be taken into account by using Erdogan's formula (equation (1.20)). He multiplied by another parameter of the form of $(X)^L$ where X is a variable such as time or frequency and L is a constant; thus, equation (1.20) becomes:

$$\dot{a}_N = A\ (\Delta K)^m\ (K_{max})^n\ (X)^L \qquad (2.15)$$

It was shown that this equation satisfactorily represented the experimental data of PMMA and A-212B steel.

Another interesting application of fracture mechanics in dynamic fatigue of polymers was that by Constable et al (1970b). They performed Wöhler type rotating bending fatigue tests on PVC cantilever specimens containing various notches of known geometry. They represented their results in the K-N curve which is similar to the S-N curve but using K (estimated according to the original notch size) instead of S. Results from sharp notches showed good correlation (independent of notch size) and a fatigue limit was revealed at a certain K value.

b) Theoretical models for cyclic crack initiation and propagation:

Most of these theoretical models are preliminary attempts to extend the models of stress cracking under constant loads to the more general case when the loads are variable. Therefore, they have the same shortcoming as the static fatigue models, i.e. the representation of the failing material at the crack tip by a very idealised model and giving a numerical solution or one restricted to very idealised conditions. Moreover, they require comprehensive and accurate data of the material structure and its viscoelastic properties.

Examples of these models were given by Williams (1967), Yokobori (1969), Knauss and Dietmann (1970) and Wnuk (1974). However, Wnuk's model shows the correlation between $\dot{a}_N$ and $(K_{max}^2 - K_{min}^2)$, the relation depends also on the frequency and some other rate sensitive factors which depend on the material properties as well as the fracture toughness, K_c.

Schapery's theory (1973) of crack growth in viscoelastic media is one of the most important and general theories at present available. When extended to the case of oscillating load, it gave a relation similar to the Paris law (equation (1.15)) where A in this case is a parameter depending in some way on the frequency, fracture and material properties and the level of loading.

However, it is hoped that the previous discussion has revealed the role of the fracture mechanics parameter K in describing the crack's behaviour under dynamic fatigue conditions in polymeric materials from both the theoretical and experimental points of view.

2.3.3 Environmental dynamic fatigue of polymers

The examination of the literature reveals that there has been very little published work on the combined effects of cyclic loading and environment, other than air, in the case of polymeric materials (to the author's knowledge, there are only three publications). Even the commercial laboratory attempts of carrying out fatigue tests in various organic environments have generally been stopped because of the extensive scatter produced on conventional S-N curves.

Pringle (1969) tested PMMA in distilled water. He made a statistical analysis of the results because of the degree of scatter, without discussing the response of the material to the environment.

The published work of Bonner et al (1973) showed that a gasoline vapour environment has very little effect on the fatigue limit of nylon 66 conventional S-N data and that the fatigue endurance of the dry resin is greater than that of the resin conditioned at 50% relative humidity in both flexural and axial tests.

However, the work of Marshall and Williams (1973) is considered to be the first actual work that deals with the problem of environmental dynamic fatigue in polymers. They studied the effect of cyclic loading on craze growth in PMMA specimens in a methanol environment. Long crazes were grown prior to fracture in a manner similar to craze growth under constant conditions (see Section 2.2.1); however, when cycling between 0 and K_o, the craze velocity, $\dot{x}_f$, was less than that obtained under constant K_o. They modified the model previously proposed by Marshall et al (1970) (equation (2.6)) to take into account variable loading conditions. The excellent correlation they demonstrated between the predicted craze growth according to the modified model and the experimental results for a test frequency of 0.1 Hz or lower, suggests that the controlling mechanism of craze growth is the same for both dynamic and static conditions. When the frequency was increased to 0.5 Hz the craze growth was faster than that predicted by the model, but

the velocity was still less than that obtained in constant K_o tests. Marshall and Williams attributed this to the difference in phase between the void size changes in the craze and the variations of K_o at high frequencies because of viscoelastic effects. This resulted in the voids not closing which gave a higher average void size and a higher average speed.

From the foregoing survey and discussion it is evident that the fracture mechanics principles and parameters are extremely powerful tools for the study of the fatigue phenomena in thermoplastics. However, from the mechanical point of view, there is still a pronounced lack of knowledge of the mechanisms of failure (e.g. detergent cracking in polyethylene) and there is a marked shortage of data on the environmental dynamic fatigue behaviour of these materials. As plastics find wider uses as structural materials, these subjects assume greater importance and should receive greater attention in future research to allow the exploitation of these materials to the utmost.

The experimental research study to be discussed in the next chapter aims at revealing the environmental effects on the behaviour of some thermoplastics under cyclic loading conditions as well as studying the effect of some other external variables such as frequency and level of loading.

CHAPTER THREE

ENVIRONMENTAL DYNAMIC FATIGUE CRACK PROPAGATION IN NYLON 66 AND HIGH DENSITY POLYETHYLENE

Most previous studies of failure phenomena in plastics have been devoted to PMMA, although it is not a true engineering plastic. This is mainly because:

a) PMMA is transparent and hence cracks can easily be seen and monitored;
b) it breaks in a reasonably brittle manner, thus allowing the description of the failure by fracture mechanics theories which were developed for glass and metals; and finally,
c) it has the viscoelastic properties of time and temperature dependence which allow the study of their effects on the fracture behaviour as an example of plastic materials.

On the other hand, fewer studies have been made of the fracture behaviour of other thermoplastics, such as polyethylene, PVC and polystyrene, although some of these are true engineering plastics and a comprehensive study of their failure behaviour might help in solving some of the practical problems (e.g. PVC pipe line failures) and widen the scope of their application. Therefore, it has been decided to study dynamic fatigue crack propagation in two engineering thermoplastics (nylon 66 and high density polyethylene) in some practical environments. It can be argued that there have not been many applications to date in which plastics suffer from the problem of dynamic corrosion fatigue failure. This may be the situation now, but certainly it will change in the future as polymers are rapidly gaining in use as structural materials (e.g. nylon is used now in making load bearing members and light duty gears where environmental dynamic fatigue failures are more likely to occur).

3.1 Experimental Procedure

3.1.1 Material and environment selection

Two engineering thermoplastics were selected for the present study

(nylon 66 and high density polyethylene).

The nylon 66 (N66) was ICI Maranyl AD 151, an injection moulded tough semicrystalline thermoplastic which is below its T_g at room temperature and has a narrow range of molecular weight distribution ($\bar{M}_w/\bar{M}_n \simeq 1.85$). The material was supplied as moulded $9\frac{1}{4} \times 3\frac{3}{8} \times \frac{3}{16}$ inch plates.

The high density polyethylene (HDPE) was BP T2000 Rigidex, a moulded semicrystalline thermoplastic with density $\rho = 0.954$ and MFI = 0.2. This material is softer than nylon 66 (it is above its T_g at room temperature) and has a higher range of molecular weight distribution ($\bar{M}_w/\bar{M}_n$ = 10-20). The material was supplied as moulded 12 x 12 x $\frac{1}{4}$ inch plates.

Tests on N66 were conducted in three different environments: air (20°C and 50% RH), distilled water and sulphuric acid of 10% concentration; while tests on HDPE were conducted in air (20°C and 50% RH) and in a detergent, Adinol (alkyl phenol polyglycol ether).

The choice of distilled water as a testing environment was based on the fact that nylons are very hygroscopic (see Section 2.1.3) and this affects the material's properties and resistance to dynamic fatigue when it is used in a humid environment. Low concentration sulphuric acid solutions are very common environments used in many chemical processes (e.g. nylon car battery cases). The susceptibility of polyethylene to stress cracking in detergents was discovered 25 years ago. Since then an intensive study of the problem has been made under static loading conditions (see Section 2.2.3(a)); therefore, it was felt that extending the study to dynamic conditions might help resolve some of the mysteries surrounding the role of detergents as cracking agents.

3.1.2 Specimen dimensions and preparation

Tests were conducted on tensile SEN specimens (Figure 5a) which were designed to satisfy the requirements of giving accurate values of the stress intensity factor according to the boundary collocation solution of Brown and Srawley (1966), i.e. the point of load application should be far enough from the plane of the crack ($\ell'/2w > 0.8$ is satisfactory for $0.1 \leqslant a/w \leqslant 0.45$, where ℓ' is the specimen free length (Figures 5a and 8b)). Other conditions should be satisfied by the test specimen, e.g. the initial crack must be as sharp as possible

to give a minimum initiation time before crack propagation under dynamic loads, and the specimen dimensions must be large enough to provide sufficient constraint around the plastic zone ahead of the crack tip and to allow the crack to propagate under mode I with the smallest possible shear lips (see Appendix A, page 277).

The following specimen dimensions were chosen:

Nylon 66: rectangular plates $9\frac{1}{4} \times 3\frac{3}{8} \times \frac{3}{16}$ inch (i.e. the moulded plates supplied by the company were used without any further machining).

HDPE: rectangular plates $11\frac{1}{2} \times 5 \times \frac{1}{4}$ inch.

Smaller rectangular specimens 6 x 2 inch were also prepared from both N66 and HDPE (for tests conducted on the Instron machine).

Two rows of equally spaced $\frac{1}{4}$ inch diameter holes were drilled at each end of the specimen to ensure firm clamping and uniform load application.

a) Method of notching: At first a saw cut was made to a length less than the required initial crack length by about 2 mm. Then a sharp crack was produced at the tip of the saw cut by forcing a razor blade into the specimen body, Figure 5b; this was carried out by mounting the razor blade in jig which was in turn fitted to a Vickers Hardness Testing Machine. Cracks were produced by this method for both N66 and HDPE specimens.

b) Specimen conditioning: HDPE specimens were left to age for about 6 weeks before testing to guarantee the stability of the mechanical properties.

N66 absorbs water and water solutions, as discussed in Chapter Two. It was therefore kept in air-tight polyethylene bags with self-indicating silica gel to absorb the moisture and keep the material dry until the time of testing. Four batches of specimens were prepared from this material:

1. A batch of dry specimens which had been kept dry as mentioned above.

2. A batch of specimens conditioned to contain 4.4% weight of distilled water.
3. A batch containing 4.4% weight of sulphuric acid hydrous solution of 10% concentration. And finally,
4. A batch which had been saturated with distilled water at 100% relative humidity (water content ≃ 9.8%).

The rate at which water is absorbed depends on the relative humidity, the thickness of the specimen and above all on temperature; while equilibrium content appears to be largely independent of temperature. Therefore, it was decided to condition the specimens in boiling distilled water to reach the required percentage of water content. It was found that 7.5 hours in boiling water was sufficient to give a water content of 4.4% in the specimen, while immersion in boiling water for 50 hours gave a water content of 8.7%. These times are much shorter in comparison with those required to reach the same water content by immersing the specimen in distilled water at room temperature (20°C), Figure 6.

Specimens conditioned in sulphuric acid (10% concentration) reached 4.4% increase in weight after immersion in the solution at room temperature for 1270 hours, Figure 7.

c) Specimen preservation: Specimens conditioned to 4.4% either in distilled water or in diluted sulphuric acid were removed from the liquid, dried well and wrapped in aluminium foil, the edges of which were sealed by self-adhesive tape. This method of wrapping isolated the specimen from the surrounding environment, even the environment between the specimen and the aluminium foil being controlled by keeping all the specimen surfaces in contact with the foil while wrapping it. This method proved sufficient to keep the specimen condition practically unchanged until the moment of testing, e.g. for a specimen containing 4.4% water wrapped by this method and kept for 1500 hours, only a loss of 0.25% was observed after this period.

Specimens conditioned in boiling water to 8.7% were kept in distilled water at room temperature. However, these specimens were still able to absorb water and it was found that the water content

was further increased by about 1% by immersion in cold water for 800 hours; no further increase was then observed.

After reaching the required condition, the specimens were left in distilled water (in the case of saturated specimens at 100% RH) or wrapped in the aluminium foil for a period of not less than three weeks to allow the water to be uniformly distributed through the specimen thickness. It should be noted that notching and drilling the specimens was conducted just before testing and not before conditioning them.

3.1.3 Testing programme

The purpose of this programme was to study the effects of the environment, loading frequency, range of loading and level of loading on crack propagation in both N66 and HDPE. Tensile dynamic fatigue tests at constant sinusoidal load amplitude were carried out on the previously described SEN specimens according to the following programme:

a) Tests on N66:

1. Dynamic fatigue crack propagation in dry N66 in air (20°C and 50% RH); the effects of load range, stress ratio R and loading frequency (0.16, 5, and 20 Hz).
2. Dynamic fatigue crack propagation in N66 (4.4% water content) in both air and distilled water; the effects of load range, R and frequency (0.16, 5, and 20 Hz).
3. Dynamic fatigue crack propagation in N66 (9.8% water content) in distilled water; the effects of load range, R and frequency (0.16, 5, and 20 Hz).
4. Dynamic fatigue crack propagation in N66 (4.4% sulphuric acid (H_2SO_4) of 10% concentration) in 10% concentration sulphuric acid environment; the effects of load range, R and frequency (0.16, 5, and 20 Hz).

b) Tests on HDPE:

1. Dynamic fatigue crack propagation in HDPE in air; the effects of load range, R and frequency (0.16, 5, and 20 Hz).
2. Dynamic fatigue crack propagation in HDPE in Adinol; the effects of load range, R and frequency (0.16, 5, and 20 Hz).

3.1.4 Testing apparatus

The tests in the preceding programme were carried out using an Instron Universal Testing Machine and a Dowty Electrohydraulic Fatigue Machine.

The Instron machine was initially designed for monotonic tests but it may be used for dynamic fatigue tests when the frequency is less than 0.5 Hz. The range of loading depends on the capacity of the load cell used: the maximum load cell capacity here was 10,000 lbf.

The Dowty is an electrohydraulic fatigue testing machine which has a range of frequency varying from 0.01 up to 100 Hz. The range of loading again depends on the capacity of the load cell used, the maximum being 12,000 lbf. The machine has the following advantages: the possibility of varying the shape of the input wave form (sinusoidal, triangular, square, etc.); the facility of making the necessary adjustments of load while the test is in progress and automatic switch-off when failure occurs, i.e. when specimen deflection exceeds a certain amount.

3.1.5 Testing procedure and the method used for calculations

Conditioning the specimens caused a slight increase in the dimensions so the measurements of specimen width and thickness were made just before testing.

In pilot tests in liquid environments there was some difficulty in preventing the environment surrounding the specimen from leaking during the test period, especially when this was long and/or the frequency was high. However, the difficulty was overcome by using "mini tanks" as shown in Figure 8. These cells were made by sealing together thin plates of glass or perspex using silicon rubber sealant, which was also used to

seal the tank to the specimen. The mini tanks with this rubbery sealer proved to be successful in preventing leakage for all materials, environments and test conditions in the experimental programme.

Each end of the specimen was bolted to a pair of steel plates, then pin loaded in the machine, Figure 8b, and the crack propagation was measured by a travelling microscope.

Tests at frequencies of 20 and 5 Hz were conducted on the Dowty machine while those at 0.16 Hz were conducted on the Instron. The possible discrepancy in the results due to the use of two different types of testing machine and two different specimen sizes was checked by conducting similar tests on both machines. The observed discrepancy was negligible in comparison with the normal scatter of dynamic fatigue test results.

Moreover, the temperature rise (measured by fixing a thermocouple on the surface of the specimen) was found to be negligible in both N66 and HDPE specimens up to the highest frequency used in the present programme (20 Hz) and the immersion of the specimen in the environment during the test period did not cause any significant change in its weight (i.e. there was a negligible increase of liquid content in the specimen).

Fracture mechanics concepts were used in analysing the crack propagation data obtained from all tests since it had previously achieved success in using the parameter K to describe the behaviour of cracks under environmental static fatigue conditions as well as dynamic fatigue in air (see Chapter Two). Also the theoretical treatment by Schapery (see pages 43 and 53) which led to describing the crack propagation by K, assuming the linearity of the viscoelastic continuum regardless of the nature of crack tip plastic zone, has supported the experimental evidence for the application of K. However, the experimental work discussed in Chapter Two shows that approximate linearity is sufficient and the behaviour of cracks is still correlated by the parameter K (e.g. Hertzberg et al (1970,1973) and Marshall et al (1972)).

In the present experiments approximate linearity may be assumed if the the maximum stresses and the rates of loading are limited (perfect linearity is approached by increasing the rate of loading and decreasing the maximum stress). A guide to approximate linearity was identified by considering the isochronous data for similar materials (Ogorkiewicz, 1970), Figures 9 and 10. It is also expected that linear behaviour would

extend to higher stresses than those shown in Figures 9 and 10 because the time of loading is much less than 100 sec (e.g. at the lowest frequency the time of loading is about 3 sec).

The stress intensity factor K for the SEN specimens used in the present programme was estimated by using the boundary collocation solution of Brown and Srawley since this solution takes account of finite plate effects. The solution was given as:

$$K = \sigma Y a^{\frac{1}{2}} \tag{3.1}$$

where σ is the gross stress, a is the crack length and Y is the finite effects correction factor, given as:

$$Y = \left\{1.99-0.41\left(\frac{a}{w}\right)+18.70\left(\frac{a}{w}\right)^2- 38.48\left(\frac{a}{w}\right)^3+ 53.85\left(\frac{a}{w}\right)^4\right\} \tag{3.2}$$

The accuracy of equation (3.1) falls rapidly as the crack length exceeds 0.5 w, so all the crack measurements were taken for $0.1 < a/w < 0.4$. Also crack growth was only considered when it occurred by opening mode crack surface displacements (i.e. cleavage mode or mode I) (see Appendix A, page 277). This mode was recognised where the shear lips occupied less than 10% of the specimen thickness and in this case K in equation (3.1) may be replaced by K_I.

3.2 Experimental Results

3.2.1 Dynamic fatigue crack propagation in dry N66 in air

It was hoped that this study would confirm the unique correlation between the cyclic crack growth rate $\dot{a}_N$ and the range of the stress intensity factor ΔK (= $K_{max} - K_{min}$) for N66, as well as reveal the effects of loading frequency and the level of loading represented by the ratio R (= $K_{min}/K_{max} = \sigma_{min}/\sigma_{max}$ at the instantaneous crack length).

Tests were carried out at frequencies of 0.16, 5 and 20 Hz, and at each frequency four ratios R were chosen (0, 0.25, 0.4 and 0.6). In any particular test under constant frequency and ratio R the crack growth

was recorded at intervals whilst the test was in progress. The relationship between crack length a and the numbers of cycles N was typically as shown in Figure 11, and this pattern of accelerating crack growth did not change with frequency or R.

From the crack growth data (e.g. Figure 11) $\dot{a}_N$ was represented by the slope of the curve at any particular crack length. The maximum and minimum values of K corresponding to this particular crack length could be determined by substituting the maximum and minimum values of the applied stress and the instantaneous crack length into equation (3.1). The magnitudes of $\dot{a}_N$ and the corresponding range of stress intensity factor ΔK are presented in Table 1 for 20 Hz test frequency. Figures 12, 13 and 14 show the correlation between log $\dot{a}_N$ and log ΔK for the different stress ratios (R) and frequencies used in the tests.

It should be mentioned that two or more specimens were used to establish the relation between $\dot{a}_N$ and ΔK at any particular frequency and ratio R (Table 1 and Figure 12) and that rest periods of up to 16 hours did not cause any significant change in the crack growth behaviour shown in Figure 11.

a) <u>$\dot{a}_N$-ΔK relation and the effect of loading ratio R</u>: By examining Figures 12, 13 and 14 it is evident that a unique relationship exists between $\dot{a}_N$ and ΔK at any particular frequency and stress ratio. On the other hand, at a constant frequency, R has an obvious effect on the cyclic crack velocity $\dot{a}_N$. At any constant ΔK an increase in R causes a similar increase in the cyclic crack velocity. However, it may be seen that when representing the experimental data in Figures 12, 13 and 14 by the Paris relation (equation (1.15)), an increase in R affects mainly the constant A, producing a decrease in the dynamic fatigue resistance, while the parameter m is hardly affected. For example, in tests conducted at 20 Hz the constant A has the values of 0.21×10^{-25}, 0.58×10^{-25}, 1.15×10^{-25} and 4.25×10^{-25} for R equals 0, 0.25, 0.4 and 0.6 respectively while m has the values of 5.83, 5.818, 5.822 and 5.811. The same effect has been found in the results obtained at the two other frequencies (see Table 2).

Another feature of the relation between log $\dot{a}_N$ and log ΔK is the tendency for deviation from the Paris power law at higher and

lower rates of cyclic crack growth. The tendency at the lower $\dot{a}_N$ seems to correspond to some apparent limiting level of ΔK for the particular level of loading. This tendency is similar to that previously observed in metals (e.g. Barsom, 1971). The tendency at the upper end results in lower values of crack growth per cycle than those predicted by the Paris law (i.e. lower values of the exponent m in equation (1.15)) which is in opposition to crack growth behaviour in metals. This behaviour of polymers may be attributed to the toughening influence of the shear lips that appear at high loads (Miller (1968) in his tests on steel, has found a decrease in the index m of equation (1.15) as a result of the increase in the effective material toughness (increase of K_{IC})). The reverse behaviour in high strength metals was attributed to K approaching K_c.

b) Frequency effect: A frequency effect may be revealed by comparing the rate of crack growth per cycle at the same ΔK and R for tests conducted at different frequencies. To facilitate the comparison, the relation between log $\dot{a}_N$ and log ΔK for tests conducted at R = 0 and different frequencies is shown in Figure 15 and it is evident that increasing the frequency affects both the parameters A and m (see Table 2) in the Paris relation in a way that produces an increase in the dynamic fatigue resistance. The same effect was found in data obtained at other R values. Figure 16 shows the relation between $\dot{a}_N$ and the frequency for various constant values of R and ΔK; it may be seen that, generally, increasing the frequency decreases $\dot{a}_N$ when data are compared at the same values of ΔK and R.

3.2.2 Dynamic fatigue crack propagation in N66 (4.4% water content) in both air (20°C and 50% RH) and distilled water

This study is the first of its kind, and aims at revealing the effect of the frequency and stress ratio on the dynamic fatigue crack propagation behaviour of N66 when it absorbs a certain amount of water. Water has a plasticising effect at room temperature and it lowers the modulus of the nylon as shown in Figure 9. Its effect on viscoelastic behaviour has been previously discussed in Chapter Two (see page 39).

Two environments were chosen for this study - water and air. Nylon may lose some of its water content in tests in air with 50% RH while it may gain some if tested in water. However, it has been found that the gain or loss of water during the test period is very small (less than 5% of the water content) and it is not expected to cause any significant variations in the properties of the conditioned nylon.

Tests were conducted at the same three frequencies as in the case of dry N66 and at each frequency, three values of R were chosen (0, 0.25, and 0.6). The typical relationship between crack growth and the number of cycles was similar to that shown in Figure 11 for dry nylon in air. The general trend of this relation was not affected by changing the environment (water or air), test frequency or stress ratio.

The relationship between log $\dot{a}_N$ and log ΔK is shown in Figures 17, 18 and 19. The first conclusion that may be drawn from these results is that testing N66 (4.4% water) either in water or air seems to have little or no effect on the relation between $\dot{a}_N$ and ΔK at a given loading frequency and stress ratio R. Therefore, it seems that the water environment has no particular effect on the plastic zone at the crack tip and its effect is only to change the mechanical and viscoelastic properties of N66 as a whole.

As in the case of dry nylon, a unique relationship exists between $\dot{a}_N$ and ΔK at any particular frequency and ratio R. Also there is a tendency for deviation from the Paris power law at low values of $\dot{a}_N$ similar to that in the case of metals. On the other hand, there are no deviations at high values of $\dot{a}_N$ up to the highest $\dot{a}_N$ obtained in these tests.

The effect of R in this test series is qualitatively similar to that on dry nylon in air. At constant test frequency increasing R affects the parameters A and m of equation (1.15) (Table 2) in a way that produces a decrease in the dynamic fatigue resistance. The same effect was observed in the results obtained at any of the three frequencies used in these tests as shown in Figures 17, 18 and 19.

The relationship between log $\dot{a}_N$ and log ΔK for tests conducted at R = 0.25 and different frequencies is shown in Figure 20. It is evident that an increase in the frequency causes a decrease in $\dot{a}_N$ when comparison is made at constant ΔK. The same frequency effect was found in data obtained at other R values. Figure 21 shows the relation between $\dot{a}_N$ and

the frequency at constant R and ΔK; the effect of frequency is similar to that which has been observed in the case of dry N66, i.e. increasing the frequency generally decreases $\dot{a}_N$ when comparison is made at constant ΔK and R.

3.2.3 Dynamic fatigue crack propagation in N66 (9.8% water content) in distilled water

The nylon in these tests was conditioned to the equilibrium point at 100% RH and tested in distilled water, the aim being to study the most drastic effects of water content and environment. Testing the saturated nylon in water did not cause any change in its water content during the test period.

Tests were carried out at the three abovementioned frequencies and at each frequency three stress ratios R were chosen (0, 0.25 and 0.45). It has been observed that increasing R to more than 0.5 has caused the crack to propagate in a rather ductile manner with a large plastic zone at its tip and sizeable shear lips; this caused a deviation from the assumed condition of plane strain at the crack tip. Moreover, the high values of the maximum applied stress in cases of $R > 0.5$ caused an increasing tendency for deviation from the assumed linear viscoelastic behaiiour of the material. Therefore, the highest chosen R was 0.45 to satisfy the assumptions required for comparing the results on a ΔK basis.

The typical relationship between crack length and number of cycles was similar to that shown in Figure 11 for dry nylon, and this pattern of behaviour did not change under any test condition. The relationship between log $\dot{a}_N$ and log ΔK for the three test frequencies is shown in Figures 22, 23 and 24.

At any particular frequency and R a unique relationship exists between $\dot{a}_N$ and ΔK as in the case of dry nylon tested in air. A tendency to a limiting value of ΔK at the low values of $\dot{a}_N$ was observed in tests at 20 and 5 Hz while this tendency was not observed in tests at 0.16 Hz even at the lowest measured $\dot{a}_N$.

The effect of R is qualitatively similar to that in the case of N66 (4.4% water content). The parameters A and m in the Paris relation (Table 2) were affected, due to increasing R, in a way that produced a decrease in the dynamic fatigue resistance; the same effect was observed

at all three test frequencies (Figures 22, 23 and 24). However, it may be inferred from the log $\dot{a}_N$ versus log ΔK curves for dry N66, 4.4% N66 and 9.8% N66 that at constant frequency, increasing the water content of the nylon makes it less sensitive to variations in the level of loading. The only exception is the case of 9.8% N66 tested at a frequency of 0.16 Hz where the vertical shifts due to increasing R (Figure 24) are somewhat greater than those in the case of 4.4% N66 (Figure 19).

Figure 25 shows the variations of $\dot{a}_N$ versus frequency at constant R and ΔK. The effect of frequency on the parameters A and m in the Paris relation is shown in Table 2. It may generally be concluded that the frequency has the same effect as in dry N66 and 4.4% N66, i.e. increasing the frequency causes a decrease in $\dot{a}_N$ at constant ΔK and R.

3.2.4 Dynamic fatigue crack propagation in N66 (4.4% H_2SO_4 of 10% concentration) in 10% H_2SO_4 environment

The effect of diluted sulphuric acid on crack propagation behaviour in N66 was investigated in this test series. The particular value of 4.4% of H_2SO_4 of 10% concentration in the nylon was chosen for the purpose of comparison with the case of N66 with 4.4% water content (i.e. zero concentration of H_2SO_4) and this may help to reveal any particular role of the acid in the crack growth process.

Tests were carried out at the same three chosen frequencies and at each frequency the chosen values of R were 0, 0.25 and 0.45. The increase of R to higher values was limited by the same reasons previously mentioned in the tests of N66 (9.8% water content). The accelerating behaviour of crack growth versus number of cycles once again was typically as shown in Figure 11 for dry nylon, and this type of behaviour did not change under any test condition.

Testing the conditioned nylon in a diluted sulphuric acid environment caused negligible variations (less than 3%) in its acid content. This small variation was not expected to cause any significant effect on the mechanical properties during the test period.

As in previous cases, the experimental data are represented as a relation between log $\dot{a}_N$ and log ΔK, Figures 26, 27 and 28. Once again a unique relationship exists between $\dot{a}_N$ and ΔK at any particular frequency and stress ratio. The deviation from the Paris relation and

the tendency to limiting values of ΔK at low values of $\dot{a}_N$ were observed in tests at all frequencies (Figures 26, 27 and 28). The effect of R on the relation between $\dot{a}_N$ and ΔK is generally the same as that previously observed in the other cases of conditioned and dry nylon.

The frequency effect on the parameters A and m of the Paris law is tabulated in Table 2 and discussed later. Figure 29 shows the relation between $\dot{a}_N$ and frequency at constant R and ΔK. The effect of frequency is qualitatively similar to that observed in other cases of conditioned and dry nylon 66.

3.2.5 Dynamic fatigue crack propagation in HDPE in air

Some attempts have been made to study dynamic crack propagation in LDPE in air as previously discussed in Section 2.3.2. Andrews and Walker (1971) related the cyclic crack growth rate to the fracture mechanics parameter τ (the rate of energy available from the stress field with respect to the crack length) with a relation similar to the Paris law (equation (2.13)). Hertzberg et al (1970,1973) suggested the validity of the Paris law for a wide range of plastics including LDPE. On the other hand, no such studies exist for HDPE. Thus, it has been decided to investigate the crack growth in this material in a series of tests similar to those on N66 to examine the correlation between the cyclic crack growth rate and the range of the stress intensity factor.

Tests were performed at frequencies of 0.16, 5 and 20 Hz, and at each frequency three stress ratios R were chosen (0, 0.3 and 0.6) except at 0.16 Hz where the maximum chosen R was limited to 0.45 for the same reasons as mentioned in Section 3.2.3. The relationship between crack length and the number of cycles was recorded for all the tested specimens and it was typically as shown in Figure 30. As in the case of N66 the experimental data are represented by a log-log plot of $\dot{a}_N$ against ΔK as shown in Figures 31, 32 and 33. It should be mentioned that more than one specimen was used to establish the relation between $\dot{a}_N$ and ΔK at any particular frequency and stress ratio.

Rest periods of up to 48 hours did not affect the crack growth behaviour shown in Figure 30.

The experimental data in Figures 31, 32 and 33 suggest the existence of a unique relationship between $\dot{a}_N$ and ΔK at any particular frequency and ratio R, moreover, the type of correlation between log $\dot{a}_N$ and log ΔK suggests the validity of the basic Paris law (equation (1.15)) for most of the crack growth history (region 2). The values of the parameters A and m in the Paris equation are tabulated in Table 2 for different frequencies and stress ratios.

The effect of increasing R on A and m is similar to that in the case of N66, i.e. at constant test frequency an increase in R affects A and m in a way that produces a decrease in the dynamic fatigue resistance. Such an effect was observed at all three test frequencies (Figures 31, 32 and 33). However, the experimental data of log $\dot{a}_N$ versus log ΔK show that the higher the frequency the less sensitive the material is to

variations in loading level.

Another feature of the log $\dot{a}_N$-log ΔK relation is the tendency for deviation from the Paris law at low rates of cyclic crack growth; this seems to indicate a limiting value of ΔK as in the case of metals and N66. No deviations were observed at the high values of $\dot{a}_N$ up to the highest $\dot{a}_N$ in these tests except in one single case. At 5 Hz and $R = 0.6$ (Figure 32), the deviation at the high $\dot{a}_N$ values was similar to that which has been observed in dry N66, and opposite to that observed in metals.

The effect of frequency on cyclic crack growth rate may be seen by comparing the data obtained at different frequencies and constant R. Figure 34 shows the relation between $\dot{a}_N$ and ΔK at different frequencies and at $R = 0.3$; it is obvious that $\dot{a}_N$ is influenced by changing the loading frequency in a manner similar to that in N66. The same frequency effect was found in the data obtained at other values of R. The effect of frequency on the parameters A and m of the Paris law is tabulated in Table 2 and the trend of variation of $\dot{a}_N$ with frequency at constant R and ΔK has been demonstrated in Figure 35. The general conclusion is that increasing the frequency has increased the dynamic fatigue resistance of the material causing a decrease in $\dot{a}_N$ when comparison is made at constant R and ΔK.

3.2.6 Dynamic fatigue crack propagation in HDPE in Adinol

This test series is aimed at revealing the effect of Adinol detergent on dynamic crack propagation in HDPE. Some data exist on the static fatigue crack propagation in this material in an Adinol environment (Marshall et al, 1972) and a unique relationship has been observed between the parameter K and the crack speed $\dot{a}$ (see page 46).

The HDPE/Adinol system is different in character from the nylon/water system. The main difference is that the bulk material does not absorb Adinol, so neither pre-soaking the polymer in Adinol before testing nor the immersion of the specimen in the environment during the test, has any effect on the mechanical properties of the material.

Tests were carried out at the three chosen frequencies and at each frequency different stress ratios R were chosen. There were some limitations in testing at high values of R, especially at low frequencies, because of the corresponding deviation from the plane strain conditions

previously noted. The relationship between crack length and the number of cycles was similar to that shown in Figure 30 for HDPE in air for all test conditions. The results are represented as log $\dot{a}_N$ versus log ΔK in Figures 36, 37 and 38.

To examine the effect of pre-soaking on the $\dot{a}_N$-ΔK relation, one of the specimens was pre-soaked in Adinol for 250 hours. The test results from this specimen are shown in Figure 36 and clearly indicate that pre-soaking up to 250 hours has no effect on the crack growth behaviour. This is expected since the bulk polymer does not absorb Adinol. Therefore, any variation in the behaviour of crack growth in Adinol from that which has been observed in tests in air should be restricted to the effect of Adinol at the crack tip region, and not to the variations of the mechanical properties of the bulk material. Also, rest periods of up to 48 hours did not affect the crack growth behaviour.

As in the case of HDPE in air a unique relationship exists between $\dot{a}_N$ and ΔK at any particular frequency and ratio R, and a tendency for deviation from the Paris law to give an apparent limiting ΔK at low values of $\dot{a}_N$ has been observed at all three test frequencies (Figures 36, 37 and 38). The tendency for high values of $\dot{a}_N$ to be overestimated by the Paris relation has only been observed at high values of R (Figures 36 and 37).

The influence of R in these tests is similar to that on HDPE in air, i.e. increasing R affects A and m of equation (1.15) (see Table 2) in a way that causes a decrease in the dynamic fatigue resistance. The effect of R was found to be the same at all test frequencies.

The frequency also has an effect similar to that on HDPE in air. Figure 39 shows the relation between $\dot{a}_N$ and the frequency at various constant ΔK and R. The general trend of the frequency effect on $\dot{a}_N$ is the same in all the previously considered cases of dry N66, conditioned N66 in different environments and HDPE in air and in Adinol.

3.3 Discussion of the Results

In the present section the experimental results will be discussed and an attempt will be made to give a rational physical explanation of the general trends of the material/environment behaviour which has been observed. A model for dynamic fatigue crack propagation will be proposed, discussed and compared with various other crack growth models.

3.3.1 An empirical model for dynamic fatigue crack growth

a) Proposed model: As shown in Section 3.2 a unique relationship exists between log $\dot{a}_N$ and log ΔK for different material/environment systems used in the experimental study. The Paris law (equation (1.15)) adequately described the experimental results of the middle region of growth, which represents most of the crack growth history, for tests conducted at constant frequency and ratio R. However, the simple relation of equation (1.15) was not capable of representing the results when tests were conducted at different levels of loading; this has been previously recognised by different investigators for a variety of materials and environments as discussed in Chapter One. Different approaches have been proposed to deal with the effect of loading level on the cyclic rate of crack growth (see Section 1.4). Some of the proposed models have been empirical equations for representing the experimental data (e.g. equation (1.21)) while others have thrown some light on the nature of the mechanism reponsible for cyclic crack growth in the material, such as the dependence of $\dot{a}_N$ on COD or the plastic zone size at the crack tip (equations (1.22) and (1.25)).

An attempt was made to represent the experimental results of the present work by the Arad formula (equation (1.25)). The equation failed to give a unique correlation between $\dot{a}_N$ and the parameter λ independent of R as shown in Figure 40 for the case of dry N66 at a frequency of 20 Hz, nor was success met in other cases. Therefore, it seemed necessary to propose a model which is capable of representing the test results, and has the generality with which to unify the different models and approaches proposed for application under specific conditions. Moreover, the proposed model should be physically rational to explain the nature of the propagation of dynamic fatigue cracks in polymers.

Following the above considerations it seems reasonable to assume the dependence of $\dot{a}_N$ on the condition at the crack tip represented by COD and/or the plastic zone size (r_p). Since both COD and r_p are proportional to K^2 (Chapter One), and the dependence could be some function of their range as well as their level, the following crack growth model is proposed:

$$\dot{a}_N = B\,(K_{max}^2 - K_{min}^2)^{\alpha}\,(K_m^2)^{\beta} \qquad (3.3)$$

the parameters B, α and β being functions of frequency, environment test condition and material properties.

Equation (3.3) may be written as:

$$\dot{a}_N = B\,(\psi)^L \qquad (3.4)$$

where $\psi = (K_{max}^2 - K_{min}^2)^{\alpha/L}\,(K_m^2)^{\beta/L}$ and $L = \alpha + \beta$.

Since $K_{max} = \frac{\Delta K}{(1-R)}$, $K_{min} = \frac{R\Delta K}{(1-R)}$ and $K_m = \frac{(1+R)\Delta K}{2\,(1-R)}$, the proposed model can also be expressed in the following form:

$$\dot{a}_N = B\,(2\,\Delta K)^{\alpha}\,(K_m)^{(\alpha+2\beta)} \qquad (3.5)$$

and

$$\dot{a}_N = B\,\psi^{\alpha+\beta} = B\left\{(\Delta K)^2\left[(0.25)^{\beta}\left(\frac{1+R}{1-R}\right)^{\alpha+2\beta}\right]^{\frac{1}{\alpha+\beta}}\right\}^{(\alpha+\beta)} \qquad (3.6)$$

b) <u>The applicability of the proposed model and comparison with other crack growth models</u>: The proposed model has the facility of being reduced to other models used in describing cyclic crack growth rates in viscoelastic materials, as well as the ability to be converted into a form of model based on COD or the cyclic crack tip plastic zone size in cases where they are considered as governing parameters of crack growth.

Mukherjee and Burns (1971) used an equation very similar to the model suggested by Erdogan (1968) (equation (1.20)); their equation was of the form:

$$\dot{a}_N = A\, f^L\, (\Delta K)^m\, (K_m)^n \qquad (3.7)$$

where f is the frequency and L, m, n and A are constants. They adequately described the experimental data of cyclic fatigue crack growth in PMMA by equation (3.7). Later, Mukherjee (1973) used K_{max} instead of K_m in equation (3.7) and showed that the new form could successfully describe experimental data from PMMA, as well as that from steel (see page 52). Equation (3.7) is similar to the proposed model when compared with equation (3.5); $B\, 2^{\alpha} = A\, f^L$ where both LHS and RHS are functions of the frequency and test conditions.

The proposed model by Arad et al (1972c) (equation (1.25)) may be expressed in the form:

$$\dot{a}_N = A\, (2\, \Delta K\, K_m)^m \qquad (3.8)$$

Both equations (3.8) and (1.25) may be considered as special forms of the proposed model, i.e. the case where the parameter β in the proposed model is equal to zero. However, Arad's model (equation (1.25)) has a shortcoming in its inability to represent the results in cases where the cyclic crack growth has a simple dependence on ΔK (equation (1.15)) irrespective of the value of R, as in the case of polycarbonate (Arad et al, 1972a). On the other hand, the Paris model (equation (1.15)) may be considered as a special form of the proposed model; i.e. the case where the parameter $\alpha = -2\beta$. In such a case, the proposed model (equation (3.6)) will be reduced to the form:

$$\dot{a}_N = B\, (2)^{\alpha}\, (\Delta K)^{\alpha} \qquad (3.9)$$

Equation (3.9) is similar to equation (1.15) where $A = B\, (2)^{\alpha}$.

The above discussion confirms the generality of the proposed model, which gives it the advantage of unifying the other models proposed for describing the cyclic crack growth in different viscoelastic materials by considering them as special cases of a more general model.

It has been pointed out by Liu (1965) that it is not the condition of stress and strain outside the plastic region that; causes fracture, but rather the environment within the plastic zone at the crack tip. Hence, it is reasonable to consider a criterion for cyclic crack growth based on the plastic zone size at the crack tip (McEvily et al, 1963) or the crack opening displacement (COD) (Hall and Shah, 1971) since both of them may be considered as a measure of the condition of the plastic zone.

The proposed model can easily be expressed in terms of crack opening displacement U since U is proportional to K^2 for small plastic zones (Appendix A, equation (A.18)). The form of dependence of $\dot{a}_N$ on COD can be derived from equation (3.3) and given as:

$$\dot{a}_N = B' (U_{max} - U_{min})^{\alpha} (U')^{\beta} \qquad (3.10)$$

where B is equal to $B'/(E \sigma_y/1 - \nu^2)^{\alpha+\beta}$ in plane strain conditions and $B'/(E \sigma_y)^{\alpha+\beta}$ in plane stress conditions, and B' may generally still be considered as depending on frequency, environment, test conditions and material properties. Equation (3.10) shows the dependence of $\dot{a}_N$ on the range of COD, as well as on some measure of the level of COD represented by $U' \alpha K_m^2$.

It has been shown by Johnson and Paris (1968) that the cyclic plastic zone size is proportional to $(\Delta K)^2$ irrespective of the value of R (see page 29). Therefore, if the governing factor of cyclic crack growth is the cyclic plastic zone size ($2r_{pc}$), this becomes a special case of the proposed model where $\alpha = -2\beta$, and equation (3.9) can easily be converted to the form:

$$\dot{a}_N = B'' (2r_{pc})^{\gamma} \qquad (3.11)$$

where $B = B''/(32\sqrt{2}\,\pi\,\sigma_y^2)^{\gamma}$ in plane strain conditions, $B = B''/(16\,\pi\,\sigma_y^2)^{\gamma}$ in plane stress conditions and $\gamma = \alpha/2$. B'' may generally still be considered as depending on frequency, environment, test conditions and materials properties.

It should be mentioned that for a small plastic zone where U is described by equation (A.18), and in the special case where $\alpha = -2\beta$, it is difficult to interpret the criterion as $\dot{a}_N$ governed by U (equation (3.10)) or by $2r_{pc}$ (equation (3.11)). In fact, either of the two parameters may be considered as the controlling parameter and the LHS of equation (3.10) is equal to the LHS of equation (3.11) multiplied by a constant. However, in the very special case where both B'' and B' are equal (i.e. when the uniaxial yield strain ε_y is rate independent and equal to $1/16\pi \simeq 2\%$ in the case of plane stress or equal to $1/32\sqrt{2}\,\pi\,(1-\nu^2) \simeq 1\%$ (for $\nu = \frac{1}{2}$) in the case of plane strain) both the criteria of COD and $2r_{pc}$ are identical and equation (3.10) is equivalent to equation (3.11). The condition of rate independence of yield strain is not unrealistic; Williams (1972) has shown that ε_y in PMMA is rate independent and approximately equal to 0.05.

Equations (3.10) and (3.11) show the ability of the model to describe the cyclic crack growth rate in rational physical terms representing the conditions prevailing at the crack tip. In particular, equation (3.11) is very useful in representing the cyclic rate of crack growth under conditions of extensive yielding at the crack tip where the stress intensity factor is no longer capable of characterising the failure process. Equation (3.10) is useful in conditions where an accurate estimation of COD can be made.

The proposed model can also be converted to represent cases where the cyclic rate of crack growth is governed by the strain energy release rate per unit area of crack extension in one cycle.

The energy available per cycle = $G_{max} - G_{min}$, and G may be related to K^2 as shown in equation (A.6) (see Appendix A) for a limited amount of plasticity at the crack tip. Thus, as a special case of the proposed model where the parameter $\beta = 0$, equation (3.3) may be rewritten as:

$$\dot{a}_N = B_1 (G_{max} - G_{min})^{\alpha} \qquad (3.12)$$

where $B = B_1/(E/(1 - \nu^2))^{\alpha}$ in plane strain and B_1/E^{α} in plane stress conditions.

The energy term G is equivalent to J (Rice contour integral) for a small plastic zone size (equation (A.19) in Appendix A). Thus, equation (3.12) may be written as:

$$\dot{a}_N = B_1 (J_{max} - J_{min}) \qquad (3.13)$$

For small plastic zone sizes both equations (3.12) and (3.13) are similar to equation (3.10) when $\beta = 0$ and the LHS of the equation is multiplied by $(\sigma_y)^{\alpha}$. Thus, either the energy parameter or the COD parameter may be considered as the controlling parameter of cyclic crack growth.

Relating the cyclic rate of crack growth to energy terms, as in equations (3.12) and (3.13) has the advantage of eliminating the restrictions put forward for describing the cyclic crack growth behaviour in K terms. The energy approach can be used in cases where the material exhibits non-linear behaviour, and there are no restrictions on the plastic zone size at the crack tip. This type of energy dependence has been shown in elastomers (Gent et al, 1964) and in LDPE (Andrews and Walker, 1971) (see page 49). However, under conditions where the cyclic crack growth rate is completely controlled by energy terms, B_1 may be considered as a function only of frequency, environment and material properties regardless of whether plane stress or plane strain conditions prevail.

Arad et al (1973b) have shown that their proposed model (equation (1.25)) can be converted to an energy formulation in the way described above to give equations similar to equation (3.12) and (3.13). They also showed that their model can be expressed in terms of COD to give an equation similar to equation (3.10) when the exponent β is equal to zero.

To summarise, the previous discussion reveals the wide range of applicability of the proposed model in conditions where the controlling parameter of cyclic crack growth behaviour is an energy term, crack opening displacement term or cyclic plastic zone size term. Any of these provides a rational physical dependence of the cyclic crack growth rate, and it has been shown by several investigators that these parameters can successfully describe the cyclic crack growth rate (Hall and Shah, 1971; McEvily et al, 1963; Andrews and Walker, 1971). In the case of a small plastic zone at the crack tip a correspondence has been shown between the three mentioned approaches. However, the COD approach (equation (3.10)) may be considered the most general one since the cyclic plastic zone size approach (equation (3.11)) is similar to equation (3.10) when $\alpha = -2\beta$ and the energy approach (equations (3.12) and (3.13)) is similar to equation (3.10) when $\beta = 0$. Moreover, the proposed model provides a unifying pattern for most of the previous cyclic fatigue laws used in viscoelastic materials and eliminates the apparent discrepancies between some laws (e.g. between the Arad model (equation (1.25)) and the Paris model (equation (1.15))) by considering them as special cases of a more general law.

c) The use of the proposed model in representing the experimental data: As previously shown all the experimental data were represented in log $\dot{a}_N$-log ΔK graphs (e.g. Figure 12). The Paris model adequately represented the results at constant frequency and stress ratio R for all tested cases. On the other hand, neither the Paris model (equation (1.15)) nor the Arad model (equation (1.25)), Figure 40 , was able to give a simple correlation of $\dot{a}_N$ independent of R.

The proposed model was used to represent the experimental results. If equation (3.4) is capable of representing the results, then it is expected that both B and $L = \alpha + \beta$ will not depend on loading conditions. According to equation (3.6) representing log $\dot{a}_N$ against log ΔK should give a straight line relation for each R value. The slope of the lines should be constant and equal to the exponent of ΔK (i.e. equal to $2(\alpha + \beta)$) regardless of the value of R, while the intersection with the log $\Delta K = 0$ axis would give

different values depending on the value of R. Examining the values of the exponent $2L$ (= m) for any particular material, environment and test frequency (Table 2) shows that $2L$ is indeed only very slightly affected by the variations of R and can reasonably be assumed constant. Direct examination of the graphs may suggest misleading values of the intercept A (e.g. it appears in Figure 17 that the value of A for R = 0.6 is greater than that for R = 0.25 while Table 2 shows a value of A two times greater for R = 0.25 than for R = 0.6). This is because the log ΔK = 0 axis is far away from the range of the experimental results, so that the intersection with this axis is very sensitive to any slight variations in the slope $2L$. If the intersection, denoted by C, is considered with an axis near the range of the results (e.g. log ΔK = 2.7 axis), this will be more realistic and will yield values which give a correct indication of the relative positions of the experimental results as shown in Table 2.

For the determination of the parameter ψ (equation (3.6)), both the exponents α and β should be known. The value of $2(\alpha + \beta)$ may be considered as equal to the mean value of the slopes of the lines representing the experimental results at different ratios R on the log $\dot{a}_N$-log ΔK graphs (e.g. Figure 12). The value of $(\alpha + 2\beta)$ may be determined as the mean value of the slopes of the lines representing the relation of log $\dot{a}_N$ against log $(1+R/1-R)$ at different constant ΔK as shown in Figure 41. Log $\dot{a}_N$ were determined at a particular ΔK for different values of R by considering the intersection of a vertical line at the particular log ΔK with the lines representing the experimental results on log $\dot{a}_N$-log ΔK graphs as shown in Figure 12. Both α and β can be determined by solving the two equations:

$$2(\alpha + \beta)_m = constant \qquad (3.14)$$

and

$$(\alpha + 2\beta)_m = constant \qquad (3.15)$$

The subscript m refers to the mean value of the quantity.

It should be mentioned that α, β and $2L$ are only considered in

all cases for the section of the experimental results which has been represented by the Paris equation.

Knowing the values of α, β and R for any particular material, environment and test frequency, the parameter ψ of equation (3.6) can be determined for any value of ΔK. The crack growth data for all the tests were replotted in terms of the parameter ψ for the medial part of the experimental results. The relationship between $\log \dot{a}_N$ and $\log \psi$ was established for different tests. Figures 42, 43 and 44 for dry N66 in air; Figures 45, 46 and 47 for N66 (4.4% water content) in both air and distilled water; Figures 48, 49 and 50 for N66 (saturated with 9.8% water content) in distilled water; Figures 51, 52 and 53 for N66 (4.4% H_2SO_4 of 10% concentration) in 10% concentrated H_2SO_4; Figures 54, 55 and 56 for HDPE in air and Figures 57, 58 and 59 for HDPE in Adinol. In all cases the figures demonstrate a linear relationship between $\log \dot{a}_N$ and $\log \psi$, and the parameter ψ successfully represented the results irrespective of the particular values of R and ΔK. This type of correlation has not been achieved by the Paris or Arad models, as previously shown. The coefficients α, β, L and B of equation (3.4) are tabulated in Table 3 for different materials and test conditions. The trends of the variations of these parameters will be discussed later after discussing the effects of frequency and environments.

3.3.2 The effect of frequency

It has been shown in Section 3.2 that, for any particular material and environment, when comparison is made at constant ΔK and R the effect of frequency was similar in all cases, i.e. increasing the frequency caused an increase in the dynamic fatigue resistance of the material, which resulted in a decrease in $\dot{a}_N$. According to the proposed model, the effect of frequency on $\dot{a}_N$ for any particular value of ψ may be revealed when comparing $\log \dot{a}_N$-$\log \psi$ curves for a particular material and environment at different frequencies. Such a comparison is shown in Figures 60 to 65 for the six material/environment conditions considered in the present study (experimental points have been omitted for the purpose of clarity). Generally speaking, the effect of frequency in all cases is similar and an increase in the frequency causes a decrease in $\dot{a}_N$ when comparison is made at a constant value of ψ. The effect of

frequency on the parameter L is shown in Table 3, and no special trend of variation can be identified in the case of N66. In the case of HDPE, tests in air showed a decrease in L with decreasing frequency, while tests in Adinol showed an increase in L with decreasing frequency.

a) Material responses due to change of frequency: It has been shown in Chapter Two (page 51) that predicting the effect of frequency variations is difficult since they produce several material responses which may have contradictory effects on the resistance of the material to dynamic fatigue crack propagation. These may be summarised as follows:

1. Effect of frequency on damping: As discussed in Chapter Two (pages 37 and 51) the loss modulus E'' and the loss tangent $tan\ \delta$ may increase or decrease with increasing frequency, depending on which side of the peak value on the f-E'' or f-$tan\ \delta$ curve the range of frequency is chosen. The magnitude of the dissipated energy (W_d) and the material damping will increase or decrease according to the variations in E'' (equation (2.3), page 37) and $tan\ \delta$. As discussed by Hertzberg et al (1973) (see page 51), viscoelastic materials which have high damping properties are more resistant to cyclic crack propagation than those with low damping properties. This is expected since increasing damping is associated with an increase of $tan\ \delta$ (the ratio of loss energy to recoverable energy) which implies that the available energy for crack propagation will be reduced and hence the cyclic crack growth rate will be decreased. Hence, the resistance to cyclic crack propagation will increase with increasing frequency if this is associated with an increase in the energy loss and vice versa.
2. Effect of frequency on the modulus E: Increasing the frequency causes an increase in the strain rate, which results in an increase in the modulus E of the material. On the other hand, increasing the frequency will increase the rate of energy dissipated per unit volume of the

material $\dot{W}_d$ (equation (2.4), page 37) - $\dot{W}_d$ also increases with increasing E'' - and the temperature rise depends on $\dot{W}_d$ (increases with increasing $\dot{W}_d$). Thus, an increase in frequency causes an increase in temperature rise which results in a decrease in the modulus of the material (Ferry, 1970). Hence, increasing the frequency has two contradictory effects on the modulus.

An increase in the modulus of the material will result in a decrease in the strain amplitude (and vice versa), when cycling under constant stress amplitude. Furthermore, the associated dynamic creep in one cycle will be an inverse reflection of modulus and frequency changes. Thus, if a failure criterion is associated with a certain amount of critical strain accumulation, the material resistance to cyclic crack propagation will vary according to frequency and modulus changes. Hertzberg et al (1973) (page 51) have shown that the higher the modulus, the more resistant the material is to cyclic crack propagation. Thus, from this point of view, the increase in frequency may have two contradictory effects on the rate of cyclic crack growth.

3. Effect of frequency on fracture toughness parameter K_c: The increase in K_c makes the material tougher and more resistant to cyclic crack propagation. Thus, if the frequency has an effect on K_c, it will have a corresponding effect on the material resistance to dynamic fatigue crack propagation. In a recent study by Marshall et al (1974) on PMMA, they showed that K_c is affected by changes in temperature and rate of strain and this is largely governed by β transitions, and they suggested that changes of K_c reflect changes in the modulus E. Similar studies do not exist for other polymeric materials; however, it is reasonable to assume that K_c in other polymers may be related to the molecular kinetics of the material and the type of associated relaxation processes. If changes in K_c reflect changes in E, the effect of frequency on K_c and the resistance to dynamic fatigue crack propagation will be

similar to that discussed above in (2).

4. Effect of frequency on the plastic zone at the crack tip: Increasing the frequency causes an increase in the strain rate which has the effect of increasing the yield stress σ_y (Williams, 1972) as well as influencing the modulus E as discussed above in (2). This results in a reduction of cyclic plastic zone size (equation (1.26)) and the crack opening displacement (equation (A.18) in Appendix A). If the cyclic crack growth rate is related to the plastic zone size (McEvily et al, 1963) or to COD (Hall and Shah, 1971) as in equations (3.10) and (3.12), then, suppressing the plastically deformed zone at the crack tip will increase the resistance to cyclic crack propagation. On the other hand, the temperature rise due to increasing the frequency will reduce both E and σ_y which has the contrary effect of decreasing the resistance to cyclic crack propagation.

b) Effect of frequency on the tested materials: It has been shown that in all the tested materials and environments, increasing the frequency increased the dynamic fatigue resistance of the material causing a decrease in $\dot{a}_N$. According to the above discussion, the temperature rise, as a result of increasing the frequency, has a significant detrimental effect on the material's resistance to cyclic crack propagation. However, the temperature rise has been found to be negligible in all the tests performed ($< 2^{o}C$) up to the highest frequency used, especially in tests in liquid environments where the generated heat was easily transferred to the environment because of the high heat transfer coefficient. Thus, the effect of temperature rise was practically eliminated in all tests and increasing the frequency is expected to increase the resistance to cyclic crack propagation due to the expected increase in E, σ_y and K_c as previously discussed in Section 3.3.2(a).

In the case of N66, tests at room temperature on the dry nylon at a frequency of 1 Hz lie to the LHS of the α peak according to Figure 4a (the dotted line). Since increasing the frequency qualitatively corresponds to shifting to higher temperatures (see

page 38), and shifts of the curve according to frequency variations are not expected to be large and may still be considered to the LHS of the α peak in the range of 0.16 to 20 Hz, a decrease may be expected in the value of *tan* δ with increasing frequency (neglecting the vertical shifts of the curve). This may result in a decrease in the dynamic fatigue resistance of the nylon. However, such an effect might have been masked by the effect of the increase in E, σ_y and K_c, and the final result is a slight increase in the cyclic fatigue resistance with increasing frequency as shown in Figure 60.

Increasing the water content in nylon to 4.4% (reasonably assumed equivalent to equilibrium near 70% RH) and 9.8% (equivalent to equilibrium at 100% RH) results in shifting the α peak to below room temperature (20°C) as shown in Figure 4b. The increase in test frequency, which roughly corresponds to shifts to higher temperatures, is expected to cause an increase in *tan* δ (Figure 4a) assuming the results in the whole frequency range to be to the RHS of the α peak in the *tan* δ-temperature curve. The expected result is an increase in damping and dynamic fatigue resistance, which agrees with the observed trend in the experimental data (Figures 61 and 62).

Unfortunately, at the present time, there is no available data on the effect of absorption of liquids other than water on the viscoelastic behaviour of nylon. Therefore, the effect of mechanical losses on the resistance to dynamic crack propagation is not possible to discuss for N66 containing 4.4% H_2SO_4 of 10% concentration.

In the case of HDPE tested at room temperature, it is expected that increasing the frequency would result in shifting the curve representing the loss modulus E'' (Figure 3) towards higher temperatures. Since the room temperature tests are expected to lie to the LHS of the α peak (Figure 3), increasing the frequency is more likely to decrease the losses (neglecting the vertical shifts in the E'' curve), resulting in a decrease in the dynamic fatigue resistance. This effect combined with the other previously discussed effects on σ_y, E and K_c have caused the observed increase in the dynamic fatigue resistance with increasing frequency (Figure 64). Testing HDPE in Adinol did not change the general trend observed in tests in air as shown in Figure 65; however, the material seems less sensitive to frequency variation.

It should be mentioned that the above discussion of the effect of frequency variations on the mechanical losses in both N66 and HDPE is over-simplified, and may only be considered as a pointer to trends of variations in the mechanical losses. Actual variations in damping according to frequency changes can only be revealed when the relationship between *tan* δ and frequency is established for the particular material and environment under test.

From the discussion of frequency effects on the resistance to cyclic crack propagation in both HDPE and N66, it may be concluded that the strain rate dependence of the mechanical properties (modulus, yield stress and fracture toughness) is the major factor causing variations in the resistance to cyclic crack propagation as a result of frequency changes in isothermal tests. On the other hand, variations in damping due to the effect of frequency changes on the mechanical losses seem to be of secondary importance.

3.3.3 Effect of environments

There is an important difference between liquid environmental tests of N66 and those of HDPE. In the case of N66 the liquid is absorbed by the material as a whole and this affects the bulk properties of the material, while for HDPE this is not so and the effect of the environment is restricted to the plastic zone at the crack tip.

a) Environmental effects on N66: In conditioned N66 of 4.4% water content tests were performed in distilled water and air. As previously shown (Section 3.2.2) changing the environment did not cause any significant change in the crack growth behaviour as long as no significant change occurred in the water content of the nylon. This suggests that the effect of a water environment is only to change the mechanical and viscoelastic properties of the material with no particular effect on the zone at the crack tip.

The effect of conditioning the nylon, at the three test frequencies, is shown in Figures 66, 67 and 68 on $\log \dot{\alpha}_N$-$\log \psi$ graphs. As previously discussed in Chapter Two (page 39), nylons absorb water and the absorbed water shifts the α, β and γ peaks to lower temperatures (Figure 4b). This lowers T_g and has a dramatic plasticising effect on nylon at room temperature, reducing the

modulus to lower values as shown in Figure 9. The explanation is that water acts to disrupt the interchain hydrogen bonds in the non-crystalline region in the nylon, thus allowing greater chain mobilities and rearrangements. In tests conducted at room temperature, shifting the α peak to below the ambient temperature may result in increasing the damping by increasing the loss tangent (Figure 4a), which causes an increase in dynamic fatigue resistance as discussed before (Section 3.3.2(a)). However, the effect of a large reduction in the modulus overcomes the effect of the increase in damping (Hertzberg et al, 1970) and the net result is a decrease in the dynamic fatigue resistance.

Figure 66, 67 and 68 show that at any of the test frequencies, when comparison is made at constant ψ parameter, increasing water content caused a decrease in cyclic fatigue crack resistance resulting in higher $\dot{a}_N$ values, except in a small range of results at frequencies of 5 and 20 Hz where the line representing the results of N66 (4.4% water content) overlaps the line representing the dry nylon at high values of $\dot{a}_N$. It may also be noticed that the value of the exponent L (equation (3.4)) decreases with increasing water content at any particular test frequency (see Table 3).

The case of conditioned nylon containing 4.4% of H_2SO_4 of 10% concentration is also shown in Figures 66, 67 and 68. The role of the sulphuric acid in the crack growth behaviour is revealed by comparing this case with that of N66 (4.4% water content), i.e. zero H_2SO_4 concentration. It is clear that the effect of sulphuric acid is a further reduction of the cyclic fatigue resistance when comparison is made at any of the test frequencies at constant ψ; furthermore, the value of the exponent L decreases at any test frequency (Table 3). Sulphuric acid attacks the interchain bonds faster than water causing greater plasticisation and leading to futher deterioration in the mechanical properties and higher rates of crack propagation.

Another aspect of plasticising nylon by water or diluted sulphuric acid is the effect on the threshold value of ΔK. Figure 69 shows the relationship between log $\dot{a}_N$ and log ΔK at f = 20 Hz and R = 0 for different conditioned nylons in different environments. A tendency to a limiting value of ΔK (= ΔK_{th}) is observed in all

cases. However, ΔK_{th} seems to be lowered by increasing the water content to 4.4%, while a further increase to 9.8% increases ΔK_{th} again. Nylon conditioned in diluted H_2SO_4 shows a tendency to ΔK_{th} comparable to that of dry nylon. The same trend of variation in ΔK_{th} has also been observed at other frequencies and values of R.

It seems that there is no simple connection between the threshold value of ΔK and the degree of plasticisation in N66. However, this point needs further experimental investigation and no general conclusion can be obtained at the present stage.

b) Environmental effects on HDPE: The effect of Adinol detergent on the crack growth behaviour in HDPE is shown in Figures 70, 71 and 72. At any of the test frequencies, when comparison is made at constant Ψ parameter, testing in Adinol increases the resistance to cyclic crack propagation resulting in a decrease in $\dot{a}_N$. This surprising result contradicts that which has been previously observed in static fatigue tests (Marshall et al, 1972). In static fatigue tests when comparison is made at a given K value, the crack speed in Adinol is higher than in air and an absorption mechanism at the crack tip has been suggested by Isaksen et al (1963) to explain stress cracking in Adinol (see Section 2.2.3(a)). However, the actual role of Adinol in the stress cracking process is not yet completely understood.

In the present dynamic fatigue test, the following points may be considered in discussing the effect of Adinol on cyclic crack growth resistance:

1. There is insufficient time, during the loading part of a loading cycle, for Adinol to be absorbed by the plastic zone and to exert internal pressure on the weakened structure (Section 2.2.3(a)), especially at high frequencies. This may explain why testing in Adinol does not increase the rate of cyclic crack propagation, but it does not give an explanation for the observed reduction in $\dot{a}_N$.
2. The local thermal softening in the plastic zone at the crack tip due to local temperature rise (Regel et al,1973)

(see page 49) may be reduced by the cooling effect of the Adinol liquid, causing an increase in the dynamic crack propagation resistance. This effect may provide an explanation for the observed reduction of $\dot{a}_N$ for tests in Adinol at high frequencies such as 20 Hz and probably 5 Hz, but it is not adequate to explain the results at low frequency (0.16 Hz).

Whilst the factors discussed above may be considered as contributory factors, they do not adequately explain the role of Adinol and the mechanism of dynamic failure in detergent environments.

Testing in Adinol has caused a decrease in the parameter B and an increase in the exponent L of equation (3.4) when their values are compared with those for tests in air, as shown in Table 3. The increase in L allows the cyclic crack growth rate in Adinol to approach its value in air at high values of $\dot{a}_N$ (Figures 70, 71 and 72).

The effect of Adinol on the threshold value of ΔK may be seen in Figure 73 which is for tests in both Adinol and air conducted at a frequency of 0.16 Hz and $R = 0$. It seems that testing in Adinol causes the crack to start propagating at a ΔK_{th} higher than its value in air. Once again this contradicts what has been previously observed in static fatigue tests (Marshall et al, 1972).

3.3.4 Trends of variation in α, β, L and B coefficients

The general COD approach of equation (3.10) may be considered the most reasonable representation of the crack growth behaviour in all materials and environments in the present work, since values of α and β (Table 3) did not give rise to any special case such as $\beta = 0$ or $\alpha = -2\beta$ as discussed in section 3.3.1(b). All the β values are negative, as shown in Table 3. Thus, according to equation (3.10), the COD level may be considered to have a retarding effect on the cyclic crack growth process; an increase in COD level at constant $\Delta(COD)$ causes a decrease in $\dot{a}_N$.

Representing the experimental results by the Arad model (equation (1.25)) as shown in Figure 40, which may be considered as an $\dot{a}_N$-$\Delta(COD)$ representation since λ is proportional to COD, shows that at constant λ

(constant $\Delta(COD)$) increasing R (i.e. increasing COD level) causes a decrease in $\dot{a}_N$. However, the negative ratio of β/α may be considered as a measure of the contribution of COD level in the dynamic crack propagation process. The lower the ratio, the greater the COD level expected to retard the crack growth process. If β/α is lowered to -0.5, i.e. $\alpha = -2\beta$, then the cyclic crack growth rate may be related to cyclic plastic zone size by equation (3.11), and hence to ΔK (in the case of a small plastic zone) irrespective of R, as in the Paris law (equation (1.15)). On the other hand, the higher the ratio β/α, the less contribution is expected from the COD level as a retarding factor, up to $\beta/\alpha = 0$. Positive values of β/α reverse the role played by the COD level and make it work as an accelerating factor in the crack propagation process. At $\beta/\alpha = 0$ (i.e. $\beta = 0$ and the COD level does not affect the process), the cyclic crack growth rate may be related to the strain energy release rate by equation (3.12) where direct correlation (in the case of a small plastic zone) with $(K_{max}^2 - K_{min}^2)$ is obtained, as in Arad's law (equation (1.25)).

Experimental results on some aluminium alloys (Johnson and Paris, 1968) and on polycarbonate tested above a certain loading rate (Arad et al, 1972a) have shown direct dependence of $\dot{a}_N$ on ΔK as in the Paris law. According to the above discussion a significant retardation effect of the COD level is expected giving $\beta/\alpha = -0.5$. On the other hand, experimental results on PMMA (Mukherjee and Burns, 1971) were described by equation (3.7) where m and n were found to be 2.13 and 2.39, respectively. According to the comparison with equation (3.5), β has a small value of 0.13 and $\alpha = 2.13$, thus, $\beta/\alpha = 0.061$. Considering the above discussion, a slight accelerating effect of the COD level is expected in the crack growth process. However, the nature of the experimental work can cause such slight variations and m may be considered as practically equal to n, i.e. $\beta/\alpha = 0$, and there is no contribution of the COD level in the process.

The values of β/α for the present work are tabulated in Table 3. A general trend may be observed when comparing dry nylon with that conditioned in water. At any of the three test frequencies there is a decrease in the ratio β/α as the water content increases, the only exception being the case of N66 (9.8% water content) at 0.16 Hz. The observed trend signifies that the more plasticised the nylon is by water,

the higher the retarding contribution of the COD level in the crack growth process.

Moreover, when comparing dry N66 (tested in air) with the softer material of HDPE (tested in air) at any particular frequency (Table 3), the ratio β/α is found to be lower for HDPE than for N66 which implies that the retarding contribution of COD level in the crack growth process is greater in HDPE than in N66.

From the results of Mukherjee and Burns (1971) on PMMA and the present results on HDPE and N66, it may be concluded that the more ductile the polymer, the higher the retarding contribution of the COD level in the crack growth process and vice versa. However, generalising this conclusion is avoided at the present stage since the available data are limited to the three polymers PMMA, N66 and HDPE and to two degrees of plasticisation of N66.

The effect of water content in N66 on the exponents L, α and β and the parameter B is shown in Table 3. A decrease in L and α and an increase in B are observed at each test frequency as the water content increases, while no specific trend of variation of the exponent β can be identified. The effect of H_2SO_4 on L, α, β and B at each test frequency may be distinguished by comparing the values of these parameters in N66 containing 4.4% of H_2SO_4 of 10% concentration and N66 with 4.4% water content. H_2SO_4 causes a decrease in L and α and an increase in B and β.

Testing HDPE in Adinol caused an increase in both L and α and a decrease in β and B when their values are compared with those of tests in air at any particular frequency.

No specific trend of variation can be identified in α, β, L and B in the case of N66 as a result of changing the test frequency. In the case of HDPE, tests in air showed a decrease in L and α and an increase in B and β with decreasing frequency, while tests in Adinol showed an increase in L and α as a result of frequency decrease.

The only possible comparison with the parameters reported in the literature is in the case of dry N66 since no previous work has been done on conditioned nylon or on HDPE. Hertzberg et al (1970) tested N66 in air at a frequency of 10 Hz and $R = 0$; estimated values of the parameters A and m ($= 2L$) in the Paris relation are 0.4165×10^{-21} and 4.155 respectively. Arad et al (1972c) tested dry nylon 66 and represented the results by the crack growth model of equation (1.25).

The values they found for the exponent m (equation (1.25)) were 3.1, 3.3 and 1.8 for frequency levels of 0.1, 5 and 20 Hz, respectively. Comparing equation (1.25) with (3.6) shows that the exponent m may be considered as equivalent to the exponent L ($= \alpha + \beta$) at least at $R = 0$. Values of L for dry N66 in the present work are 3.06, 3.13 and 2.91 for frequencies of 0.16, 5 and 20 Hz, respectively. There is reasonable agreement between m and L in Arad's results and the present results at low and medium frequencies, while at high frequency (20 Hz) L is higher than m by about 60%.

According to the above comparison, it should be mentioned that erroneous conclusions may be obtained when comparing the exponents of various sets of data obtained from various tests performed by different workers. Polymeric materials are sensitive to many factors that affect their basic material properties. Therefore, care must be taken to check any difference in the mechanical or viscoelastic properties of the materials due to the methods of production, subsequent treatments (e.g. annealing), handling the material, specimen preparations and conditions of testing.

CHAPTER FOUR

ENVIRONMENTAL DYNAMIC FATIGUE CRACK GROWTH IN LOW DENSITY POLYETHYLENE

It has been shown in the preceding chapter that an empirical modelling approach was useful and successful in studying environmental effects on the dynamic fatigue crack propagation process in nylon and HDPE. It was difficult to assess the correlation between dynamic and static fatigue crack growth in the case of nylon, since cracks did not propagate in either dry or conditioned nylons tested in distilled water or diluted sulphuric acid under sustained loads. In HDPE the cyclic crack growth rate in an adinol environment was less than that in air, while the reverse was true in static fatigue tests, and it seems that the environmental failure mechanism operating in dynamic fatigue differs from that in static fatigue. Therefore, it was decided to extend the study to the case of LDPE, where crack growth data under static loading conditions are available for two grades of this material in two different environments (Marshall et al, 1969b) in the form of K-da/dt graphs (see page 46).

An approach for correlating environmental dynamic and static fatigue crack growth is already available (Wei and Landes, 1969, see page 31) and it has been shown to be substantially correct for metals. However, the linear superposition of environmental static and inert environment dynamic fatigue contributions as in equation (1.27) suggests that the same mechanism of failure due to the aggressive environment is operating in both dynamic and static fatigue, and that the type of failure behaviour is the same in both inert and aggressive environments. These assumptions are not generally easy to justify in the case of polymers, since the role of the aggressive environment may be different in dynamic and static conditions, and the type of failure behaviour may differ between inert and aggressive environments. For example, PMMA fails in air (inert environment) by crack propagation in both dynamic (Arad et al, 1971) and static (Marshall et al, 1969a) conditions, whereas in alcoholic environments failure is by craze formation and growth in both static and dynamic conditions at low frequencies (Marshall et al, 1970; Marshall and Williams, 1973).

In this chapter an attempt will be made to apply the superposition model to dynamic fatigue crack growth in LDPE in a methanol environment, in the hope of finding a correlation between dynamic and static loading conditions.

Although LDPE is a soft plastic which behaves in a ductile manner in air, a complete transition to environmental brittle stress cracking occurred in alcohols (Marshall et al, 1969b) and the test results were independent of the specimen thickness, indicating a prevailing plane strain condition. Therefore, there is no difficulty in applying fracture mechanics concepts in such environmental tests.

4.1 Experimental Procedure

4.1.1 Material, environment and specimen preparation

The selected material was LDPE (ρ = 0.912) of MFI(7) and methanol was chosen as the testing environment; these are the same material and environment as have previously been used in static fatigue tests (Marshall et al, 1969b).

Tests were conducted on SEN specimens (Figure 5a) of 6 in. length x 2 in. width x $\frac{1}{8}$ in. thickness. Specimens were notched by forcing a razor blade into the specimen body (Figure 5b) to obtain an initial crack length of ($0.1\,w < a < 0.2\,w$). One row of $\frac{1}{4}$ in. diameter equally spaced holes was drilled on each end of the specimen for clamping purposes.

4.1.2 Testing procedure and testing programme

Perspex mini-tanks, as shown in Figure 8a, were used to maintain the methanol surrounding the specimen during the test period. The tanks were sealed to the specimen by silicone rubber sealer. Each end of the specimen was bolted to a pair of steel plates and pin loaded in the Instron Universal Testing Machine. A small capacity load cell was fitted in the machine since the required loads were small. Crack propagation was monitored by a travelling microscope.

It was intended in this programme to study the dynamic crack growth of LDPE in a methanol environment at constant frequency and stress ratio R. Thus, tests were conducted at a frequency of approximately 0.125 Hz corresponding to a crosshead speed of 0.2 in/min and the load varied from zero to maximum then to zero (i.e. R = 0) in a cyclic ramp form. Fracture mechanics was used in analysing the crack propagation data

obtained, as in the case of static fatigue tests and for the same reasons previously discussed in the case of HDPE and N66 (see page 62). The stress intensity factor K for the SEN specimen geometry used was calculated using equation (3.1), and crack growth measurements were therefore only considered in the range of $0.1 \leqslant a/w \leqslant 0.4$ to guarantee accuracy.

It should be mentioned that there was no discernible temperature rise during all tests, also that the fracture surfaces produced by cracks grown by cyclic loading were completely flat with no sign of ductility or shear lips which assume the cleavage mode of failure.

4.2 Results and Discussion

In all tests, the relationship between crack length, a, and the number of cycles, N, was typically as shown in Figure 74. From these crack growth data, plots of ΔK versus cyclic crack growth rate $\dot{a}_N$ were made for each specimen. $\dot{a}_N$ represents the slope of the a-N curve at any particular crack length and ΔK, corresponding to this particular crack length, was determined by substituting the values of the maximum applied stress and the instantaneous crack length in equation (3.1) (see page 63). Figure 75 shows the log $\dot{a}_N$-log ΔK relationship for different specimens. The results obtained demonstrate that, within the test limits, there is a unique relationship between ΔK and the cyclic crack speed (the scatter in results is of the order of ±5%, which is acceptable for this type of test). The results seem reasonably representable by a straight line for $\dot{a}_N > 3.2 \times 10^{-4}$ in/cycle; below this value a tendency towards limiting ΔK has been observed as in the case of N66 and HDPE (Chapter Three).

An auxiliary test was performed in air under the same test frequency and stress ratio R used in the methanol tests; the observed cyclic crack growth rate was much lower. Moreover, up to $\Delta K = 350$ lbf/in$^{3/2}$ there was no sign of crack propagation after 20,000 cycles, which indicates that this value is less than the ΔK threshold in air. Since the highest ΔK applied in the methanol tests was 200 lbf/in$^{3/2}$, which corresponded to the highest observed $\dot{a}_N$ ($= 1.45 \times 10^{-2}$ in/cycle), it is reasonable to assume that the cyclic crack growth up to the highest ΔK in methanol tests is only due to the environmental effect of methanol at the crack tip without any contribution from growth in an inert environment such as

air. It should be mentioned that methanol is a precipitant for polyethylene thus, it is not likely to be absorbed by the bulk material and it has no effect on the mechanical properties; its effect is only at the highly stressed crack tip zone.

Therefore, according to the above discussion, and since the type of failure is the same in both dynamic and static fatigue of this material (in both cases failure was by crack propagation), it was decided to examine the applicability of the linear superposition model proposed by Wei and Landes (1969) to the present test results.

4.2.1 Wei and Landes model

Reference has been made to the linear superpositon model by Wei and Landes in Chapter One (see page 31); now the graphical solution of equation (1.27) will be considered in more detail.

The environmental contribution in the environmental dynamic fatigue process (i.e. $(da/dN)_{environment}$ in equation (1.27)) was assumed by Wei and Landes to be expressed in the form:

$$\left(\frac{da}{dN}\right)_{enviroment} = \int_{\tau} \frac{da}{dt}\, dt \qquad (4.1)$$

where τ is the period of one cycle = $1/f$. The crack growth rate in the integral is a function of the stress intensity factor, which is in turn a function of time, i.e.

$$\frac{da}{dt} = \frac{da}{dt}\,[K(t)] \qquad (4.2)$$

A schematic diagram which illustrates the graphical method of evaluating $(da/dN)_{corrosion\ fatigue}$ as the sum of two contributions (equation (1.27)) is shown in Figure 76. In the present study, the contribution of dynamic fatigue in an inert environment may be considered as equal to zero, and equation (1.27) is reduced to:

$$\left(\frac{da}{dN}\right)_{corrosion\ fatigue} = \left(\frac{da}{dN}\right)_{environment} \qquad (4.3)$$

where $\left(\frac{da}{dN}\right)_{environment} = \int_{\tau} \frac{da}{dt}\,[K(t)]\,dt$ (from equations (4.1) and (4.2)).

4.2.2 The applicability of the superposition model to the present results

Static fatigue results of LDPE of MFI(7) in a methanol environment were previously obtained by Marshall et al (1969b); Figure 77 shows the relationship between K and log da/dt. To check any discrepancy in the behaviour due to changes in the material properties (e.g. changes due to the ageing effect), a static fatigue test was performed and the results obtained are shown in Figure 77. The results are within the scatter band previously determined by Marshall et al (1969b), but tend to fall within its lower half.

The graphical method schematically shown in Figure 76 was applied, considering the middle curve in Figure 77. The curve according to equation (4.3) is shown in Figure 75. The first glance at Figure 75 suggests that the linear superposition method is not applicable to LDPE; however, this might not be the case if the rate dependence of K at which the crack starts to propagate is considered.

It has been shown by Marshall et al (1969b) that in monotonic constant strain rate tests on notched specimens of LDPE of MFI(7) in a methanol environment, the value of K at which the crack starts to propagate is strain rate dependent, and the higher the strain rate the higher the value of K_{th} will be. The relation between K_{th} and the strain rate can be deduced from Marshall's results; Figure 78 shows the curve representing this relation.

In the present study tests were conducted at a machine crosshead speed of 0.2 in/min and the effective length of the specimen between the clamps (Figure 8b) ℓ' was equal to 4.5 in. The strain rate in the cyclic loading was thus equal to 0.0445 min^{-1} which corresponds to K_{th} = 133 $lbf/in^{3/2}$ as shown in Figure 78. Therefore, it is expected in the present cyclic fatigue tests, that the crack will not start to

propagate unless the value of K exceeds K_{th} = 133 lbf/in$^{3/2}$. The graphical method schematically shown in Figure 76 was applied considering the upper, middle and lower curves in Figure 77 and assuming there is no crack growth below K = 133 lbf/in$^{3/2}$. The resulting three curves and the points representing the experimental results are shown in Figure 79. Most of the experimental points fall within the lower half of the scatter band. Considering that this tendency has been observed in the static fatigue results (Figure 77), it may be concluded that the superposition model suggested by Wei and Landes for metals is applicable in the case of LDPE in methanol when the rate sensitivity of the stress intensity factor is considered. However, LDPE may be considered as a special case in which the contribution of pure dynamic fatigue (inert environmental dynamic fatigue) is negligible compared to the environmental part.

CHAPTER FIVE

ENVIRONMENTAL ROTATING BENDING TEST OF PMMA AND HDPE

The cheapest and most widely used simple method for comparing fatigue lives of different materials is the Wöhler type rotating bending fatigue test. This test is used in both commercial and research fields to establish the relation between the applied loading stress and the number of cycles to failure for unnotched specimens. The results are usually presented in the form of S-N curves. The use of unnotched specimens makes the results difficult to analyse or interpret because of the unknown stresses induced by the inherent flaws in the material. It would therefore appear more logical to induce initial cracks or notches of predetermined size, rather than measuring the behaviour of undetermined flaws.

As previously shown in Chapter Two, the concepts of fracture mechanics, which are based on the assumption of flawed material, can be used in studying crack behaviour in different polymeric materials. The simplest application of fracture mechanics in rotating bending tests of polymers was that by Constable et al (1970b). They showed that, for PVC sharp-notched specimens, in the rotating bending test, representing the results in a K_o-N curve rather than the conventional S-N curve would give direct correlation between K_o and N independent of notch size, since K_o effectively includes notch size representation.

In the present study an attempt will be made to reveal the environmental effect on two thermoplastics using the simple Wöhler rotating bending test. Notched specimens are used in the hope of finding a correlation between the initial stress intensity factor K_o and the number of cycles to failure, similar to that observed by Constable et al in the case of PVC in air.

5.1 Experimental Procedure

5.1.1 Materials, environments and specimen preparation

The two selected thermoplastics were HDPE and PMMA. High density polyethylene was supplied as ½ in diameter rods of BP T2000 Rigidex with density ρ = 0.954 and MFI = 0.2, and PMMA was supplied by ICI as rods of

½ in diameter machined from cast sheets.

HDPE was tested in both air and Adinol environments; PMMA was tested in air and methanol. These combinations of polymer and environment were chosen because much of the work done on the environmental effects on the dynamic and/or static fatigue behaviour of thermoplastics has been conducted on one or more of these combinations (e.g. Marshall et al, 1969a, 1970, 1972; Marshall and Williams, 1973 and the work presented in Chapter Three).

Tests were conducted on circular cross-section notched specimens as shown in Fibure 80a. The induced notches should be as sharp as possible to satisfy the requirements of fracture mechanics principles. In the case of HDPE, notches were induced by forcing a razor blade into the specimen body. The notching process was performed on a lathe. The specimen was inserted into the chuck and allowed to rotate slowly while the razor, which was attached in a special attachment fixed on the lathe crosshead, was forced into the specimen to the required depth. The blade was free to slide in the vertical direction perpendicular to the horizontal axis of the specimen as shown in Figure 80b. This technique of notching was successful in HDPE specimens, but in the case of PMMA the razor induced uncontrollable cracks ahead of its tip. PMMA specimens were therefore machine notched with a dead sharp 60° lathe tool to give a notch root radius of approximately 0.0005 in.

5.1.2 Testing apparatus and procedure

Tests were performed on four rotating bending rigs specially designed for testing plastics. As shown in Figure 81, each rig consists of an electric motor coupled to a speed variator to give a range of speeds between 450 rpm and 4500 rpm. The thicker end of the specimen was inserted into a chuck driven by the motor, while the other end was fitted with a bearing from which the end of a lever arm was hung. This design allowed the applied load P to be increased by a factor of $1\frac{1}{2}$-2, depending on the chosen loading point, and also resulted in a more stable system, overcoming vibrational problems especially at small loads and high frequencies (Constable et al, 1970b). When failure occurs the lever arm falls on the cut-out switch and switches off the motor. For tests conducted at a much lower speed (2 rpm), an additional set of reduction gears was introduced into the system.

In tests conducted in liquid environments, the specimen was enclosed in the environment by a sleeve made of a soft flexible material which carries negligible stresses with respect to the tested specimen. A thin rubber or polyethylene tube of 1/16 in thickness was fitted around the thicker end of the specimen as shown in Figure 80a and the other end of the tube was sealed off by a rubber plug. The space between the tube and the thin part of the specimen was filled with the liquid environment. The effect of the sleeving on fatigue life was tested using specimens of HDPE, which is above its T_g at room temperature and much softer than PMMA. Specimens with and without sleeves and having the same notch depth were tested at constant frequency in air. The results obtained (Figure 84) show that the effect of the sleeves on specimen lives was negligible. However, even any minor effect could be eliminated by substituting rubber sleeves, which are more flexible, for those made of polyethylene.

5.1.3 Testing programme

It was intended in this programme to study the effect of environment on the dynamic fatigue life using the simple rotating bending fatigue test, and to check the correlation between the initial stress intensity factor and the number of cycles to failure for specimens with various notch depths.

Tests on HDPE were conducted at a speed of 2000 rpm in both air ($20^{\circ}C$, 50% RH) and Adinol. Four notch depths varying from 0.01 to 0.09 in, were used for tests in Adinol, while in air tests, three notch depths were chosen varying from 0.02 to 0.09 in.

Tests on PMMA were conducted at a speed of 2000 rpm in both air ($20^{\circ}C$, 50% RH) and methanol. A notch depth of 0.04 in was used for tests in air, while three notch depths varying from 0.01 to 0.09 in were used for tests in methanol. Another batch of PMMA specimens of notch depth 0.04 in were tested at a speed of 500 rpm in methanol and at a speed of 2 rpm in both air and methanol.

Fracture mechanics was used in analysing and correlating the results; this was encouraged by the successful application of its concepts in crack and craze studies in different thermoplastics.

The stress intensity factor, K, for the round notched bars in bending used in the present study, was calculated using the approximate

method suggested by Williams and Isherwood (1968). The solution was given by Williams and Constable (1969) as:

$$K = F\,\sigma\left\{\pi\left(\frac{D-d}{2}\right)\right\}^{\frac{1}{2}} = \left((3\sigma_m + \sigma_n)/4\right)\left\{\pi\,(D-d)/2\right\}^{\frac{1}{2}} \qquad (5.1)$$

where F is the finite effects correction factor (F is unity for the infinite case), σ is the applied gross stress at the cracked section, D is the bar diameter, d is the diameter at the notched section, σ_m is the mean stress over the crack area and σ_n is the nominal stress at the crack tip ignoring stress concentration effects.

In the case of a round bar in bending, the maximum gross section stress $\sigma = 32\,M/\pi\,D^3$, where M is the bending moment and σ_m is given as:

$$\sigma_m = \frac{\sigma}{2}\left[\frac{D}{d} + 1\right]/D/d \qquad (5.2)$$

and

$$\sigma_n = \sigma\,(D/d)^3 \qquad (5.3)$$

From equations (5.1), (5.2) and (5.3):

$$K = \left\{\frac{1}{4}\left[\frac{3}{2}\left(\frac{D/d + 1}{D/d}\right)\right] + \left(\frac{D}{d}\right)^3\right\}\sigma\,(\pi\,a)^{\frac{1}{2}} \qquad (5.4)$$

where a is the notch depth ($= (D-d/2)$).

The simple approximate solution of K as given by equation (5.4) was examined by measuring the fracture stress intensity factor K_{IC} in PMMA round notched bars in bending and correcting the results by considering the finite effects as in equation (5.4) (Williams and Constable, 1969). The solution gave constant values of K_{IC} for different D/d ratios, which agreed with K_{IC} obtained by other solutions for other loading systems and K_{IC} obtained by equation (5.4), indicating the validity of the approximate solution in bending. Equation (5.4) may be used for D/d ratios up to 2.

5.2 Results and Discussion

5.2.1 HDPE in air and in Adinol environments

The results are represented as K_o versus log N (number of cycles to failure). Figure 82 shows the relation between K_o and log N for HDPE specimens of different notch dpeths tested in Adinol at a speed of 2000 rpm. Figure 83 shows the effect of notch depth on the K_o versus log N relation at a speed of 2000 rpm in air (20°C, 50% RH), while Figure 84 shows the effect of sleeving in polyethylene tubes and blowing air at the cracked section.

It should be mentioned that in all cases represented in Figures 82, 83 and 84, failures were entirely by true dynamic fatigue crack propagation without any indication of thermal softening. This has been confirmed by the study of the fatigue crack surfaces, Figure 85a. However, in tests in Adinol some specimens with notch depths of 0.01 in failed by cyclic thermal softening rather than crack propagation as shown in Figure 85b (these results are not included in Figure 82). This type of failure occurred due to temperature rise during the test (see Section 2.3.1) because of the increase in the rate of dissipated energy per unit volume as the cyclic stress increased (equation (2.4)). The thermal failure occurred at a distance of about 0.15 in from the change in section and not at the notched section as shown in Figure 85b. This implies that the area of maximum temperature did not coincide with the area of maximum stress, as previously observed by Constable et al (1970a).

The results shown in Figure 84 indicate that polyethylene sleeves have no effect on the specimen life. On the other hand, blowing air at the notched section has the effect of increasing specimen life, as previously observed by Regel et al (1973) in their tests on nylon 6 and polyvinylalcohol and attributed to the local rise in temperature at the crack tip (see page 49).

a) The effect of notch depth on the results of HDPE: As shown in Figures 82 and 83, increasing the notch depth causes an increase in the number of cycles to failure in both air and Adinol environments when comparison is made at a constant value of K_o. These results contradict the previous findings of Constable et al (1970b); they found that K_o-log N relation was independent of notch size in PVC

thermoplastic. Representing the results on the basis of the maximum gross stress (σ) or the nominal stress at the crack tip (σ_n) did not eliminate the notch depth effect and the number of cycles to failure still depends on the initial notch size as shown in Figure 86 for HDPE in Adinol.

It was therefore decided to conduct a theoretical analysis based on the existence of a unique relationship between $\dot{a}_N$ and ΔK at constant frequency and stress ratio (as shown in Chapter Three) to reveal the effect of notch size on fatigue life.

i. Analytical prediction of notch depth effect on fatigue life of HDPE: In this analysis, the dynamic fatigue crack propagation will be considered for the case of tensile SEN specimens (previously studied in Chapter Three) tested at a frequency of 20 Hz and with $R = 0$ in both Adinol and air. As shown in Chapter Three (sections 3.2.5 and 3.2.6), the correlation between $\dot{a}_N$ and ΔK may be represented by the Paris power law (equation (1.15)). Equation (1.15), in the case of $R = 0$, may be written in the integral form:

$$\int_0^N dN = \int_{a_o}^{a} A^{-1} \, (K_{max})^{-m} \, da \qquad (5.5)$$

i.e.
$$N = \int_{(a_o/w)}^{(a/w)} w \, A^{-1} \, (K_{max})^{-m} \, d(\frac{a}{w}) \qquad (5.6)$$

where a_o is the initial crack length, a is the current crack length and w is the specimen width.

For SEN specimens K is given by equation (3.1), thus equation (5.6) may be expressed as:

$$N = \int_{(a_o/w)}^{(a/w)} w^{1-\frac{m}{2}} A^{-1} \, (\frac{a}{w})^{-\frac{m}{2}} \, \sigma^{-m} \, [1.99 - 0.41 \, (\frac{a}{w}) + 18.70 \, (\frac{a}{w})^2$$

$$- 38.48 \, (\frac{a}{w})^3 + 53.85 \, (\frac{a}{w})^4]^{-m} d(\frac{a}{w}) \qquad (5.7)$$

For the case of HDPE in air, the parameters A and m are given as 0.37239×10^{-15} and 3.123 respectively (Table 2). As shown in Figure 31, the power law representation holds for most of the growth history (K in the range of (630-2000 lbf/in$^{3/2}$). Below K = 630 lbf/in$^{3/2}$ the value of $\dot{a}_N$ drops rapidly as K decreases, indicating some threshold value of K. For the case of HDPE in Adinol, A and m have the values of 0.189376×10^{-18} and 4.067 respectively as tabulated in Table 2. Figure 36 shows that the power relationship holds from K = 575 to 2000 lbf/in$^{3/2}$; below K = 575, $\dot{a}_N$ again decreases rapidly as K approaches some threshold value.

However, it is reasonable to assume that the initiation period (observed in SEN tests) is dependent only on the stress condition at the crack tip, material and environmental properties and testing conditions such as frequency, stress ratio (R), ambient temperature, cyclic wave form, etc., while it is independent of geometric factors such as crack length and type of loading. For tests conducted at the same conditions for a particular material/environment combination the initiation period would be expected to depend only on the stress condition at the crack tip. Since the stress distribution at a sharp crack tip is the same for all cases, and only the magnitude varies by the scalar parameter K, the initiation period would be expected to be the same for tests conducted at the same K_o and different notch depths, providing that the initial notches are dead sharp with the same tip geometry. The total fatigue life N_t may be represented by:

$$N_t = N_i \text{ (initiation)} + N_p \text{ (propagation)} \qquad (5.8)$$

where N_i is independent of initial notch depth for a particular material/environment combination at the same test conditions and the same K_o value and N_p may be

determined by an equation similar to (5.7). The upper limit of integration in equation (5.7) corresponds to a relatively high value of $\dot{a}_N$ where a negligible number of cycles is still required to complete failure. In the case considered, in both air and Adinol environments, the upper limit of integration was determined by K reaching 2000 lbf/in$^{3/2}$.

A computer program was used to integrate equation (5.7). The computation was carried out for four values of K_o and five of a_o in each environment, for specimens of width w = 5 in. The computer program was stopped when K reached 2000 lbf/in$^{3/2}$ or when a/w exceeded 0.65, as the formula for calculating K loses its accuracy for large values of a/w, and even for a/w > 0.55 the degree of accuracy of equation (3.1) falls rapidly. The results are tabulated in Tables 4 and 5 and shown in Figures 87 and 88. As may be seen, there is an obvious notch depth effect on the value of N_p at any particular value of K_o. An increase in the notch depth causes an increase in N_p and there appears to be an optimum notch depth effect since N_p is less for a_o/w = 0.35 than for a_o/w = 0.225 when comparison is made at any constant K_o (the dotted curves in Figures 87 and 88). However, the results for a_o/w = 0.35 may not be accurate enough to rely upon since the final a/w exceeded 0.55 at all chosen K_o values except at the highest ones (Tables 4 and 5). The same pattern of behaviour would be expected when representing the results as K_o versus log N_t curves, since at any given K_o the same value of N_i will be added to the different values of N_p.

Similar analysis for the case of rotating bending tests, is extremely difficult, since it necessitates knowing crack propagation behaviour, which requires crack growth measurements in the radial direction during the test. Thus, the above results, for tensile SEN specimens, are not directly applicable to the rotating bending case. However, the principles and assumptions are the same for both cases. Therefore, it is believed that the analysis

for the rotating bending case would not yield very different results.

The experimental results of the rotating bending test (Figures 82 and 83) showed a continuous increase in N with increasing a_o up to the highest chosen notch depth, without the reversing behaviour shown in the predicted results for SEN specimens. This might be attributed to the temperature effect discussed below. However, more data are needed at different notch depths (say 0.055, 0.065 and 0.075) to confirm the presence or absence of an optimum value of a_o.

ii. The effect of temperature rise: Another factor that might help in explaining the observed notch depth effect on the results is the rate of energy dissipated per unit volume of the material $\dot{W}_d$ (equation (2.4)). For tests of constant stress amplitude conducted at the same frequency and the same initial stress intensity factor, a decrease in the notch depth necessitates an increase in the stress σ to obtain the same value of K_o (equation (5.4)). Thus, at constant K_o, decreasing the initial notch depth causes an increase in $\dot{W}_d$ (equation (2.4)) which results in a greater temperature rise during the test. The effect of temperature rise is to further reduce the material dynamic fatigue resistance (the effect of temperature rise was included in the discussion of the frequency effect - Section 3.3.2). This may explain the observed reduction in life when the notch depth was decreased at the same K_o (Figures 82 and 83).

In summary, the apparent notch depth effect in the experimental results may be explained to some extent by the analytical results of SEN specimens, and by the effect of the increase in temperature as the initial notch becomes shorter in tests conducted at the same K_o.

b) The effect of Adinol on the results of HDPE: At any particular notch depth and K_o, testing in Adinol increases the fatigue life (as

shown in Figures 84 and 89). This effect is definitely not due to lack of adequate controls, since sleeving has no effect on the results and even cooling by blowing air at the notched section could not cause the observed increase in life, Figure 84. This striking feature of the results contradicts that which has previously been observed in static fatigue (Marshall et al, 1972) and agrees with the observed behaviour in dynamic tensile fatigue of SEN specimens (see Section 3.3.3(b)) and may be discussed in the same way. However, no definitive conclusion can be reached about the role of Adinol in dynamic fatigue of HDPE, which is certainly different from its role in static fatigue of the same material. It seems, hypothetically, that Adinol, in dynamic fatigue, has the effect of reducing the friction between the molecules in the plastic zone at the crack tip - lubricational effect - and increases the fatigue life. This hypothesis is certainly not proven but it is at least feasible in the light of the observed results.

5.2.2 PMMA in air and in methanol environments

The results of PMMA in both air and methanol at a speed of 2000 rpm are shown in Figure 90 in K_o versus log N representation, while the results at a speed of 2 rpm are shown in Figure 91. The effect of test speed on the results of PMMA in methanol is shown in Figure 92 for two speeds (2000 and 500 rpm) and the notch depth effect is shown in Figure 93.

All failures were caused by crack propagation without any indication of thermal softening, as confirmed by the striations appearing on the fracture surfaces.

a) The effect of methanol environment: It has been shown by Marshall et al (1970) and Marshall and Williams (1973) (see pages 40 and 54) that the failure of PMMA in methanol in both static and dynamic (low frequency) conditions is by craze formation and growth, then subsequent void coalescence within the craze itself; while failure in air, in both static and dynamic conditions, is by crack propagation (Marshall et al, 1969a; Arad et al, 1971 - see pages 44 and 52). However, in the present study, testing PMMA in methanol at high frequency results in a mixed pattern of

continuous craze growth and crack growth by void coalescence within the craze up to the crticical point where fast crack propagation occurs.

For tests in methanol at a speed of 2000 rpm, the region of fast crack propagation and the region of craze/crack growth are shown in Figure 94a, while Figure 94b shows that voids coalesce in the craze in cyclic steps as indicated by the striations. In air tests at 2000 rpm, the two regions of fast crack propagation and fatigue crack growth may be seen in Figure 94c. Figure 94d shows that the fatigue crack grows in cyclic steps in air. The region of fast crack growth is similar in both air and methanol environments, while the region of fatigue growth is different. In air the fatigue crack grows directly in cyclic steps, while in methanol first the craze grows, then complete separation occurs by void coalescence starting at different points in the craze, in a stepwise manner as shown in Figure 94b.

Comparing the results of air and methanol at a speed of 2000 rpm (Figure 90) shows that at high values of K_o testing in methanol increases the fatigue life, while at low values of K_o (below 540 lbf/in$^{3/2}$) testing in methanol decreases the fatigue life. Results show a fatigue limit in air at about 450 lbf/in$^{3/2}$, and in methanol at 275 lbf/in$^{3/2}$. At high values of K_o, methanol plasticises the material at the crack tip, then craze growth causes stress relaxation in the crazed part. Failure by void coalescence within the relaxed craze takes more time than direct fatigue crack growth, which results in K_c being reached after a few cycles and the occurrence of fast crack propagation as in air tests. At low values of K_o, methanol crazes are still able to initiate and propagate while cracks in air are almost stationary (Marshall et al, 1970). Under dynamic conditions, the material reaches its fatigue limit in air at K_o = 450 lbf/in$^{3/2}$ while methanol induced crazes are still able to initiate and propagate below this value, which leads to subsequent void coalescence starting in the weak ligaments of the craze and failure of the crazed section. Therefore, the fatigue limit in methanol occurs at a value lower than that in air.

The change of the behaviour of PMMA due to testing in an aggressive environment (methanol) as shown in Figure 90 is similar

to that previously observed in metals (e.g. carbon steel in air and in water (McAdam, 1926)). The observed behaviour in metals was attributed to the cooling effect of the liquid environment which increases the life in low cycle fatigue, while the corrosive effect of the environment takes place in high cyclic fatigue resulting in decreased life.

The effect of methanol at the speed of 2 rpm as shown in Figure 91 is to increase the fatigue life for specimens tested at K_o > 500 lbf/in$^{3/2}$ which agrees with the results obtained at the speed of 2000 rpm and may be attributed to the same causes. However, more results are still needed at low values of K_o in both air and methanol environments to clarify the effect of methanol on the fatigue limit at low speeds.

b) Effect of test speed and notch depth on PMMA in methanol: The general aspects of polymeric material responses to frequency changes have been previously discussed in Chapter Three (Section 3.3.2). As shown in Figure 92, when comparison is made at constant K_o, increasing the frequency from 500 to 2000 rpm caused an increase in the fatigue life and fatigue limit. Similar trends due to frequency changes have been observed in PMMA tested in air* when the frequency was increased from 1500 to 3000 rpm. These results indicate that increasing the frequency within the range used in tests causes an increase in the dynamic fatigue resistance of the material in both air and methanol environments. This means that there is no significant temperature rise, which would cause deterioration of the dynamic fatigue resistance, due to increasing frequency.

The initial notch depth effect on specimen life is similar to that previously discussed in the case of HDPE; as shown in Figure 93 there is a tendency for the fatigue life to increase as a result of increasing the notch depth in tests conducted at the same K_o. However, no analytical treatment (as in the case of HDPE) will be considered since there are no available data on the relation between cyclic crack/craze speed and the applied stress intensity factor.

---

* I. Constable (unpublished data).

However, the above discussion reveals the complexity of the behaviour of PMMA in methanol since it is not direct crack propagation as in air (even in air the plastic zone at the crack tip is a crazed material) but a combination of craze growth and crack propagation by void coalescence within the craze. For a better understanding of the mechanism of dynamic failure in methanol a close detailed study of the criteria of void coalescence in the craze is necessary. Such a study of void coalescence and craze growth in the particular geometry of round notched bars is presented in the next chapter.

CHAPTER SIX

CRAZE GROWTH AND VOID COALESCENCE IN PMMA ROUND NOTCHED BARS

Most of the previous studies of craze phenomena in polymers were concerned with the craze structure and craze kinetics (see Section 2.2.1 and Appendix B) while there are few studies concerned with the aspects of the failure process that occurs in the craze itself (e.g. Murray and Hull, 1970 - see page 287 in Appendix B). Even the studies of craze kinetics were mostly on SEN specimens (e.g. Marshall et al, 1970 - see page 40) with the exception of one study on surface notches (Parvin, 1972 - see page 42). Marshall et al (1970) first studied the kinetics of methanol crazes in PMMA SEN specimens under constant loading conditions (see page 40) then extended their study to craze growth under cyclic loads (Marshall and Williams, 1973 - see page 54) by modifying the model previously proposed for the static case to include load variations.

The present work represents a study of the failure mechanisms and craze growth kinetics for environmental attack in PMMA using notched circular bar specimens (as used in rotating bend tests) in an effort to provide a background for the explanation of environmental crazing phenomena in this particular geometry.

6.1 Experimental Procedure

6.1.1 Material, environment and specimen preparation

The circular cross-section notched specimen used in these tests is shown in Figure 95a. The specimens were prepared from $\frac{1}{2}$ in diameter rods machined from PMMA cast sheets, and machine notched with a dead sharp 60° lathe tool to give a root radius of approximately 0.0005 in. All the specimen surfaces were polished to allow the transmission of light through them, Figure 95b. Similar specimens having different notch depths and diameters were also prepared. Methanol was used as the testing environment in the present study.

6.1.2 Testing apparatus and procedure

The specimens were pin loaded in single lever rigs which maintained

the load constant throughout the test. As illustrated in Figure 95b, each clamp contained a plane mirror inclined at 45° to the axis of the specimen to reflect the light transmitted through the specimen and microscope (1) was used to observe the surface of the craze formed at the notched section. A closed circuit television camera was attached to the microscope and the process of void coalescence within the craze was recorded on video tape. A transparent container was used to maintain the methanol around the notched section and to allow the light from a second source to be reflected at the craze. This light was received by microscope (2) to which a still camera was attached, with which photographs were taken at intervals. Craze growth measurements were taken from these photographs.

6.1.3 Testing programme

This programme had two aims; first, a detailed study of the failure process, as recorded on the video tape and by microscopic examination of the fracture surfaces. Secondly, a study of the effect of initial condition at the crack tip on the craze growth behaviour. Therefore, specimens with different notch depths and diameters were subjected to various constant loads to give different stress intensity factors K_o (evaluated using the gross stress and initial crack length as indicated later).

6.2 Results and Discussion

6.2.1 Craze growth

For craze growth measurements, only tests which gave a symmetrical radial craze growth with respect to the specimen axis as shown in Figure 96d were considered. Measurements of the radial craze growth versus time were taken from these photographs, which were enlarged using a projector. The average radial craze length x was determined from:

$$x = \frac{d}{2}\left[1 - \frac{1}{2}\left(\frac{b}{B} + \frac{a}{A}\right)\right] \qquad \text{(Figure 96b)}$$

where d is the notch diameter and a, A, b and B were measured on the projector screen.

Typical curves obtained for radial craze growth versus time for specimens subjected to different initial stress intensity factors, K_o, are shown in Figure 97. In some cases there was a tendency for the craze to accelerate as it approached the centre of the specimen, Figure 97, possibly due to early void coalescence in the craze which may cause a further increase in the K value.

6.2.2 Void coalescence

It has been mentioned previously that crazes are a network of small cracks or voids interconnected by ligaments of the original material (see Appendix B). The failure of these links allows the small voids to grow by coalescence. The stresses carried by the material within the craze increases with time due to two factors:

1. The craze growth itself, which reduces the material at the crazed section carrying the original load on the specimen; and,
2. The plasticising action caused by the diffusion of methanol in the craze (see (d) in Appendix B). Such plasticisation causes unequal stresses in the ligaments of the material in the craze, i.e. the less softened ligaments in the newly formed part of the craze carry more load and thus become more likely to fail than the more softened ones in the older part of the craze.

The process of void coalescence was clearly shown on the TV screen. There are two distinct features of void coalescence; the first type is a cluster of very small voids (each of the order of 3-4 x 10^3 Å as measured from the fracture surface (Figure 98), appearing as a dark area in the craze (e.g. Figure 99d). The second type is the individual separate voids which grow much larger than the first type, and appear in the craze at different points, Figure 99f. Once the local failure process started it continued to give either one of the previously mentioned void forms, or resulted in both void features in one craze, Figure 99i and 99j. Voids usually started to coalesce when the craze had almost completely covered the cross-section of the specimen (Figure 99a), however, in some cases, especailly when K_o was high, void

coalescence started earlier. Final failure was caused by void growth and coalescence eventually leading to complete separation (Figure 99w). It was usually observed that the large voids (type 2) grew faster and caused final failure before coalescence occurred between the clusters of small voids if the two patterns were found in one craze.

The pressure inside the voids is low, allowing part of the methanol to evaporate, and voids are thus full of methanol and methanol vapour, Figure 99t and 99u. The movement of methanol vapour bubbles was clear; when the large voids grew in size and coalesced, the bubbles moved to join each other (Figure 99u) forming one large bubble filling the space above the liquid in the void.

Some tests of unloading and reloading the crazed specimens, which contained the larger voids with bubbles inside, have established the existence of the two phases of methanol in the void. When the specimen was unloaded, the craze relaxed, the two surfaces of the void approached each other, the pressure increased and the bubbles became progressively smaller until they disappeared. When the specimen was reloaded, the pressure in the void decreased and after a delay of approximately five minutes the bubbles suddenly reappeared. This is a similar process to that which is observed when pressure is reduced at the surface of some methanol in a container.

It has been noticed that void coalescence starts inside the craze away from the original crack or notch near to the centre of the specimen. This means that failure in the craze starts internally and grows towards the notch in a radial direction. It is thought that this rather surprising phenomenon occurs because the material within the craze is plasticised by the methanol, and the effect increases with time, so that the material is more plasticised in the craze near the notch than near the centre. Thus, most of the load is carried by the central section, and if a fault or weak link is present there it will cause void coalescence to start and lead to the final failure.

It seems that this type of failure is different from that observed in crazed SEN specimens in which the original crack propagates in the craze causing the final failure (Graham et al, 1972, see page 42). However, in the SEN case, the crack may be forced to propagate in that way because the specimen is not completely symmetrical with respect to the loading axis, as shown in Figure 100a. This causes bending, which

forces the original crack to propagate in the craze. As evidence of this, additional tests were made on SEN specimens. The load in these tests was controlled to allow the craze to propagate to more than three-quarters of the specimen width and to leave a length of uncrazed material ahead of the craze approximately equal to the original crack length. The material ahead of the craze was then removed and the specimen quickly reloaded in methanol but with a smaller load, Figure 100b. Complete failure of all these specimens was caused by void coalescence in the newly formed part of the craze at the end remote from the original crack and the crack started and propagated from this end while the original crack remained stationary.

6.2.3 Fracture surface

The fracture surface patterns produced by void coalescence and crack propagation through the wet craze distinguish this sort of failure from others (e.g. fracture in air).

The first distinct zone is the featureless part in which "puddles" appear, Figure 101. However, in some cases radial marks appear in this zone pointing to the centre of the specimen, as shown in Figure 102. The puddles represent the maximum size of the voids before fracture starts, and the radial marks indicate the direction of craze propagation. In some cases these puddles have very definitive boundaries (Figure 103) and usually have radial marks pointing to the origin of void coalescence (Figure 104) and showing the direction of void growth. However, these marks have no relation to those showing the direction of craze propagation; they may intersect them at any angle, Figure 102.

In the featureless region (Figure 101), mating surfaces are identical. It is thought that the crack was propagating slowly through the centre of the craze which would give two identical surfaces with hills and valleys of the order of 300 Å (the average spacing between the sites of inhomogeneities in the material, as shown later). This feature would be difficult to see, however, even with a powerful microscope. Alternatively, it is thought that any micro-features which might have been formed in this region were obliterated by the relaxation of the highly stressed craze.

It was noticed that the clusters of small voids which appear as dark areas in the craze before failure did not usually leave any feature on the fracture surface. However, in some cases, when these clusters were

formed in that part of the craze where fast crack propagation occurred, the features were seen on the fracture surface, e.g. Figure 99w. Comparison of this Figure with Figure 99o and Figure 99v shows that some of these clusters have disappeared from the fracture surface where there was slow crack propagation while others are still visible where there was fast crack propagation.

The second distinct zone is the island structure (Figure 105) with its definitive type of island and crater features which may give an indication of discontinuous propagation along the craze/matrix interface, i.e. the crack transferring across the craze thickness in an irregular manner. The transition to this type of feature, Figure 106, may be the result of the crack within the craze reaching its instability condition, causing a transition from slow to fast crack propagation. The parabolic markings at the zone boundary are similar to those found in the region of fast crack propagation in a PMMA craze in air (Berry, 1962 - see page 288 in Appendix B) and are thought to represent the intersection of an expanding void in the craze and a radial crack moving at a high speed.

6.3 Analysis of Craze Growth

A previous model for craze formation and growth (Marshall et al, 1970 - see page 40) was based on the crack opening displacement approach, in conjunction with a simple flow analysis to describe the movement of the liquid environment within the craze. The present analysis is based on the same concepts and, moreover, takes into account the viscoelastic behaviour of the material.

Crazing occurs when the lateral contraction of the highly stressed extending material at the crack tip is restrained by the material outside the plastic zone ahead of the crack. This causes a triaxial stress system in this region and leads to the formation of voids at the sites of inhomogeneities in the material. The average spacing between such sites is termed the process zone size ℓ_o. The formation of voids allows the liquid to diffuse into the voided zone ahead of the crack and to plasticise it. To maintain equilibrium, the plastic zone with its yield stress σ_y grows ahead of the liquid front (Marshall et al, 1970). Again the liquid diffuses through the voids of the plastic zone formed ahead of the wet craze tip and softens it. This process continues and the craze grows in length ahead of the crack tip.

6.3.1 Void area

It has been shown that the average voiding area A (Figure 107c) at the wet craze tip (Williams and Marshall, 1975) is given by:

$$A = \frac{\ell_o^2}{2d_o} U_b \qquad (6.1)$$

where U_b is the displacement at the wet craze tip and d_o is the height of the section which has the displacement U_b.

It may be assumed that there is a section d_o at the crack tip which may be considered as the original crack tip diameter. This section extends causing a crack displacement U_a and voids form in this extended section. The liquid diffuses in these voids and softens the material. For equilibrium the plastic zone with its original height d_o grows ahead of the liquid front. The strain in the craze $\varepsilon = U/d_o$ has a limiting value ε_o due to workhardening in the craze ligaments. Kambour (1964a,b) has reported an average value of 50% for void contents for fully formed wet and dry crazes in many polymers, so that ε has a limiting value of unity since the void contents $v = 1 - 1/1+\varepsilon$ (Williams and Marshall, 1975). The results of Marshall et al (1973) and Williams (1972) showed a limiting value of COD in air of 2 μm; hence for $\varepsilon_o = 1$, $d_o = 2$ μm.

However, displacements greater than $\varepsilon_o d_o$ will result in more material being drawn into the craze in order to maintain ε_o, so that d_o will increase.

6.3.2 Craze velocity

The craze growth characteristics may be relaxation controlled or flow controlled (Williams and Marshall, 1975 - see page 41). However, the representation of craze growth versus time on a log-log scale gives slopes greater than 0.6, Figure 108, and this suggests that the process is flow rather than relaxation controlled since in the latter case the slope would be expected to be much lower (typically 0.1). To maintain the craze speed equal to that of the environment requires formation of the porous plastic zone ahead of the liquid front faster than, or at least equal to, the speed of the environment at the craze tip. This

means that the environment at the craze tip should always find a void in front of it waiting for it to diffuse through, a condition which is reasonable since the diffusion and softening effect of the environment occurs over the short process zone of length ℓ_o (Marshall et al, 1970).

That the craze should be as a homogeneous porous system has been previously proposed (Marshall et al, 1970). The liquid will move within the pores because of the pressure upon it, assuming the pressure in the void ahead of the liquid front to be zero. An exact solution for this flow is not possible at this time. Consequently, the medium will be considered as a series of long filaments extending in the radial direction with a pressure gradient along the filament $dP/dx \simeq P/x$. The velocity V of the liquid at the tip of the craze may be approximated, assuming simple laminar channel flow, as:

$$V = \frac{P}{x} \frac{h^2}{12\ \eta} \qquad (6.2)$$

where P is the pressure drop along the radial distance x, x is the craze length in the radial direction, Figure 107a, η is the liquid viscosity and h^2 may be looked upon as the mean effective voiding area A.

6.3.3 Displacement at the craze tip (U_b)

The craze and the colinear plastic zones are schematically represented in Figure 107b. Inspection of this Figure and Figure 107a shows that the craze is similar to a Dugdale line plastic zone (Appendix A). However, the stress over the wet craze is much lower than σ_y due to the softening effect, and it is assumed to be uniform and to have an average value σ_c along the craze, whilst the material at the tip is not yet softened and is still at σ_y, the bulk material yield stress, Figure 107b.

To evaluate U_b consider the Rice contour integral J. For extended plastic zones ahead of the crack, $J = \sigma_c\ U_a$ according to equation (A.16) (Appendix A). However, if the plastic zone is small, J approaches the energy dissipated per unit area $G = K^2(1+\xi)/8\mu$ (equation (A.19)), i.e. $U_a = K^2/\sigma_c .\ 1+\xi/8\mu$.

To consider the situation of a crack having a long crazed zone, it is

necessary to model the extended crack by an equivalent crack having the same stress field at its tip as had the original crazed zone. This field is described by the equivalent stress intensity factor K_e. It is then possible to assume, in case of extended cracks, that $J = G = K_e^2 . (1+\xi)/8\mu$, where G here is equivalent to the total energy per unit area expended during the initial loading of the crack and the extension of the zone at its tip. The equivalent crack has a displacement U_b at its tip equal to that at the tip of the extended zone of the original crack because of the similarity of the two stress fields (in each case K_e is the same). Therefore, for the equivalent crack, $U_b = K_e^2/\sigma_y . (1+\xi)/8\mu = J/\sigma_y$, where σ_y is the stress at its tip (equal to the stress at the tip of the extended zone in the original case).

The case of round notched bars, in which there are no shear lips at the notch tip, may be considered as entirely plane strain and U_b may be given as:

$$U_b = \frac{K_e^2 \, (1 - \nu)}{E \; \sigma_y} \tag{6.3}$$

Poisson's ratio ν is essentially constant in polymeric materials (Schapery, 1972) while both E and σ_y are time dependent parameters because of the viscoelastic behaviour of the material, i.e. $E = E(t)$ and $\sigma_y = \sigma_y(t)$. Therefore,

$$U_b = \frac{K_e^2 \, (1 - \nu^2)}{E(t) \; \sigma_y(t)} \tag{6.4}$$

which indicates that the plastic zone maintaining equilibrium at the craze tip has to change in size with the increase of time and craze length.

From equations (6.1), (6.2) and (6.4) the craze velocity may be expressed as:

$$\frac{dx}{dt} = \frac{\ell_o^2}{24 \, \eta \, d_o} \cdot \frac{P}{x} \cdot \frac{K_e^2 \, (1 - \nu^2)}{E(t) \; \sigma_y(t)} \tag{6.5}$$

where P, the pressure of the liquid, is the atmospheric pressure for shallow immersion of the crazed section.

6.3.4 Evaluation of $E(t)$ and $\sigma_y(t)$

It has been found that both E and σ_y vary similarly at different times and strain rates. σ_y/E has the value of 0.05 independent of strain rate (Williams, 1972).

i.e. $$\frac{E(t_1)}{E(t_2)} = \frac{\sigma_y(t_1)}{\sigma_y(t_2)}$$

Moreover, there was an agreement between the modulus determined from the creep data when converted to a strain rate basis and the modulus determined from constant strain rate tests (Williams, 1972), and it was found that an equation of the form:

$$E(t) = 10^5 \left[0.95 + 3.98\ (\dot{\varepsilon}_1)^{0.109}\right] \text{ lbf/in}^2 \quad (\dot{\varepsilon} \text{ sec}^{-1}) \qquad (6.6)$$

provides the best representation of the data. This equation could be converted again to a time basis using $\dot{\varepsilon} \simeq \varepsilon/t = 0.035/t$ where $\varepsilon = 0.035$ is the strain at which the modulus was determined, and it was considered appropriate for the craze tip region (Williams, 1972).

The previous equation may be expressed in another form for convenience:

$$E_o/E(t) = 1.179 + 8.9453 \times 10^{-2}\ ln\ (t) \quad (t \text{ mins}) \qquad (6.7)$$

where E_o is the modulus appropriate to the short loading time $\simeq$ 0.1 minutes. Consequently,

$$\sigma_o/\sigma_y(t) = 1.179 + 8.9453 \times 10^{-2}\ ln\ (t) \quad (t \text{ mins}) \qquad (6.8)$$

6.3.5 Evaluation of K_e

Because of the similarity between the craze and the Dugdale model plastic zone, Figure 107a, the solution for such a crazed zone is an infinite plate subjected to uniform stress σ may be given by:

$$\frac{\sigma}{\sigma_c} = \frac{2}{\pi} \cos^{-1} \left(\frac{a}{x + a}\right) \tag{6.9}$$

and the crack opening displacement by:

$$U_a = \frac{\xi + 1}{\pi \mu} \sigma_c \, a \, ln \left(\frac{x + a}{a}\right) \tag{6.10}$$

In such a case

$$J = \sigma_c U_a = K_e^2 \frac{1 + \xi}{8\mu} \tag{6.11}$$

From equations (6.9), (6.10) and (6.11):

$$K_e = \frac{K \left[ln \left(\frac{x + a}{a}\right)^2\right]^{\frac{1}{2}}}{\cos^{-1} \left(\frac{a}{x + a}\right)} \tag{6.12}$$

where $K = \sigma \sqrt{\pi a}$ is the original stress intensity factor for the crack alone without any extended zone.

However, in the case of a circular notched bar, a correction must be made to allow for the finite effects and the change in geometry. The numerical results for such a correction do exist for a round circular notched bar subjected to uniform axial load (Hayes and Williams, 1972) and are available in tables for different values of a/R_o, a dimensionless crack opening displacement U^* (given by $U^* = 2 \pi U_a \mu/\sigma_c R_o (\xi + 1)$), the ratio σ/σ_c and $a/(a+x)$.

The total dissipated energy per unit area may be expressed as

$J = U_a \sigma_c$ and hence

$$J = \frac{(\xi + 1)}{2 \pi \mu} U^* \sigma_c^2 R_o \tag{6.13}$$

i.e. $$J \frac{8 \mu}{(1 + \xi)} = K_e^2 = \frac{4}{\pi} U^* \sigma_c^2 R_o \tag{6.14}$$

To put K_e in a dimensionless form we introudce the factor $K = \sigma \sqrt{\pi a}$ for the infinite plate. Therefore,

$$\frac{K_e^2}{\pi \sigma^2 a} = \frac{4}{\pi^2} \frac{U^*}{(\frac{\sigma}{\sigma_c})^2 (\frac{a}{R_o})} \tag{6.15}$$

Thus, for each value of a/R_o the value of $K_e^2/\pi\sigma^2 a$ can be computed for different values of x/a using the corresponding values of U^* and σ/σ_c from the tables and substituting in the right hand side of equation (6.15). Curves of $\pi\sigma^2 a/K_e^2$ versus x/a for different values of a/R_o are shown in Figure 109. These curves could be expressed in the form of algebraic equations for convenience and an example of such equations is given below:

For $a/R_o = 0.4$:

$$\frac{\pi\sigma^2 a}{K_e^2} = 0.40639 - 0.2732 (\frac{x}{a}) + 0.1282 (\frac{x}{a})^2 - 0.02609 (\frac{x}{a})^3 \tag{6.16}$$

For $a/R_o = 0.2$:

$$\frac{\pi\sigma^2 a}{K_e^2} \quad 0.64825 - 0.22147 (\frac{x}{a}) + 0.05613 (\frac{x}{a})^2 - 0.005841 (\frac{x}{a})^3 \tag{6.17}$$

6.3.6 The craze growth equation

From equations (6.5), (6.7) and (6.8):

$$\frac{dx}{dt} = \frac{\ell_o^2(1-\nu^2)}{24\ \eta\ d_o}\ \frac{P}{x}\ \frac{K_e^2}{E_o\ \sigma_o}\ (1.179 + 8.9453 \times 10^{-2}\ ln\ (t))^2 \qquad (6.18)$$

which may be written in the form:

$$\frac{\pi\sigma^2 a}{K_e^2}\ (\frac{x}{a})\ d(\frac{x}{a}) = \frac{\ell_o^2\ P\ \pi\ \sigma^2 a\ (1-\nu^2)}{24\ \eta\ d_o\ E_o\ \sigma_o\ a^2}\ (1.179 + 8.9453 \times 10^{-2}\ ln\ (t))^2\ dt \qquad (6.19)$$

Using equation (6.19) and replacing the term $\pi\sigma^2 a/K_e^2$ with the appropriate function of (x/a) as given by equations (6.16) and (6.17), then integrating between the limits of (x/a) from zero to (x/a) and t from 0.1 to t, gives an equation of the form:

$$f(\frac{x}{a}) = B\ f(t) \qquad (6.20)$$

where $f(t) = \left(1.195t + 0.195t\ ln(t) + 8 \times 10^{-3} t\ (ln\ t)^2 - 8 \times 10^{-2}\right)$,

$$B = \frac{\ell_o^2\ P\ \pi\ \sigma^2\ a\ (1-\nu^2)}{24\ \eta\ d_o\ E_o\ \sigma_o\ a^2}$$

and $f(x/a)$ is a variable function depending on the ratio a/R_o.

For example, for $a/R_o = 0.4$:

$$f(\frac{x}{a}) = 0.2032(\frac{x}{a})^2 - 0.091067(\frac{x}{a})^3 + 0.03205(\frac{x}{a})^4 - 0.005218(\frac{x}{a})^5 \qquad (6.21)$$

and for $a/R_o = 0.033$:

$$f\left(\frac{x}{a}\right) = 0.41842 \left(\frac{x}{a}\right)^2 - 0.06824 \left(\frac{x}{a}\right)^3 \ln \left(\frac{x}{a}\right) \qquad (6.22)$$

A logarithmic representation of $f(t)$ against t is shown in Figure 110 and it is a straight line relation which may be represented by the equation:

$$f(t) = 1.23\, t^{1.13} \qquad (6.23)$$

The error obtained by using this equation in evaluating $f(t)$ instead of the original one is not more than ±4% for times extending from 2 minutes to 17 hours. The error increases for times less than 2 minutes. However, the error is acceptable considering that the actual time measured during craze growth was between 1 minute and 17 hours.

Moreover, the logarithmic representation of $f(x/a)$ against (x/a) shows that these functions could be represented by parallel straight lines having the same slope for different values of a/R_o (e.g. Figure 111). Therefore, it could be represented by an equation of the form:

$$f\left(\frac{x}{a}\right) = \overline{c} \left(\frac{x}{a}\right)^{1.78} \qquad (6.24)$$

where $\overline{c}$ varies with different values of a/R_o as shown in Figure 112. The error due to the use of this equation in evaluating $f(x/a)$ is not more than ±5% for the whole craze length except for very short crazes.

Substituting for $f(t)$ and $f(x/a)$ from equations (6.23) and (6.24) in equation (6.20) gives:

$$x = \left(\frac{(1-\nu^2)\, \ell_o^2\, P}{19.5\, \eta\, d_o\, E_o\, \sigma_o}\right)^{0.562} \left(\frac{\pi\, \sigma^2 a}{a^{0.22}\, \overline{c}}\right)^{0.562} t^{0.635} \qquad (6.25)$$

The maximum error in the value of x due to the two previous approximations by using equations (6.23) and (6.24) is not more than ±5%.

If $c = \pi\sigma^2 a/K_o^2$, where K_o is the initial stress intensity factor before craze growth obtained from Hayes' (1970) calculations for round bar geometry (Figure 112), the relation between c and $\bar{c}$ could be obtained (Figure 113) as:

$$\bar{c} \simeq 0.42\, c^{1.206} \tag{6.26}$$

for a/R_o varying between 0.03 and 0.7.

Substituting in equation (6.25):

$$x \simeq \left(\frac{(1-\nu^2)\, \ell_o^2\, P}{8.2\, \eta\, d_o\, E_o\, \sigma_o}\right)^{0.562} \left(\frac{K_o^2}{a^{0.22}\, c^{0.206}}\right)^{0.562} t^{0.635} \tag{6.27}$$

The maximum error in the value of x evaluated by using equation (6.27) is not more than ±9% due to the previous approximations by using equations (6.23), (6.24) and (6.26).

Equation (6.27) describes the craze length as a function of time and initial stress intensity factor, but depends only slightly on the crack length and the correction factor because of their low power.

In accordance with equation (6.27) the results of craze growth were represented on a basis of craze length (x) against $t^{0.635}$ as shown in Figure 114. It can be seen that the relation holds for most of the craze history; however, there is a tendency for the craze speed to increase more than expected when the craze becomes long, and this may be due to the early void coalescence process which may occur within the craze, causing an increase in the K value and accelerating the craze growth.

If the flow parameter is taken as $(x/t^{0.635})$ and plotted for each specimen against the term $(K_o^2/a^{0.22} c^{0.206})^{0.562}$, the relation obtained will be as shown in Figure 115. However, Figure 115 shows that the flow parameter does not increase continuously with increasing K_o, possibly because craze bifurcations occur as the stress becomes high and the craze grows more slowly than expected giving a lower flow parameter. The results in Figure 115 could be represented by a straight line according to equation (6.27), the slope of which is:

$$51685 = \left(\frac{8.2\ \eta\ d_o\ E_o\ \sigma_o}{\ell_o^{\,2}\ P\ (1-\nu^2)} \right)^{0.562}$$

To calculate the material constant ℓ_o, take:

$P = 14.5\ \text{lbf/in}^2$

$\eta = 0.6\ \text{cp} = 0.1443 \times 10^{-8}\ \text{lbf.min/in}^2$

$\sigma_o = 16 \times 10^3\ \text{lbf/in}^2$

$E_o = 32 \times 10^4\ \text{lbf/in}^2$

$d_o = 2\ \mu\text{m} = 0.7874 \times 10^{-4}\ \text{in}$

$\nu = 0.5$

(The values of σ_o and E_o being those obtained via Williams (1972) at $t = 0.1$ min). Hence, $\ell_o = 340$ Å.

This figure agrees well with direct observations by Kambour and Holik (1969a) and X-ray scattering by Zhurkov et al (1969) for estimating the void spacing value in different polymers.

6.3.7 Estimation of σ_c dependence on time and U_b and U_a variations with craze length for SEN specimens

A useful cross-check on the method may be made by comparing the estimated U_a value with that obtained experimentally by Marshall (1972) for SEN specimens.

It has been shown that, for plane strain conditions,

$$U_b = \frac{K_e^{\,2}\ (1-\nu^2)}{E(t)\ \sigma_y(t)}$$

where $$\frac{1}{E(t)\,\sigma_y(t)} = \frac{(1.179 + 8.9453 \times 10^{-2}\ ln\ t)^2}{E_o\,\sigma_o}$$

from equations (6.7) and (6.8) and K_e could be evaluated in the same manner as in the case of round notched bars using the numerical results by Hayes and Williams (1972) for SEN specimens.

The specimen used had the dimensions: crack length a = 0.256 in, width w = 2 in, and thickness t = 0.068 in, and was subjected to force P = 55 lbf.

For a/w = 0.13:

$$\frac{\pi\sigma^2 a}{K_e^2} = 0.6929 - 0.24652\left(\frac{x}{a}\right) + 0.05343\left(\frac{x}{a}\right)^2 - 0.005308\left(\frac{x}{a}\right)^3 \qquad (6.28)$$

Therefore,

$$U_b = \frac{(1-\nu^2)\left[(1.179 + 8.9453 \times 10^{-2}\ ln(t))^2\right]\pi\sigma^2 a}{E_o\sigma_o\left[0.6929 - 0.24652\left(\frac{x}{a}\right) + 0.05343\left(\frac{x}{a}\right)^2 - 0.005308\left(\frac{x}{a}\right)^3\right]} \qquad (6.29)$$

where σ = 411.76 lbf/in^2, E_o = 32 x 10^4 lbf/in^2, σ_o = 16 x 10^3 lbf/in^2, and $\nu = \frac{1}{2}$. Thus, U_b can be evaluated at different values of x and t taken from the growth history of the craze shown in Figure 116 and substituted in equation (6.29), and $\sigma_y(t)$ can be evaluated for different values of t using equation (6.8). σ_c can be obtained for different values of x from Hayes' numerical results shown graphically in Figure 117, while J can be evaluated from the equivalent crack, as shown previously (Section 6.3.3), as $J = U_b\sigma_y$. Hence, U_a for a crack with a long extended zone is equal to J/σ_c.

Table 6 shows the values of U_b, $\sigma_y(t)$, J, $\sigma_c(t)$, U_a and $\sigma_y(t)/\sigma_c(t)$ at different time intervals and craze lengths. Figure 118 shows that both U_b and U_a increase linearly with increasing craze length and that the computed value of U_a agrees reasonably well with that obtained experimentally.

$\sigma_c(t)$ is obtained at different time intervals, for other specimens with different values of a/w and K_o, using Figure 117 and the craze growth history for each specimen. The variation of $\sigma_c(t)$ with t is shown graphically on a log-log scale (Figure 119) and it suggests that there is a unique relationship between t and σ_c which confirms the validity of representing the craze by a Dugdale model.

Moreover, it is shown in Figure 120 that σ_c decreases with time as does σ_y. However, the rate of decrease of σ_c is greater than that of σ_y, i.e. σ_y/σ_c increases with time. This is to be expected because the stressed material within the craze suffers from the effects of both relaxation and plasticisation.

The above analysis provides a more precise solution for craze behaviour in the particular geometry of circumferentially notched round bars under constant tensile loads, since it considers the time dependent properties of the material. The analysis showed good agreement with the experimental data of growth rates and it provides a basis for predicting the craze behaviour in other geometries.

6.3.8 Analysis of craze growth based on simple liquid flow and geometrical effects

Another analytical model, which also showed good agreement with the experimental data, was based on the equation of simple liquid flow in a disc to a sink (Williams, 1975)*. In this method, the craze was regarded as a series of discs each of height h and the craze radial velocity is equal to that of the liquid (see page 118). The expression for the radial craze length, x, (Figure 107a) was derived as:

$$R_1^2/4 - R_1^2/2\ (1 - \frac{x}{R_1})(\tfrac{1}{2} - ln\ (1 - \frac{x}{R_1})) = \frac{P\ h^2}{12\ \eta}\ t \qquad (6.30)$$

Equation (6.30) may be written as:

---

* J.G. Williams, private communication.

$$\phi(x) = \frac{P(1-\nu^2)\ \ell_o^2}{24\ \eta\ E_o\ \sigma_o\ d_o} K_o^2\ t \qquad (6.31)$$

(For details of the analysis, see Appendix C).

In accordance with equation (6.31) the results of craze growth were represented on a basis of $\phi(x)$ against t as shown in Figure 121. It can be seen that the straight line relation holds for most of the craze history. If the flow parameter is taken as $\phi(x)/t$ and plotted for each specimen against K_o^2, the relation obtained will be as shown in Figure 122. However, Figure 122 is similar to Figure 115 and may be discussed in the same way (see page 126). The calculated material constant (ℓ_o), according to the slope of Figure 122, is ℓ_o = 445 Å; this value is 30% higher than that obtained previously according to the slope of Figure 115 (see page 127).

The above analysis has the advantage of simplicity. However, it has the shortcoming of considering the craze voiding area (A) as being constant during craze growth and equal to its initial value at the beginning of the test (determined by the initial condition at the crack tip (equation (C.7) in Appendix C)) neglecting the time dependence of the modulus and yield stress and ignoring the variations in the stress intensity factor as the craze increases in length.

CONCLUSIONS

The study of fatigue failures of some polymeric materials in aggressive environments which has been conducted in the present work successfully demonstrates the applicability of linear fracture mechanics concepts in characterising the environmental fatigue failure process in viscoelastic materials providing approximate linearity of the materials' mechanical behaviour.

The fluctuating sinusoidal dynamic tensile fatigue studies of notched specimens of conditioned nylon 66 in different environments (air of 50% RH, distilled water and diluted sulphuric acid) and high density polyethylene in both air and Adinol have shown that variations in test frequency and amplitude and level of the stress intensity factor (ΔK and R respectively) have a remarkable influence on the material's resistance to cyclic crack propagation in any of the test environments. In all cases, an increase in ΔK or R resulted in a rise in the value of $\dot{a}_N$ (rate of cyclic crack propagation). On the other hand, increasing test frequency caused a decrease in $\dot{a}_N$. The discussion of the frequency effect according to the present results has led to the conclusion that: in isothermal tests the strain rate dependence of the modulus, the yield stress and the fracture toughness is the major factor that causes variations in the rate of cyclic crack propagation, while variations in damping seem to have only a secondary effect.

The environmental effect on the resistance of nylon 66 to cyclic crack propagation has been attributed to variations in the mechanical and viscoelastic properties of the material as a whole, since the environments are absorbed by the bulk material. Under the same test conditions an increase in the water content of the nylon caused an increase in $\dot{a}_N$. Nylon containing 4.4% of H_2SO_4 of 10% concentration has shown a decrease in the cyclic crack propagation resistance when compared with nylon containing 4.4% distilled water; this indicates an additional role of sulphuric acid in deteriorating the mechanical properties of the nylon by attacking the interchain molecular bonds. On the other hand, Adinol is not absorbed by HDPE as a bulk material, thus, it does not affect the properties of the material as a whole and the effects are restricted to the plastic zone ahead of the crack tip. The results from HDPE in Adinol have shown an increase in the resistance to cyclic crack propagation

when compared with the results in air. This surprising behaviour contradicts that previously observed in static fatigue tests by other investigators and it suggests that the main role of Adinol is different in dynamic conditions from that in static conditions.

Since previously suggested crack growth models did not adequately represent the results, an empirical model has been proposed having the form:

$$\dot{a}_N = B\ \psi^L$$

where $L = \alpha + \beta$ and

$$\psi = (K_{max}^2 - K_{min}^2)^{\alpha/L}\ (K_m^2)^{\beta/L} = \left\{(\Delta K)^2\ \left[(0.25)^{\beta}\ \left(\frac{1+R}{1-R}\right)^{\alpha+2\beta}\right]^{\frac{1}{\alpha+\beta}}\right\}$$

The proposed model adequately represented the experimental data from HDPE and N66 under all test conditions. At any particular test frequency and environment a unique relationship exists between $\dot{a}_N$ and the parameter ψ irrespective of the specific values of R and ΔK. The above model provides a unifying pattern for most of the previous cyclic fatigue laws used in the case of polymeric materials and eliminates the apparent discrepancies between some laws by considering them as special cases of the proposed model. Moreover, the presented model can easily be expressed in terms of COD, the cyclic plastic zone size (r_{pc}) or the energy available for crack propagation (G) where any of these terms provides a rational physical dependence of the cyclic crack growth rate, and it had been shown by several investigators that these parameters can successfully describe the cyclic crack growth rate.

The fluctuating tensile dynamic fatigue study of low density polyethylene in a methanol environment at low frequency (0.125 Hz) has shown good correlation between dynamic and static fatigue crack growth when the type and mechanism of failure are the same in both dynamic and static conditions. The linear superposition model previously suggested for metals has been shown to be applicable in the case of LDPE in methanol when the rate sensitivity of the stress intensity factor is considered. The LDPE/methanol system may be considered as a special case, since the contribution of dynamic pure fatigue (inert environmental

dynamic fatigue) in environmental fatigue crack growth was found to be negligible.

The environmental fatigue studies of the present project have been extended to the widely known Wöhler type rotating bending fatigue test in an effort to outline a simple and reliable routine technique for environmental dynamic fatigue testing of polymers. The results from round notched specimens of HDPE in both air and Adinol and PMMA in both air and methanol were represented on a stress intensity factor basis (K–N curve); such a representation has been shown to be inadequate to give direct correlation between the initial stress intensity factor amplitude and the numbers of cycles to failure independent of notch depth. The apparent notch depth effect has been justified to some extent by analytical treatment and by the expected increase in temperature as the initial notch depth decreases at the same initial value of K. The observed environmental effect of Adinol is to increase the fatigue life of HDPE, which agrees with the results of the tensile dynamic fatigue tests of SEN specimens, while the effect of methanol is to increase the fatigue life at high K values and decrease it at low values, reducing the fatigue limit. Such effects have been attributed to the plasticising effect of methanol and the low value of K at which the methanol crazes initiate.

From considerations of the dynamic failure process in PMMA in methanol (continuous craze growth and void coalescence) a closely detailed study of the criteria of void coalescence has been made for the particular geometry of round notched bars under tensile static fatigue conditions. Two types of void coalescence have been observed; the first is a cluster of very small voids (each of the order of $3\text{-}4 \times 10^3$ Å), and the second are the individual separate voids which grow in size and eventually cause the final failure before coalescence occurs between the clusters of small voids if the two patterns are found in one craze. The voids are full of methanol and methanol vapour due to the low pressure inside them. Void coalescence usually starts in the craze away from the original notch (near the centre of the specimen) and grows towards the notch in a radial direction; this has been attributed to the time dependent plasticising effect of methanol on the material.

Craze growth in round circumferentially notched bars has been analytically treated and the predicted radial craze length has been shown

to be:

$$x = A \left(\frac{K_o^2}{a^{0.22} c^{0.206}} \right)^{0.562} t^{0.635}$$

where A is a constant based on craze void dimensions and material and fluid parameters. The analysis has shown good agreement with the experimental data of growth rates which suggests that the fluid flow controls the craze growth behaviour in circular notched specimens, and provides a basis for predicting the craze behaviour in other geometries. The derived value of the average distance between the sites of inhomogeneities in the material has been shown to be in agreement with the direct observations of other investigators, which confirms the applicability of the analysis. A cross-check on the analytical method has been conducted by comparing the calculated COD value with that determined experimentally by other investigators for SEN crazed specimens, and reasonable agreement has been achieved.

Finally, as polymer science is a much younger field than is metallurgy, the fracture of polymeric materials is still less well understood. Environmental dynamic fatigue, in particular, has only now been recognised as a subject of importance. It is hoped that the present study represents an encouraging step towards further studies of the environmental dynamic fatigue behaviour of different plastics, since these are rapidly growing in use and finding wider application as structural materials. Such studies should receive greater attention in future to allow the exploitation of polymers to the utmost.

RECOMMENDATIONS FOR FUTURE STUDIES

As the importance of environmental dynamic fatigue studies of polymers has only very recently been recognised, the field is relatively unexplored and a lot of experimental study is needed to reveal the behaviour of different plastics, which differ widely in nature and properties, in different aggressive environments. Such studies might help in understanding the mechanisms of failure under these severe conditions. Examples of polymer/environment combinations that need to be studied are: nylon in metallic salts (dissolved either in water or in organic media), polycarbonate in alcohol and polystyrene in white spirits. Different types of failure may be obtained, such as failure by craze growth and breakdown or failure by crack propagation.

A study of environmental dynamic fatigue of any particular polymer/environment combination should include the effect of some of the different variables, such as frequency, level of loading, wave form, type of wave form (e.g. stress or strain wave form), mode of deformation (e.g. uniaxial or flexural), molecular orientation in anisotropic materials, ambient temperature, etc.

The proposed empirical model for failure by crack propagation presented in this thesis should be tested in other polymer/environment systems where the mode of failure is also by crack propagation. The model may be further generalised by introducing other variable parameters, such as frequency, temperature or degree of plasticisation. The effect of the environment and the level of loading on the threshold value of K should be closely examined for any particular polymer/environment system.

On the other hand, environmental static fatigue studies should accompany or even precede the dynamic ones, since this may help in finding the correlation between the two types of failure under the appropriate conditions (e.g. the study of LDPE included in this thesis). Moreover, an understanding of the failure mechanism and the role of the environment under static conditions will help in understanding the failure process under the more complicated dynamic conditions. The existing studies, from the mechanical point of view, are only concerned with very few polymers and they should be extended to include various engineering plastics.

The present study of craze growth and failure in circular notched

specimens (PMMA/methanol system) provides a basis for future studies under dynamic fatigue conditions.

As regards the rotating bending test, still more data are needed to reveal the exact effect of notch depth on the K–N curves for different polymer/environment systems and the studies should be extended to include the effect of test speed on the results.

As a final point, it should be mentioned that in environmental fatigue studies of polymers, a better understanding of failure mechanisms and the trends of variation in behaviour necessitates a comprehensive knowledge of the basic material mechanical and viscoelastic properties. Unfortunately, the lack of such data for many polymers severely limits the fulfilment of a complete fatigue study in such cases.

TABLE 1

Cyclic Crack Growth Rate Data for Dry Nylon 66 Tested in Air at a Frequency of 20 Hz

	$\dot{a}_N$ in/cycle	ΔK lbf/in$^{3/2}$	log ($\dot{a}_N \times 10^9$)	log ΔK	log ψ
Specimen 1 $R = 0$	1.236×10^{-7}	1823.896	2.092	3.261	6.7103
	1.396 "	1837.384	2.145	3.2642	6.71667
	2.014 "	1872.84	2.304	3.2725	6.73327
	3.048 "	1909.85	2.484	3.281	6.7503
	4.207 "	2014.19	2.624	3.3041	6.7965
	5.649 "	2108.63	2.752	3.324	6.83627
	10.046 "	2339.91	3.002	3.3692	6.92667
	15.849 "	2523.48	3.200	3.402	6.99227
	28.907 "	2824.88	3.461	3.451	7.09027
	31.623 "	2832.04	3.500	3.4521	7.0924
	53.95 "	3206.27	3.732	3.506	7.20027
	119.95 "	3589.22	4.079	3.555	7.29827
	170.22 "	3872.58	4.231	3.588	7.36427
	226.46 "	4265.8	4.355	3.630	7.4483
	364.75 "	4682.74	4.562	3.6705	7.52927
	490.91 "	5105.05	4.691	3.708	7.6043
	662.22 "	5559.04	4.821	3.745	7.67827
Specimen 2 $R = 0$	2.213×10^{-7}	1925.307	2.345	3.2845	6.75727
	2.780 "	1995.72	2.444	3.3001	6.78847
	3.811 "	2065.38	2.581	3.315	6.81827
	5.521 "	2182.73	2.742	3.339	6.8663
	7.943 "	2304.62	2.900	3.3626	6.91347
	11.776 "	2398.83	3.071	3.380	6.94827
	19.23 "	2695.88	3.284	3.4307	7.0497
	39.99 "	3061.96	3.602	3.486	7.16027
	83.18 "	3358.149	3.920	3.5261	7.2405
	110.41 "	3732.5	4.043	3.572	7.33227
	181.134 "	4080.37	4.258	3.6107	7.4097
	283.79 "	4634.47	4.453	3.666	7.5203
	530.88 "	5284.45	4.725	3.723	7.63427
Specimen 3 $R = 0$	4.446×10^{-6}	2971.666	3.648	3.473	7.13427
	9.397 "	3568.62	3.973	3.5525	7.29327
	24.89 "	4441.2	4.396	3.6475	7.48327
	38.02 "	5011.87	4.58	3.700	7.58827

TABLE 1

(Continued)

	$\dot{a}_N$ in/cycle	ΔK lbf/in$^{3/2}$	log ($\dot{a}_N \times 10^9$)	log ΔK	log ψ
Specimen 4 $R = 0.25$	1.049×10^{-7}	1514.258	2.021	3.1802	6.70115
	1.39 "	1538.15	2.143	3.187	6.71475
	1.811 "	1574.34	2.258	3.1971	6.73495
	2.349 "	1599.56	2.371	3.204	6.7487
	2.884 "	1650.82	2.460	3.2177	6.77615
	3.758 "	1702.16	2.575	3.231	6.80275
	5.176 "	1770.92	2.714	3.2482	6.83715
	6.471 "	1864.66	2.811	3.2706	6.88195
	7.834 "	1933.3	2.894	3.2863	6.91335
	9.141 "	2030.02	2.961	3.3075	6.95575
	11.803 "	2118.36	3.072	3.326	6.9927
	14.825 "	2223.31	3.171	3.347	7.0347
	17.824 "	2301.97	3.251	3.3621	7.0649
	23.121 "	2393.32	3.364	3.379	7.0987
	29.854 "	2495.74	3.475	3.3972	7.13515
	43.752 "	2648.5	3.641	3.423	7.18675
	66.069 "	2768.85	3.820	3.4423	7.22535
	102.09 "	3004.00	4.009	3.4777	7.2961
	158.130 "	3338.11	4.199	3.5235	7.3877
	209.89 "	3655.11	4.322	3.5629	7.4665
	302.69 "	4003.13	4.481	3.6024	7.54555
	349.95 "	4197.59	4.544	3.623	7.58675
	405.51 "	4391.37	4.608	3.6426	7.6259
	480.84 "	4623.81	4.682	3.665	7.67075
	547.02 "	4871.92	4.738	3.6877	7.71615
Specimen 5 $R = 0.25$	6.31×10^{-7}	1809.26	2.800	3.2575	6.85575
	10.19 "	1969.7	3.008	3.2944	6.9295
	16.63 "	2133.04	3.221	3.329	6.9987
	21.88 "	2177.71	3.34	3.338	7.01675
	33.27 "	2382.87	3.522	3.3771	7.0949
	41.69 "	2501.5	3.620	3.3982	7.1371
	49.89 "	2631.48	3.698	3.4202	7.1811
	55.98 "	2754.23	3.748	3.440	7.22075
	77.09 "	2901.35	3.887	3.4626	7.26595
	120.2 "	3054.92	4.080	3.485	7.31075
	154.170 "	3218.1	4.188	3.5076	7.35595
	204.17 "	3513.18	4.310	3.5457	7.43215
	267.30 "	3953.67	4.427	3.597	7.53475
	388.15 "	4290.42	4.589	3.6325	7.6057
	544.5 "	4753.35	4.736	3.677	7.6947

TABLE 1

(Continued)

	$\dot{a}_N$ in/cycle	ΔK lbf/in$^{3/2}$	log ($\dot{a}_N \times 10^9$)	log ΔK	log ψ
Specimen 6 $R = 0.4$	1.312×10^{-7}	1327.39	2.118	3.123	6.68718
	1.660 "	1364.9	2.22	3.1351	6.71138
	2.193 "	1400.23	2.341	3.1462	6.73358
	3.020 "	1469.94	2.480	3.1673	6.77578
	4.074 "	1510.00	2.610	3.1790	6.79918
	5.20 "	1557.4	2.716	3.1924	6.82598
	7.112 "	1624.43	2.852	3.2107	6.8626
	8.933 "	1695.12	2.951	3.2292	6.89958
	11.117 "	1766.04	3.046	3.247	6.93518
	14.125 "	1858.23	3.150	3.2691	6.97938
	18.707 "	1954.79	3.272	3.2911	7.02338
	23.33 "	2089.3	3.368	3.3200	7.08118
	26.300 "	2172.70	3.420	3.337	7.11518
Specimen 7 $R = 0.4$	3.767×10^{-7}	1490.05	2.576	3.1732	6.7876
	3.936 "	1539.93	2.595	3.1875	6.81618
	6.309 "	1631.55	2.800	3.2126	6.86638
	8.433 "	1748.24	2.926	3.2426	6.92638
	11.588 "	1846.29	3.064	3.2663	6.97378
	17.378 "	1988.84	3.240	3.2986	7.03838
	30.62 "	2165.21	3.486	3.3355	7.11218
	43.85 "	2291.39	3.642	3.3601	7.16138

TABLE 1

(Continued)

	$\dot{a}_N$ in/cycle	ΔK lbf/in$^{3/2}$	log ($\dot{a}_N \times 10^9$)	log ΔK	log ψ
Specimen 8 $R = 0.6$	0.712×10^{-7}	1032.76	1.853	3.0145	6.63006
	0.839 "	1042.32	1.924	3.018	6.63806
	0.997 "	1053.17	1.999	3.0225	6.64706
	1.197 "	1064.14	2.078	3.027	6.6561
	1.355 "	1076.713	2.132	3.0321	6.66626
	1.581 "	1096.48	2.199	3.040	6.68206
	1.866 "	1123.31	2.271	3.0505	6.70306
	2.089 "	1136.32	2.320	3.0555	6.71306
	2.559 "	1167.88	2.408	3.0674	6.73685
	3.055 "	1196.74	2.485	3.078	6.75804
	4.159 "	1273.50	2.619	3.105	6.81206
	6.397 "	1368.04	2.806	3.1361	6.87426
	9.057 "	1422.66	2.957	3.1531	6.90826
	11.194 "	1475.71	3.049	3.169	6.94007
	12.134 "	1524.05	3.084	3.183	6.96804
	16.14 "	1611.02	3.208	3.2071	7.01626
	23.88 "	1692.39	3.378	3.2285	7.05906
	28.84 "	1770.11	3.460	3.248	7.09806
	39.63 "	1851.4	3.598	3.2675	7.13706
	57.54 "	1985.18	3.760	3.2978	7.19766
	72.78 "	2084.97	3.862	3.3191	7.24026
	103.04 "	2162.72	4.013	3.335	7.2721
	120.23 "	2225.87	4.080	3.3475	7.29707
	145.88 "	2277.71	4.164	3.3575	7.31707
Specimen 9 $R = 0.6$	1.574×10^{-7}	1079.22	2.197	3.033	6.66828
	2.065 "	1155.58	2.315	3.0628	6.7277
	3.177 "	1223.24	2.502	3.0875	6.77708
	5.248 "	1288.84	2.720	3.1102	6.2204
	7.638 "	1373.128	2.883	3.1377	6.8775
	14.588 "	1538.51	3.164	3.1871	6.9763
	19.14 "	1619.2	3.282	3.2093	7.02066
	34.75 "	1791.02	3.541	3.2531	7.1083
	50.12 "	1963.86	3.700	3.293	7.1883
	157.04 "	2204.4	4.196	3.3433	7.2887

TABLE 2

Parameters m, A and C of Equation (1.15)
for Various Test Conditions

a) Dry N66 tested in air (20°C, 50% RH)

Frequency f (Hz)	Ratio R	m (=2L)	A (at log ΔK = 0)	C (at log ΔK = 2.7)
20	0	5.830	0.21074×10^{-25}	0.11608×10^{-9}
20	0.25	5.818	0.5811×10^{-25}	0.29706×10^{-9}
20	0.4	5.822	1.15305×10^{-25}	0.604294×10^{-9}
20	0.6	5.811	4.02532×10^{-25}	1.97016×10^{-9}
5	0	6.266	0.10606×10^{-26}	0.87852×10^{-10}
5	0.25	6.252	0.28563×10^{-26}	2.16872×10^{-10}
5	0.4	6.260	0.635331×10^{-26}	5.06991×10^{-10}
5	0.6	6.262	2.6442×10^{-26}	21.3646×10^{-10}
0.16	0	6.123	0.74046×10^{-26}	0.252117×10^{-9}
0.16	0.25	6.118	1.7902×10^{-26}	0.590883×10^{-9}
0.16	0.4	6.116	3.97924×10^{-26}	1.29718×10^{-9}
0.16	0.6	6.123	11.4499×10^{-26}	3.89854×10^{-9}

b) N66 (4.4% water content) tested in air and distilled water

Frequency f (Hz)	Ratio R	m (=2L)	A (at log ΔK = 0)	C (at log ΔK = 2.7)
20	0	4.303	$0.1455794 \times 10^{-19}$	0.604227×10^{-8}
20	0.25	4.260	0.267301×10^{-19}	0.849182×10^{-8}
20	0.6	4.460	$0.1342765 \times 10^{-19}$	1.479108×10^{-8}
5	0	4.120	0.1122×10^{-18}	0.149277×10^{-7}
5	0.25	3.960	0.465586×10^{-18}	0.229087×10^{-7}
5	0.6	4.042	0.505359×10^{-18}	0.414×10^{-7}
0.16	0	4.392	0.35789×10^{-19}	0.26318×10^{-7}
0.16	0.25	4.462	$0.3057736 \times 10^{-19}$	0.3410358×10^{-7}
0.16	0.6	4.580	$0.3499452 \times 10^{-19}$	0.8128306×10^{-7}

TABLE 2

(Continued)

c) N66 (9.8% water content) tested in distilled water

Frequency f (Hz)	Ratio R	m (=$2L$)	A (at log ΔK = 0)	C (at log ΔK = 2.7)
20	0	3.432	0.127174×10^{-15}	0.181228×10^{-7}
20	0.25	3.450	$0.1244515 \times 10^{-15}$	0.268411×10^{-7}
20	0.45	3.385	0.228×10^{-15}	0.444503×10^{-7}
5	0	3.571	0.624849×10^{-16}	0.240159×10^{-7}
5	0.25	3.538	0.979659×10^{-16}	0.3322×10^{-7}
5	0.45	3.650	0.56234×10^{-16}	0.4282×10^{-7}
0.16	0	4.385	0.301648×10^{-18}	0.20845×10^{-6}
0.16	0.25	4.442	$0.3478564 \times 10^{-18}$	0.34261×10^{-6}
0.16	0.45	4.493	0.399025×10^{-18}	0.539635×10^{-6}

d) N66 (4.4% of H_2SO_4 of 10% concentration) tested in H_2SO_4 of 10% concentration

Frequency f (Hz)	Ratio R	m (=$2L$)	A (at log ΔK = 0)	C (at log ΔK = 2.7)
20	0	3.786	0.313401×10^{-17}	0.5227576×10^{-7}
20	0.25	3.901	$0.1855026 \times 10^{-17}$	0.632485×10^{-7}
20	0.45	3.893	0.310081×10^{-17}	1.00595×10^{-7}
5	0	3.923	$0.1457975 \times 10^{-17}$	0.5699675×10^{-7}
5	0.25	3.825	$0.5056791 \times 10^{-17}$	1.074917×10^{-7}
5	0.45	3.952	0.2734×10^{-17}	1.279966×10^{-7}
0.16	0	3.436	$0.1889296 \times 10^{-15}$	0.357684×10^{-6}
0.16	0.25	3.501	$0.1684031 \times 10^{-15}$	0.477584×10^{-6}
0.16	0.45	3.383	$0.7112954 \times 10^{-15}$	0.968612×10^{-6}

TABLE 2

(Continued)

e) HDPE tested in air (20°C, 50% RH)

Frequency f (Hz)	Ratio R	m (=$2L$)	A (at log ΔK = 0)	C (at log ΔK = 2.7)
20	0	3.123	0.372392×10^{-15}	0.100716×10^{-6}
20	0.3	3.204	$0.2329164 \times 10^{-15}$	$0.10423176 \times 10^{-6}$
20	0.6	3.033	$0.8624337 \times 10^{-15}$	0.133299×10^{-6}
5	0	2.931	$0.2412404 \times 10^{-14}$	0.1977653×10^{-6}
5	0.3	2.923	0.296534×10^{-14}	0.2313×10^{-6}
5	0.6	2.906	$0.4366164 \times 10^{-14}$	0.306408×10^{-6}
0.16	0	2.332	$0.8390735 \times 10^{-12}$	0.166035×10^{-5}
0.16	0.3	2.212	2.83923×10^{-12}	0.266441×10^{-5}
0.16	0.45	2.356	1.314014×10^{-12}	0.3018561×10^{-5}

f) HDPE tested in Adinol

Frequency f (Hz)	Ratio R	m (=$2L$)	A (at log ΔK = 0)	C (at log ΔK = 2.7)
20	0	4.067	0.189376×10^{-18}	0.181228×10^{-7}
20	0.3	3.968	0.519039×10^{-18}	0.268411×10^{-7}
20	0.6	4.085	$0.4153125 \times 10^{-18}$	0.444503×10^{-7}
5	0	3.996	0.39021×10^{-18}	0.240159×10^{-7}
5	0.3	4.062	0.358096×10^{-18}	0.3322×10^{-7}
5	0.45	4.122	0.31787×10^{-18}	0.4282×10^{-7}
0.16	0	4.362	0.596417×10^{-19}	0.357232×10^{-7}
0.16	0.25	4.198	3.76964×10	0.8145165×10^{-7}

TABLE 3

Parameters B, α and β of Equation (3.4)
for Various Test Conditions

a) Dry N66 tested in air (20°C, 50% RH)

Frequency f (Hz)	B	α	β	$L = \alpha + \beta$	$\alpha + 2\beta$	β/α
20	0.634965×10^{-26}	3.82	-0.91	2.91	2	-0.238
5	0.021147×10^{-26}	4.36	-1.23	3.13	1.9	-0.2825
0.16	0.15506×10^{-26}	4.23	-1.17	3.06	1.89	-0.27652

b) N66 (4.4% water content) tested in air and distilled water

Frequency f (Hz)	B	α	β	$L = \alpha + \beta$	$\alpha + 2\beta$	β/α
20	0.140443×10^{-20}	3.63	-1.46	2.17	0.71	-0.4015
5	2.79254×10^{-20}	3.45	-1.43	2.02	0.59	-0.4145
0.16	$0.3311311 \times 10^{-20}$	3.42	-1.18	2.24	1.06	-0.345

c) N66 (9.8% water content) tested in distilled water

Frequency f (Hz)	B	α	β	$L = \alpha + \beta$	$\alpha + 2\beta$	β/α
20	216.272×10^{-19}	3.21	-1.51	1.70	0.19	-0.4705
5	96.16123×10^{-19}	3.09	-1.30	1.79	0.49	-0.421
0.16	$0.4305266 \times 10^{-19}$	3.35	-1.13	2.22	1.09	-0.3375

TABLE 3

(Continued)

d) N66 (4.4% of H_2SO_4 of 10% concentration) tested in H_2SO_4 of 10% concentration

Frequency f (Hz)	B	α	β	$L = \alpha + \beta$	$\alpha + 2\beta$	β/α
20	0.401791×10^{-18}	2.98	-1.05	1.93	0.88	-0.3525
5	0.400867×10^{-18}	3.02	-1.07	1.95	0.88	-0.3543
0.16	58.34454×10^{-18}	2.55	-0.83	1.72	0.89	-0.3255

e) HDPE tested in air (20°C, 50% RH)

Frequency f (Hz)	B	α	β	$L = \alpha + \beta$	$\alpha + 2\beta$	β/α
20	0.584117×10^{-16}	2.89	-1.33	1.56	0.23	-0.46
5	5.140437×10^{-16}	2.61	-1.15	1.46	0.31	-0.4405
0.16	5211.95×10^{-16}	1.67	-0.52	1.15	0.63	-0.3115

f) HDPE tested in Adinol

Frequency f (Hz)	B	α	β	$L = \alpha + \beta$	$\alpha + 2\beta$	β/α
20	0.339625×10^{-19}	3.37	-1.35	2.02	0.67	-0.4005
5	0.365174×10^{-19}	3.42	-1.39	2.03	0.64	-0.392
0.16	0.291407×10^{-19}	3.12	-0.98	2.14	1.16	-0.3145

TABLE 4

Variation of Number of Cycles to Failure with Initial Notch Depth at Various Constant Initial K - HDPE SEN Specimens Tested in Air at f = 20 Hz

Initial K ($lbf/in^{3/2}$)	Initial a/w	Number of Cycles	Final K ($lbf/in^{3/2}$)	Final a/w	Nominal Initial Stress (lbf/in^2)
650.0	0.075	0.122595×10^7	2015.63	0.320	517.80
650.0	0.125	0.152677×10^7	2001.70	0.400	379.08
650.0	0.175	0.168622×10^7	2037.90	0.465	297.57
650.0	0.225	0.176056×10^7	2037.25	0.515	240.88
650.0	0.350	0.171634×10^6	2024.06	0.620	149.10
750.0	0.075	0.761813×10^6	2037.33	0.285	597.46
750.0	0.125	0.953596×10^7	2018.64	0.365	437.40
750.0	0.175	0.105503×10^7	2000.21	0.425	343.34
750.0	0.225	0.110930×10^7	2025.72	0.480	277.94
750.0	0.350	0.108016×10^6	2032.85	0.590	172.04
850.0	0.075	0.498205×10^6	2017.80	0.250	677.13
850.0	0.125	0.627512×10^6	2003.82	0.330	495.72
850.0	0.175	0.695417×10^6	2015.22	0.395	389.12
850.0	0.225	0.733661×10^6	2028.85	0.450	314.99
850.0	0.350	0.712432×10^6	2010.67	0.560	194.97
950.0	0.075	0.334499×10^6	2001.21	0.220	756.79
950.0	0.125	0.425705×10^6	2038.01	0.305	554.04
950.0	0.175	0.472835×10^6	2007.13	0.365	434.90
950.0	0.225	0.501103×10^6	2010.70	0.420	352.05
950.0	0.350	0.491240×10^6	2010.93	0.535	217.91

TABLE 5

Variation of Number of Cycles to Failure with Initial Notch Depth at Various Constant Initial K - HDPE SEN Specimens Tested in Adinol at f = 20 Hz

Initial K ($lbf/in^{3/2}$)	Initial a/w	Number of Cycles	Final K ($lbf/in^{3/2}$)	Final a/w	Nominal Initial Stress (lbf/in^2)
575.0	0.075	0.663109×10^7	2035.12	0.355	458.06
575.0	0.125	0.842480×10^7	2033.06	0.435	335.34
575.0	0.175	0.941945×10^7	2000.85	0.490	263.23
575.0	0.225	0.992219×10^7	2010.18	0.540	213.08
575.0	0.350	0.978157×10^7	2013.27	0.645	131.89
675.0	0.075	0.342342×10^7	2015.67	0.310	537.72
675.0	0.125	0.435702×10^7	2038.70	0.395	393.66
675.0	0.175	0.487492×10^7	2031.25	0.455	309.01
675.0	0.225	0.513672×10^7	2026.54	0.505	250.14
675.0	0.350	0.506248×10^7	2006.37	0.610	154.83
775.0	0.075	0.191912×10^7	2026.42	0.275	617.38
775.0	0.125	0.245020×10^7	2008.12	0.355	451.98
775.0	0.175	0.275521×10^7	2026.34	0.420	354.79
775.0	0.225	0.290373×10^7	2007.95	0.470	287.20
775.0	0.350	0.285929×10^7	2006.79	0.580	177.77
900.0	0.075	0.101125×10^7	2013.78	0.235	716.96
900.0	0.125	0.129958×10^7	2005.01	0.315	524.88
900.0	0.175	0.146885×10^7	2013.77	0.380	412.01
900.0	0.225	0.154791×10^7	2022.06	0.435	333.52
900.0	0.350	0.153091×10^7	2035.86	0.550	206.44

TABLE 6

Values of Various Parameters at Different Time Intervals - Constant Load Test of PMMA SEN Specimens in Methanol

x (in)	t (min)	$U_b \times 10^4$ (in)	$\sigma_y(t) \times 10^{-2}$ (lbf/in^2)	J (lbf/in^2)	$\sigma_c(t) \times 10^{-2}$ (lbf/in^2)	$U_a \times 10^3$ (in)	$\sigma_y(t)/\sigma_c(t)$
0.0	0.1	0.290	16	0.464	-	0.029	-
0.0197	1.4	0.435	13.20	0.5742	30.96	0.185	4.264
0.0394	3.25	0.505	12.42	0.6272	19.58	0.320	6.343
0.0591	6.25	0.567	11.88	0.6736	15.23	0.442	7.800
0.0787	10.0	0.619	11.52	0.7131	13.05	0.546	8.828
0.1181	20.0	0.713	11.03	0.7864	10.76	0.731	10.251
0.1575	30.5	0.79	10.75	0.8493	9.35	0.908	11.497
0.1969	42.25	0.864	10.54	0.9107	8.54	1.066	12.342
0.2362	53.5	0.933	10.39	0.9694	7.96	1.218	13.05
0.2756	65.5	1.004	10.27	1.0311	7.54	1.368	13.62
0.315	77.5	1.072	10.17	1.0902	7.29	1.495	13.951
0.3543	89.25	1.14	10.09	1.1503	7.03	1.636	14.353
0.3937	101.0	1.209	10.02	1.2114	6.80	1.781	14.735
0.5512	148.0	1.488	9.81	1.4597	6.35	2.299	15.449

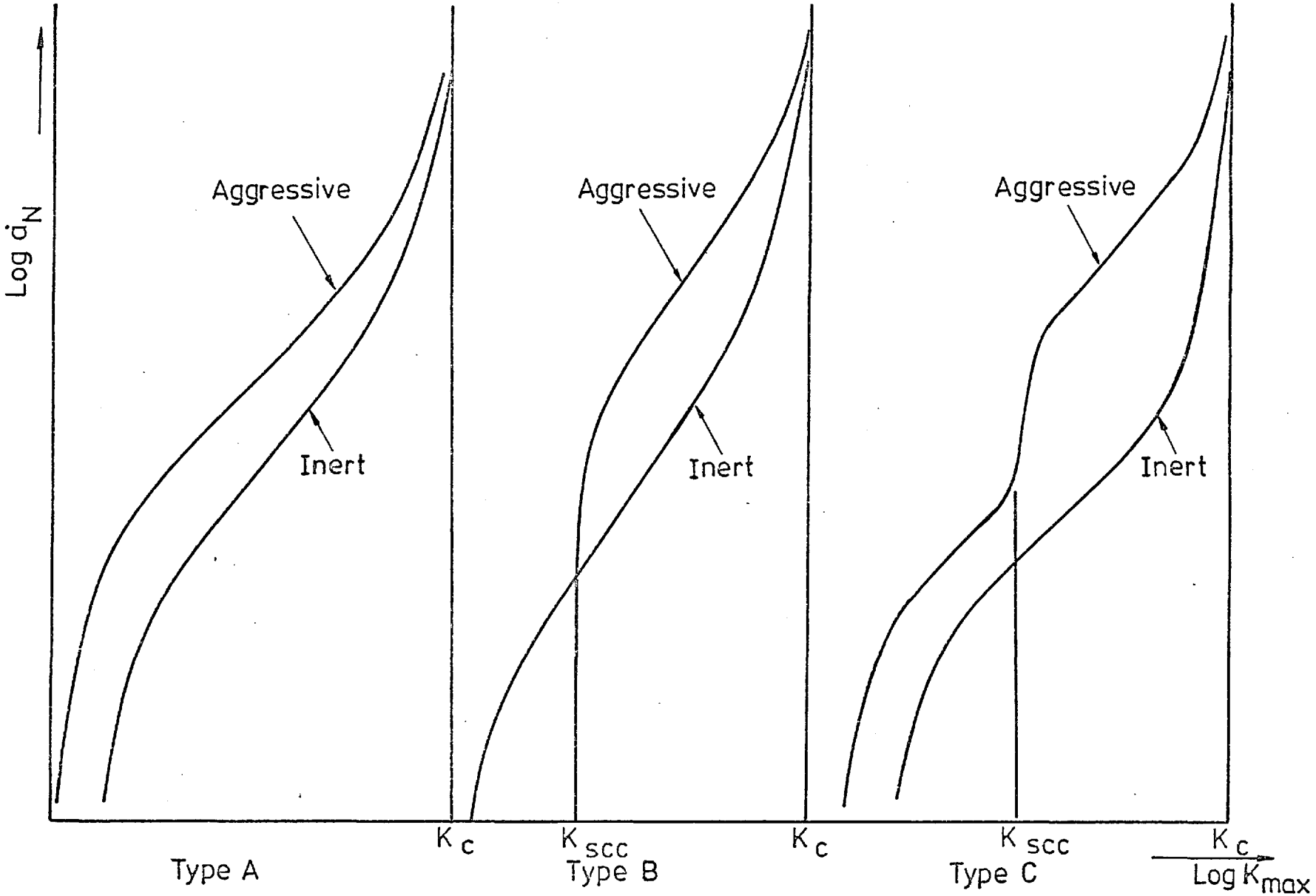

Figure 1: Types of fatigue crack growth behaviour in metals (after McEvily and Wei, 1971)

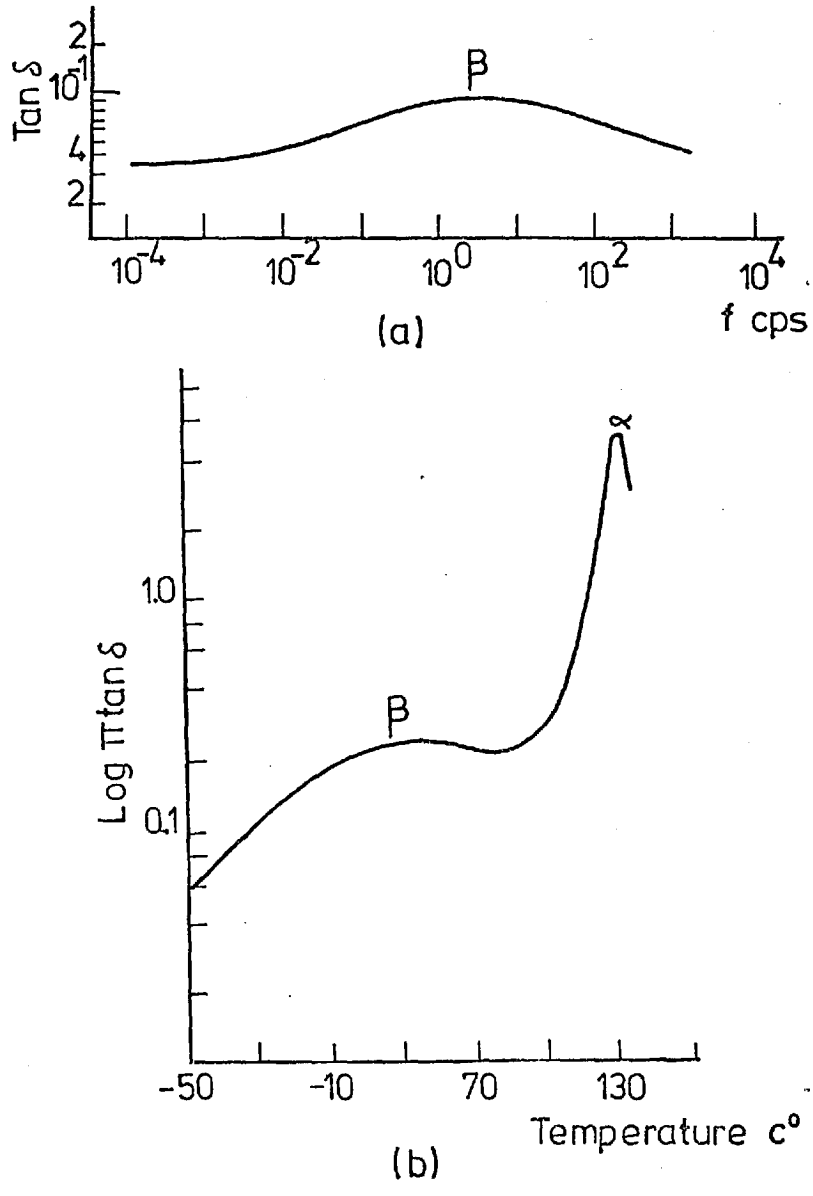

Figure 2: (a) Loss tangent of PMMA near 25°C (after Koppelmann, 1958)

(b) Temperature dependence of tan δ for PMMA at 1 cps (after Nielsen, 1962)

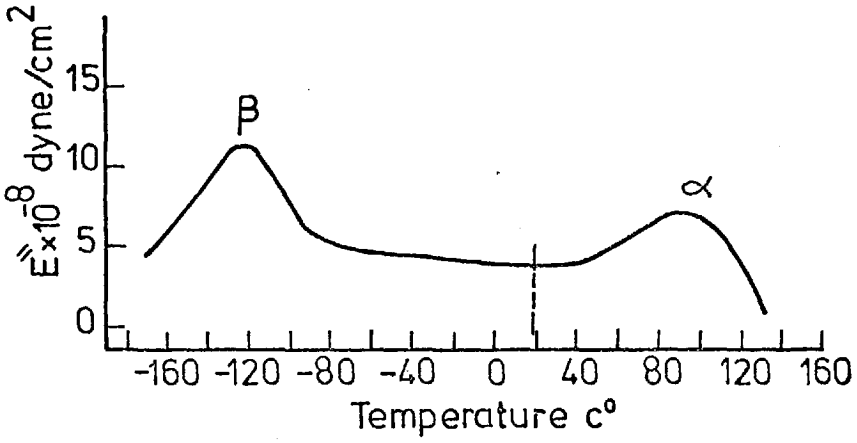

Figure 3: Loss modulus against temperature for polyethylene at 110 cps (after Takayanagi, 1967)

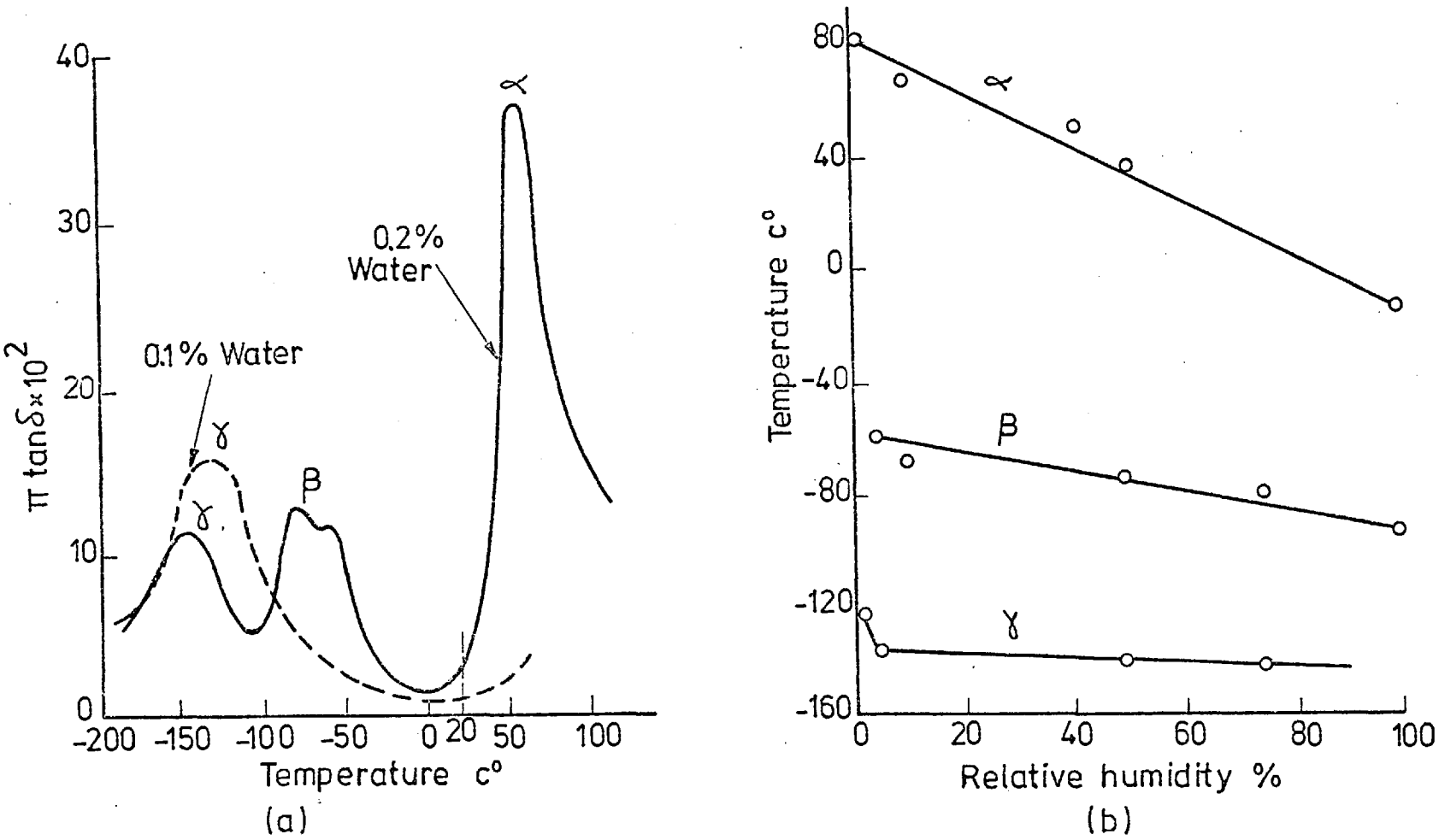

Figure 4: (a) Loss tangent against temperature for almost dry nylon 66, f = 1 cps (after Starkweather, 1973)

(b) Peak temperature dependence on water content in nylon 66, (nylon 66 saturated at different relative humidities) (after Starkweather, 1973)

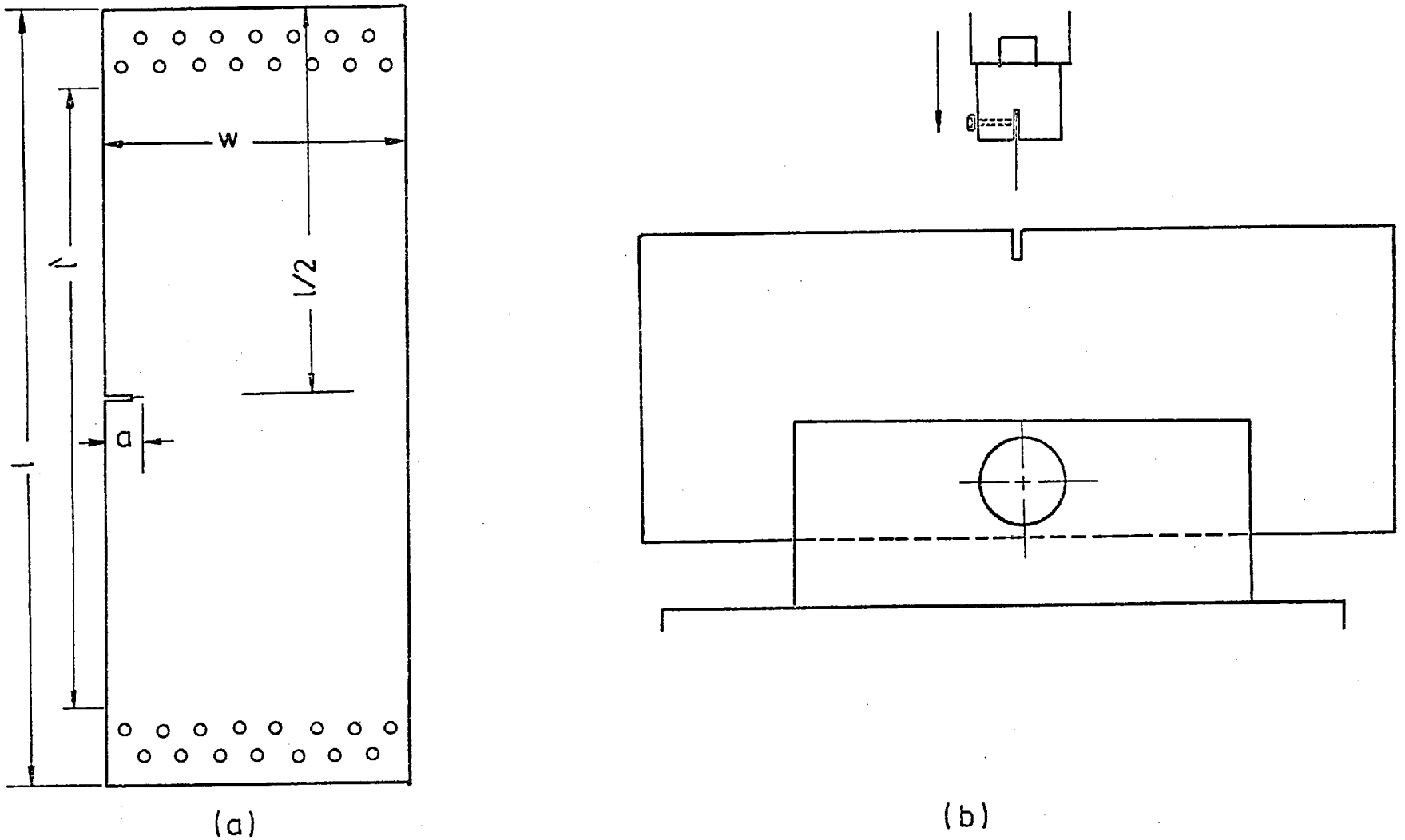

Figure 5: (a) SEN specimen geometry

(b) Method of notching

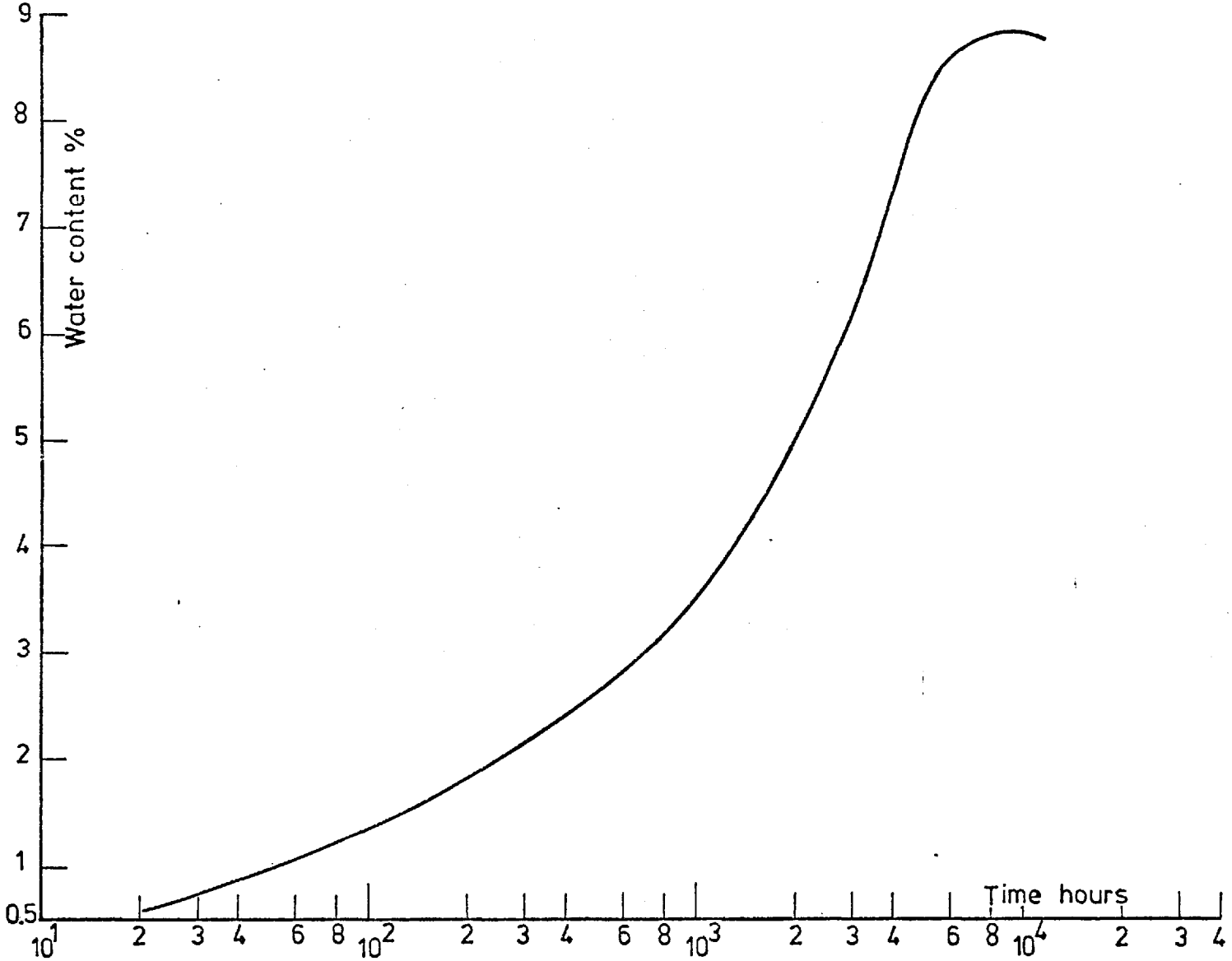

Figure 6: Rate of water absorption of N66 (Maranyl AD151) in distilled water (100% RH) at 20°C

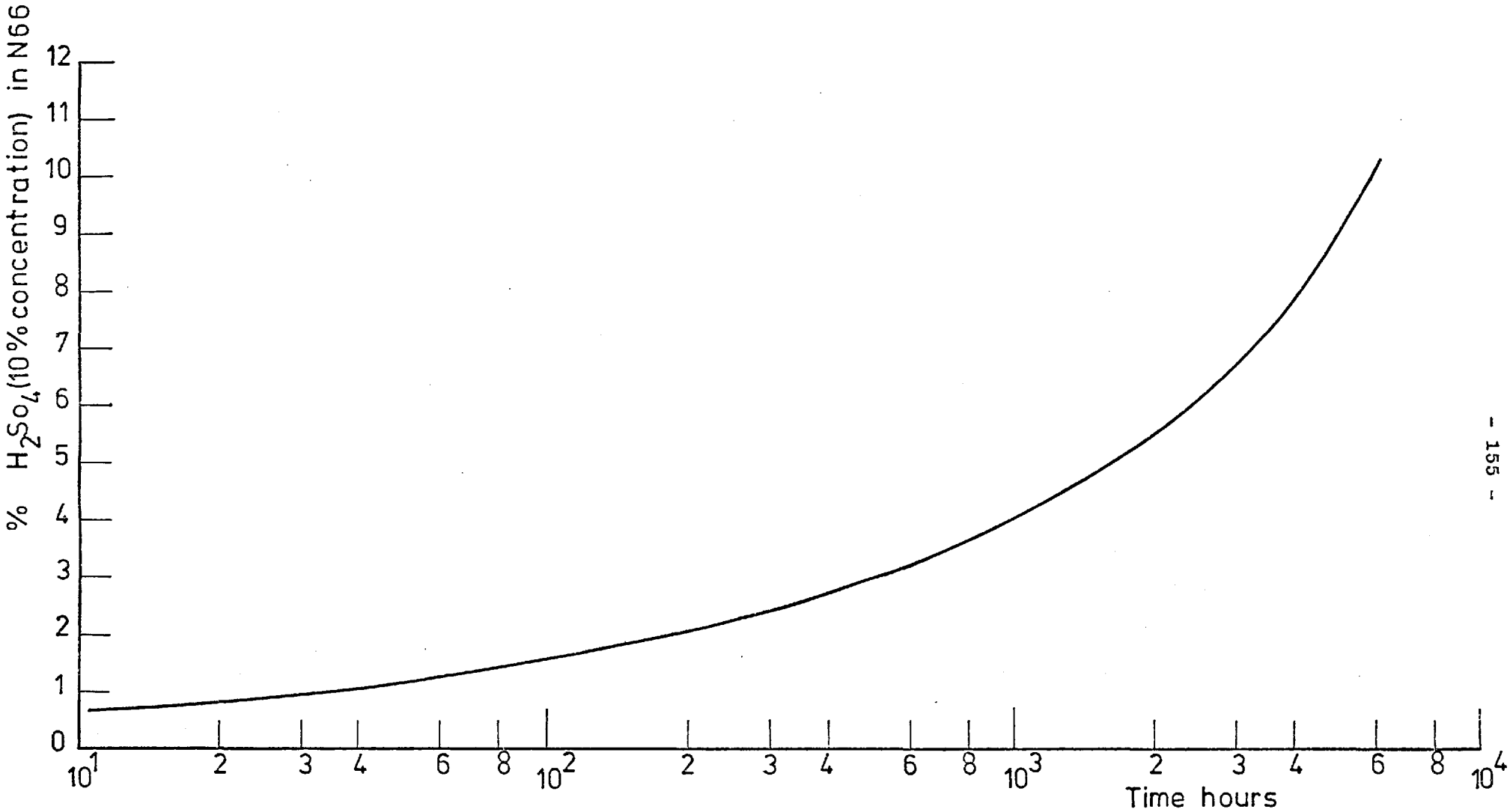

Figure 7: Rate of absorption of diluted H_2SO_4 (10% concentration) - N66 in an environment of H_2SO_4 of 10% concentration at 20°C

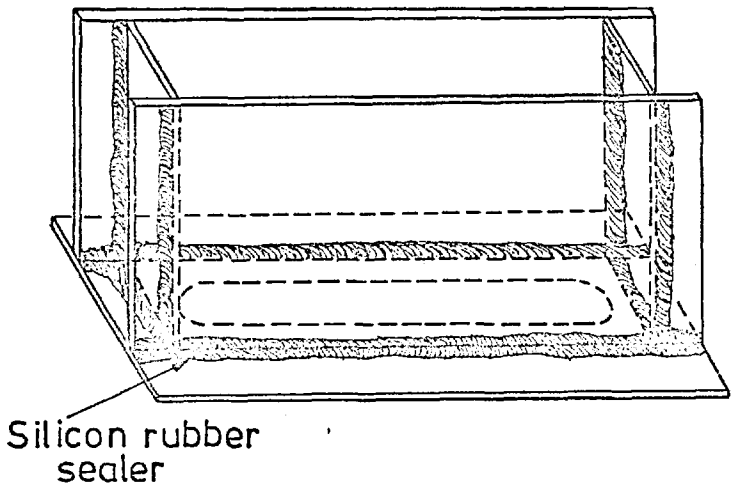

(a)

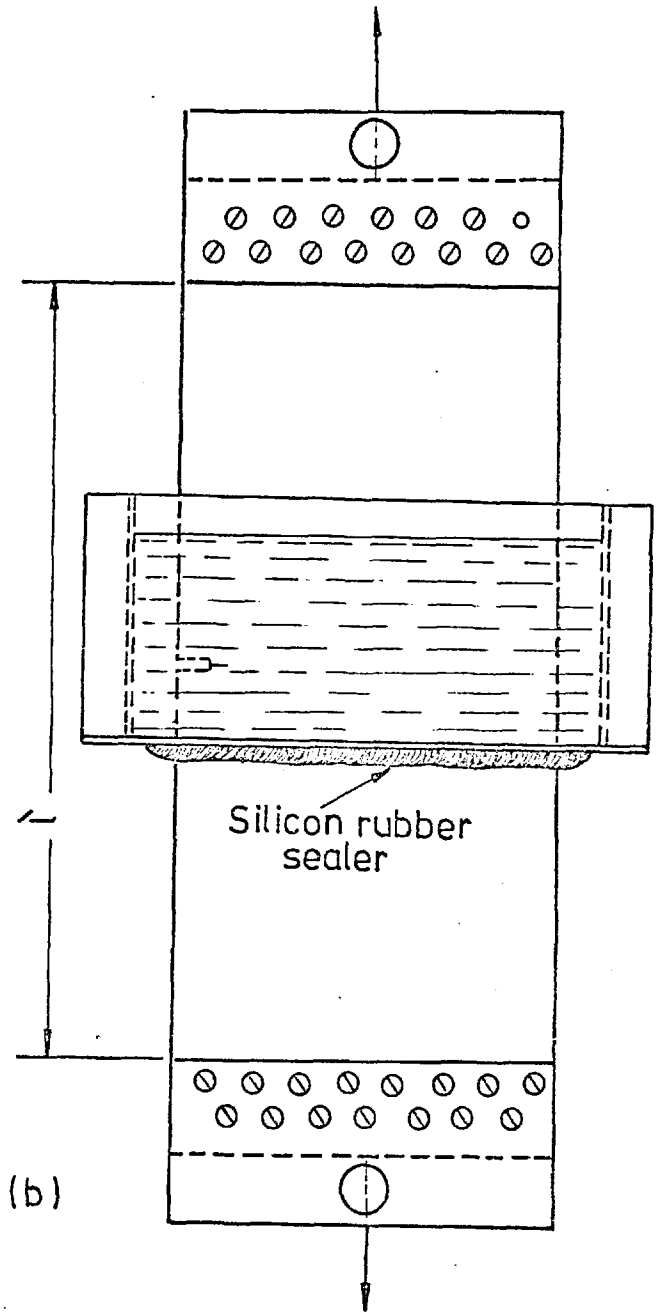

Figure 8: (a) The mini-tank

(b) Specimen in mini-tank and bolted to two pairs of steel plates

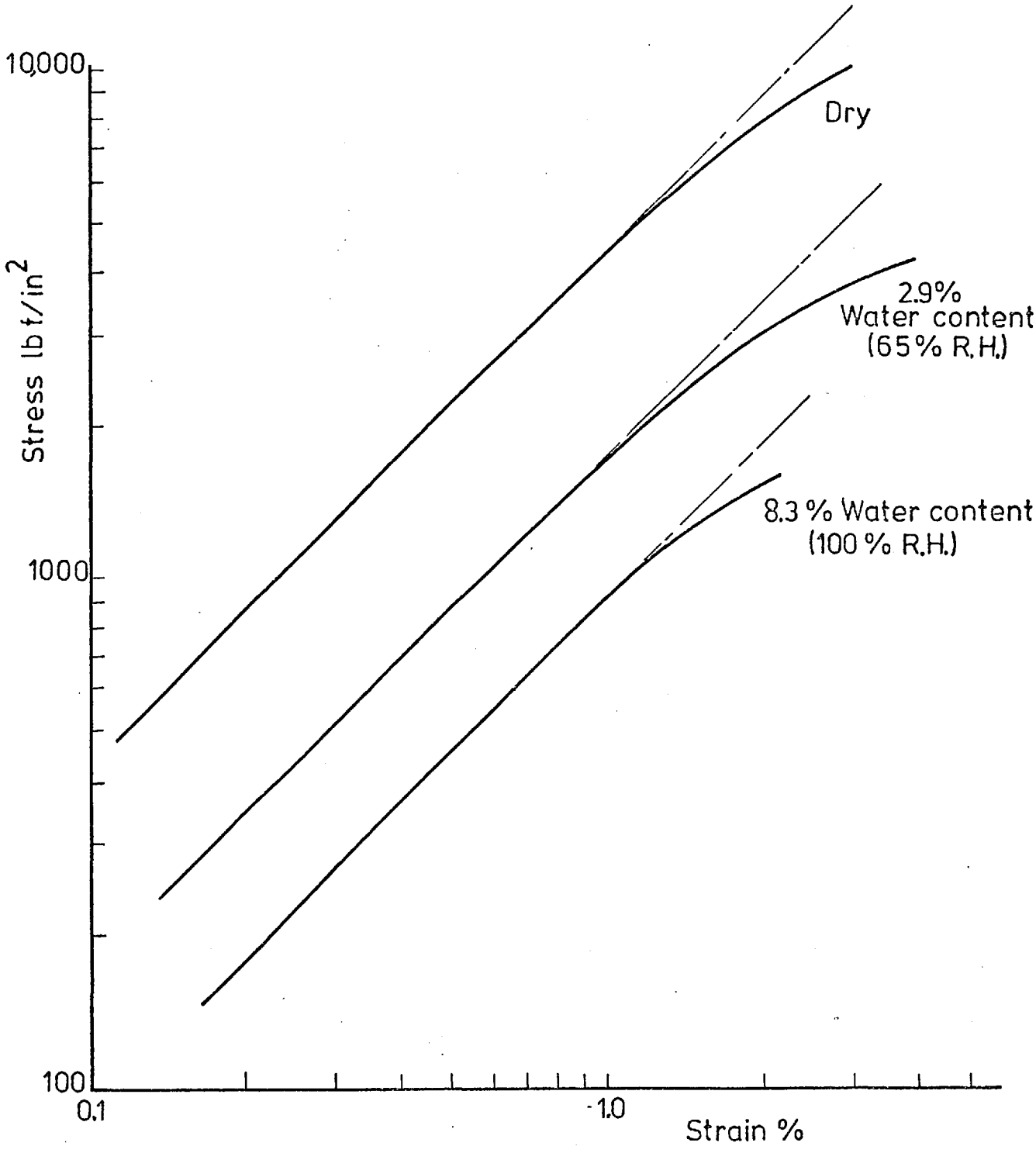

Figure 9: Isochronous stress vs. strain curve, 20°C, 100 sec, log axes. Effect of water content. Nylon 66 (Maranyl A100, A101) (after Ogorkiewicz, 1970)

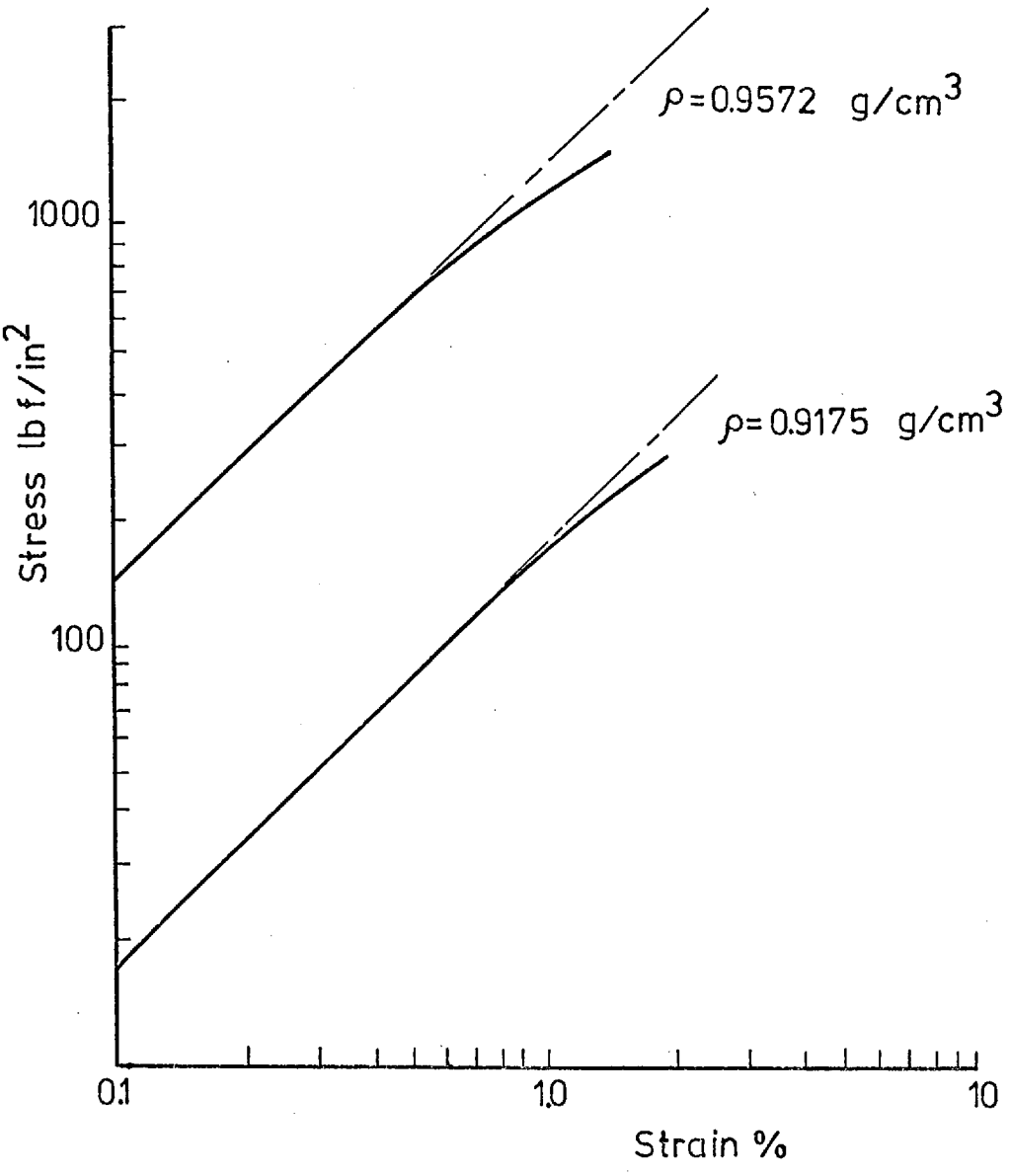

Figure 10: Isochronous stress vs. strain curve, 20°C, 100 sec, log axes. Effect of density on non-linearity, quenched from 190°C. Polyethylene, low density and high density grades (after Ogorkiewicz, 1970)

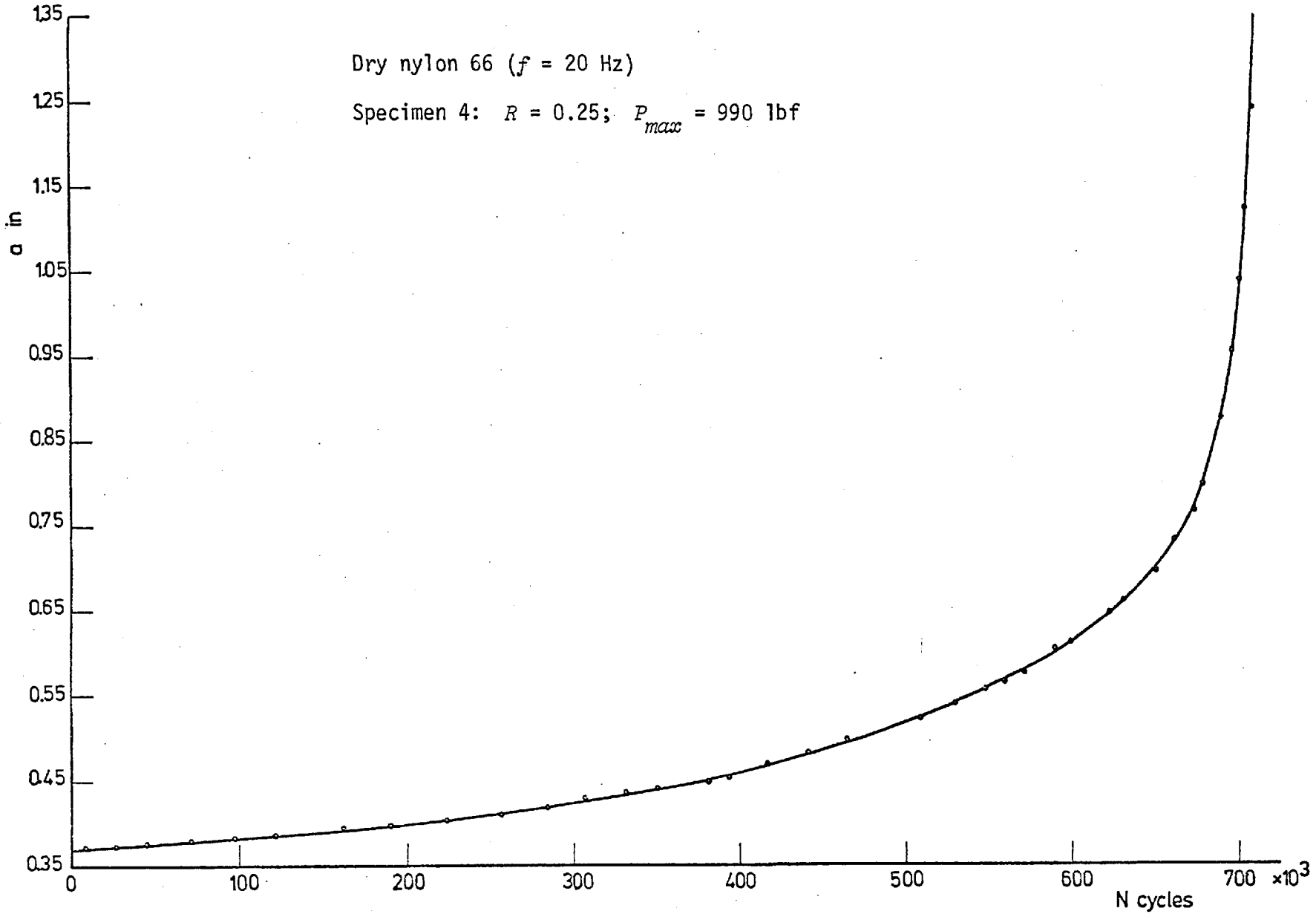

Figure 11: Crack length vs. number of cycles - dry nylon 66 tested in air

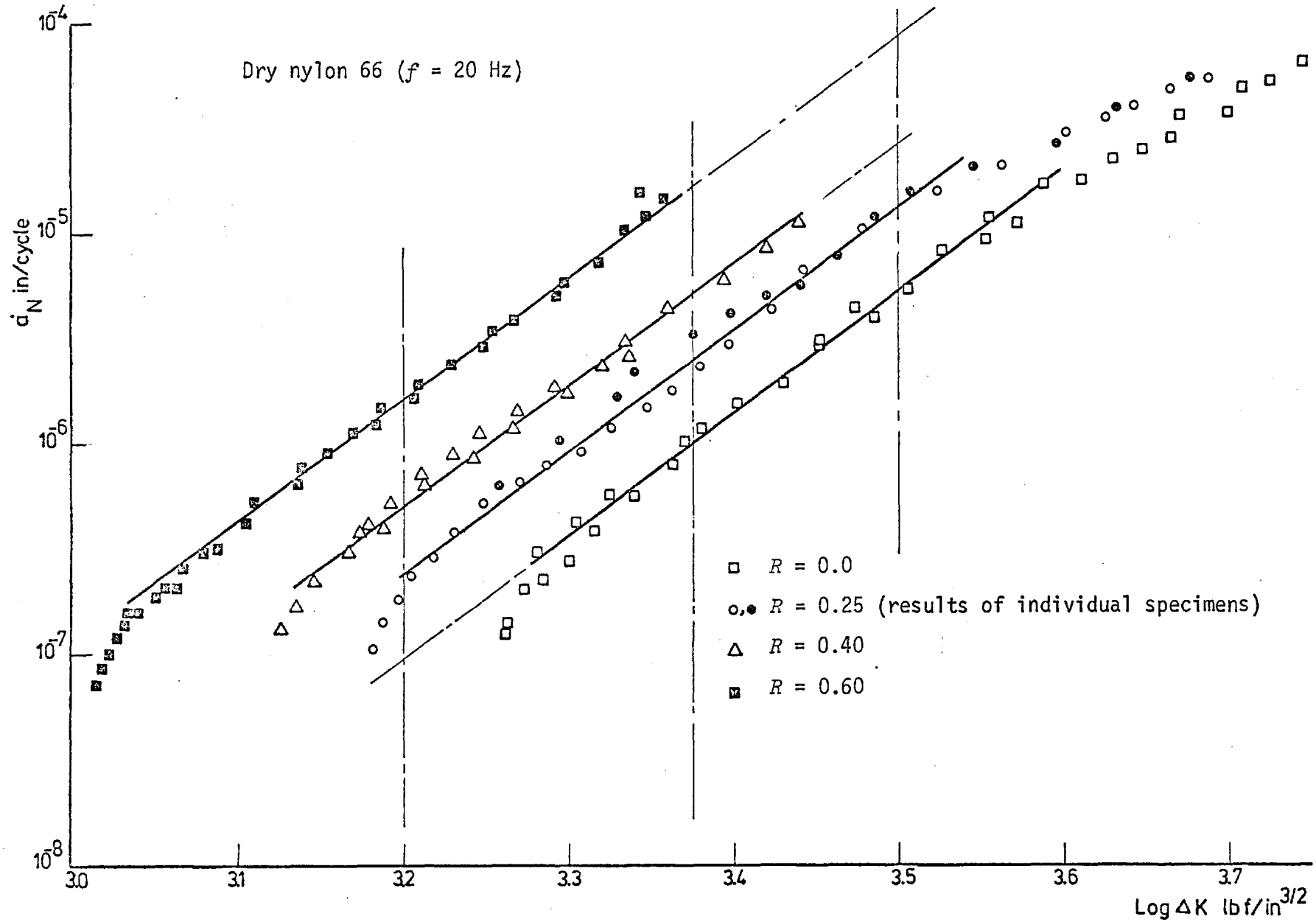

Figure 12: The relationship between log $\dot{a}_N$ and log ΔK for dry nylon 66 tested in air (20°C, 50% RH) at f = 20 Hz

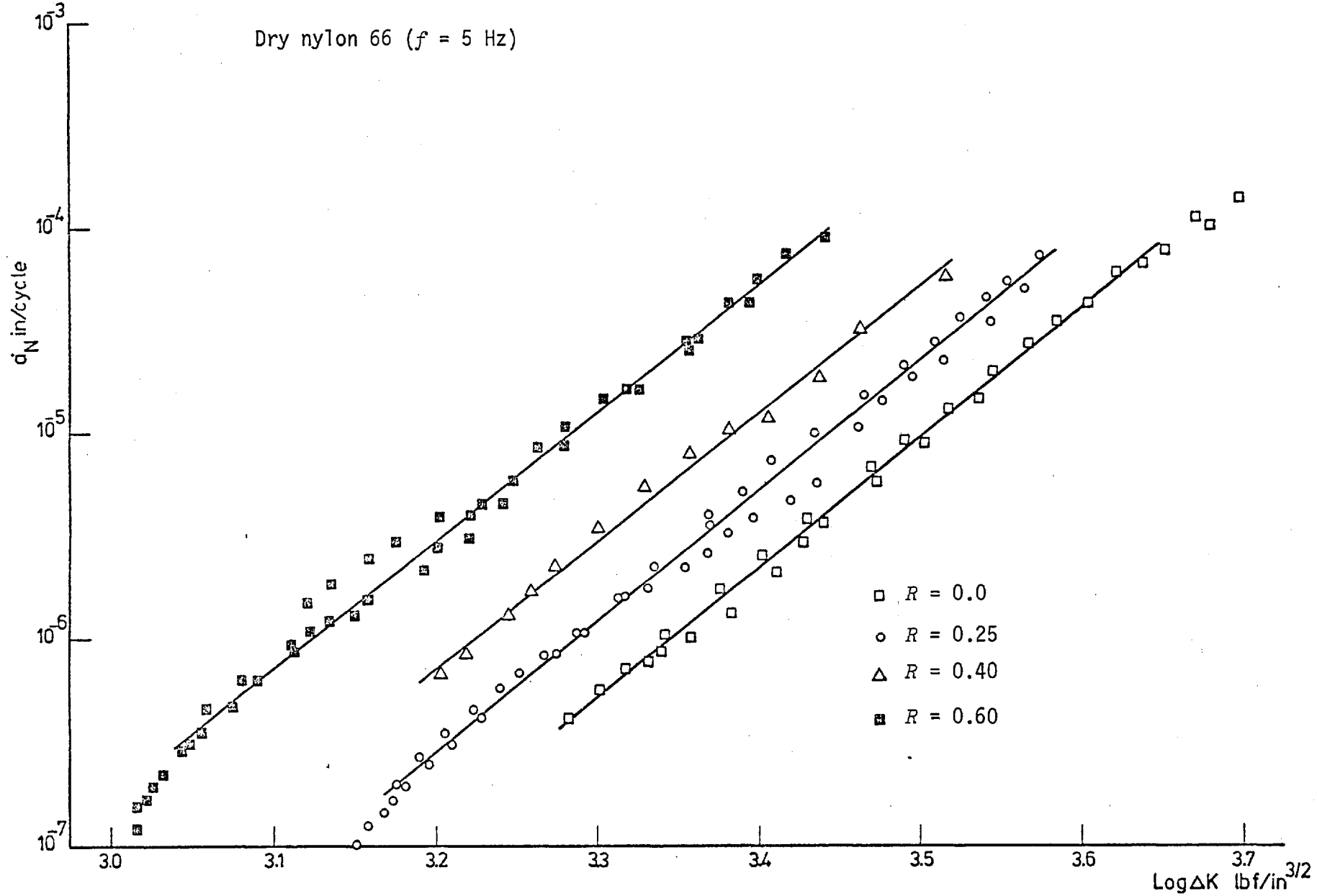

Figure 13: The log $\dot{a}_N$-log ΔK relationship of dry nylon 66 tested in air (20°C, 50% RH) at f = 5 Hz

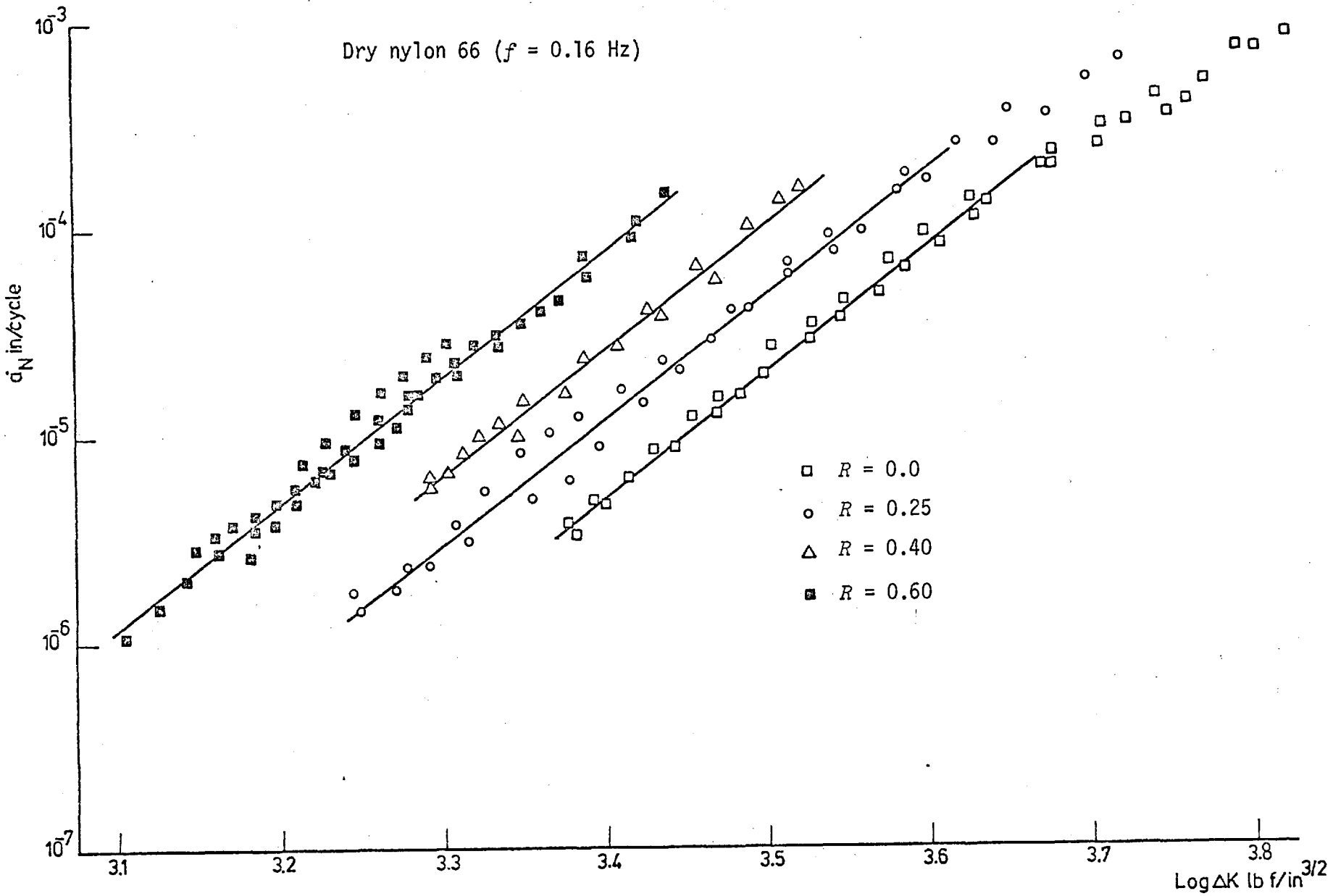

Figure 14: The log $\dot{a}_N$-log ΔK relationship of dry nylon 66 tested in air (20°C, 50% RH) at f = 0.16 Hz

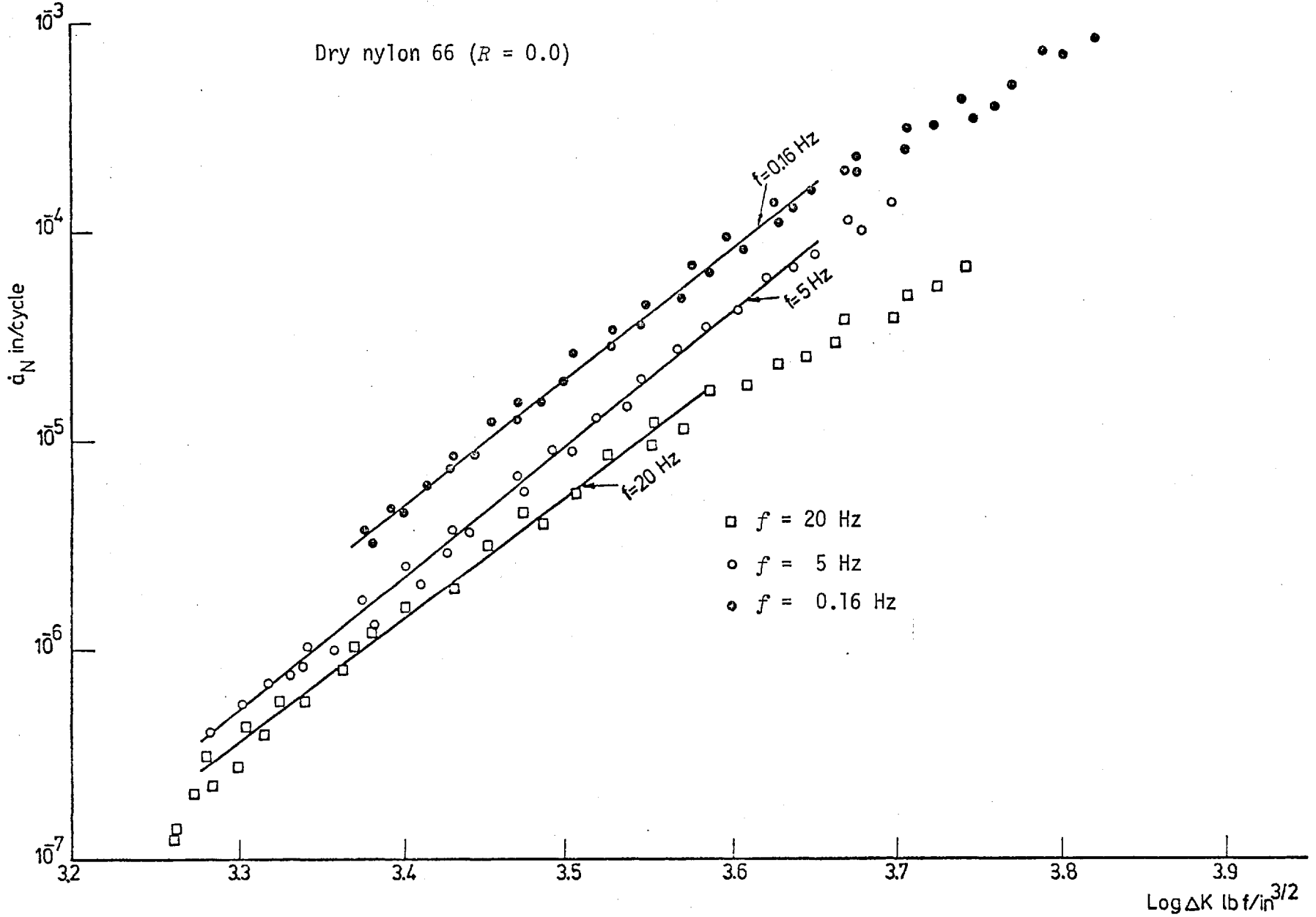

Figure 15: The log $\dot{a}_N$-log ΔK relationship of dry nylon 66 tested in air at R = 0.0 at different frequencies

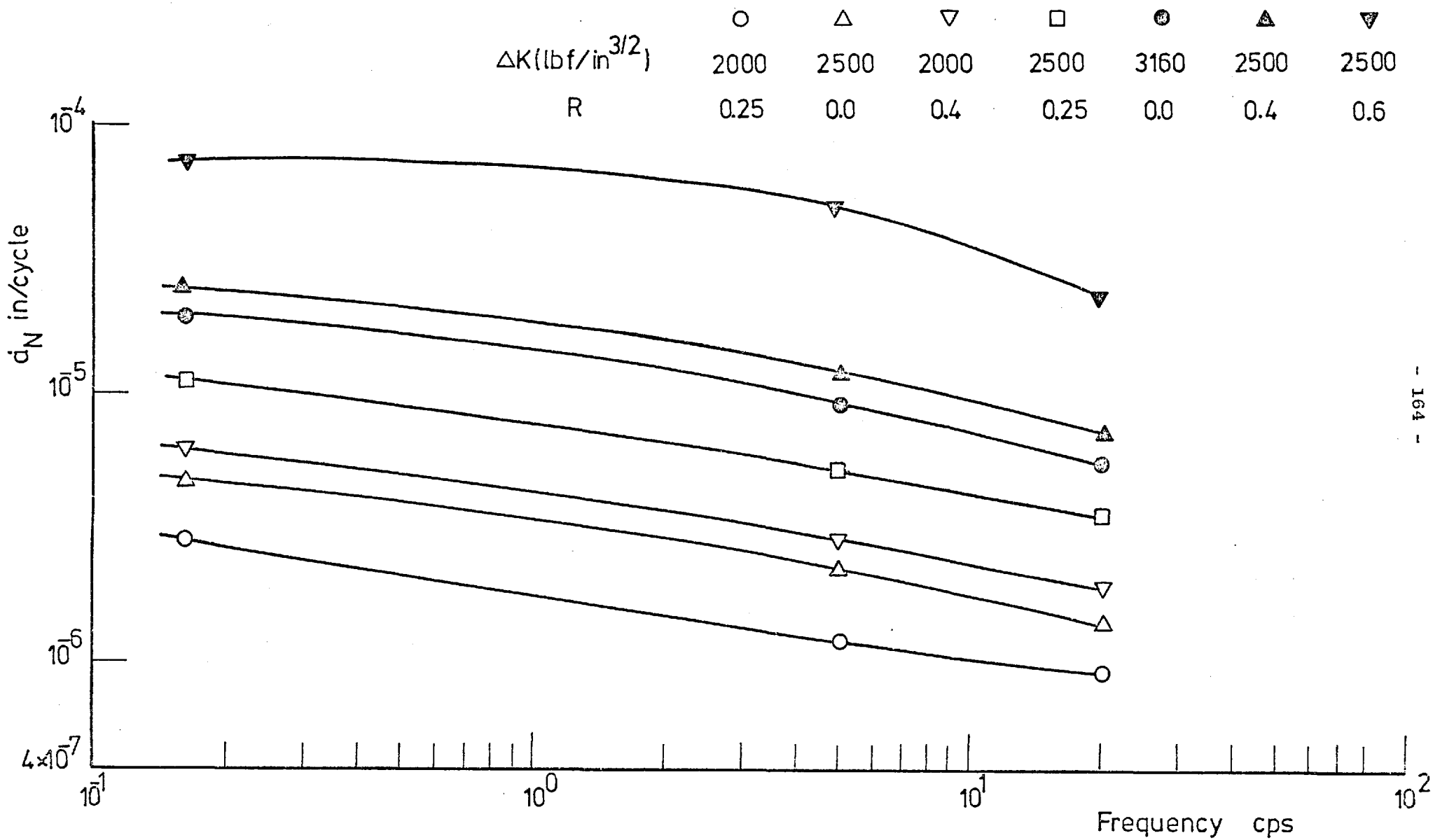

Figure 16: Variation of $\dot{a}_N$ with frequency, for dry N66, in air at different constant values of R and ΔK

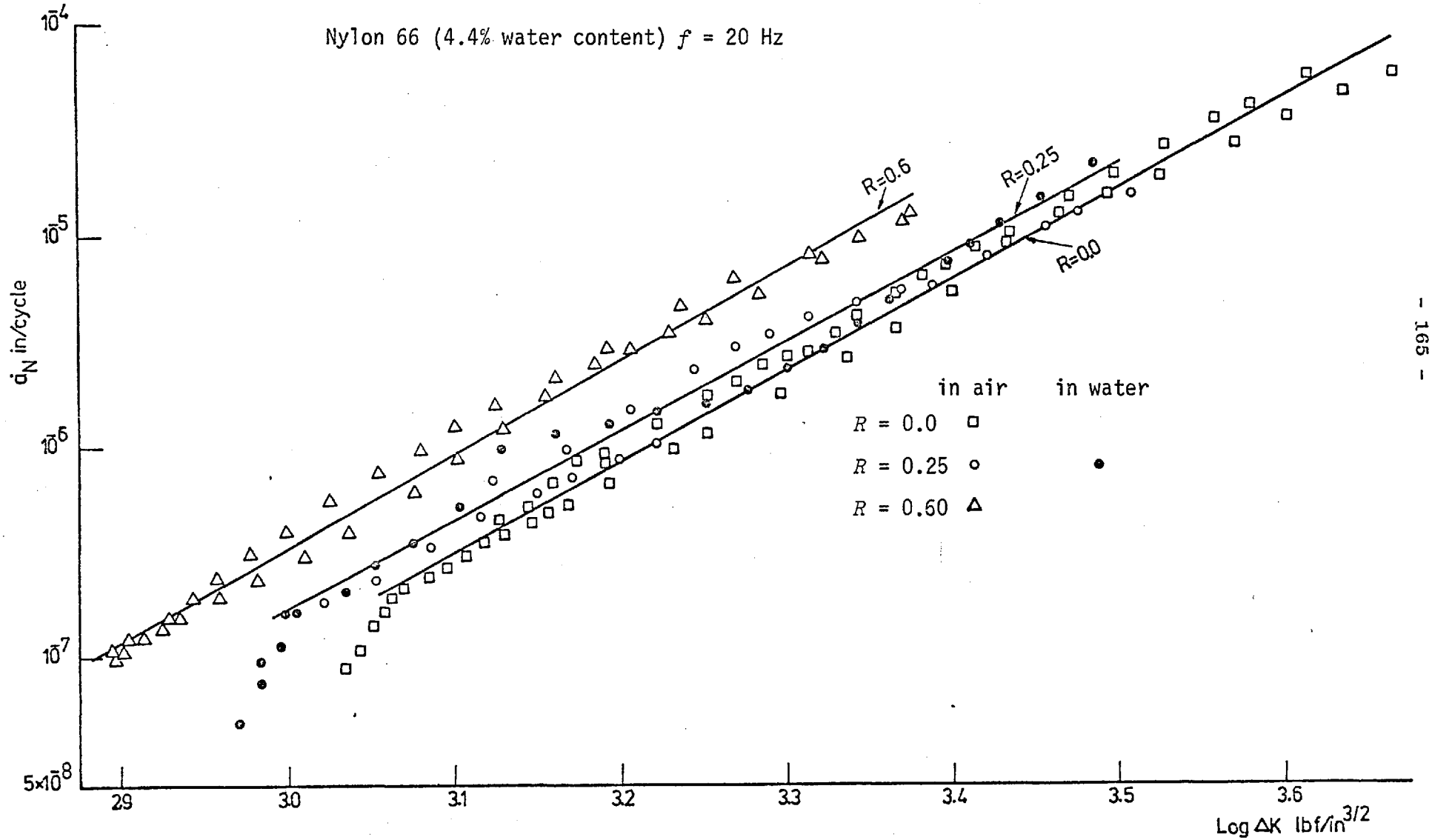

Figure 17: The log $\dot{a}_N$-log ΔK relationship of N66 (4.4% water content) tested in air and distilled water at f = 20 Hz

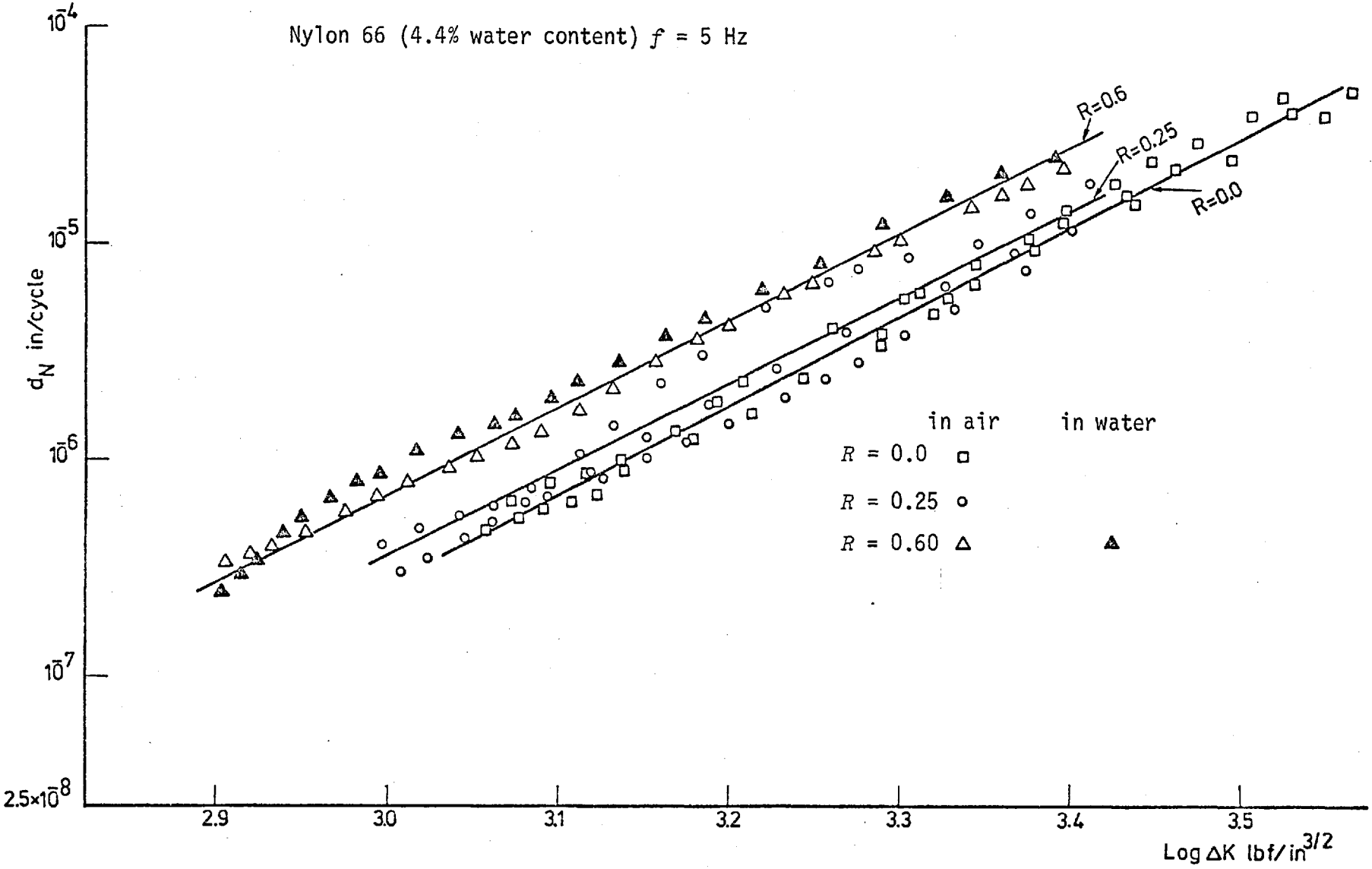

Figure 18: The log α_N-log ΔK relationship of N66 (4.4% water content) tested in air and distilled water at f = 5 Hz

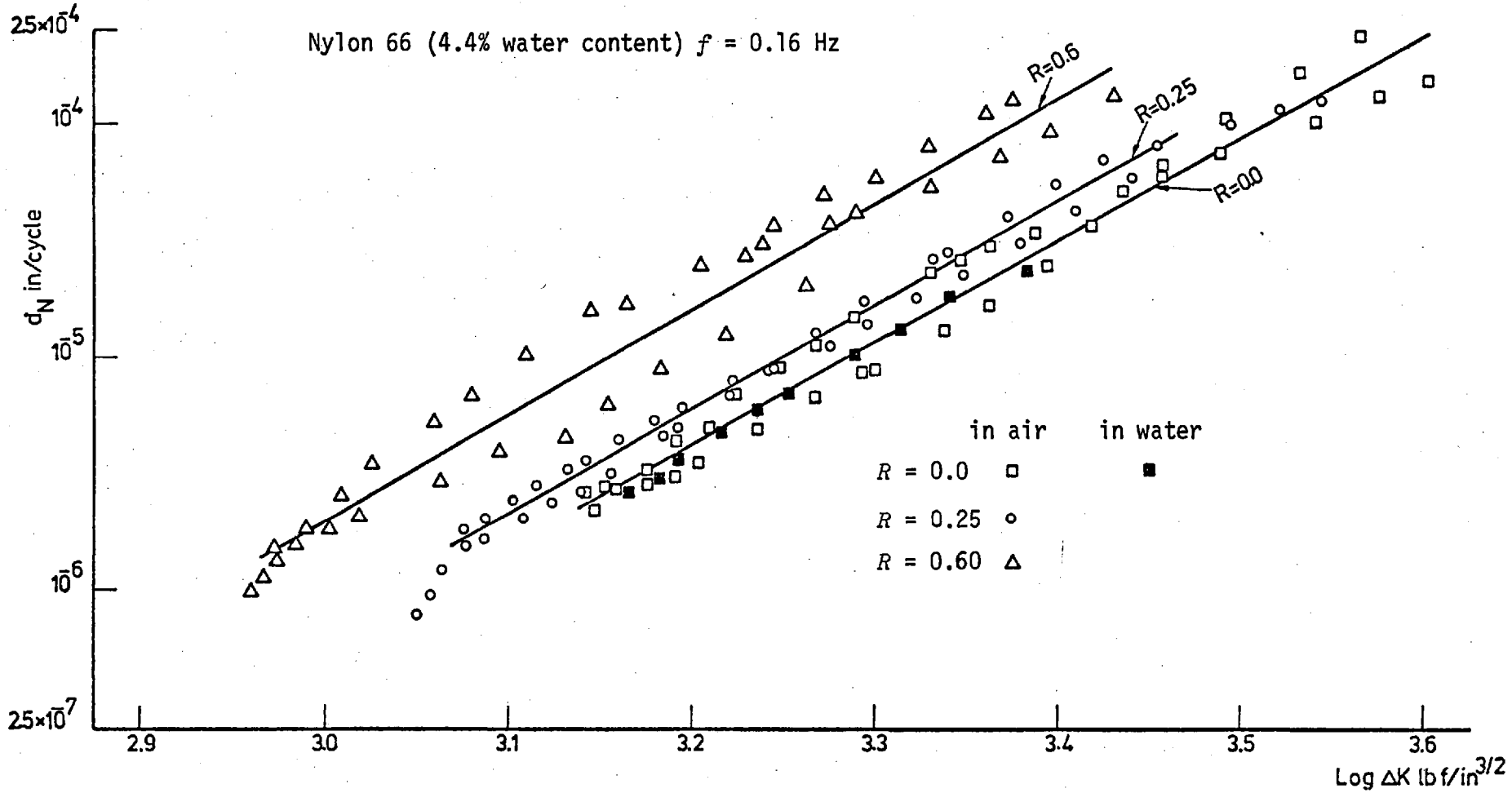

Figure 19: The log $\dot{a}_N$-log ΔK relationship of N66 (4.4% water content) tested in air and distilled water at f = 0.16 Hz

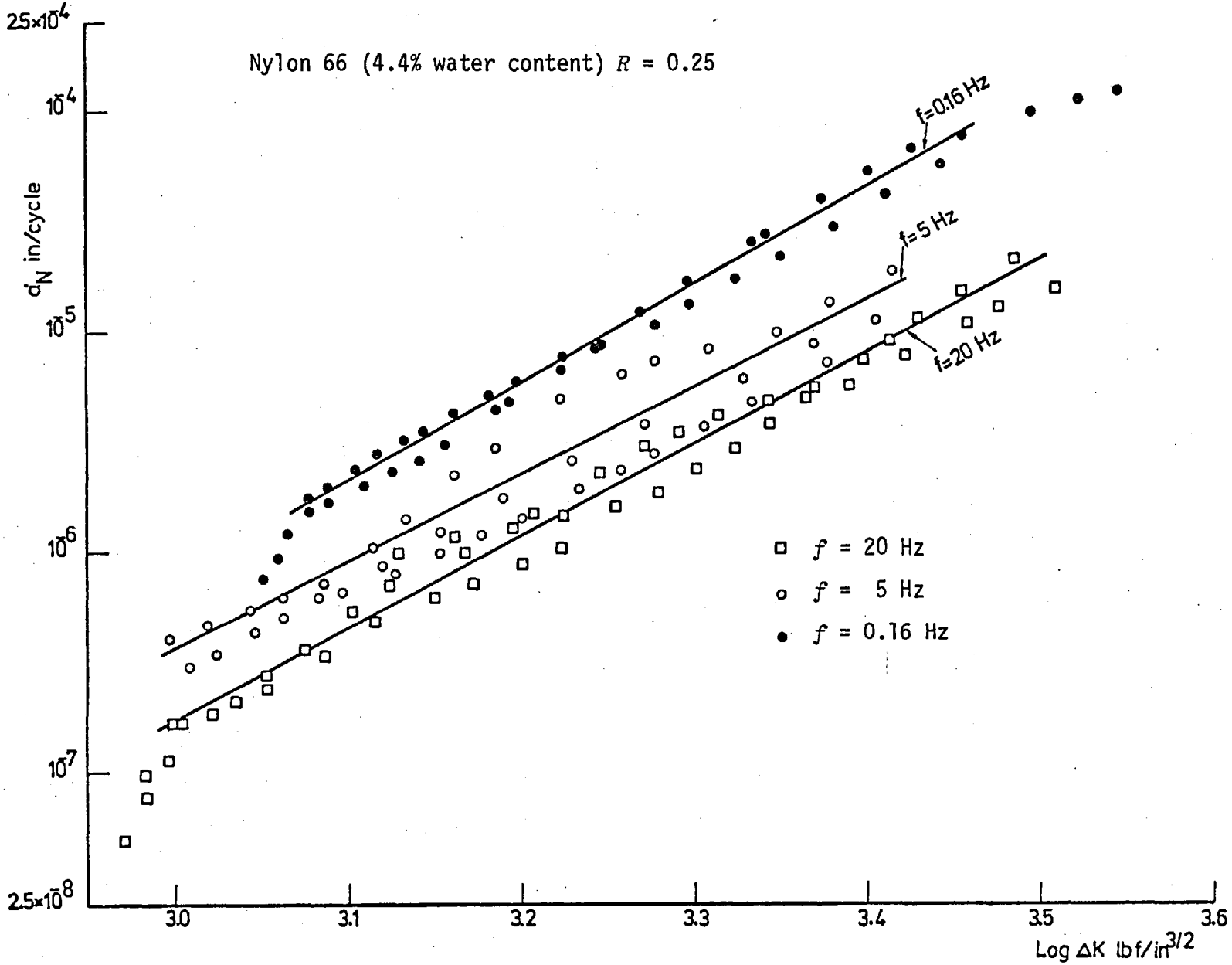

Figure 20: The log α_N-log ΔK relationship of N66 (4.4% water content) tested in air and distilled water at R = 0.25 and different frequencies

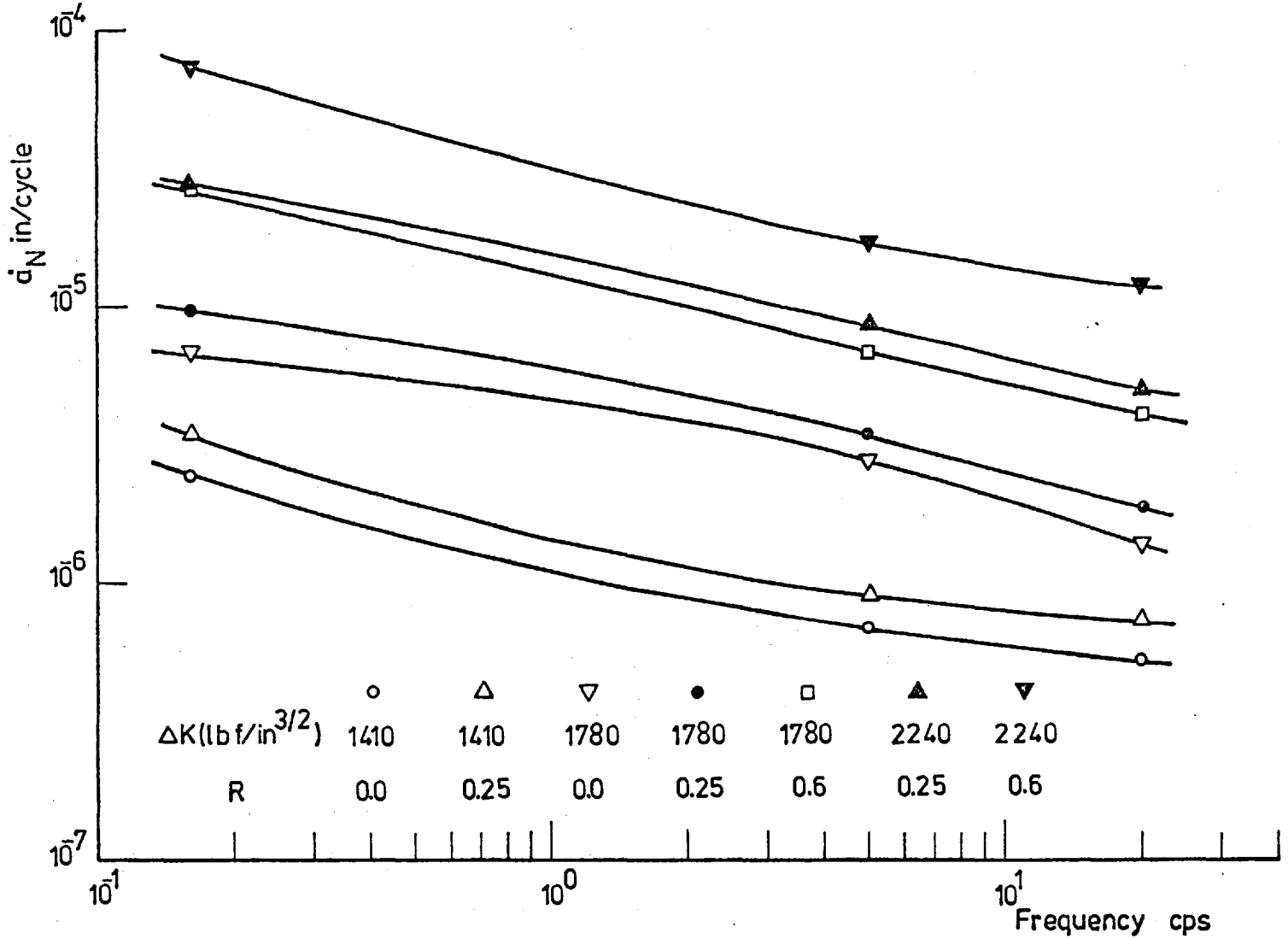

Figure 21: Variation of $\dot{a}_N$ with frequency, for N66 (4.4% water content) in air and distilled water, at different constant values of R and ΔK

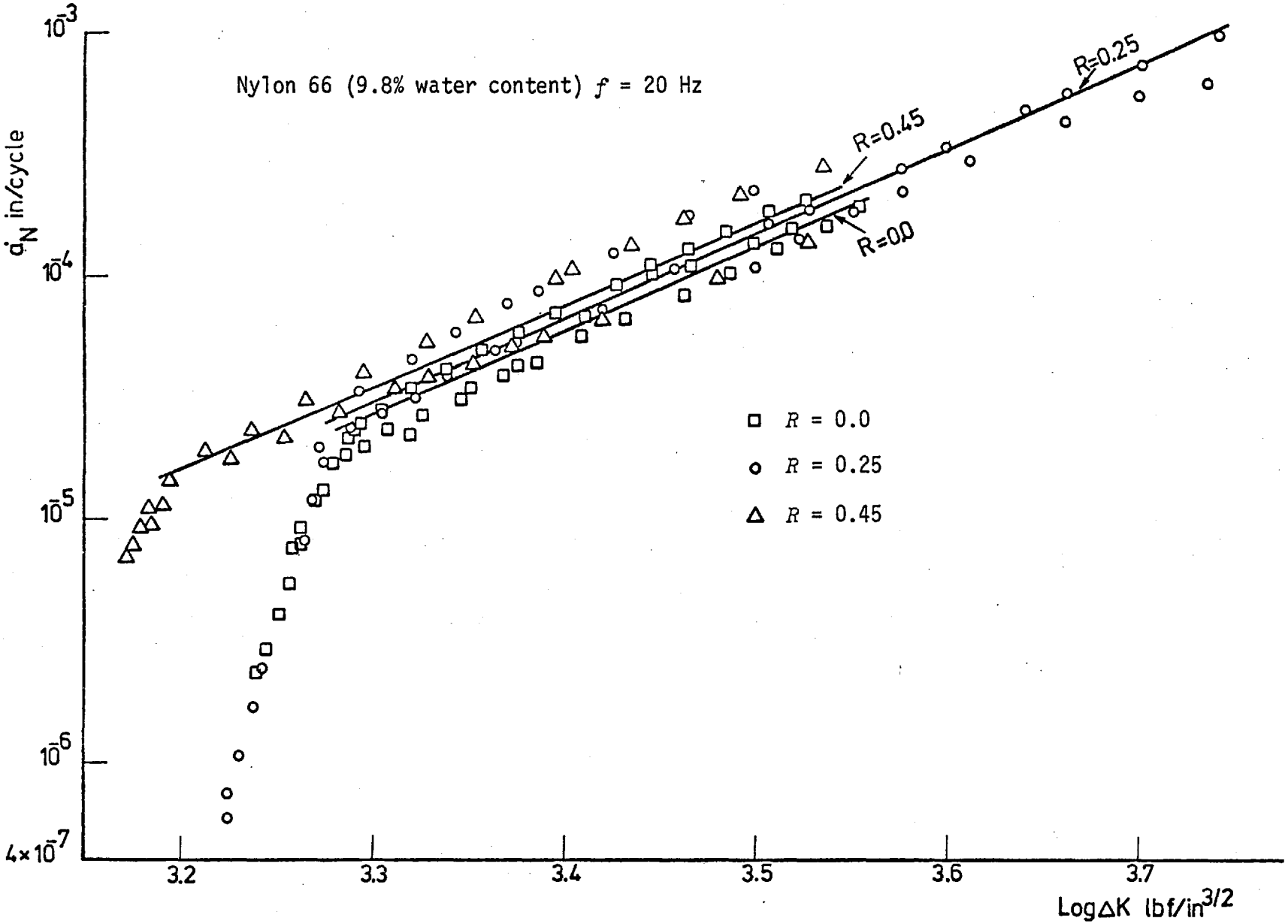

Figure 22: The log $\dot{a}_N$-log ΔK relationship of N66 (9.8% water content) tested in distilled water

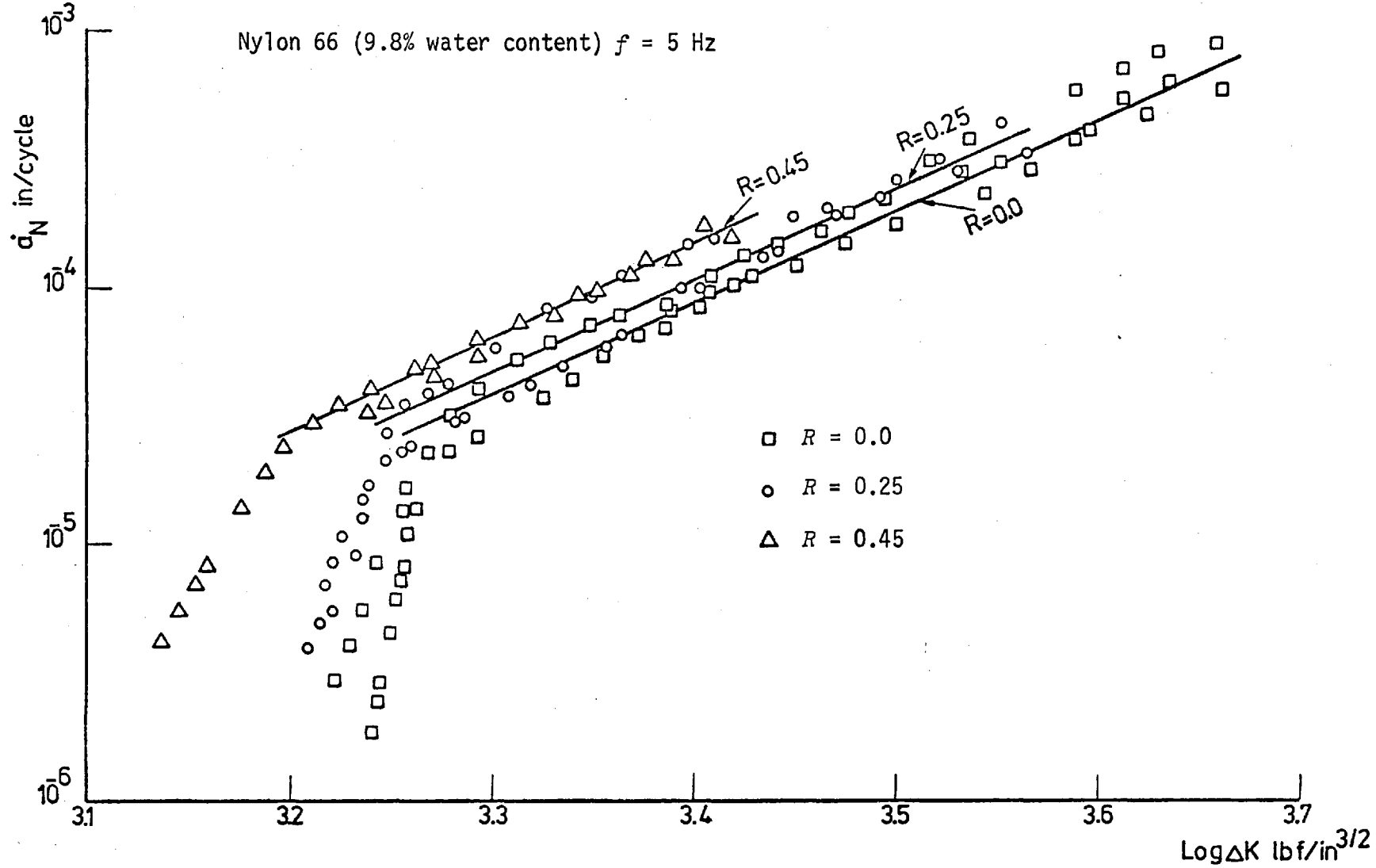

Figure 23: The log $\dot{a}_N$-log ΔK relationship of N66 (9.8% water content) tested in distilled water at f = 5 Hz

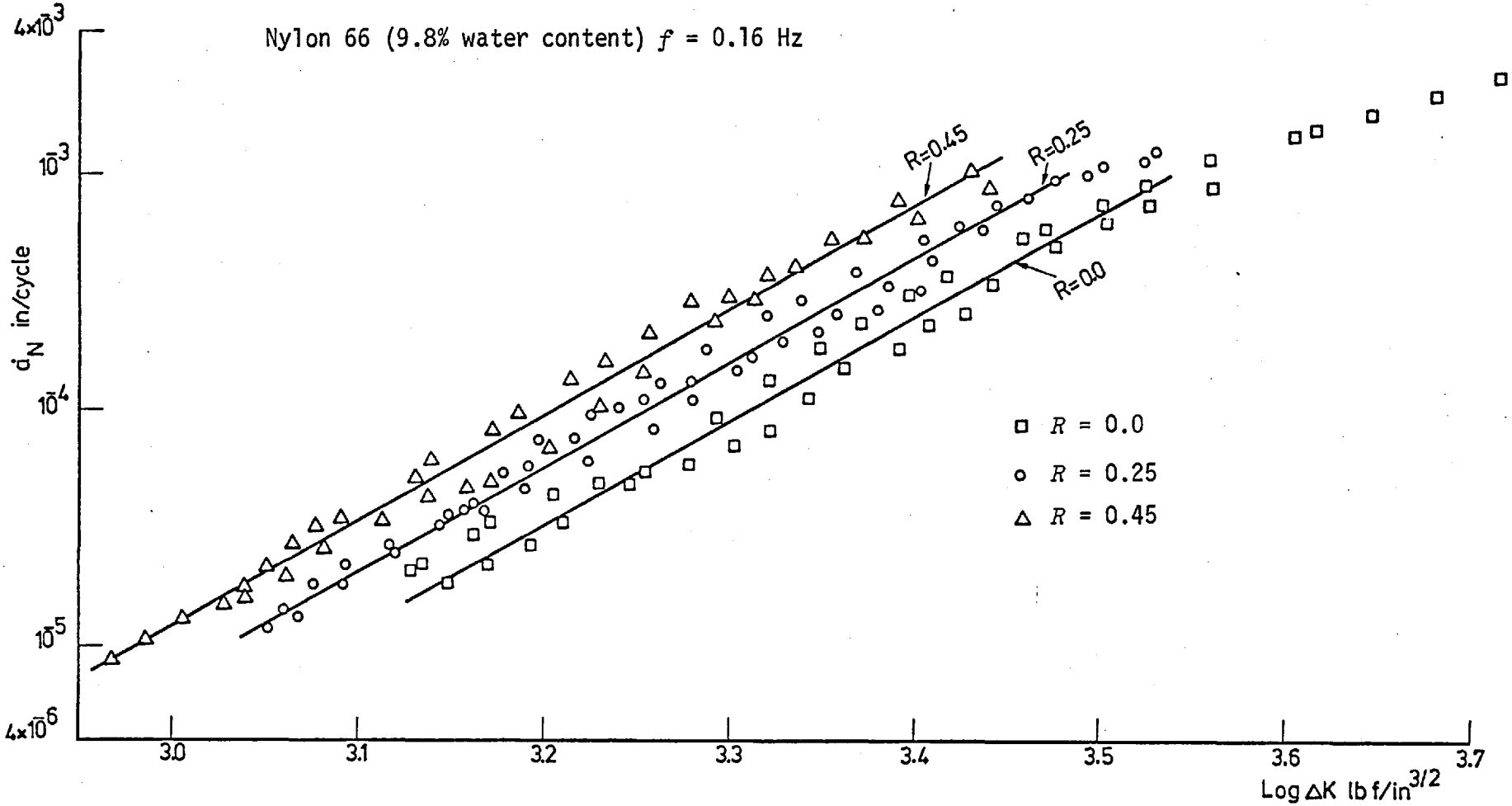

Figure 24: The log $\dot{a}_N$-log ΔK relationship of N66 (9.8% water content) tested in distilled water at f = 0.16 Hz

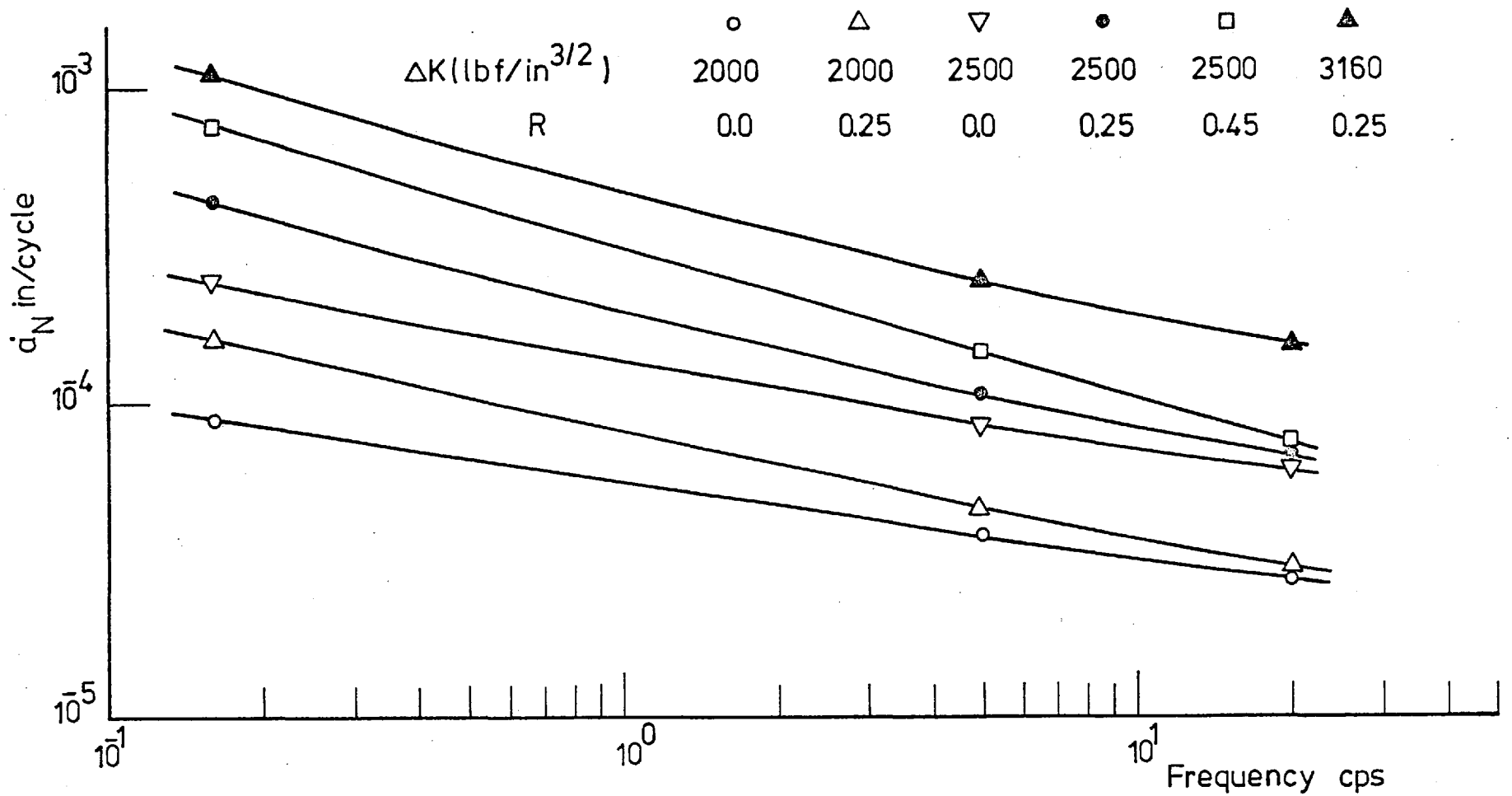

Figure 25: Variation of $\dot{a}_N$ with frequency at different constant values of R and ΔK for N66 (9.8% water content) in distilled water

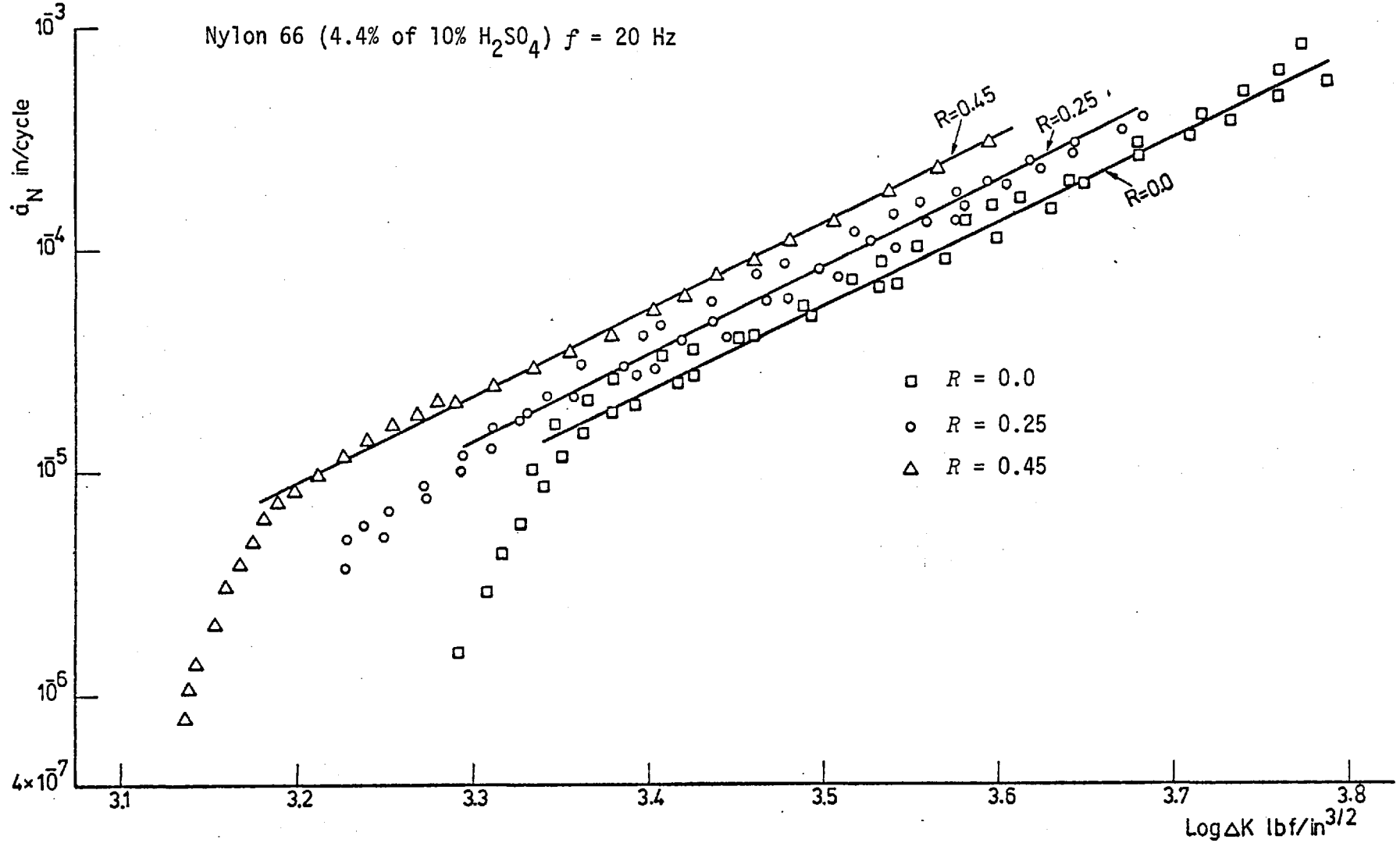

Figure 26: The log $\dot{a}_N$-log ΔK relationship of N66 (4.4% of H_2SO_4 of 10% concentration) tested in 10% H_2SO_4 at f = 20 Hz

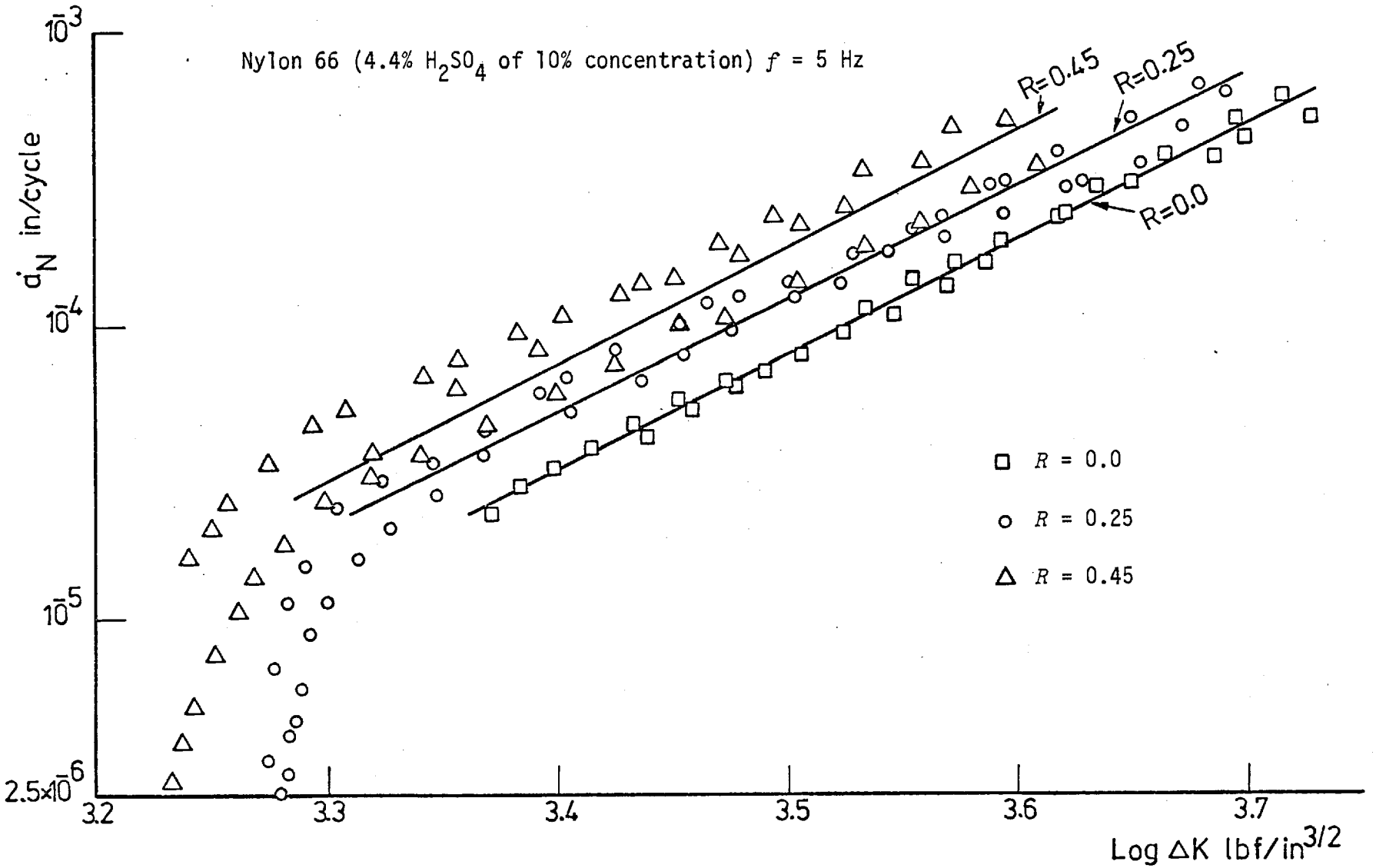

Figure 27: The log $\dot{a}_N$-log ΔK relationship of N66 (4.4% H_2SO_4 of 10% concentration) tested in 10% H_2SO_4 at f = 5 Hz

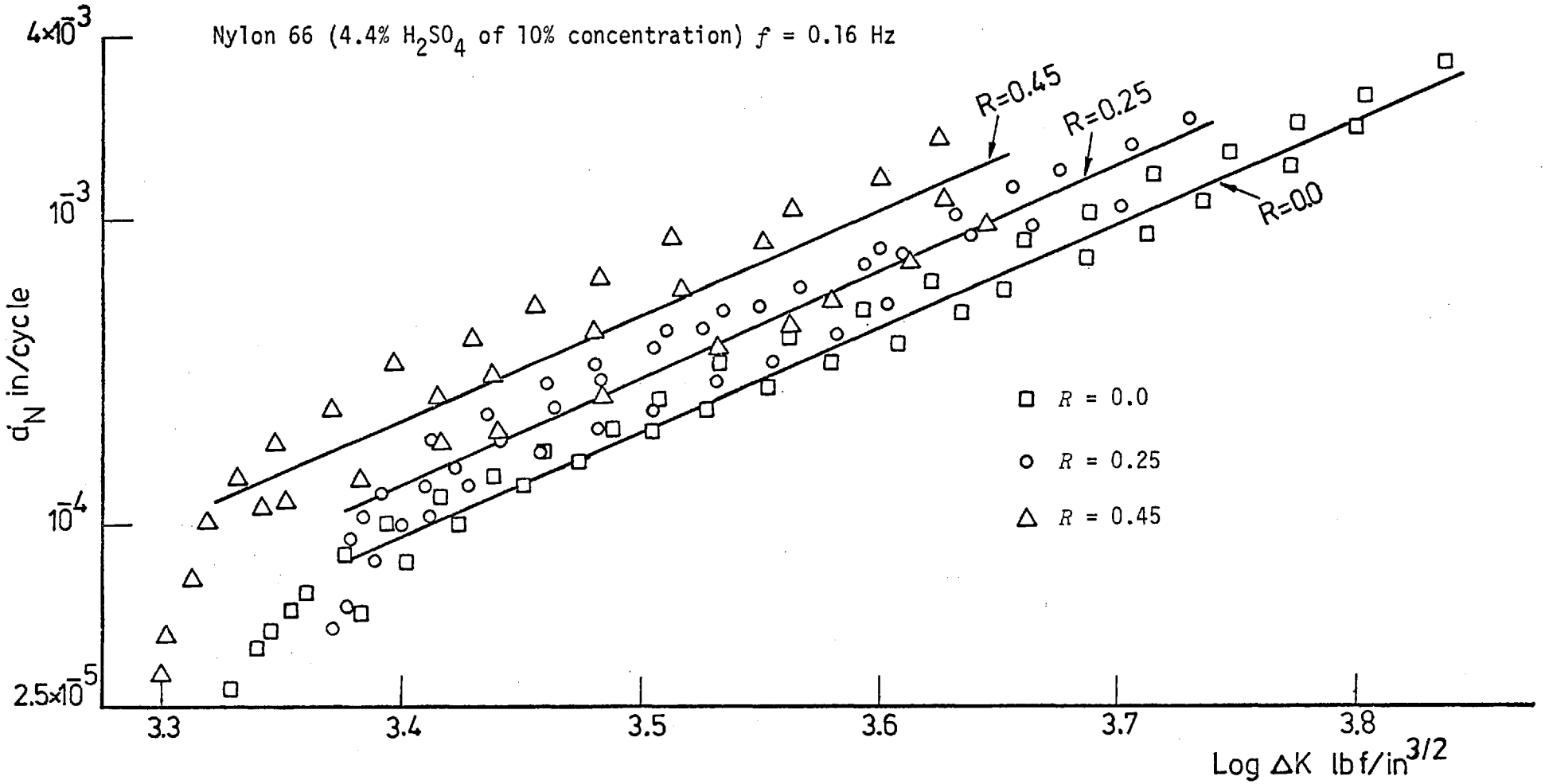

Figure 28: The log $\dot{a}_N$-log ΔK relationship of N66 (4.4% H_2SO_4 of 10% concentration) tested in 10% H_2SO_4 at f = 0.16 Hz

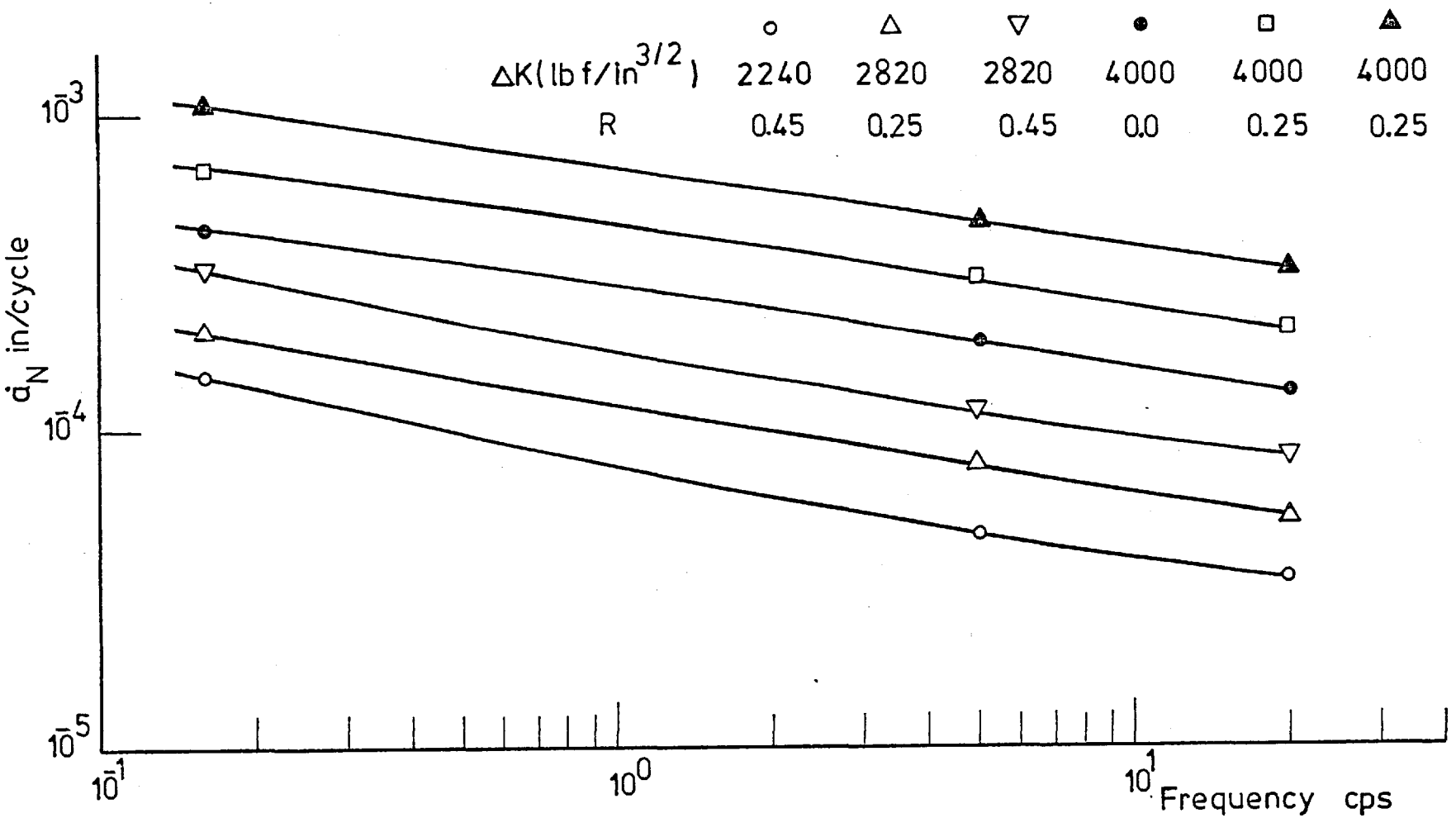

Figure 29: Variation of $\dot{a}_N$ with frequency at different constant values of R and ΔK for N66 (4.4% of 10% H_2SO_4) in 10% H_2SO_4 environment

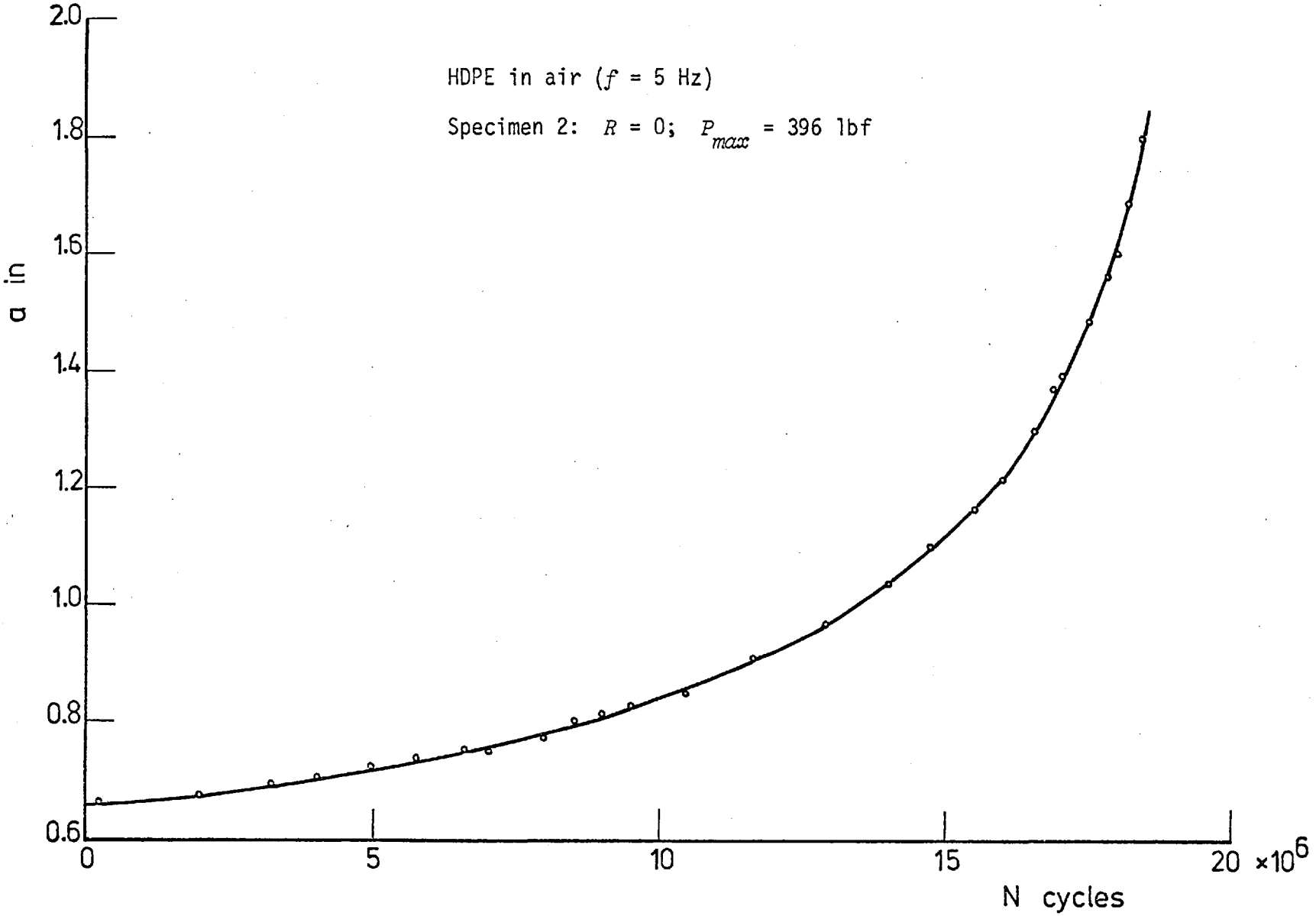

Figure 30: Crack length vs. number of cycles - HDPE tested in air

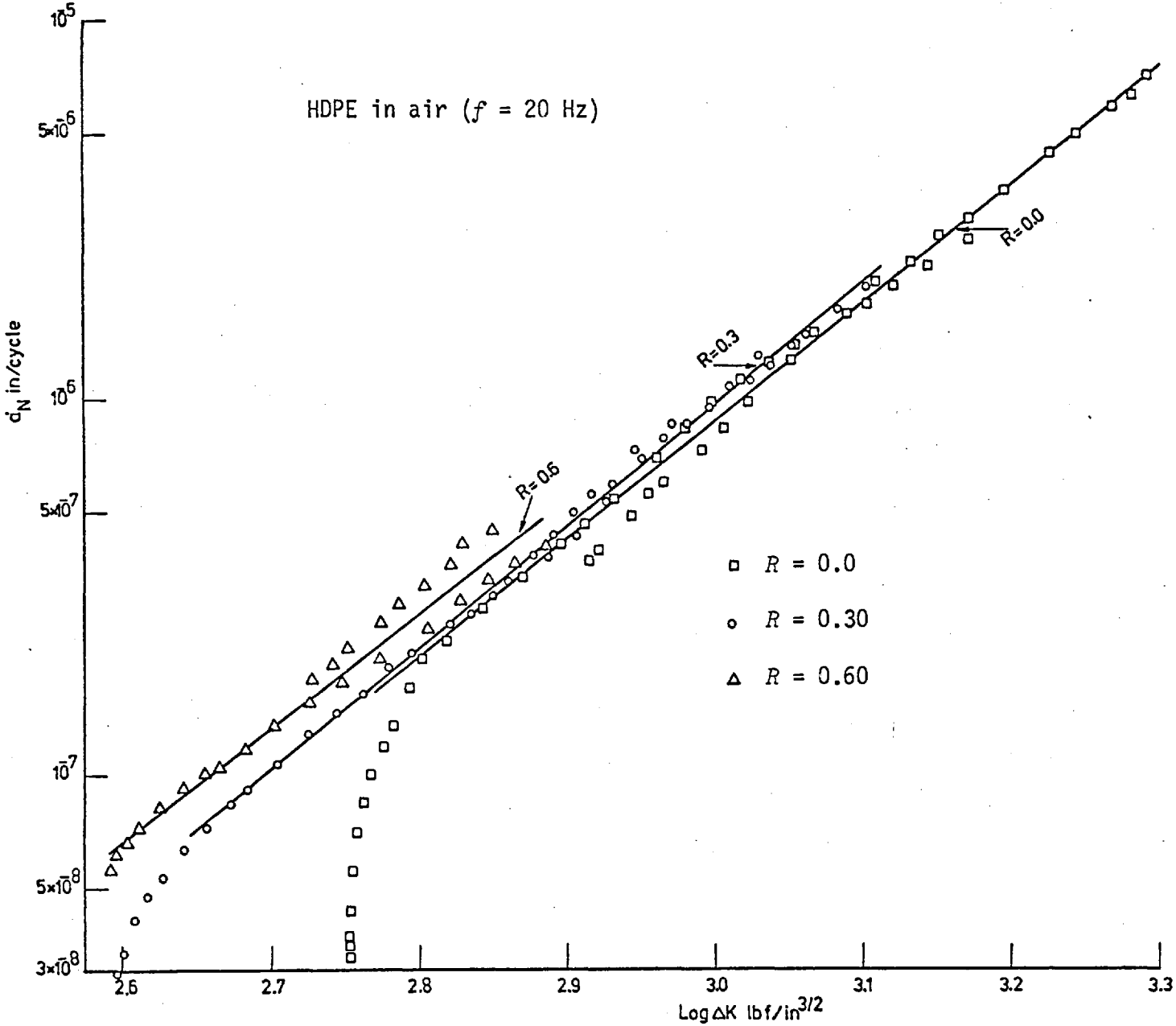

Figure 31: The log $\dot{a}_N$-log ΔK relationship of HDPE tested in air at f = 20 Hz

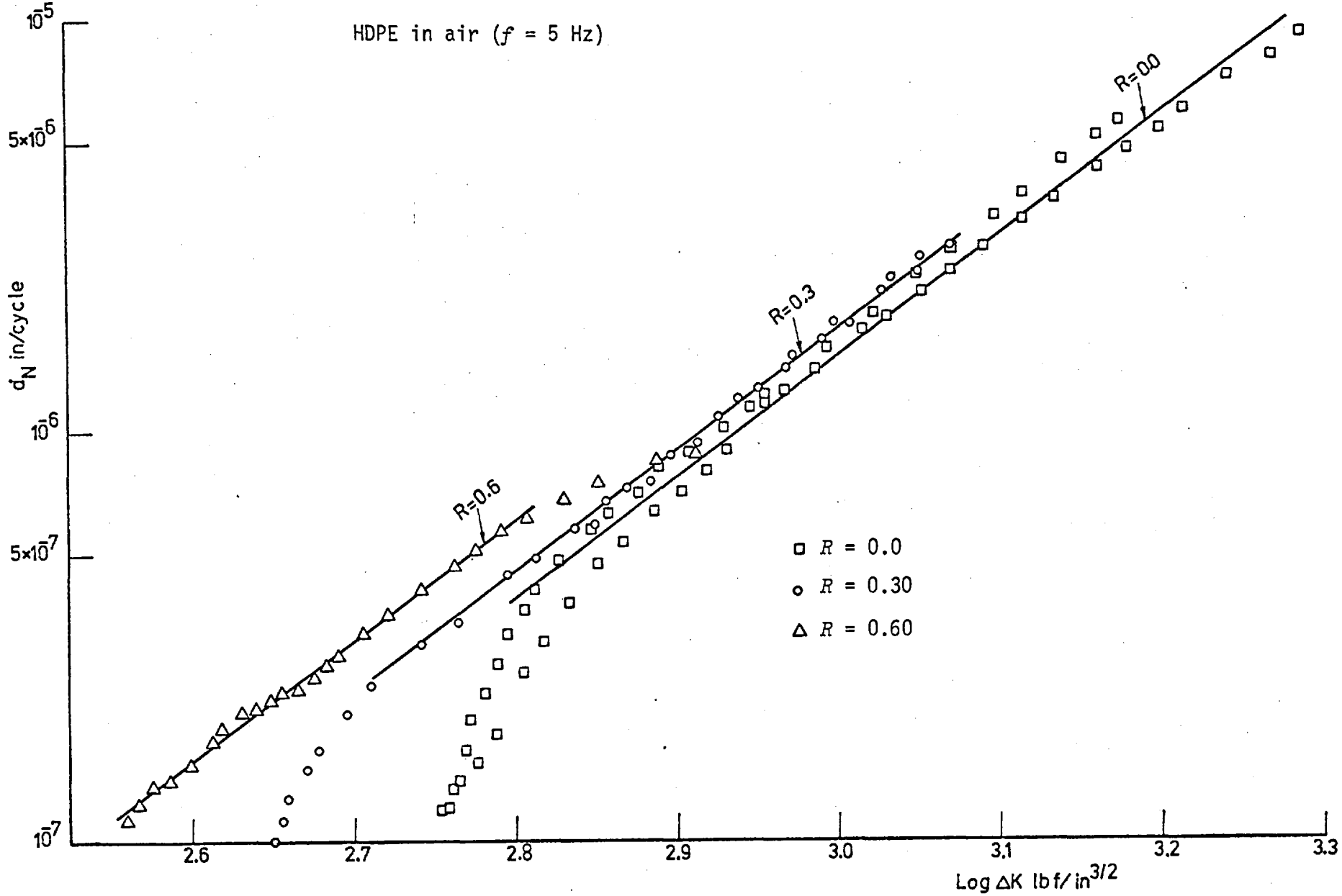

Figure 32: The log $\dot{a}_N$-log ΔK relationship of HDPE tested in air at f = 5 Hz

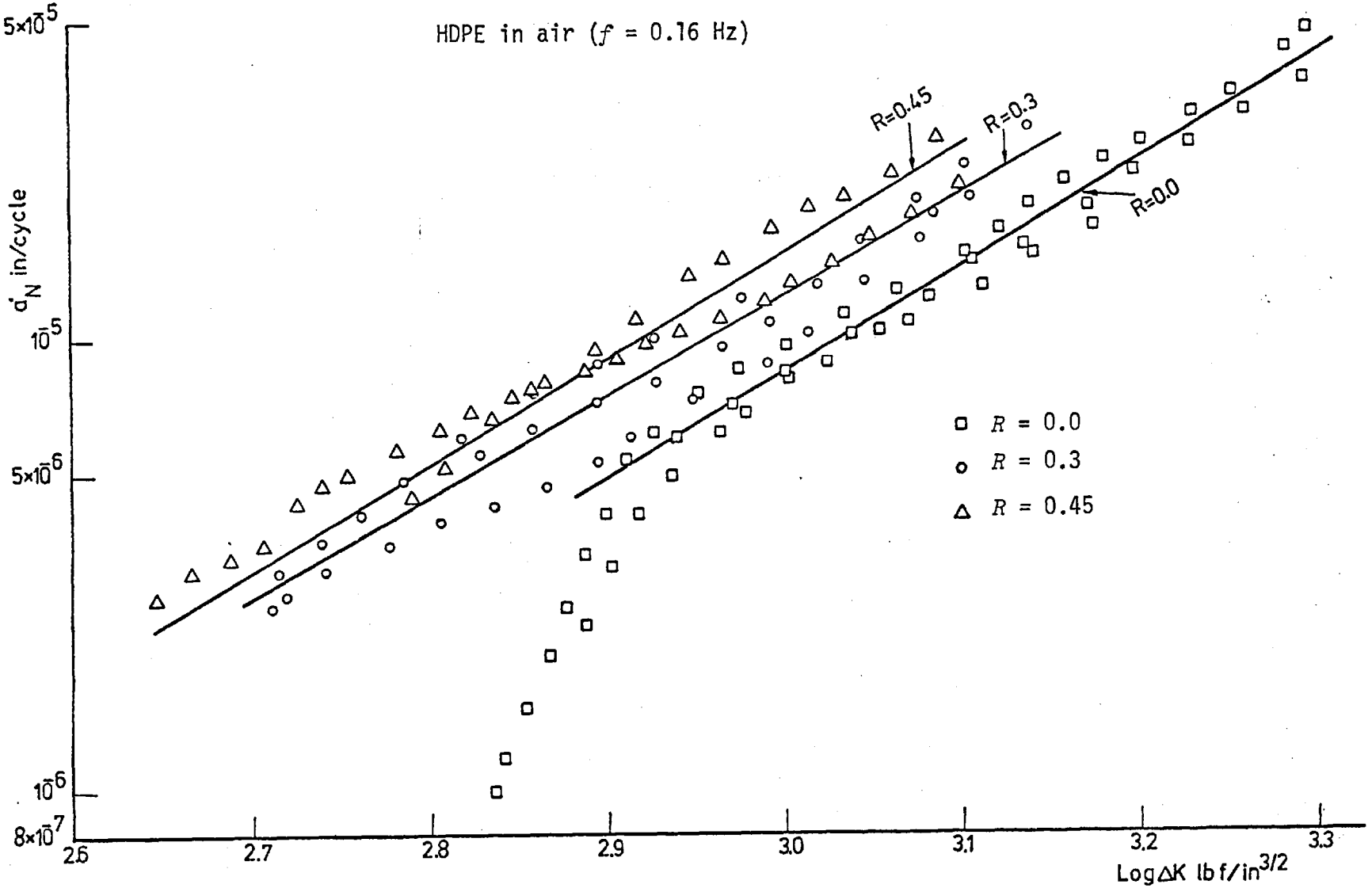

Figure 33: The log $\dot{a}_N$-log ΔK relationship of HDPE tested in air at f = 0.16 Hz

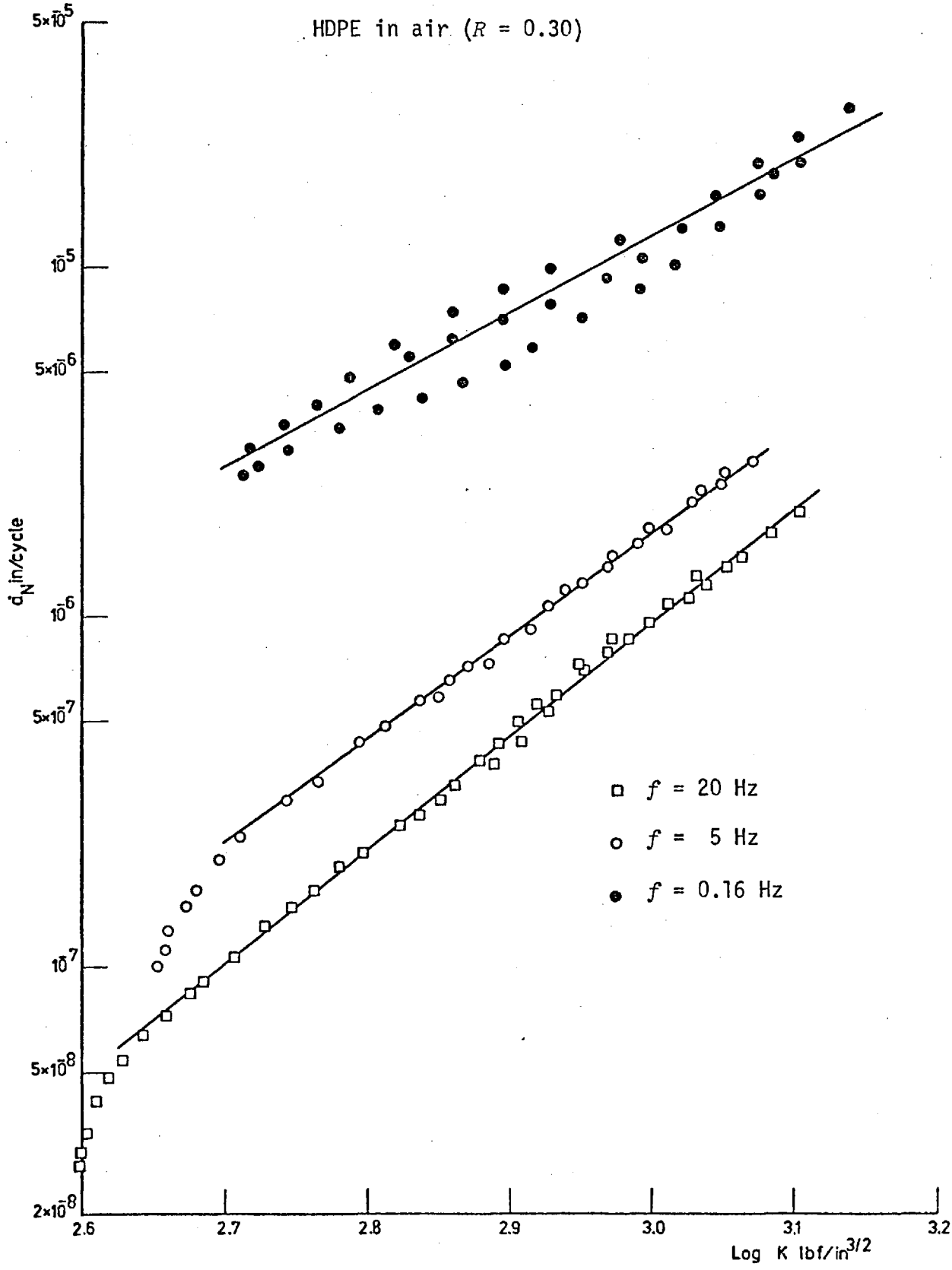

Figure 34: The log $\dot{a}_N$-log ΔK relationship of HDPE tested in air at R = 0.30 and different frequencies

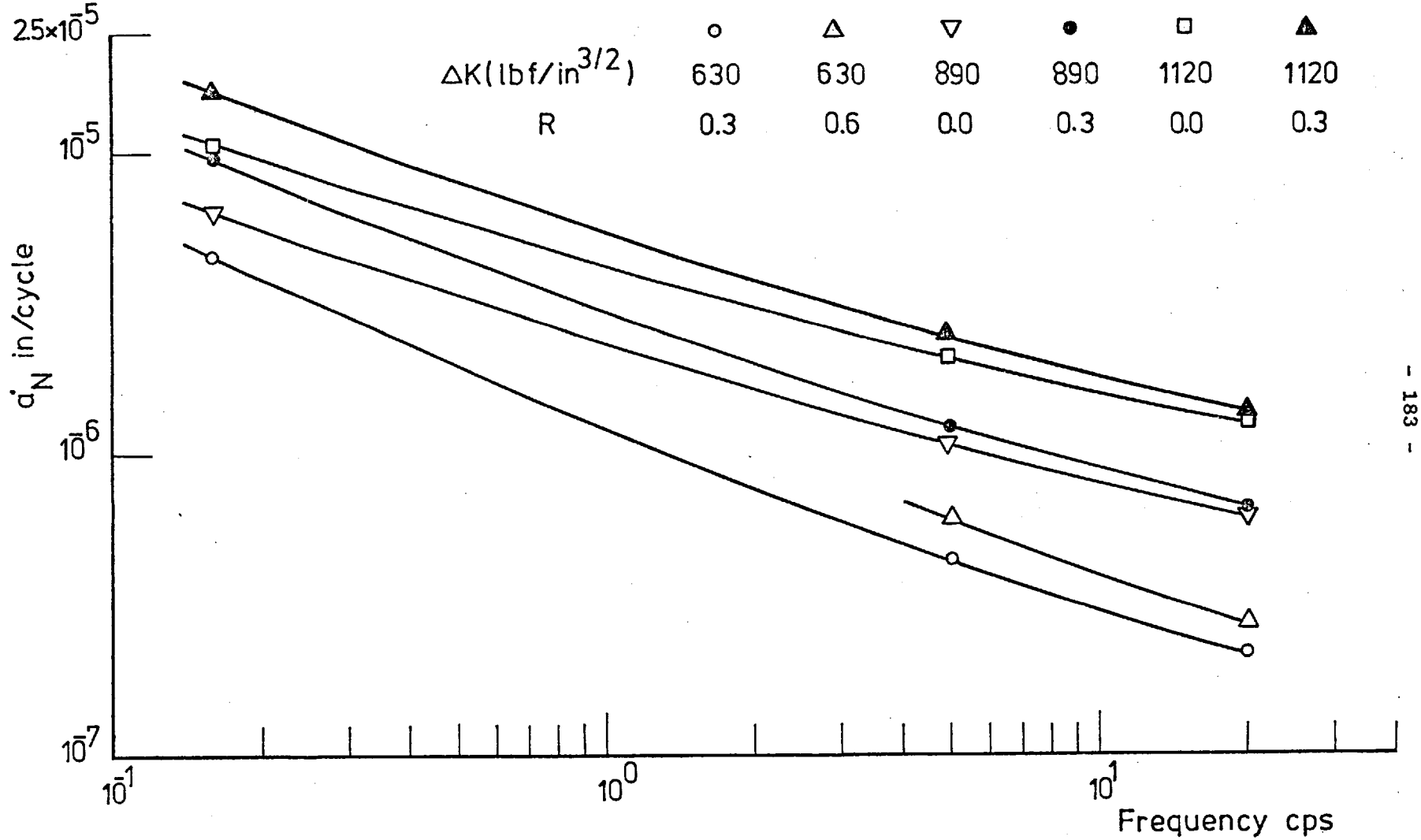

Figure 35: Variation of $\dot{a}_N$ with frequency, for HDPE in air, at different constant values of R and ΔK

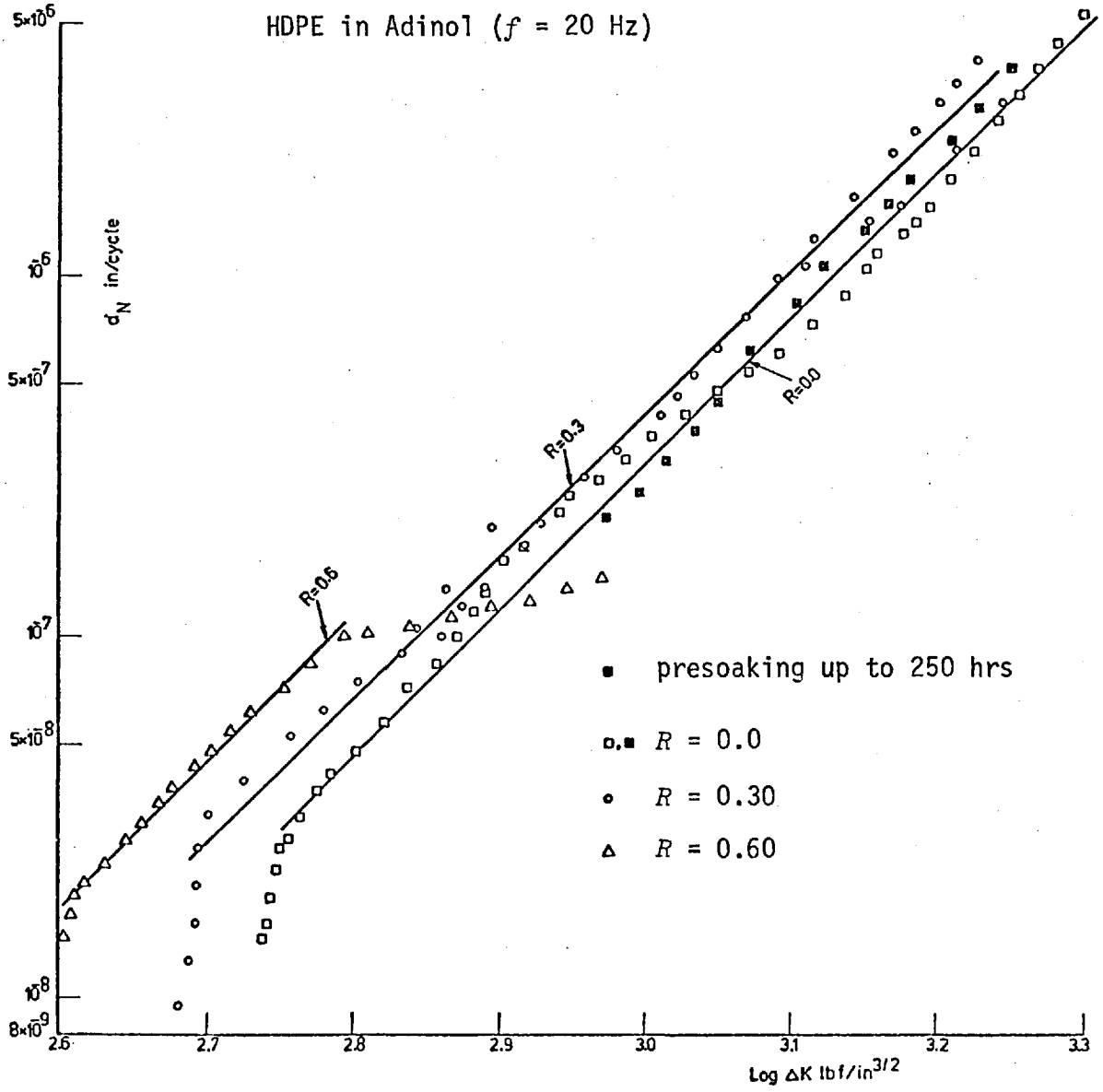

Figure 36: The log $\dot{a}_N$-log ΔK relationship of HDPE tested in Adinol at f = 20 Hz

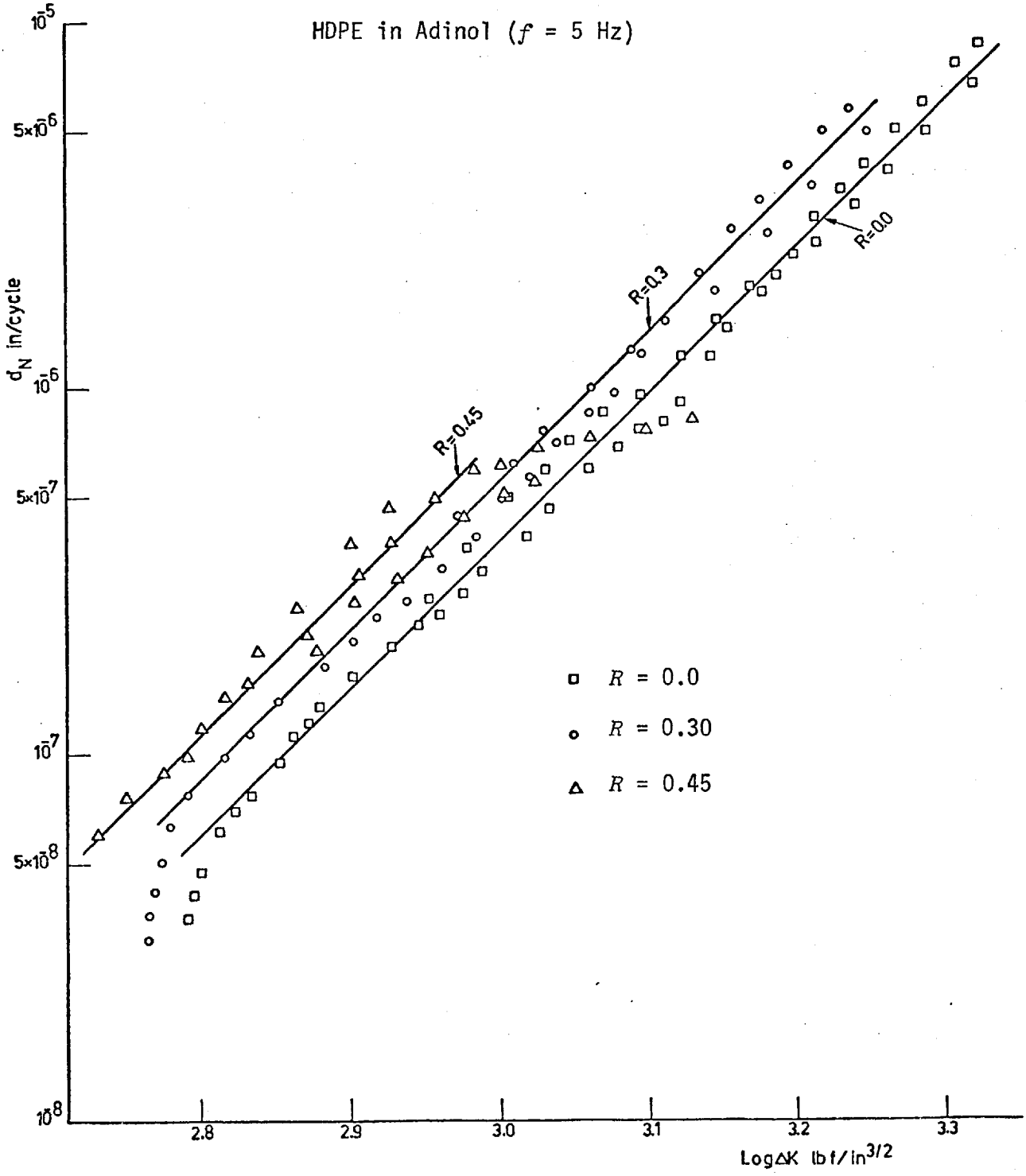

Figure 37: The log $\dot{a}_N$-log ΔK relationship of HDPE tested in Adinol at f = 5 Hz

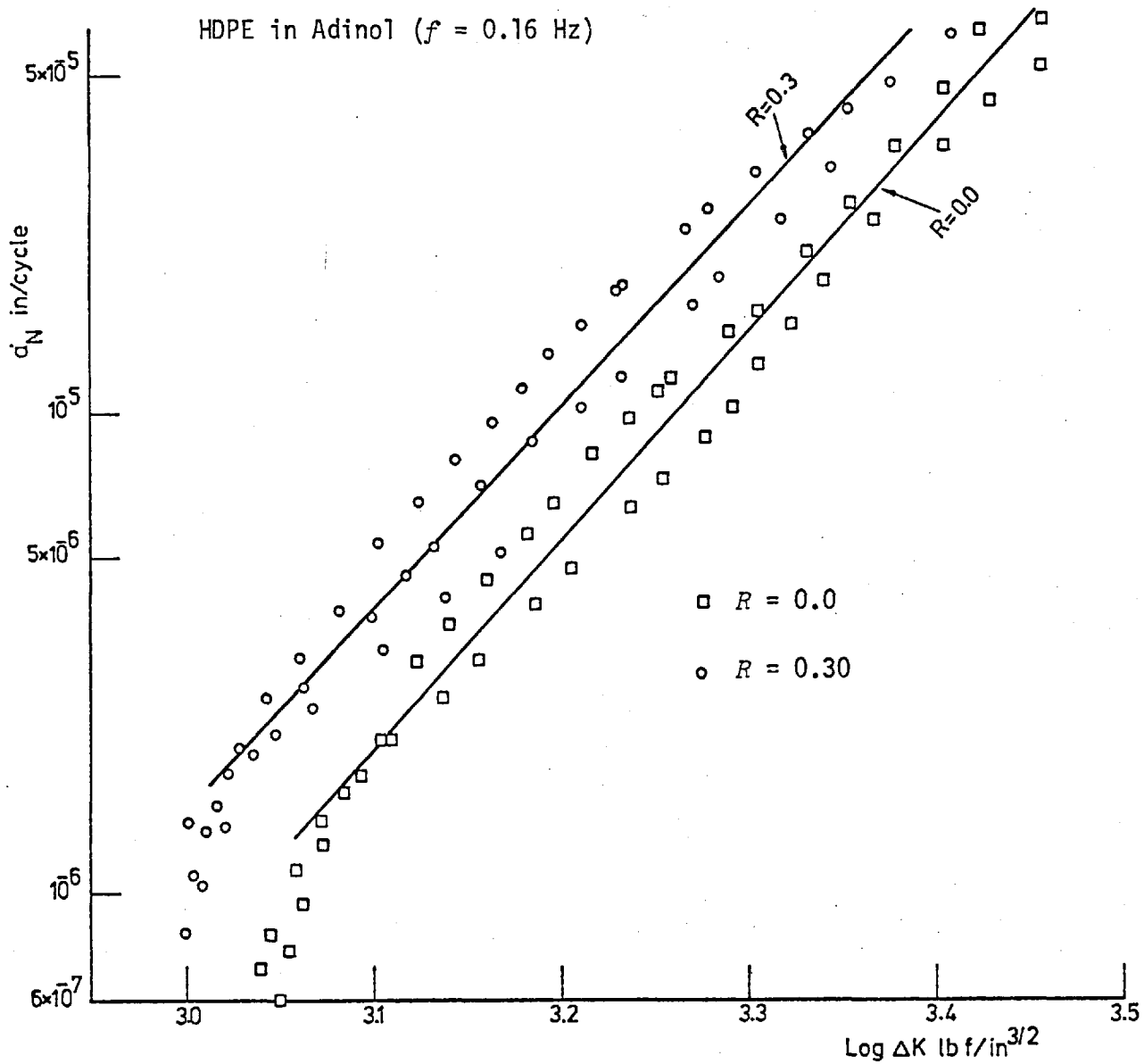

Figure 38: The log $\dot{a}_N$-log ΔK relationship of HDPE tested in Adinol at f = 0.16 Hz

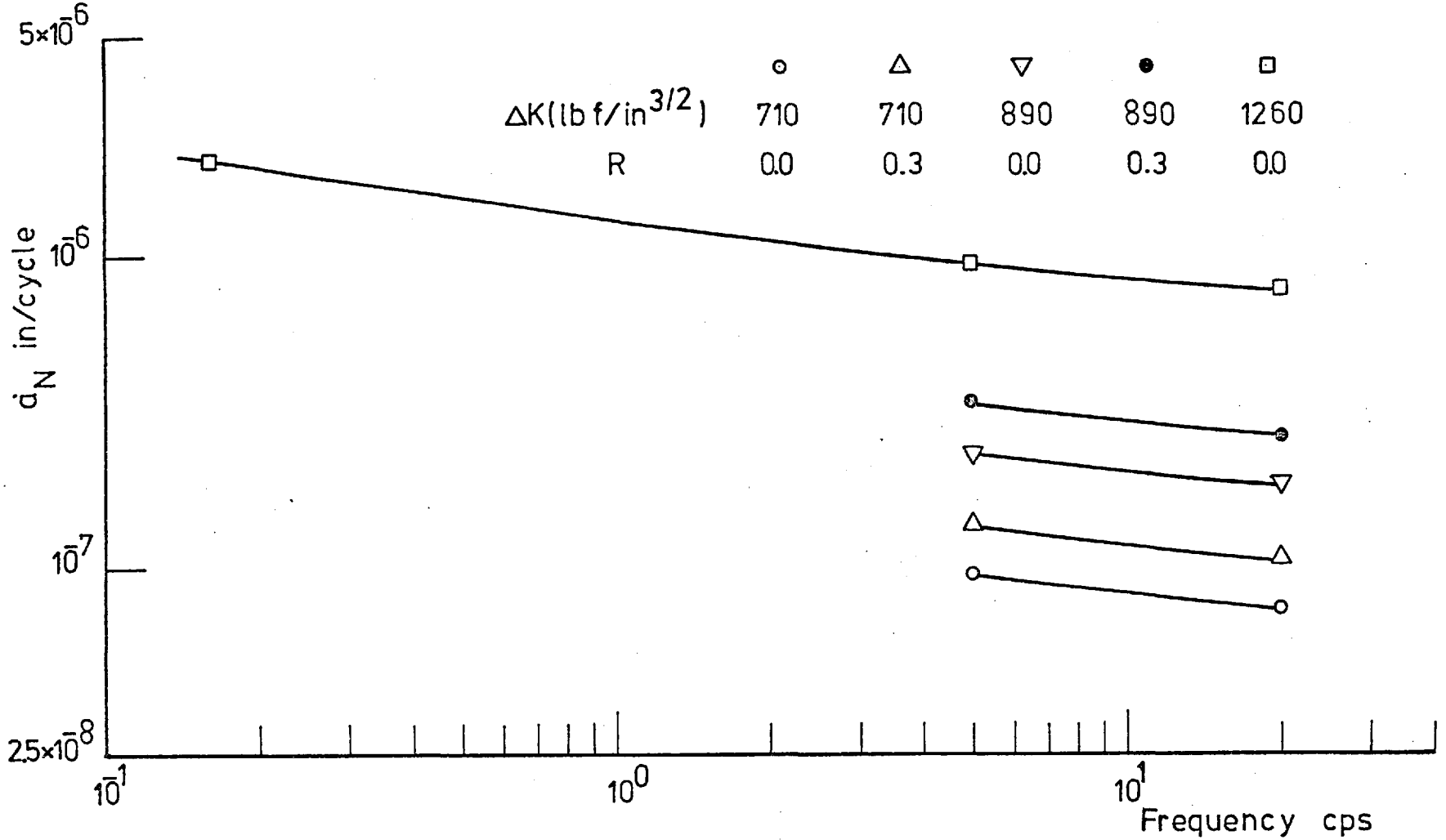

Figure 39: Variation of $\dot{a}_N$ with frequency, for HDPE in Adinol, at different constant values of R and ΔK

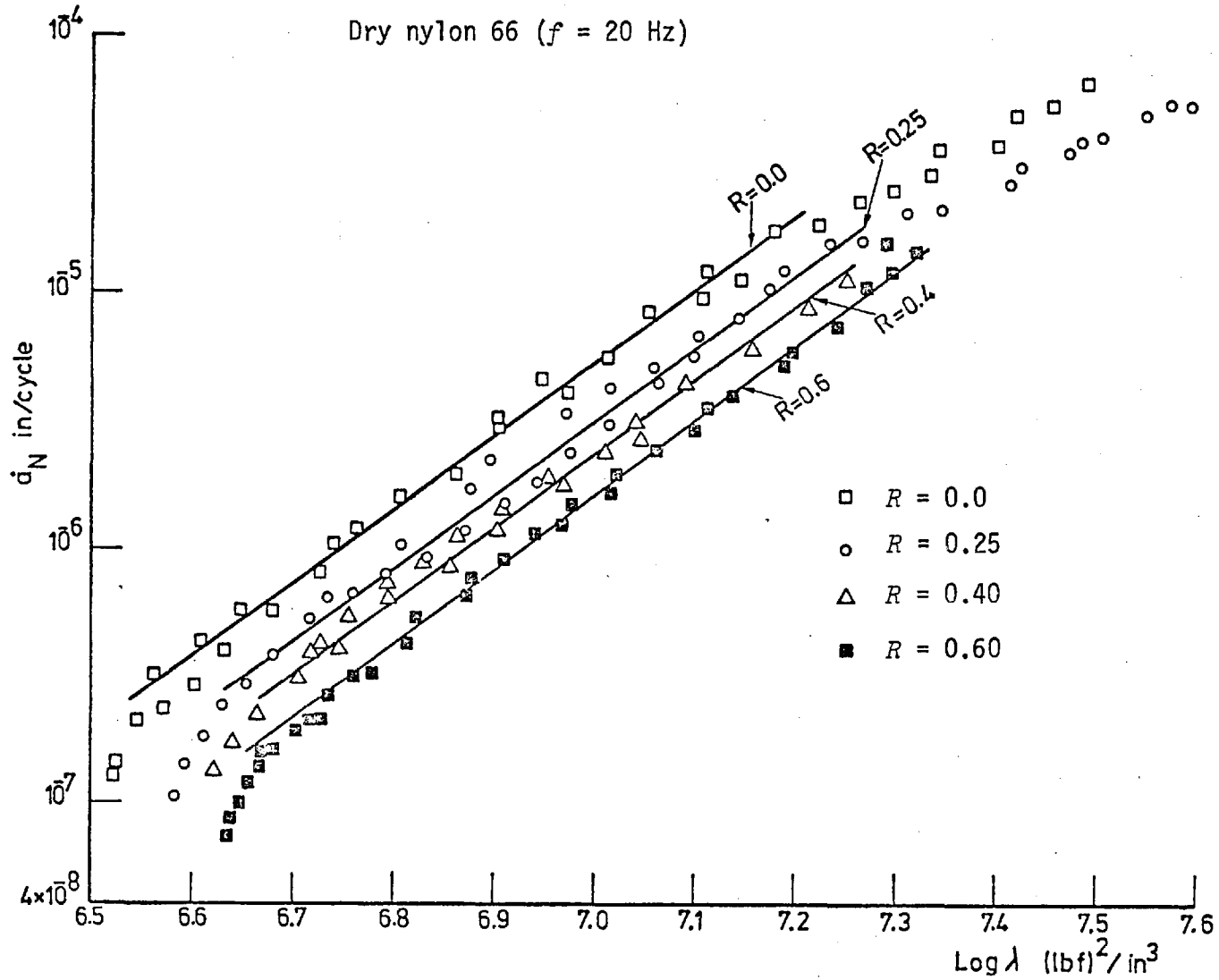

Figure 40: Variation of crack growth rate with λ (equation (1.25)) - dry N66 tested in air at f = 20 Hz

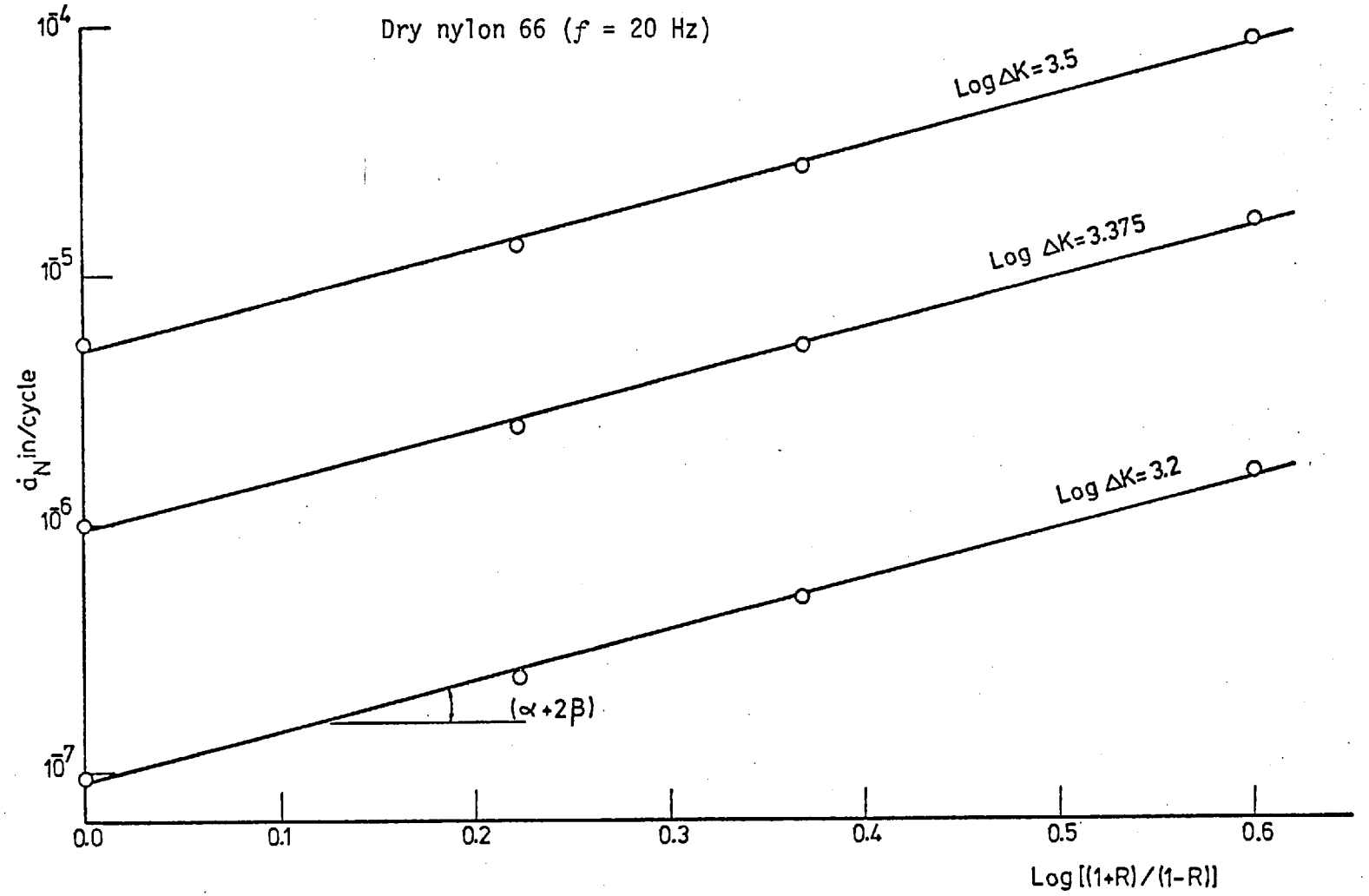

Figure 41: Variation of crack growth rate with *(1+R)/(1-R)* at constant ΔK - dry N66 tested in air at f = 20 Hz

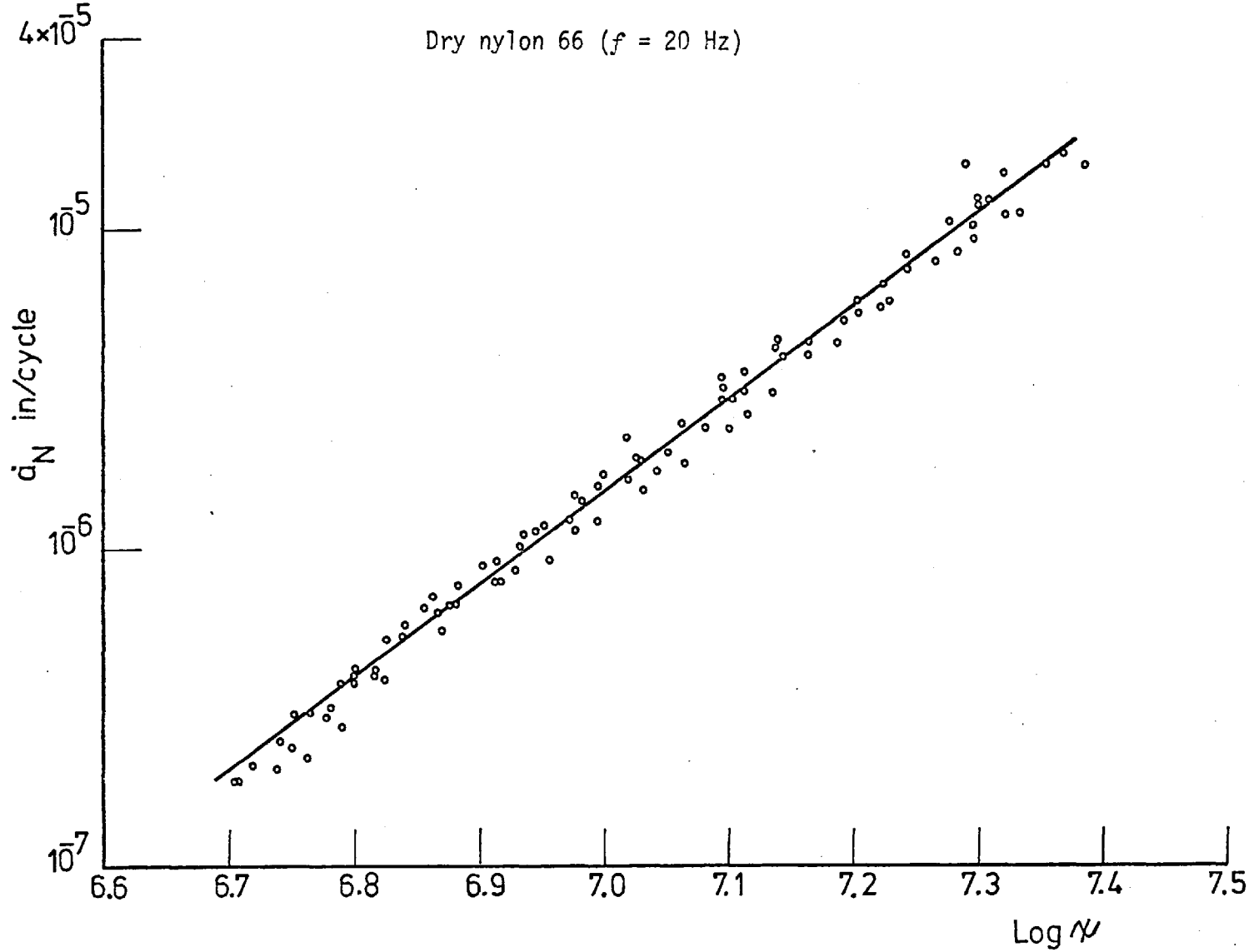

Figure 42: The log $\dot{a}_N$-log ψ relationship of dry nylon 66 tested in air at f = 20 Hz

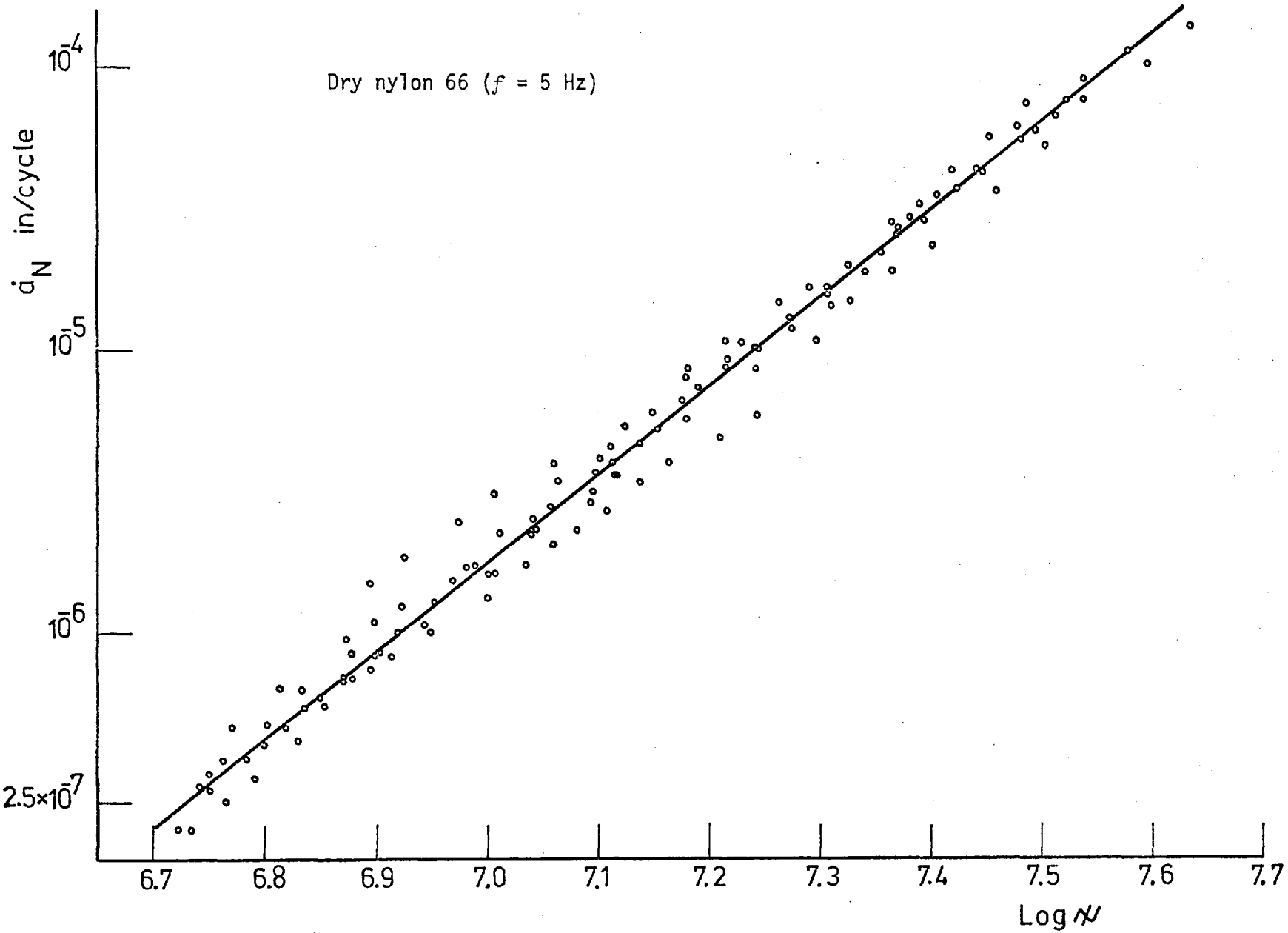

Figure 43: The log $\dot{a}_N$-log ψ relationship of dry nylon 66 tested in air at f = 5 Hz

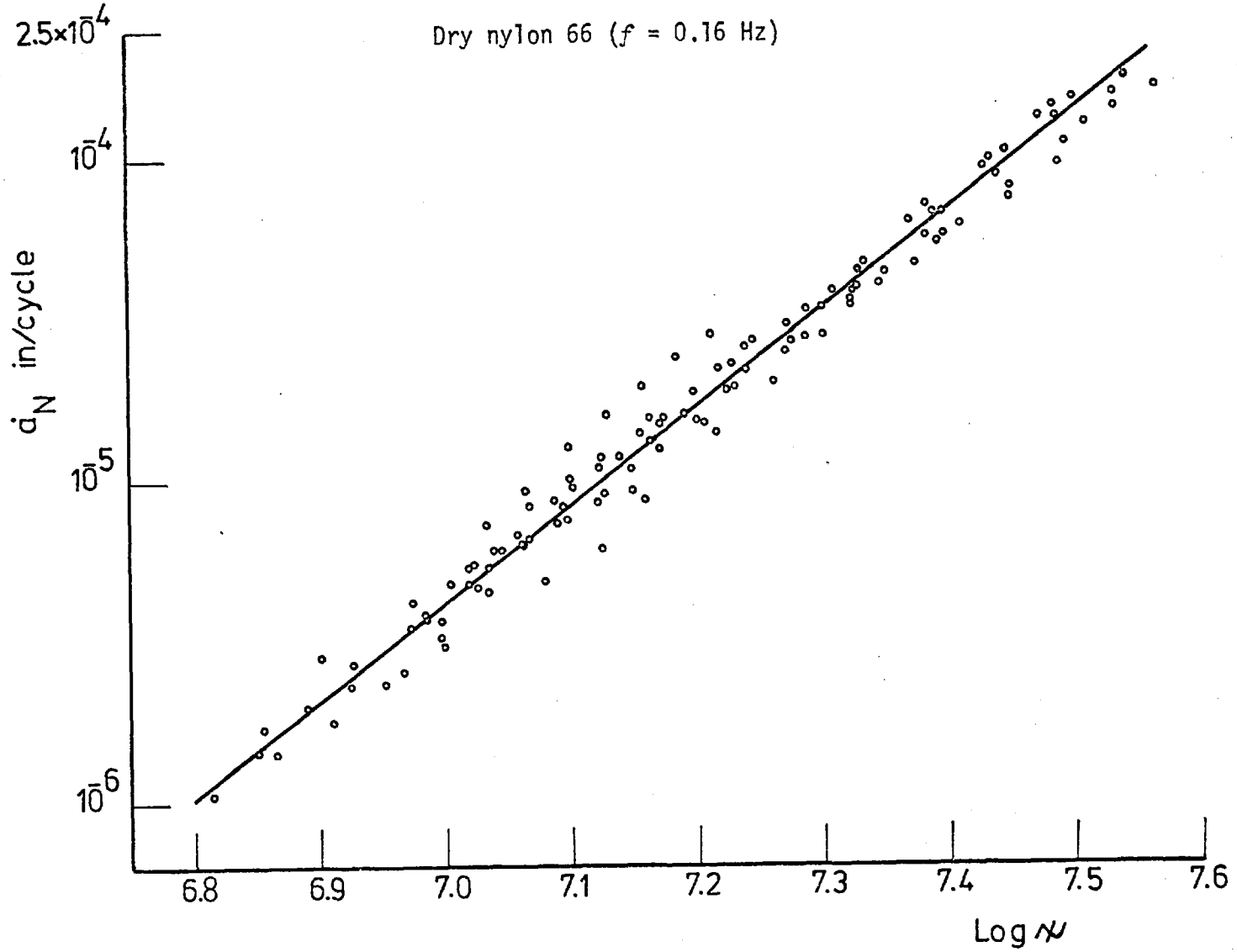

Figure 44: The log $\dot{a}_N$-log ψ relationship of dry nylon 66 tested in air at f = 0.16 Hz

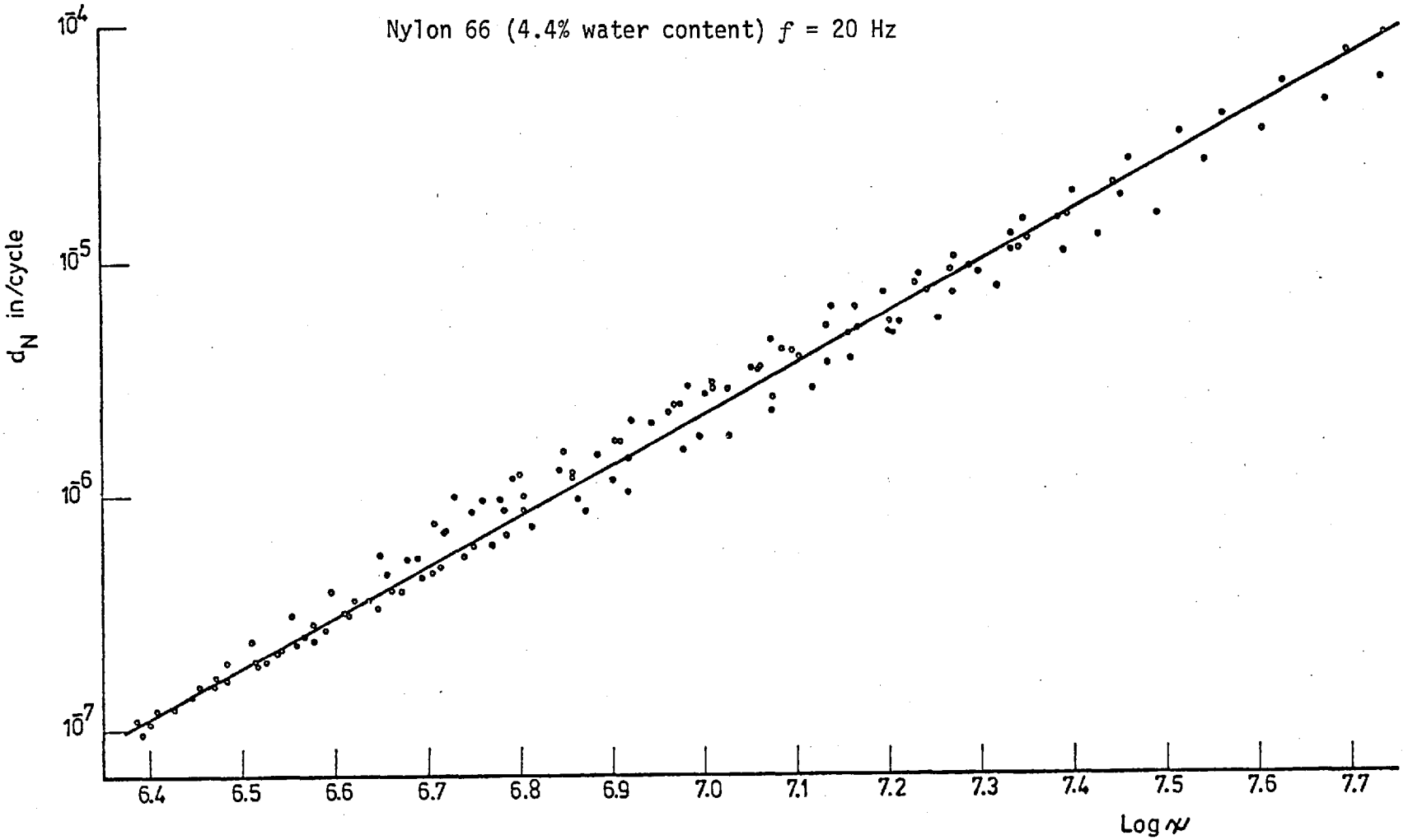

Figure 45: The log $\dot{a}_N$-log ψ relationship of N66 (4.4% water content) tested in air and distilled water at f = 20 Hz

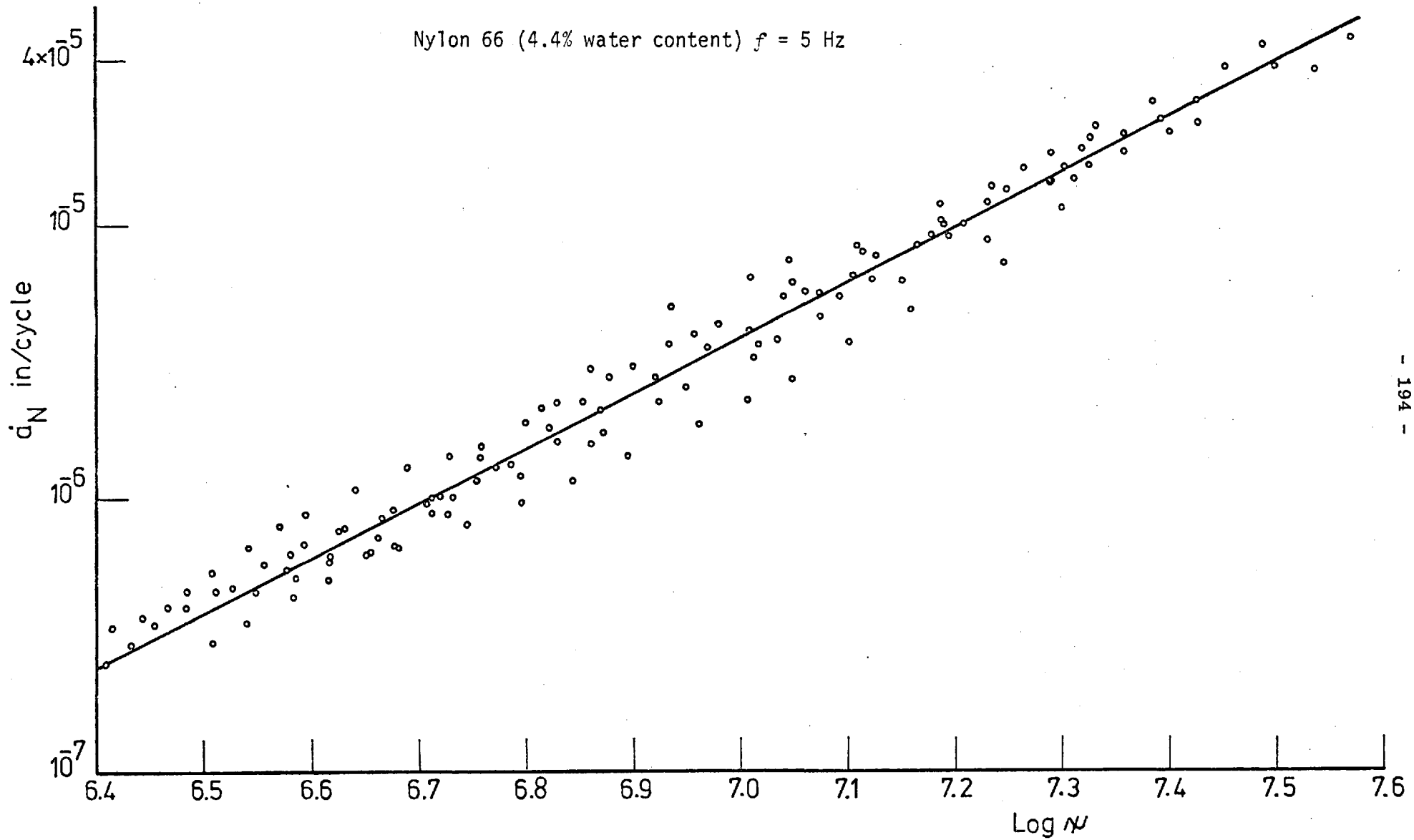

Figure 46: The log $\dot{a}_N$-log ψ relationship of N66 (4.4% water content) tested in air and distilled water at f = 5 Hz

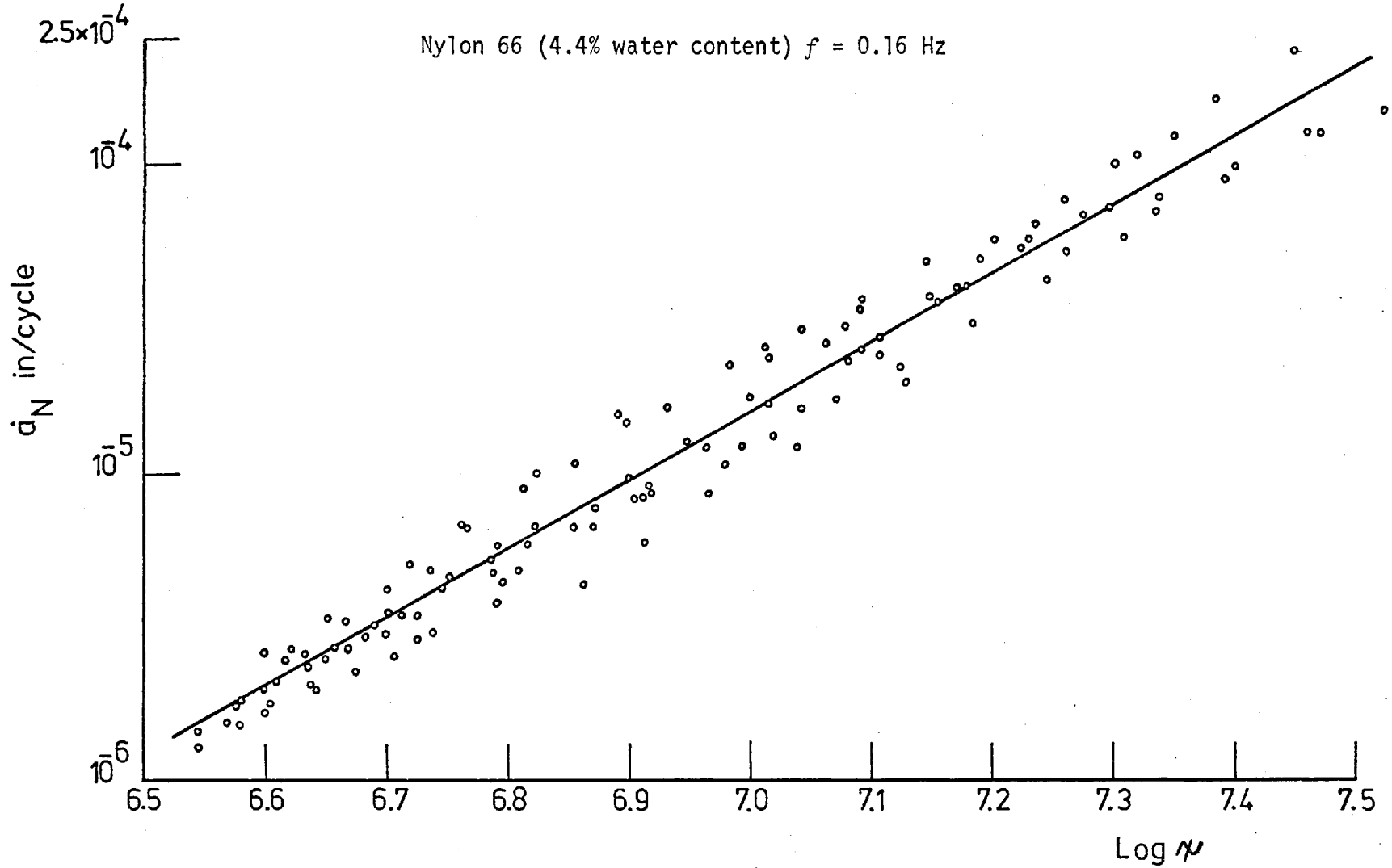

Figure 47: The log $\dot{a}_N$-log ψ relationship of N66 (4.4% water content) tested in air and distilled water at f = 0.16 Hz

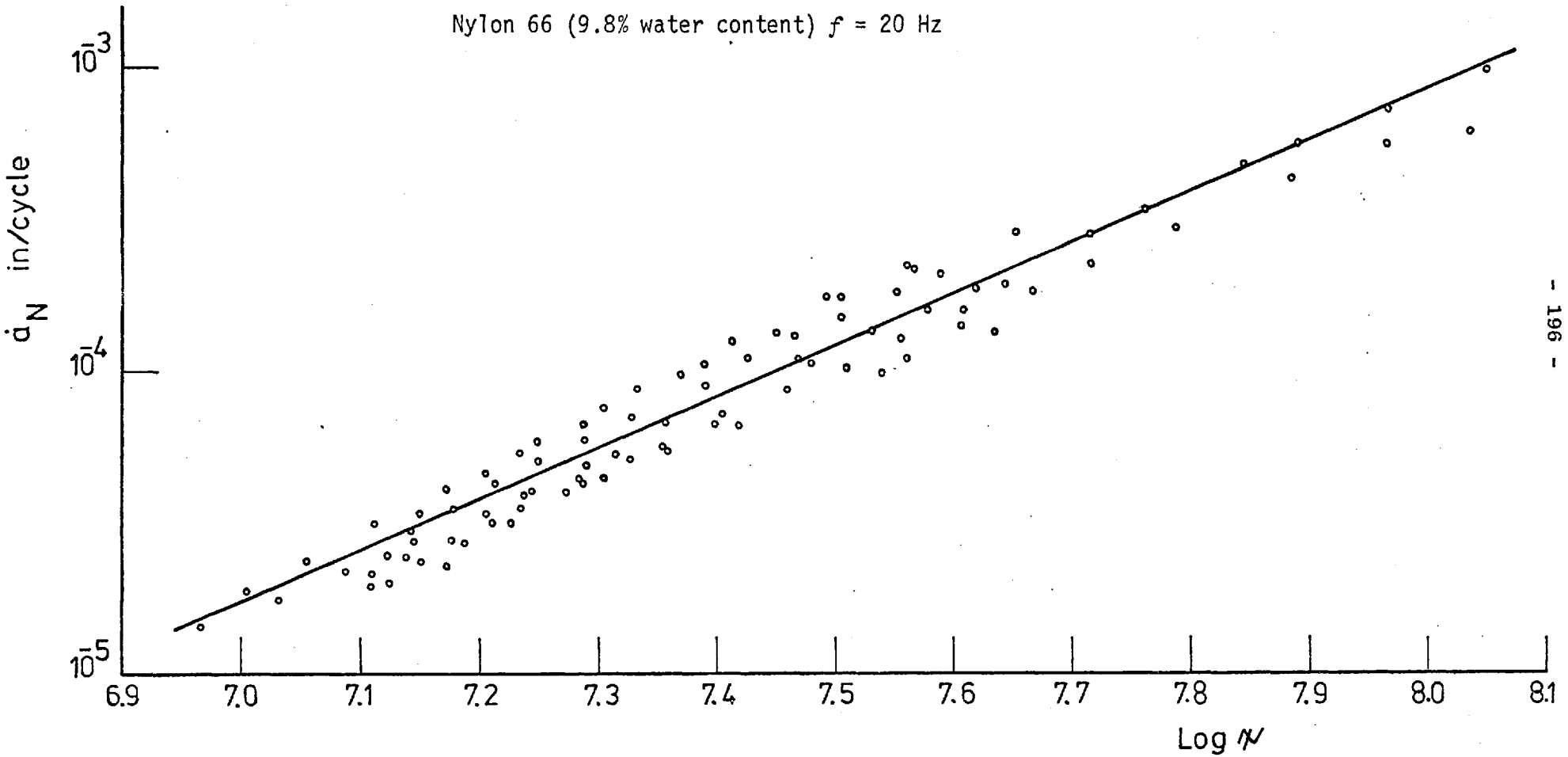

Figure 48: The log $\dot{a}_N$-log ψ relationship of N66 (9.8% water content) tested in distilled water at f = 20 Hz

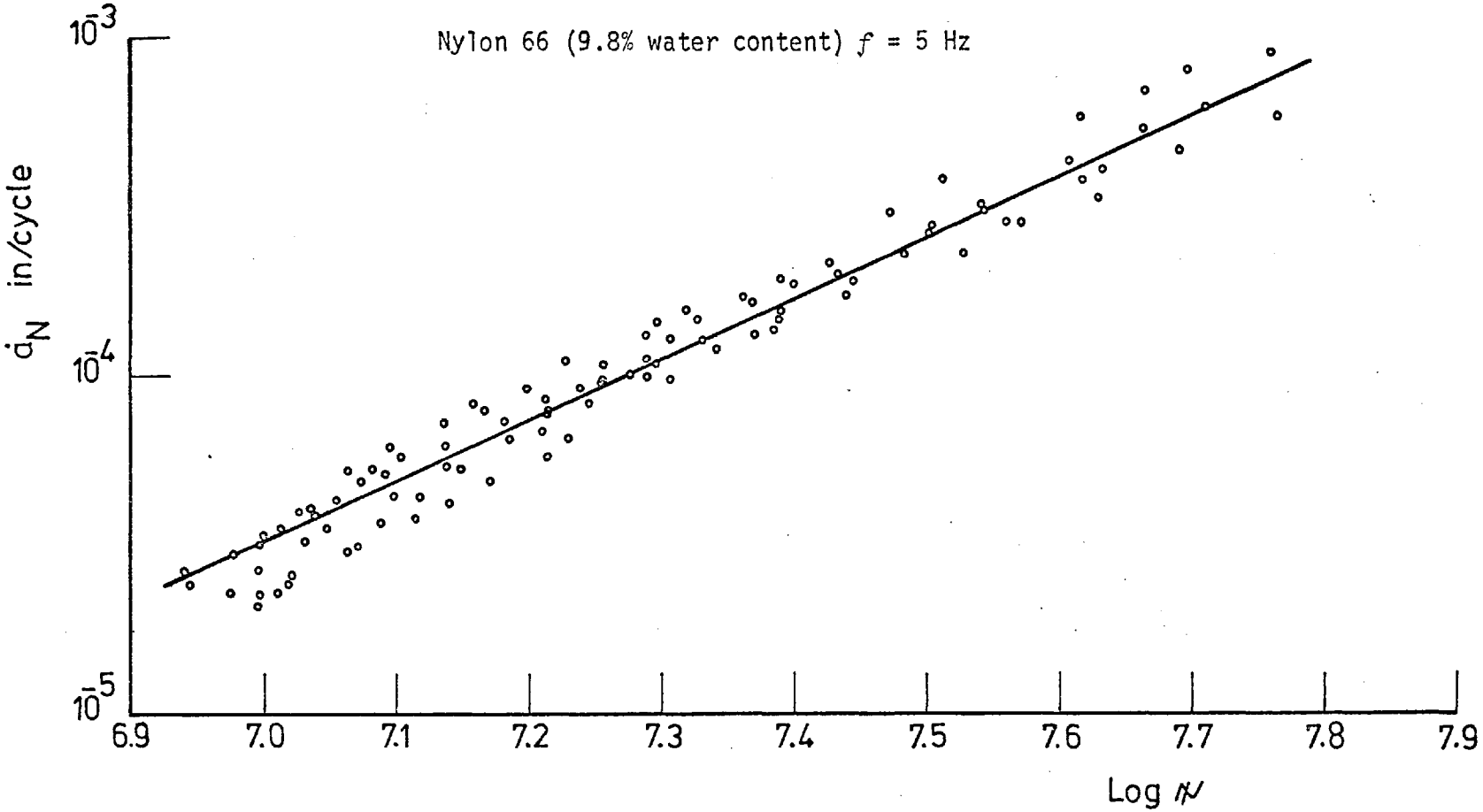

Figure 49: The log $\dot{a}_N$-log ψ relationship of N66 (9.8% water content) tested in distilled water at f = 5 Hz

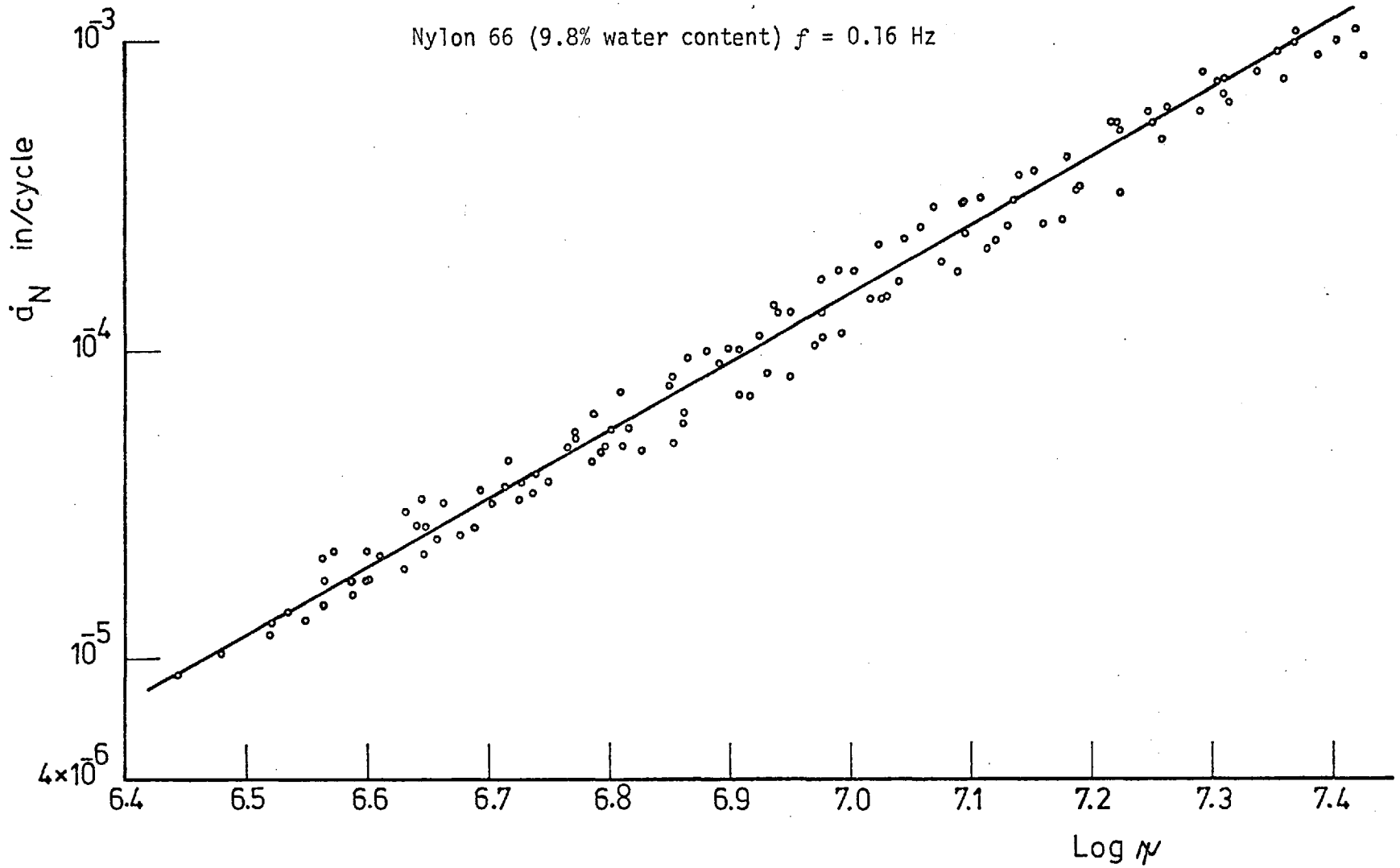

Figure 50: The log $\dot{a}_N$-log ψ relationship of N66 (9.8% water content) tested in distilled water at f = 0.16 Hz

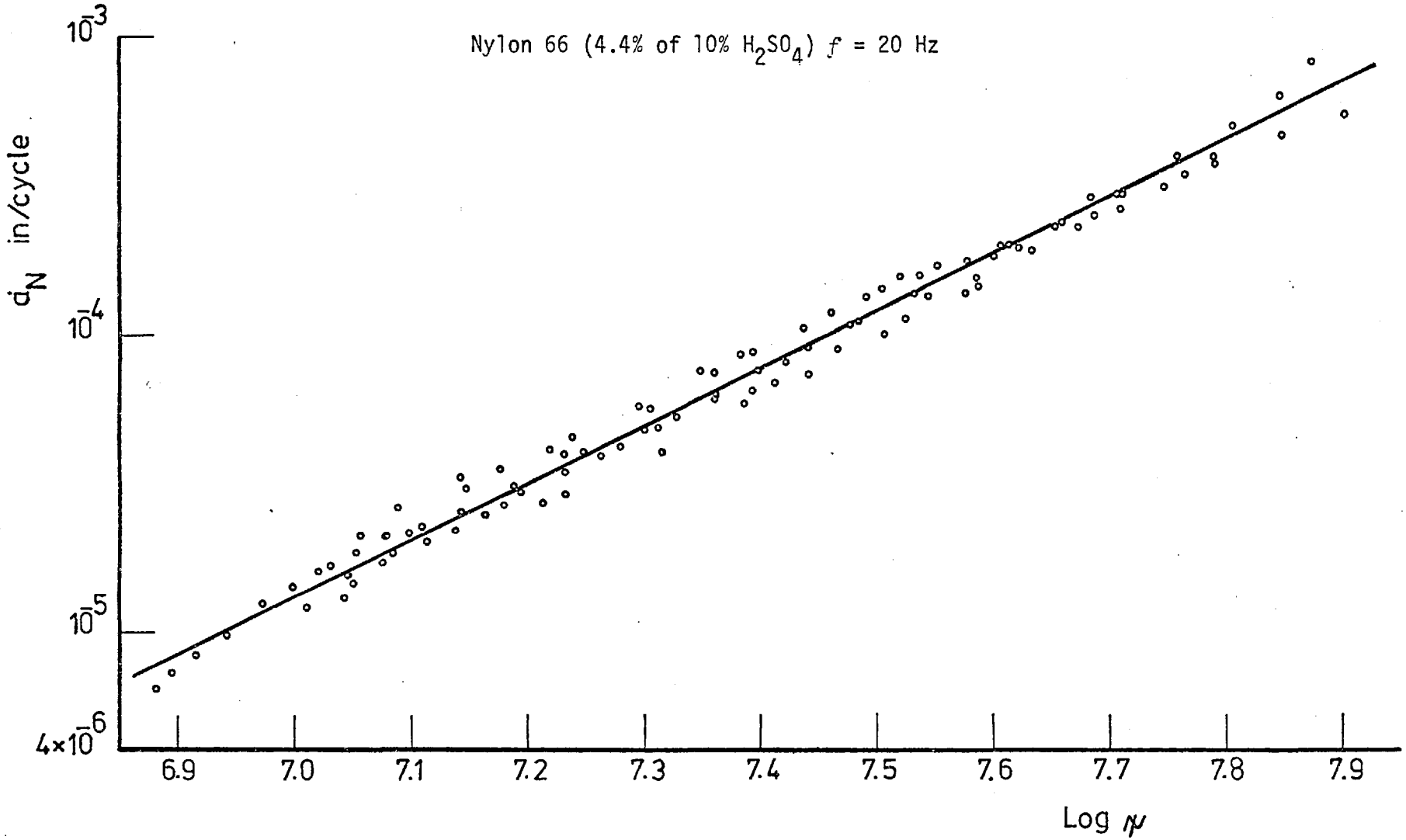

Figure 51: The log $\dot{a}_N$-log ψ relationship of N66 (4.4% of H_2SO_4 of 10% concentration) tested in 10% H_2SO_4 at f = 20 Hz

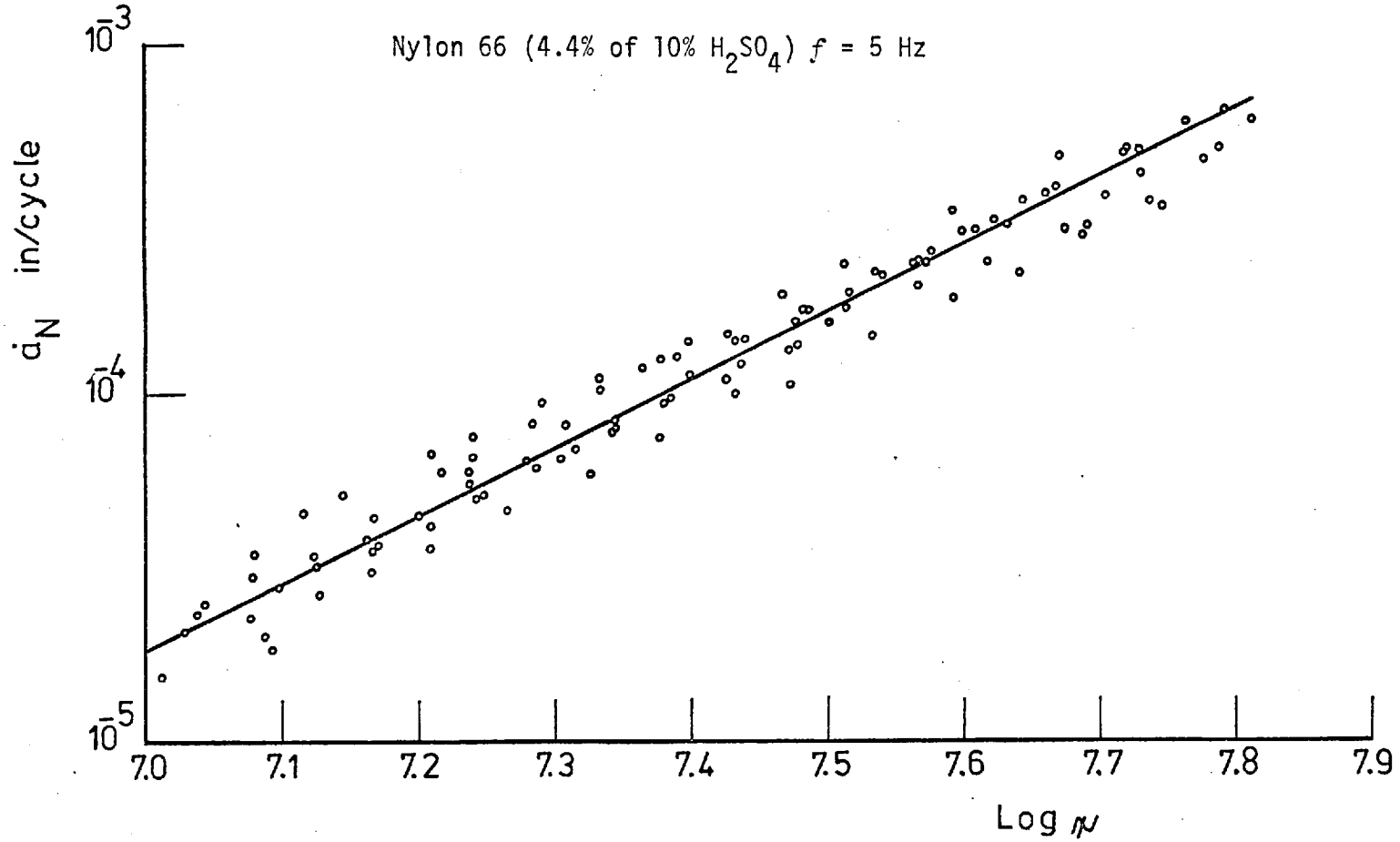

Figure 52: The log $\dot{a}_N$-log ψ relationship of N66 (4.4% of H_2SO_4 of 10% concentration) tested in 10% H_2SO_4 at f = 5 Hz

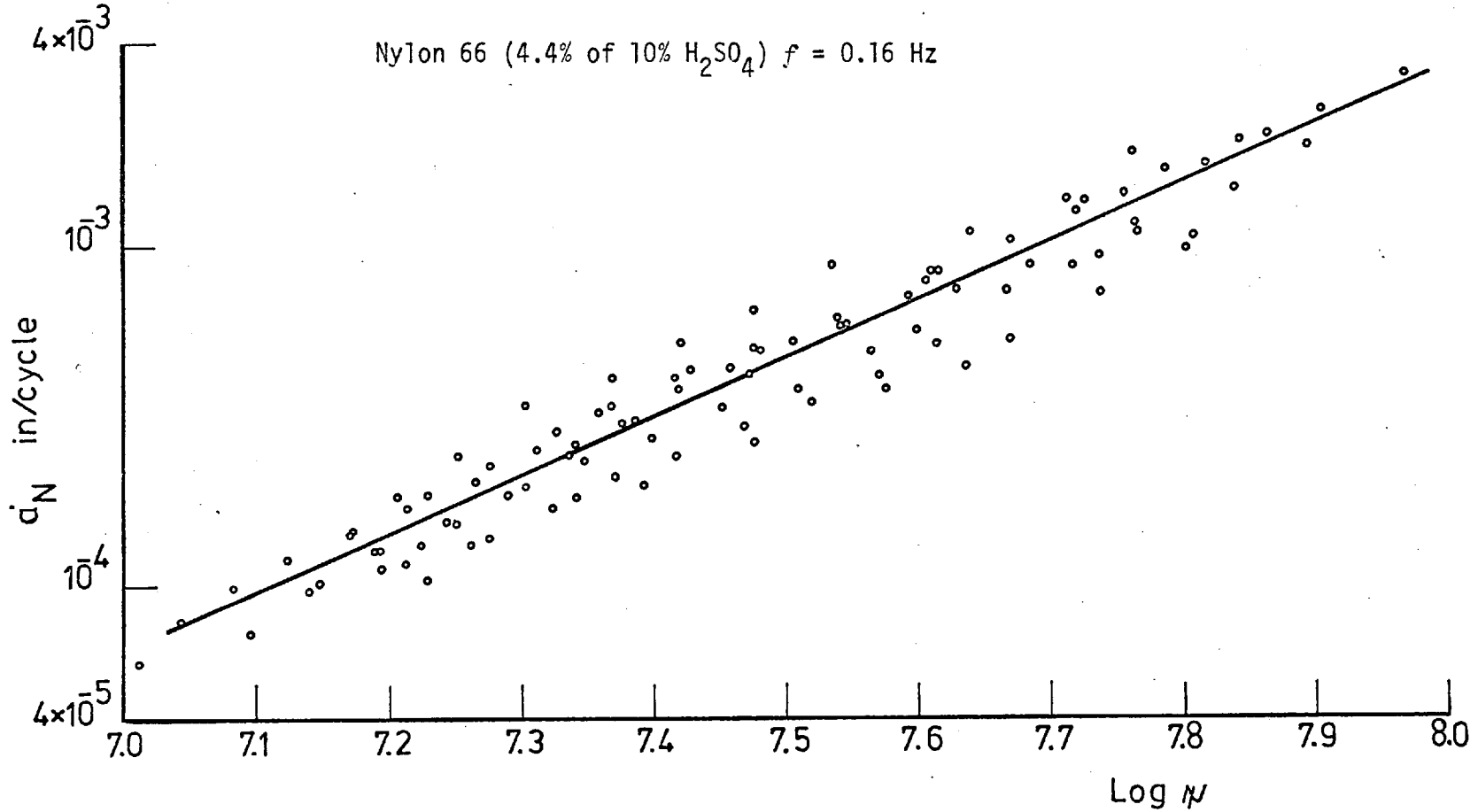

Figure 53: The log $\dot{a}_N$-log ψ relationship of N66 (4.4% of H_2SO_4 of 10% concentration) tested in 10% H_2SO_4 at f = 0.16 Hz

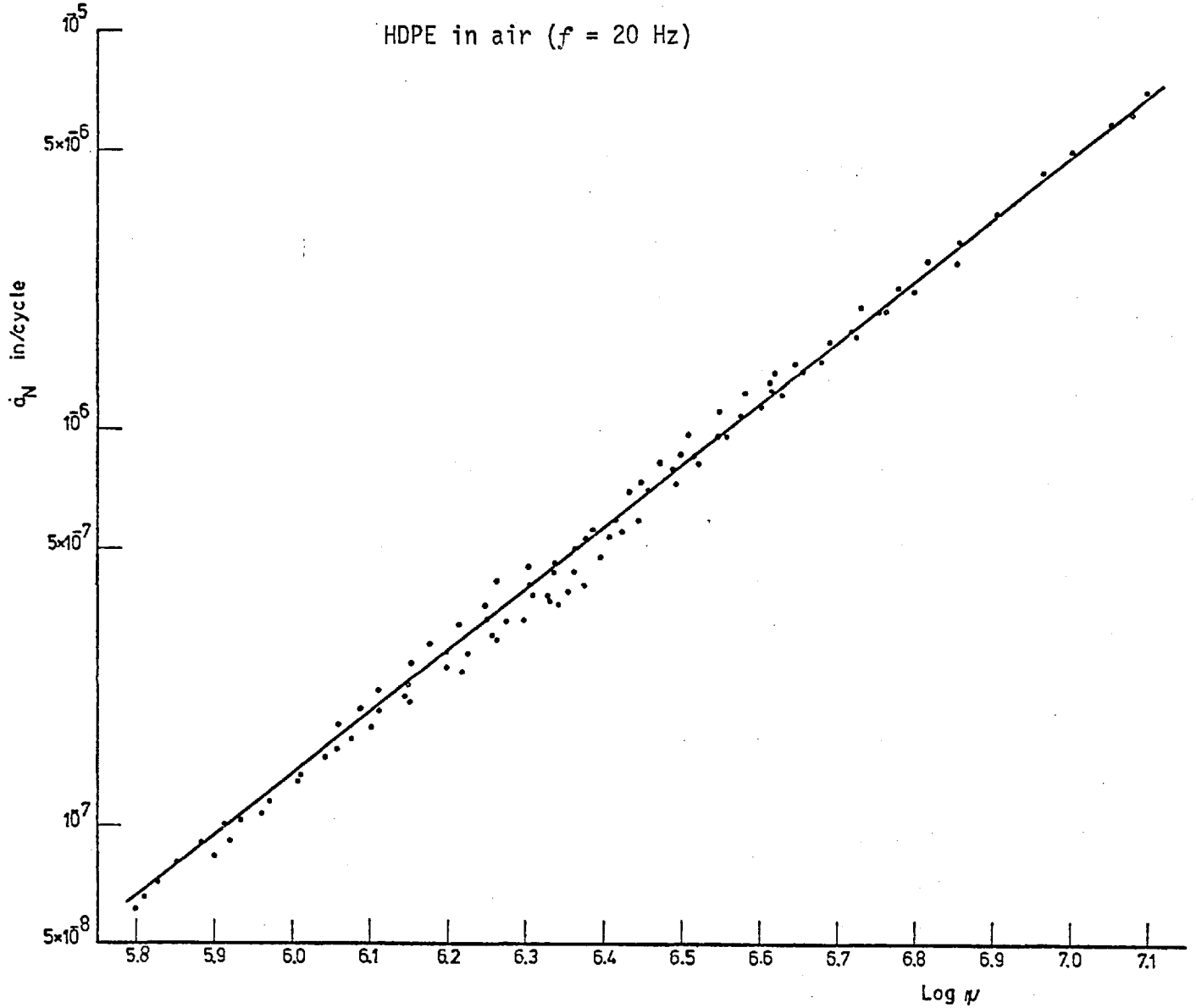

Figure 54: The log α_N-log ψ relationship of HDPE tested in air at f = 20 Hz

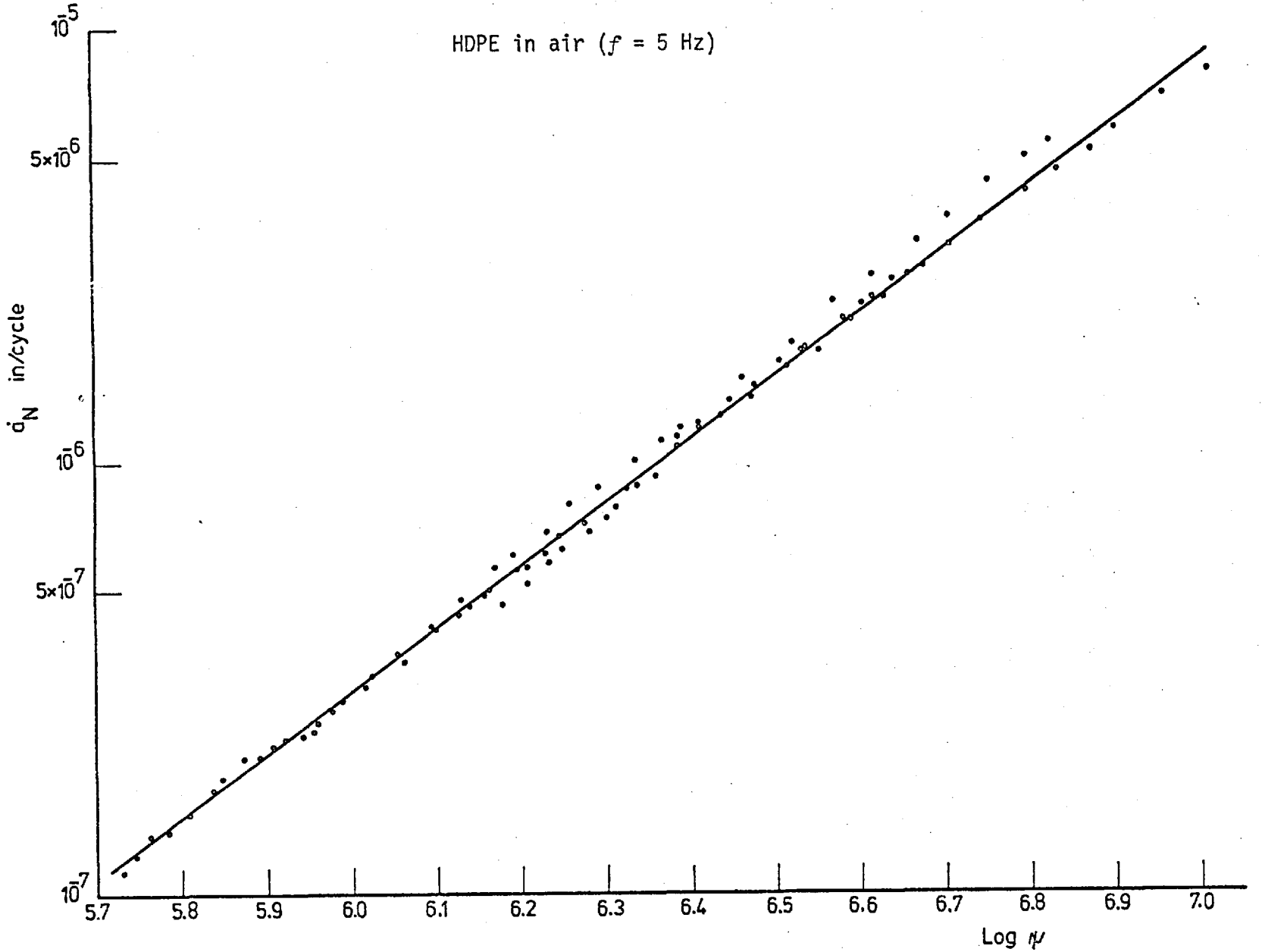

Figure 55: The log $\dot{a}_N$-log ψ relationship of HDPE tested in air at f = 5 Hz

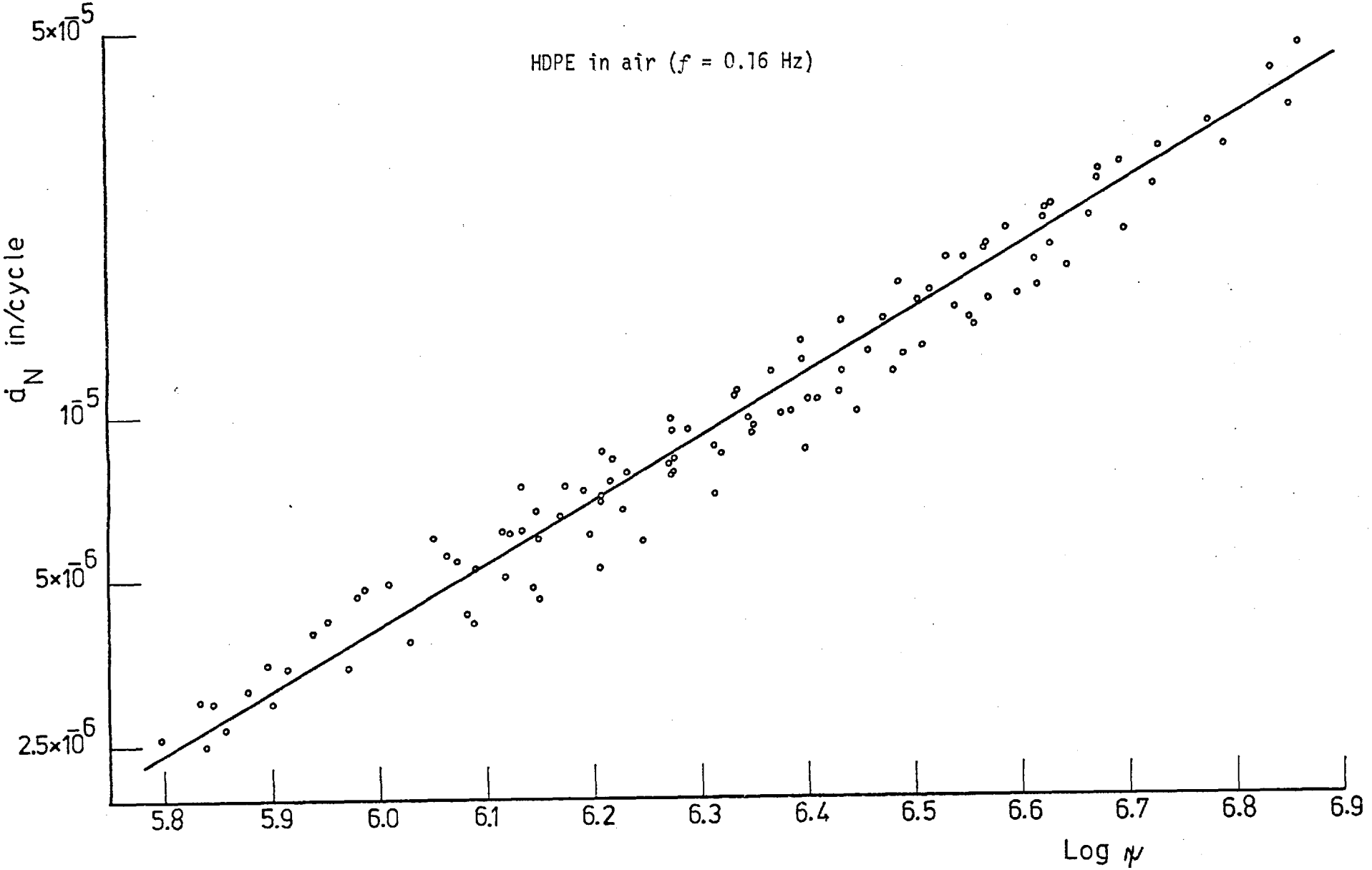

Figure 56: The log $\dot{a}_N$-log ψ relationship of HDPE tested in air at f = 0.16 Hz

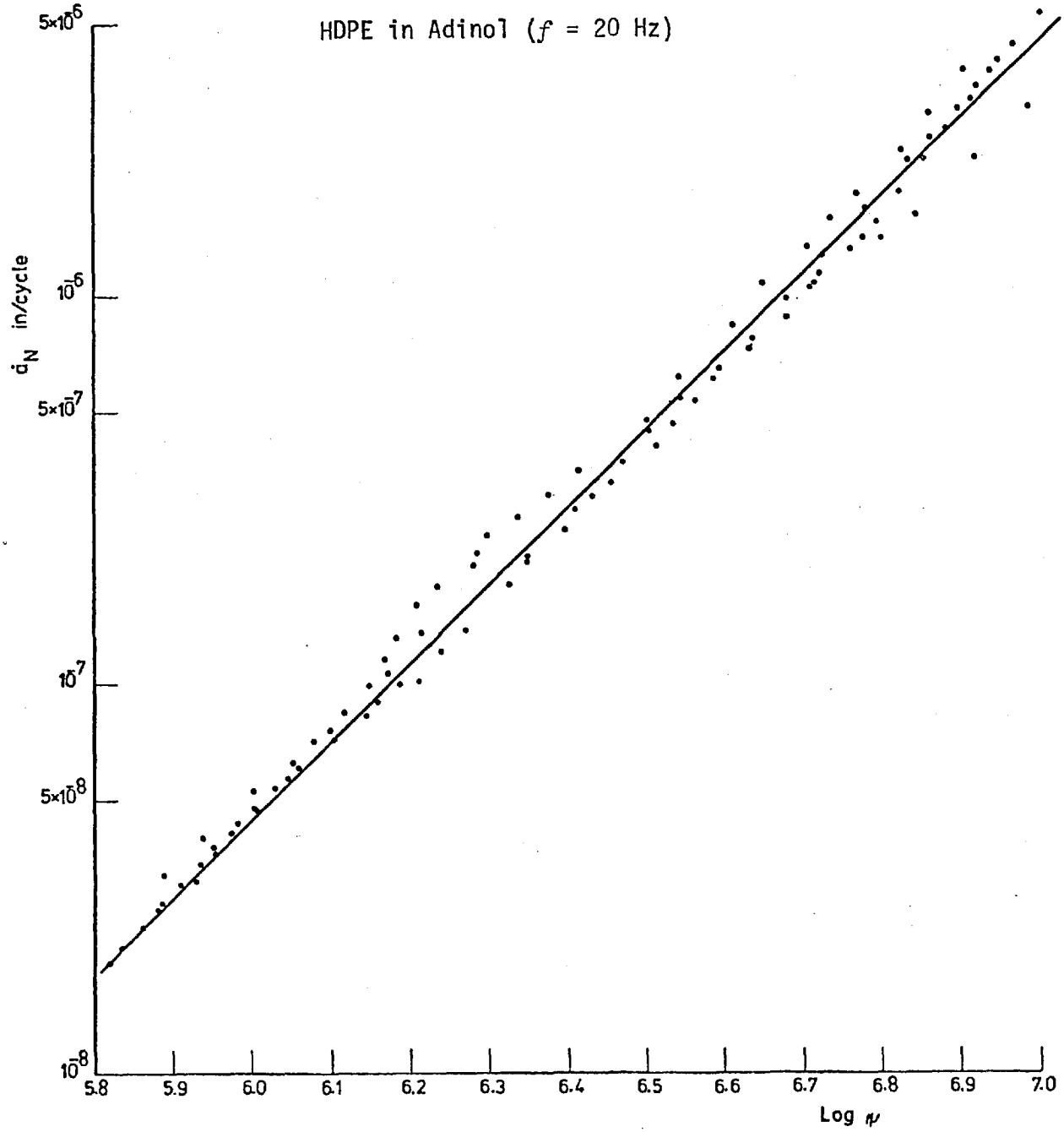

Figure 57: The log $\dot{a}_N$-log ψ relationship of HDPE tested in Adinol at f = 20 Hz

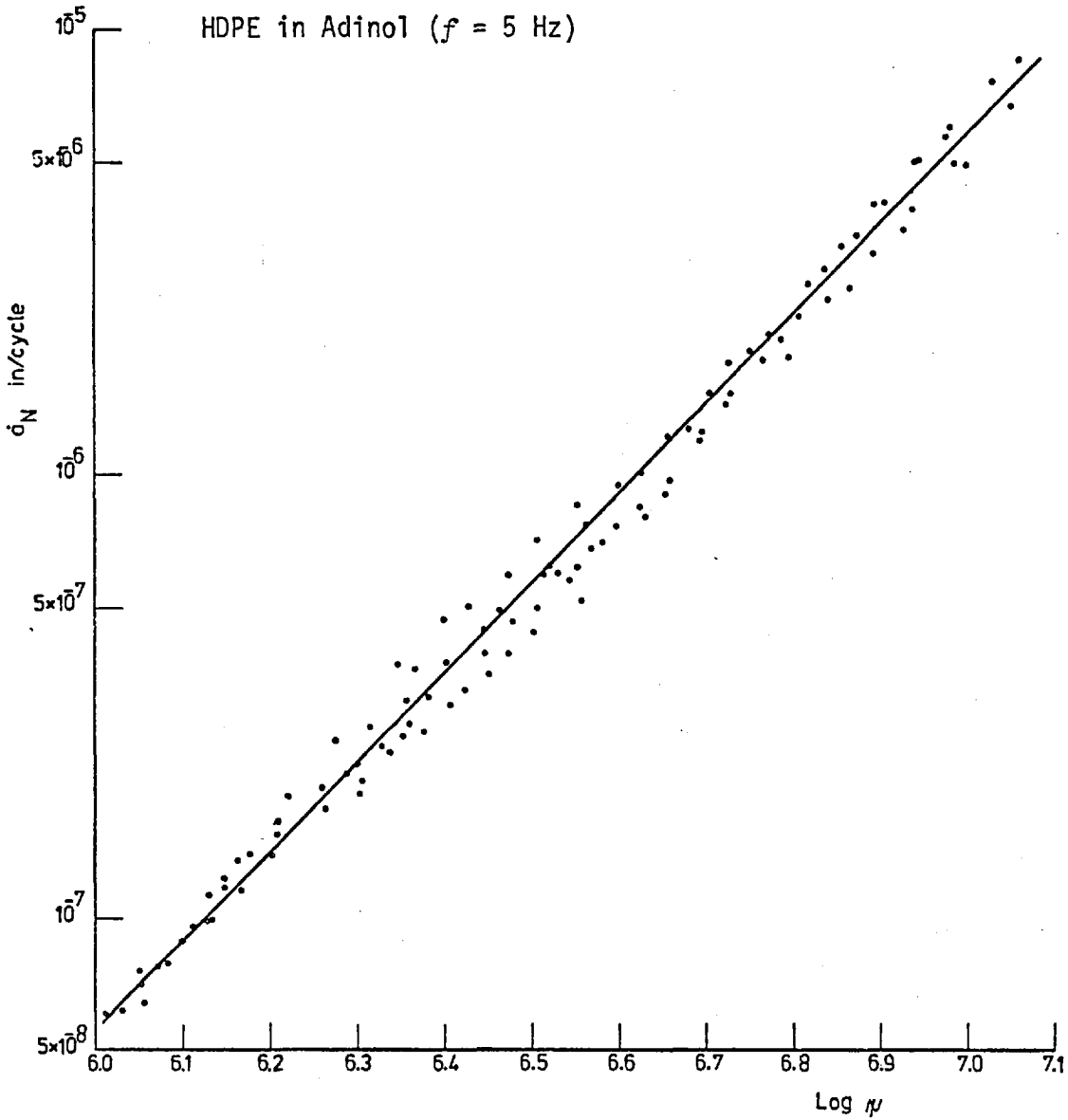

Figure 58: The log α_N-log ψ relationship of HDPE tested in Adinol at f = 5 Hz

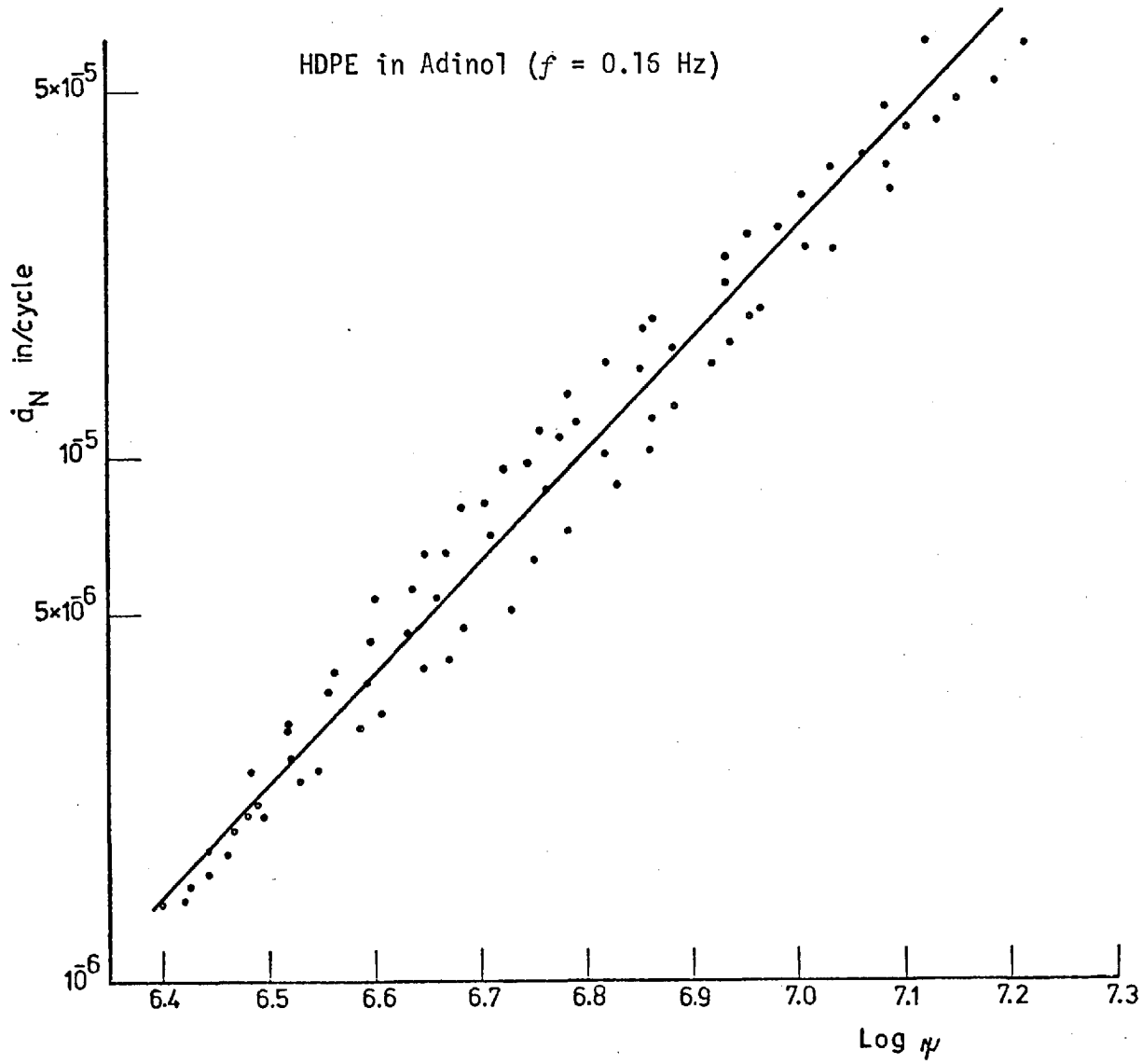

Figure 59: The log $\dot{a}_N$-log ψ relationship of HDPE tested in Adinol at f = 0.16 Hz

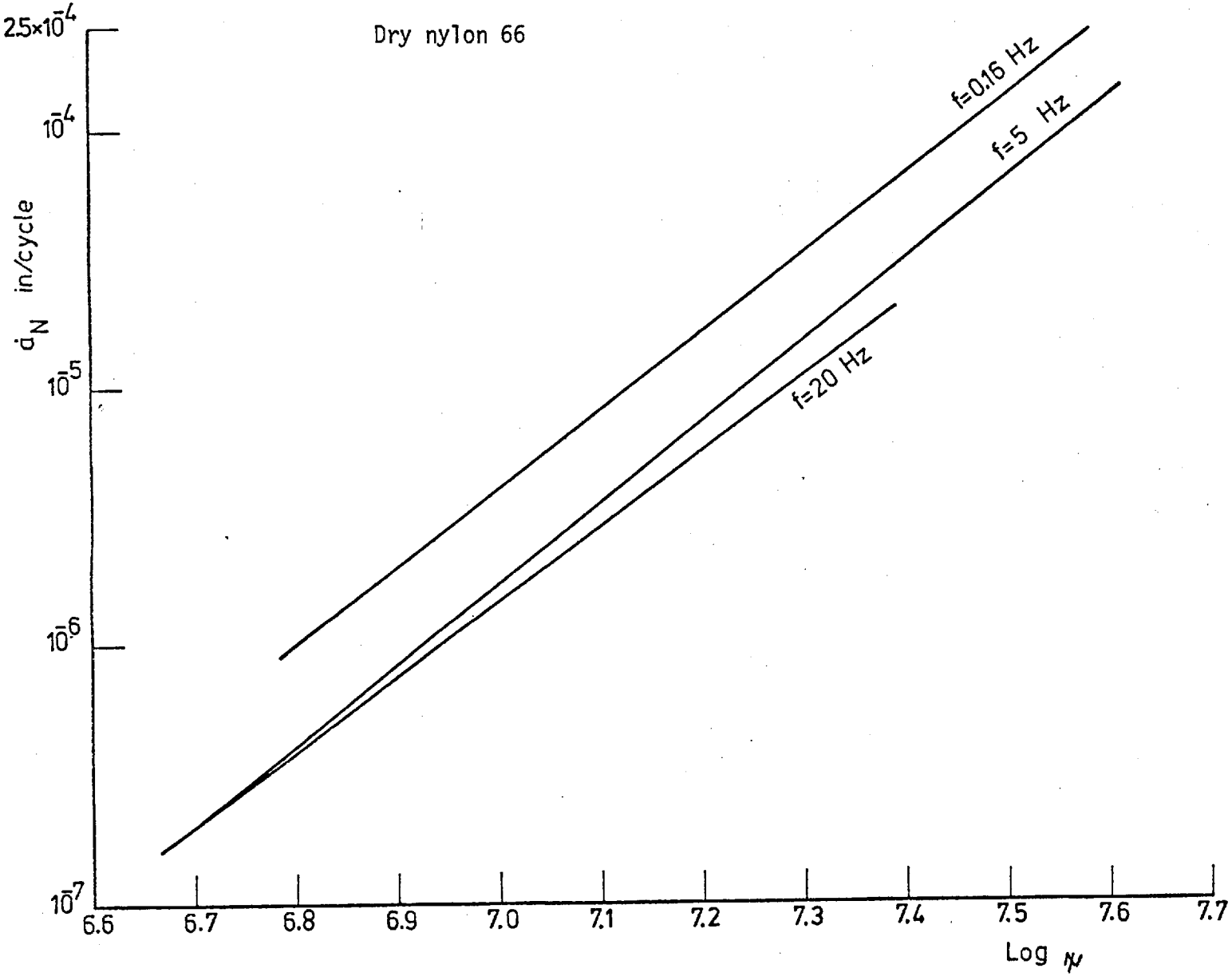

Figure 60: The log $\dot{a}_N$-log ψ relationship of dry N66 tested in air at different frequencies

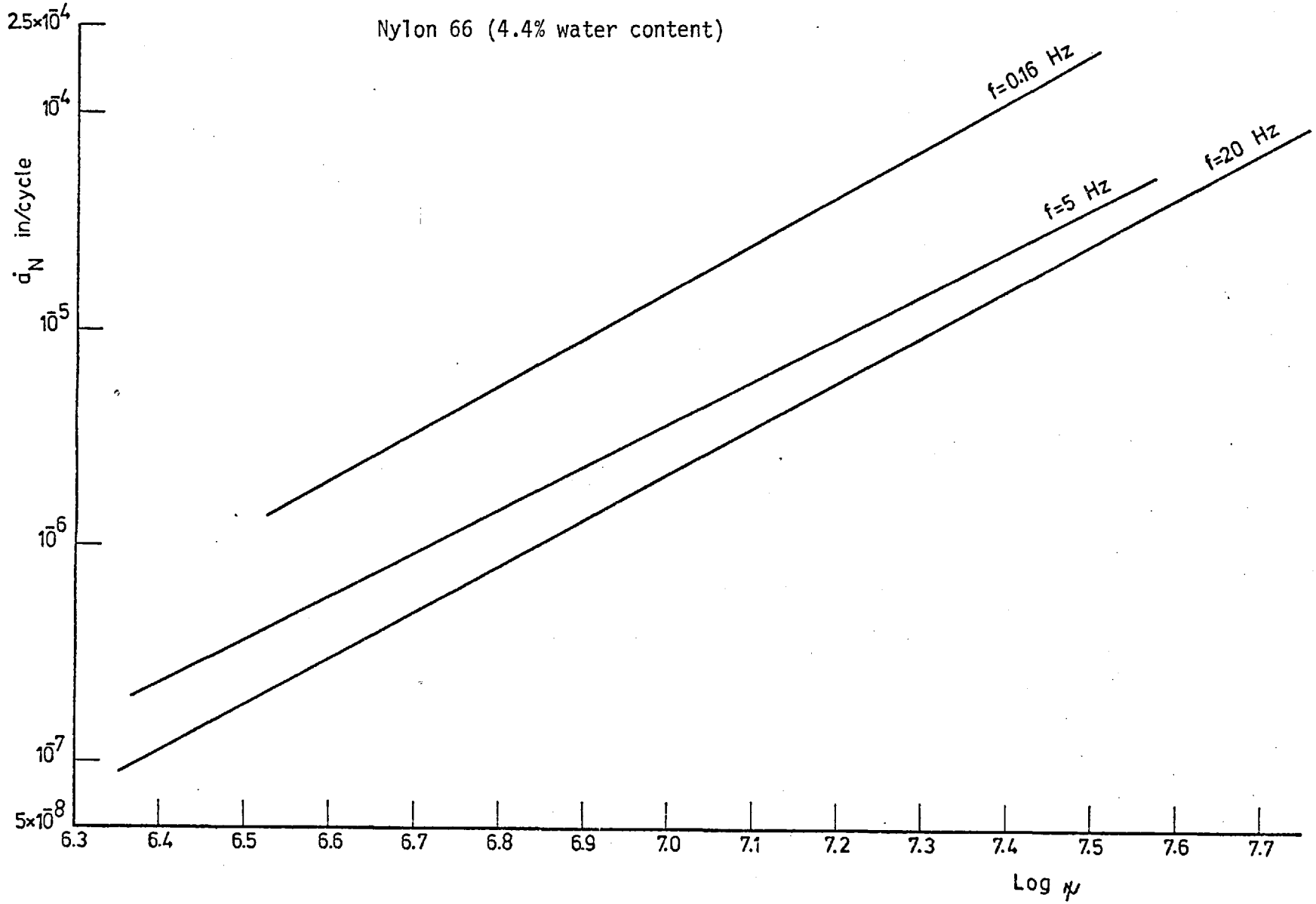

Figure 61: The log $\dot{a}_N$-log ψ relationship of N66 (4.4% water content) tested in air and distilled water at different frequencies

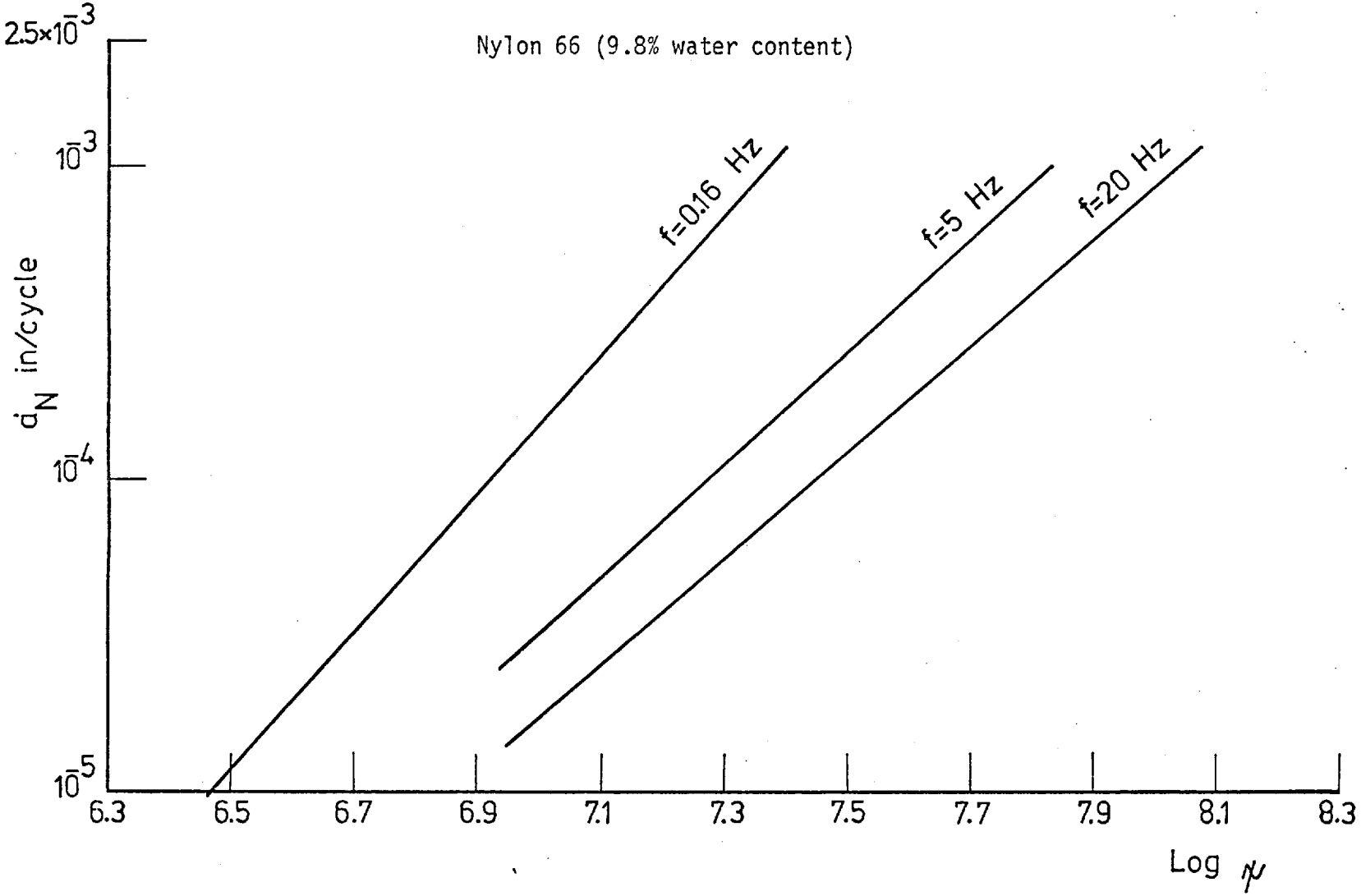

Figure 62: The log $\dot{a}_N$-log ψ relationship of N66 (9.8% water content) tested in distilled water at different frequencies

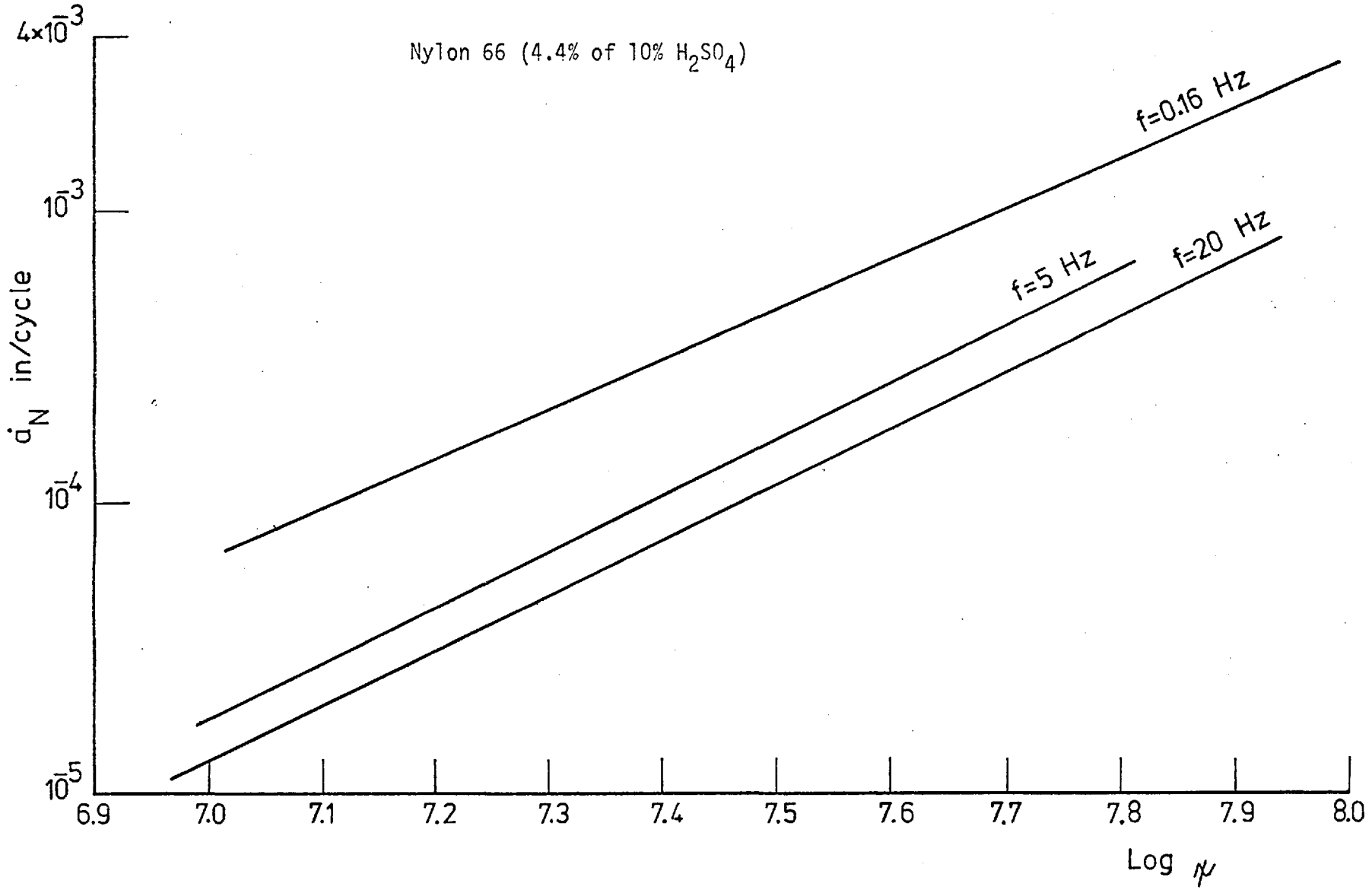

Figure 63: The log $\dot{a}_N$-log ψ relationship of N66 (4.4% of H_2SO_4 of 10% concentration) tested in 10% H_2SO_4 at different frequencies

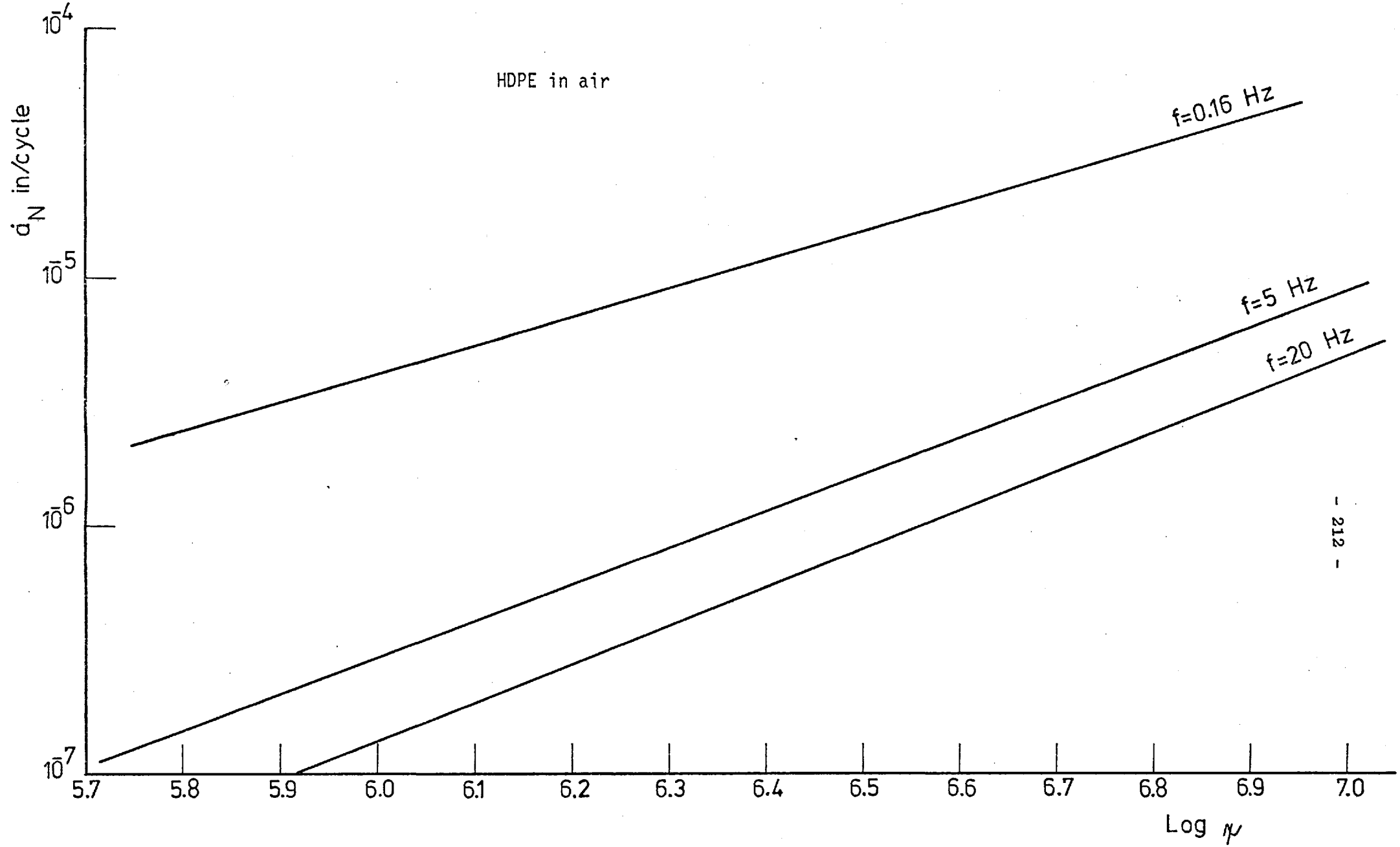

Figure 64: The log $\dot{a}_N$-log ψ relationship of HDPE tested in air at different frequencies

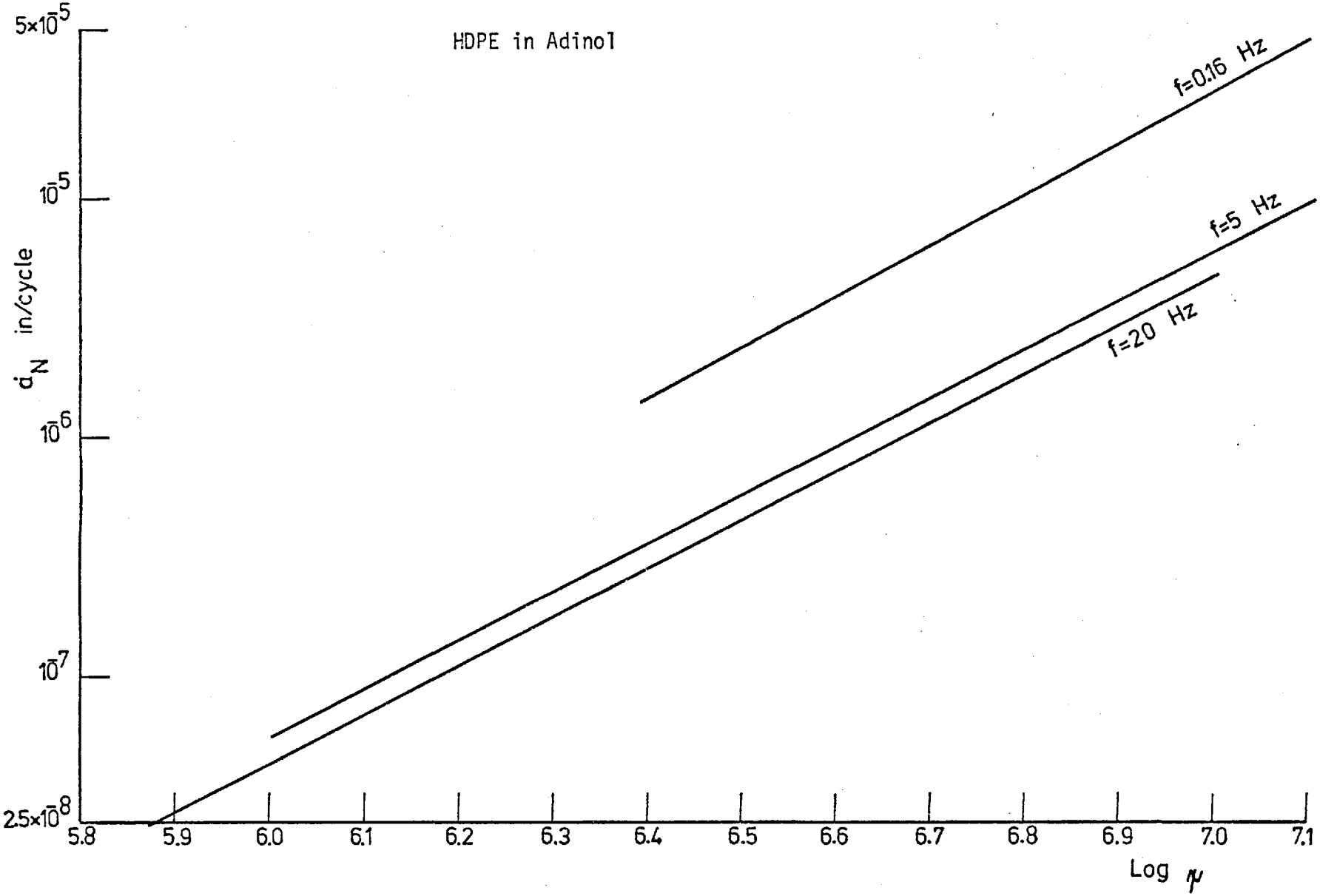

Figure 65: The log $\dot{a}_N$-log ψ relationship of HDPE tested in Adinol at different frequencies

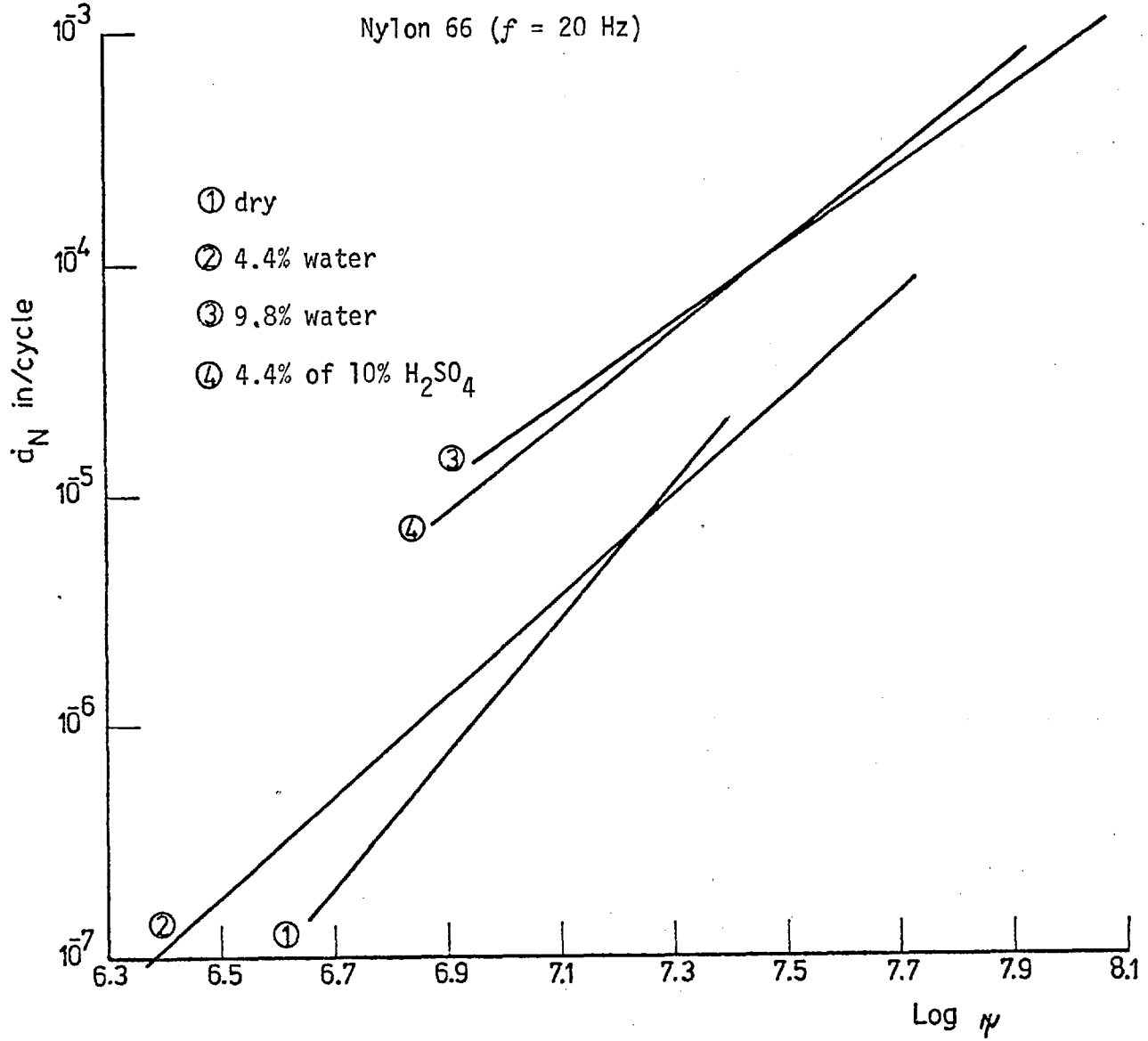

Figure 66: The log $\dot{a}_N$-log ψ relationship of conditioned N66 at f = 20 Hz

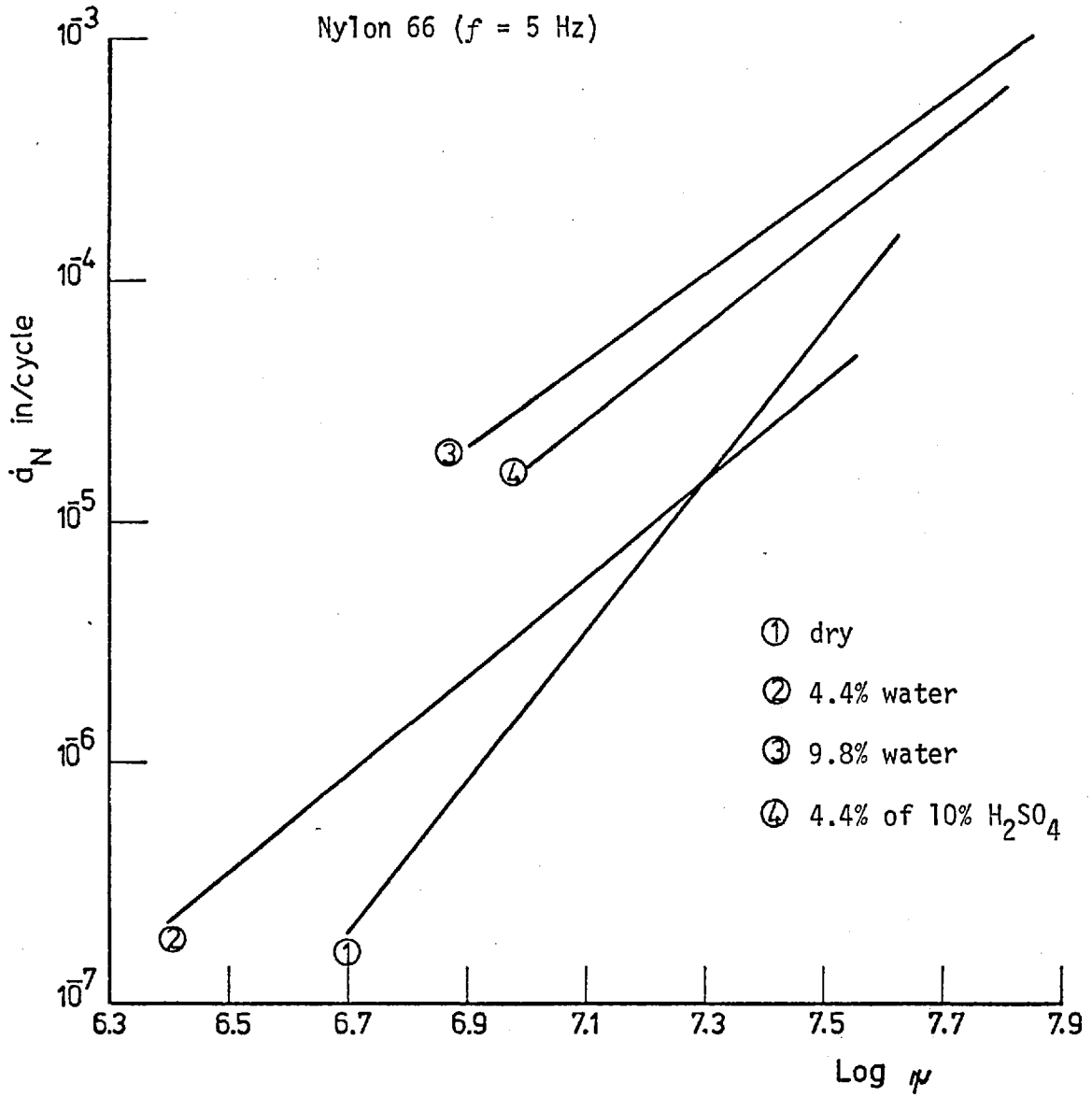

Figure 67: The log $\dot{a}_N$-log ψ relationship of conditioned N66 at f = 5 Hz

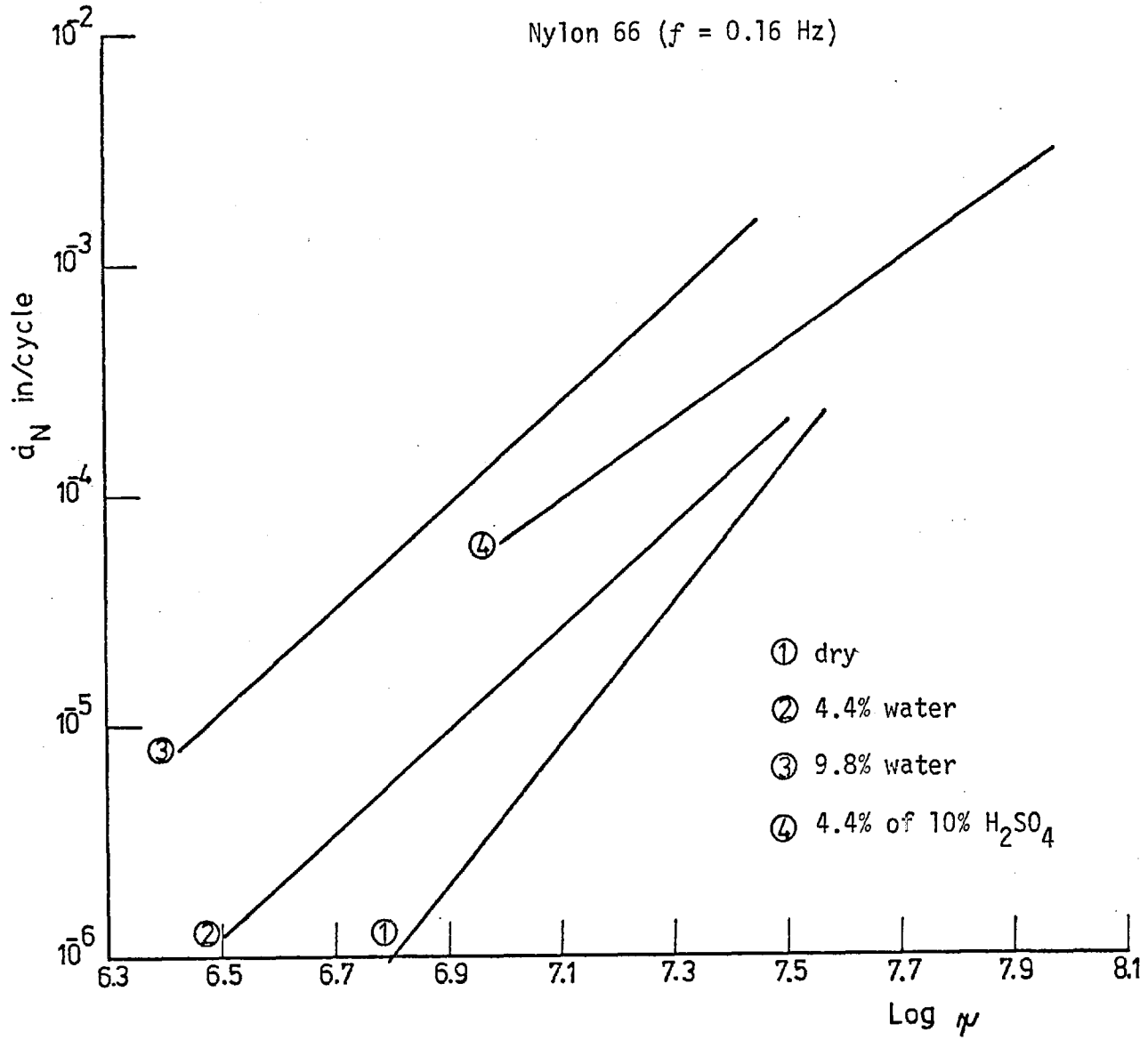

Figure 68: The log $\dot{a}_N$-log ψ relationship of conditioned N66 at f = 0.16 Hz

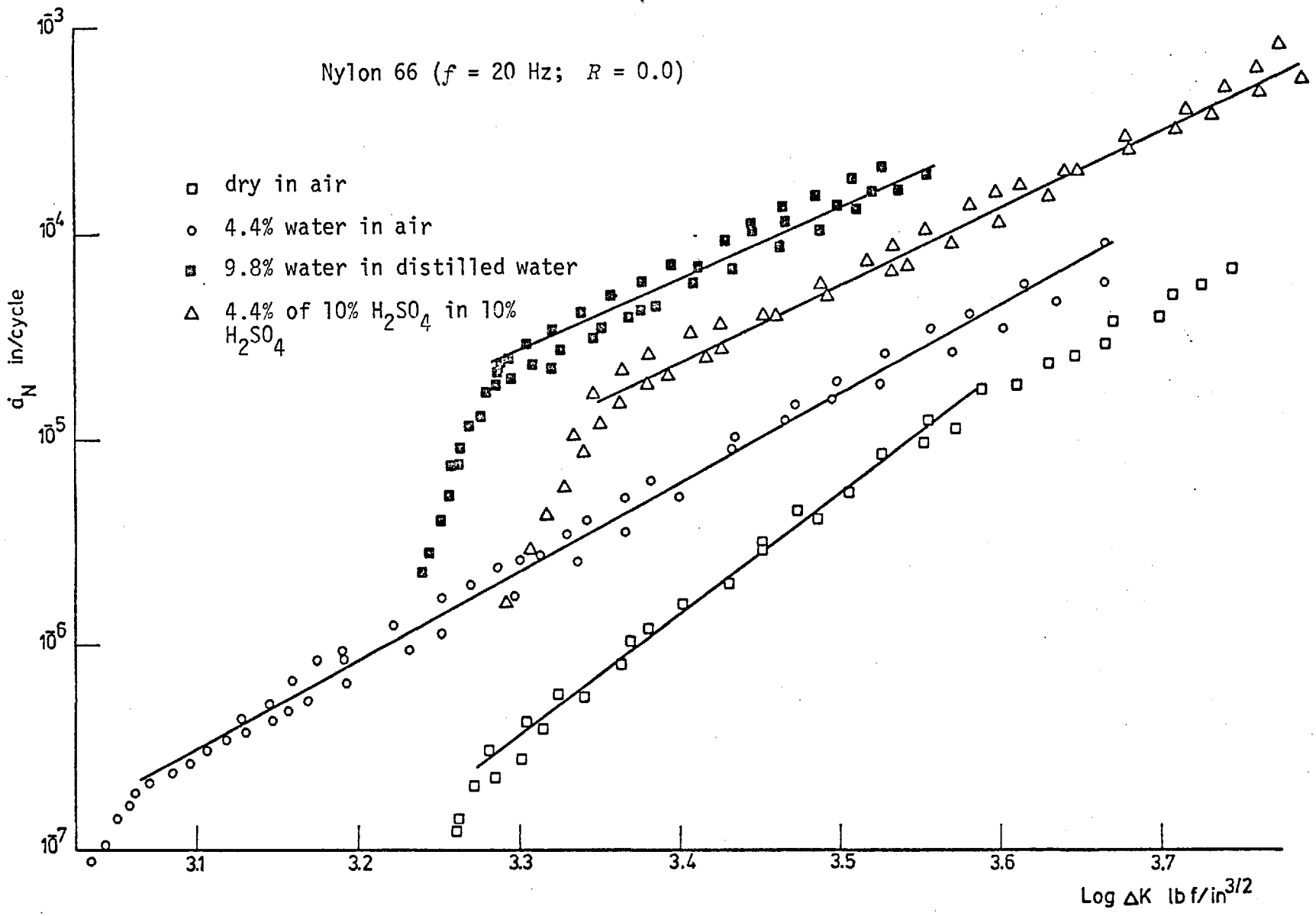

Figure 69: The log $\dot{a}_N$-log ΔK relationship of conditioned N66 at f = 20 Hz and R = 0

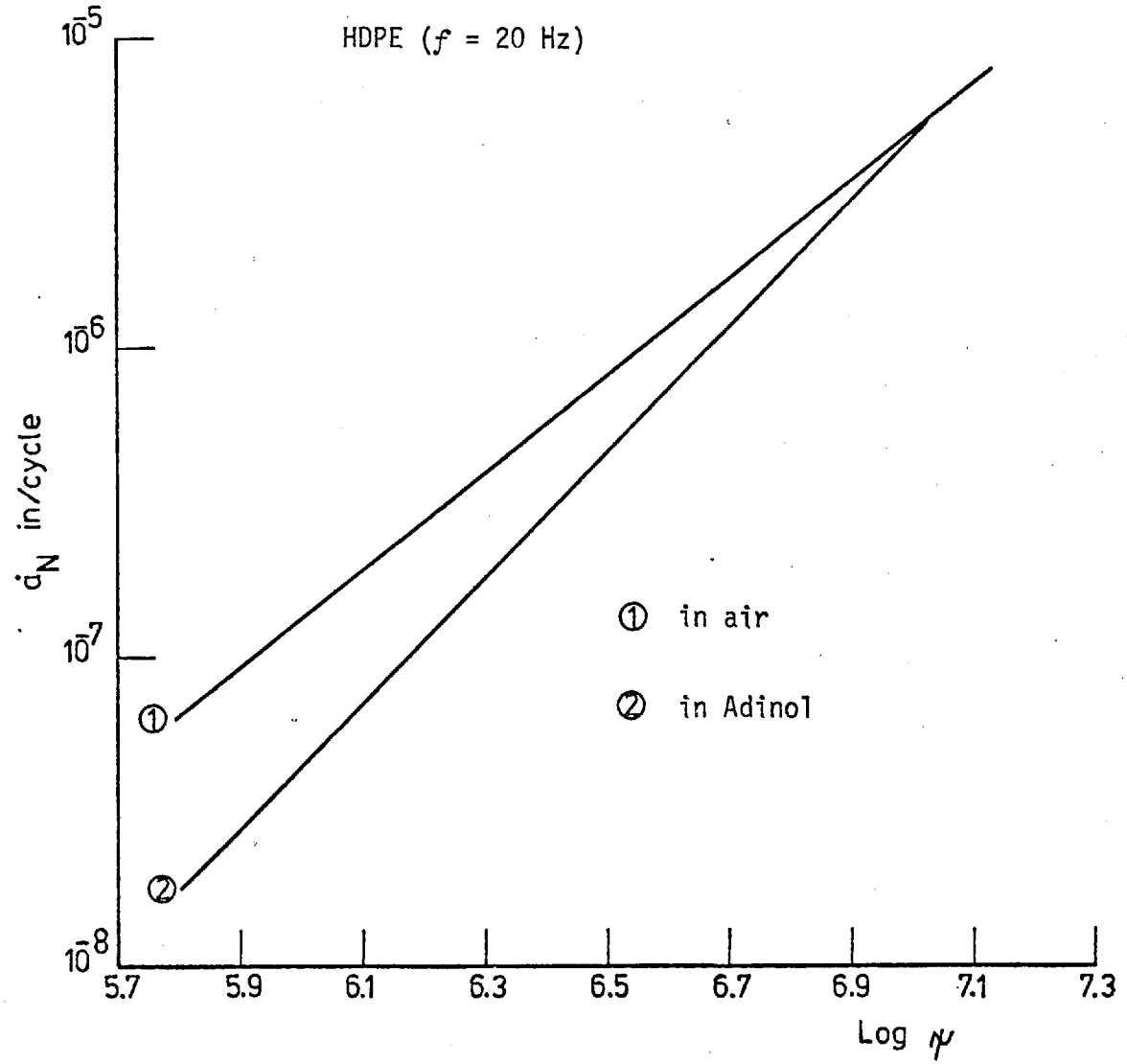

Figure 70: The log $\dot{a}_N$-log ψ relationship of HDPE in air and Adinol at f = 20 Hz

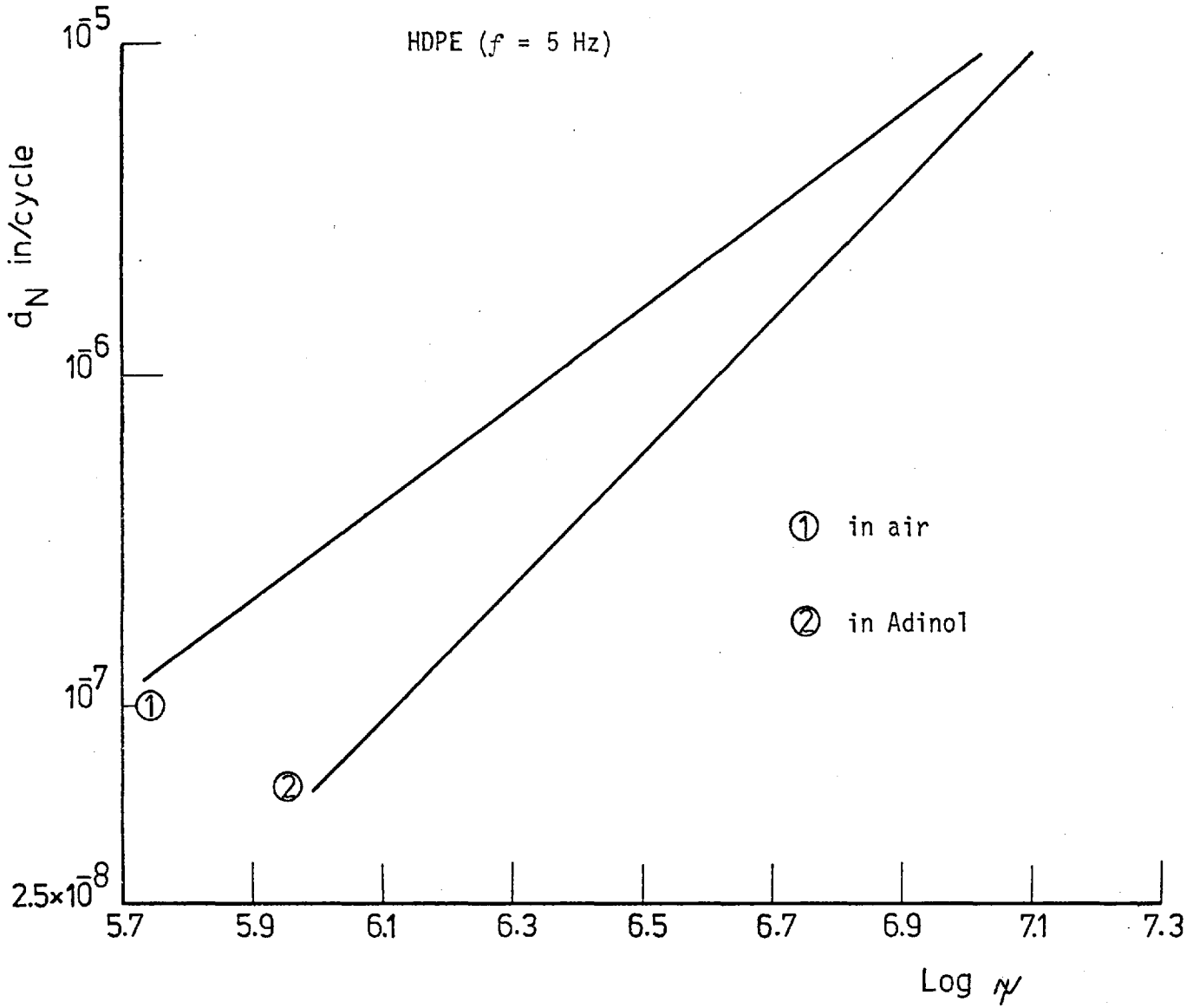

Figure 71: The log $\dot{a}_N$-log ψ relationship of HDPE in air and in Adinol at f = 5 Hz

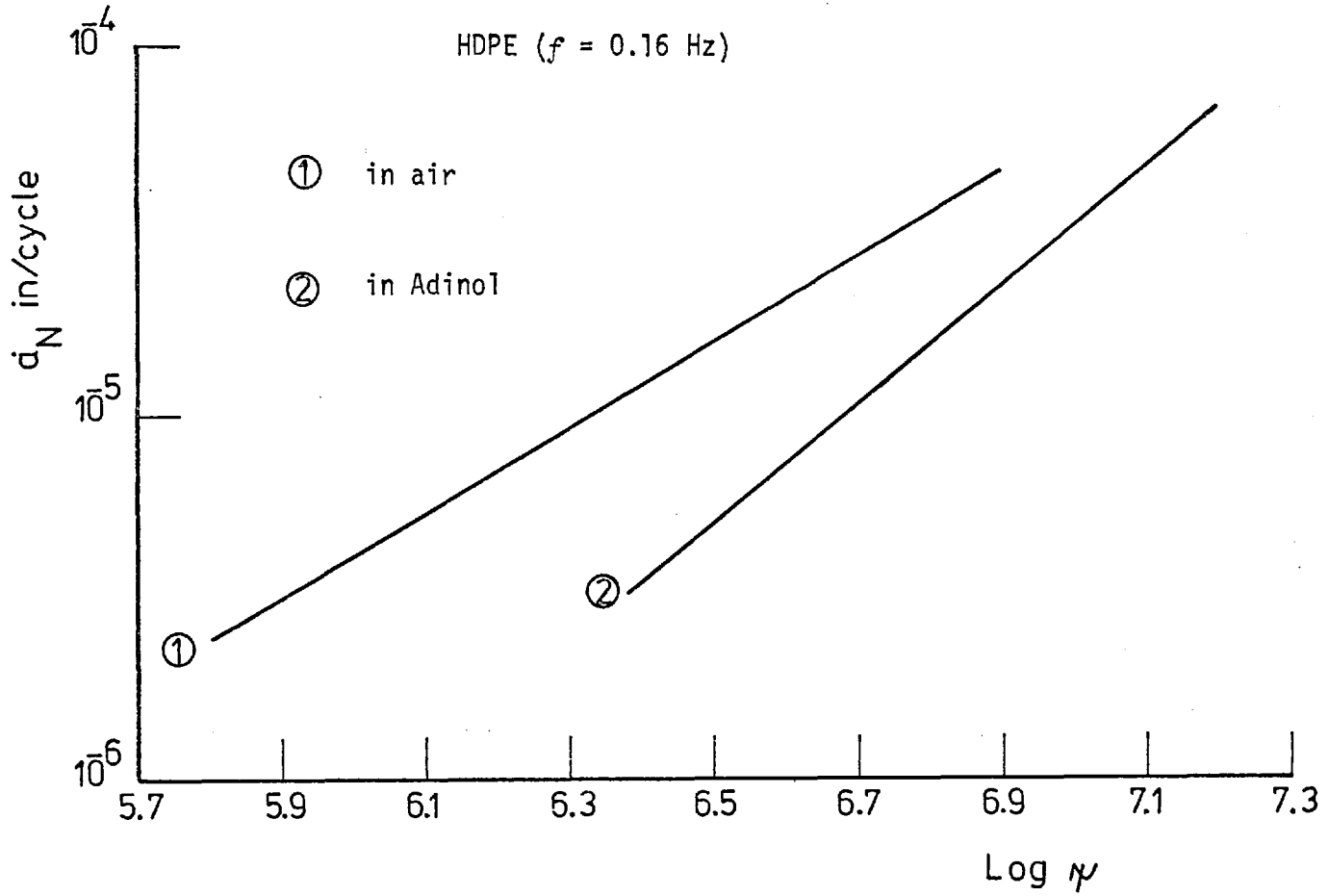

Figure 72: The log $\dot{a}_N$-log ψ relationship of HDPE in air and in Adinol at f = 0.16 Hz

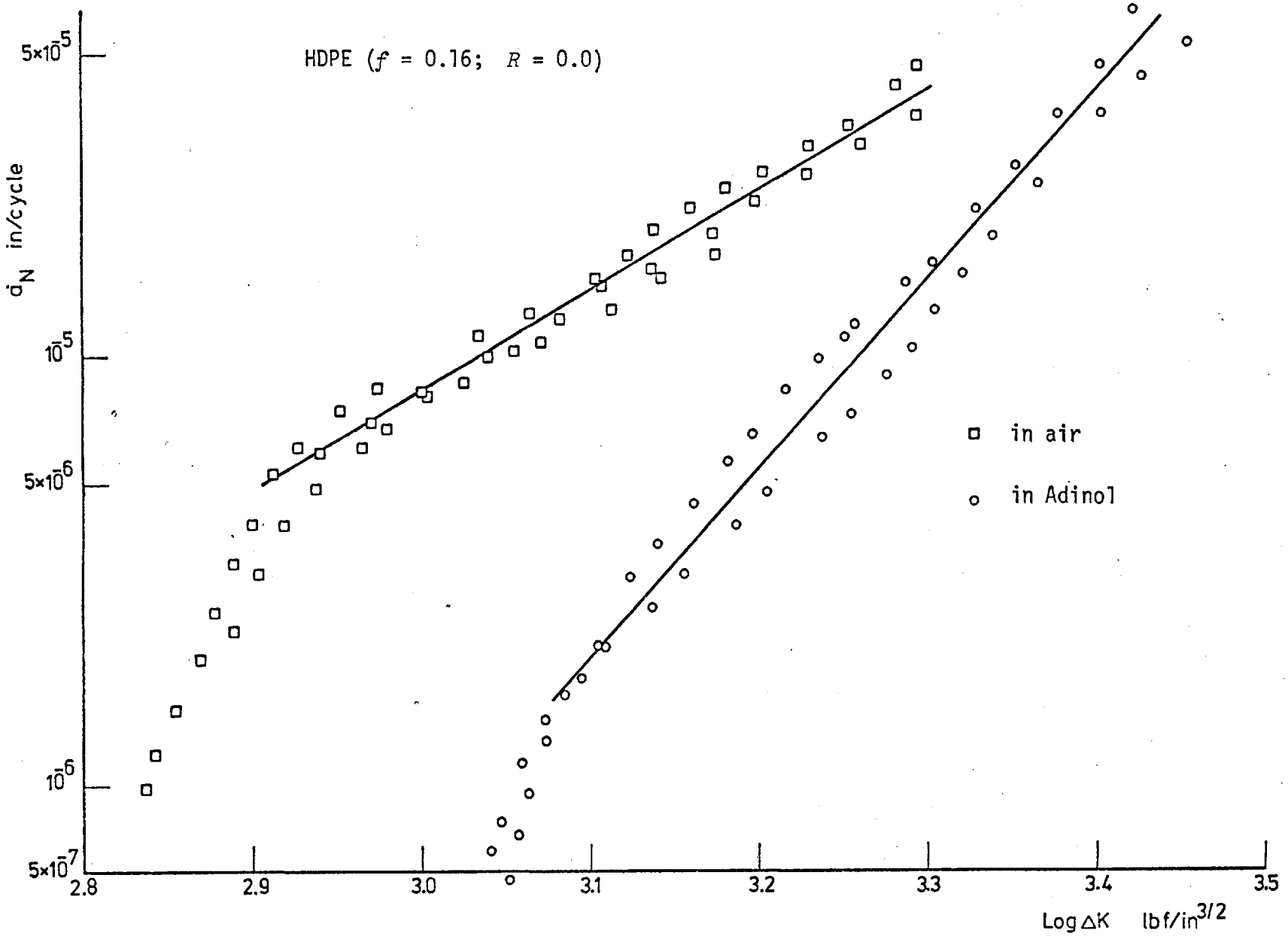

Figure 73: The log $\dot{a}_N$-log ΔK relationship of HDPE in air and Adinol at f = 0.16 Hz and R = 0

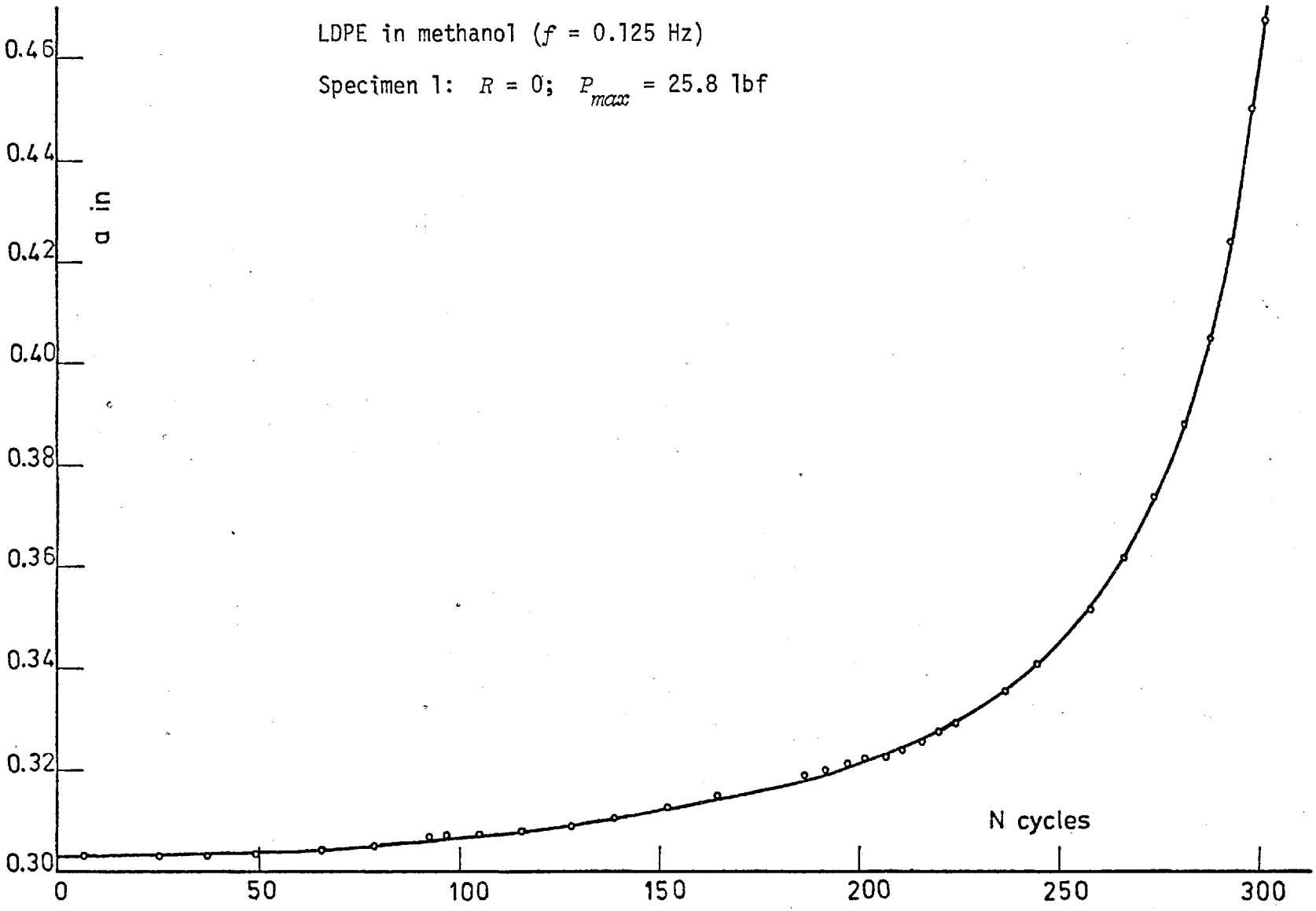

Figure 74: Crack length vs. number of cycles - LDPE tested in methanol

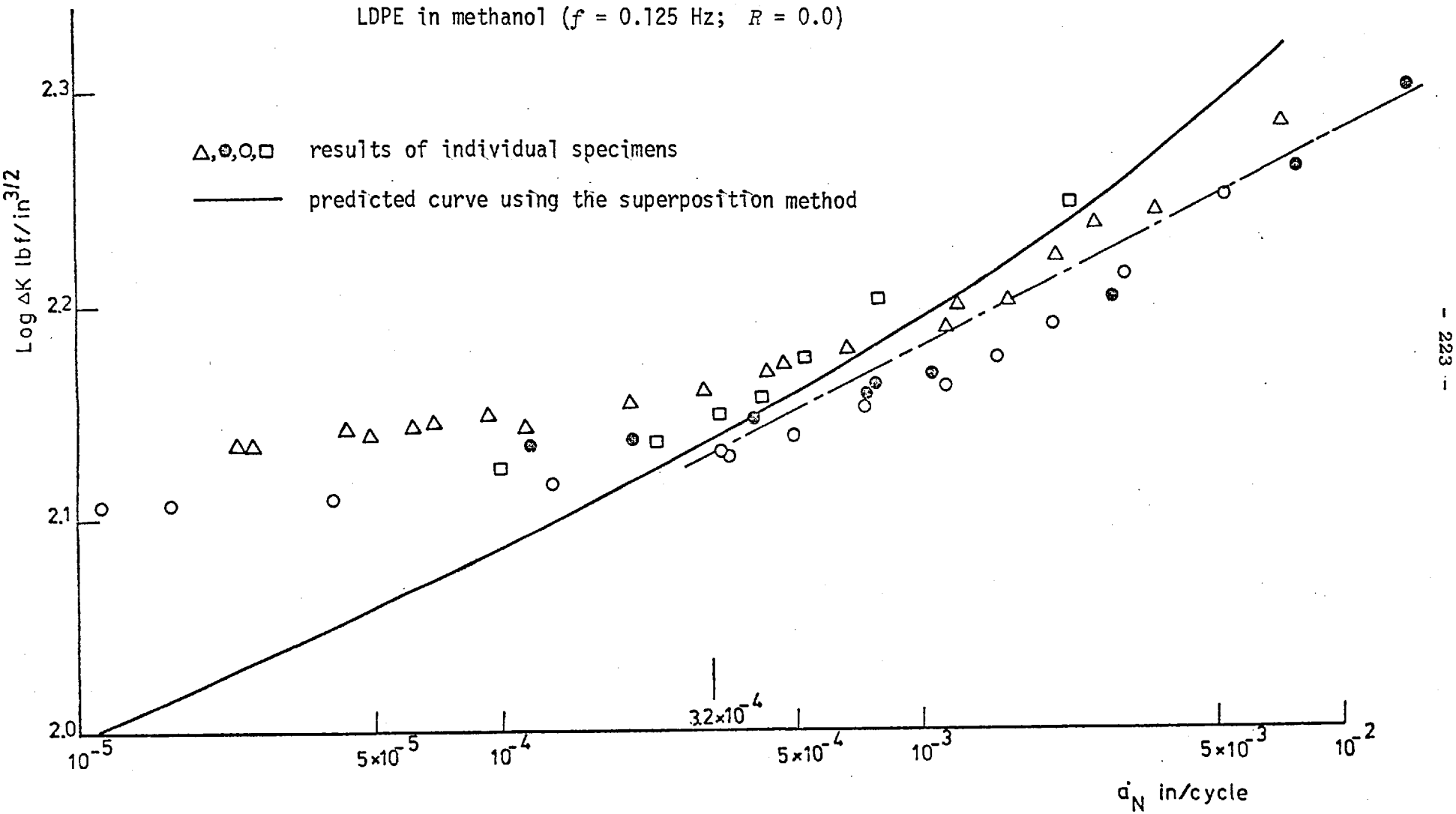

Figure 75: The log $\dot{a}_N$-log ΔK relationship of LDPE tested in methanol at f = 0.125 Hz and R = 0

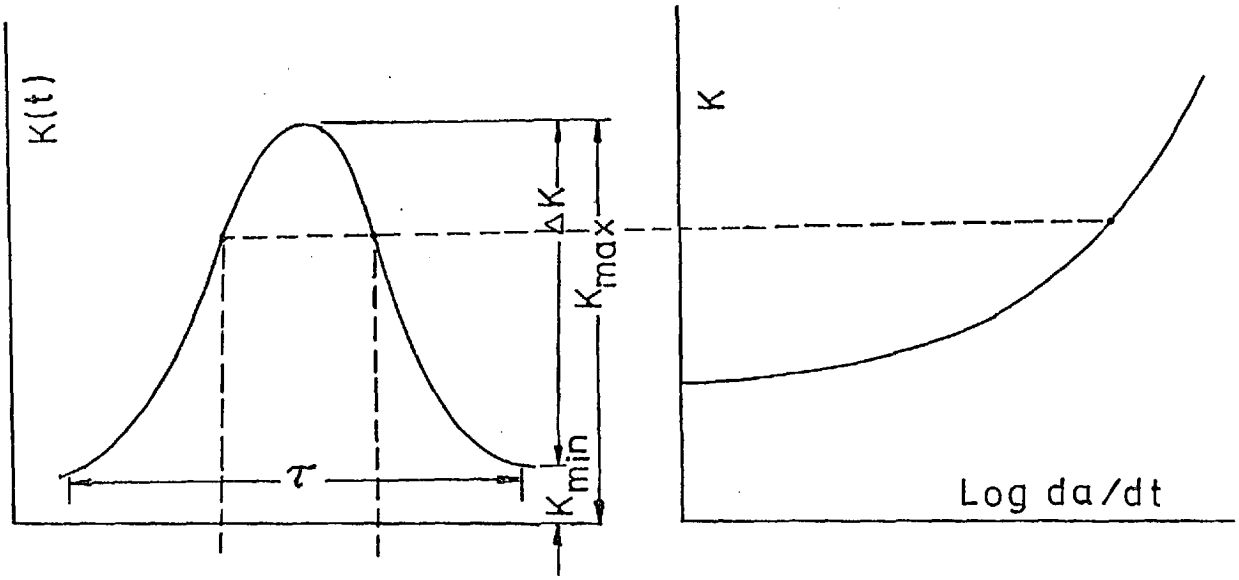

(a) Stress intensity factor as a function of time in dynamic fatigue

(b) Static fatigue: rate of crack growth under sustained load in an aggressive environment

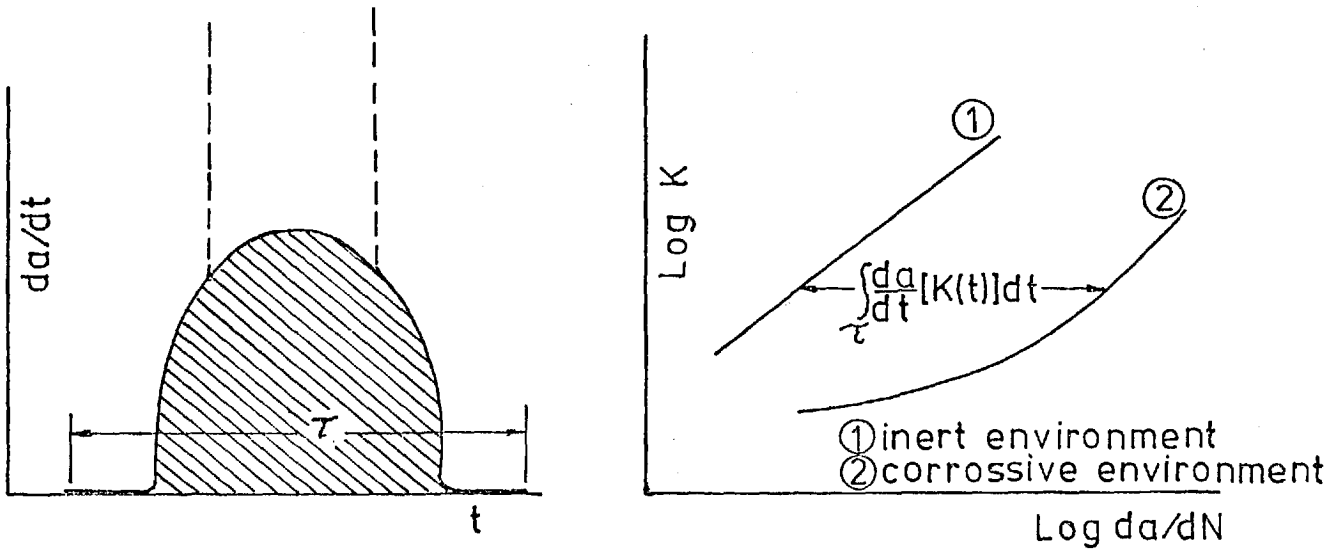

(c) The area under the curve represents the environmental contribution to crack growth in dynamic fatigue

(d) Resulting effect of adding the two contributions on cyclic fatigue crack growth rate

$$= \int_{\tau} \frac{da}{dt} \left[K(t)\right] \, dt$$

Figure 76: Schematic diagram illustrating the graphical method of the superposition analysis (after Wei and Landes, 1969)

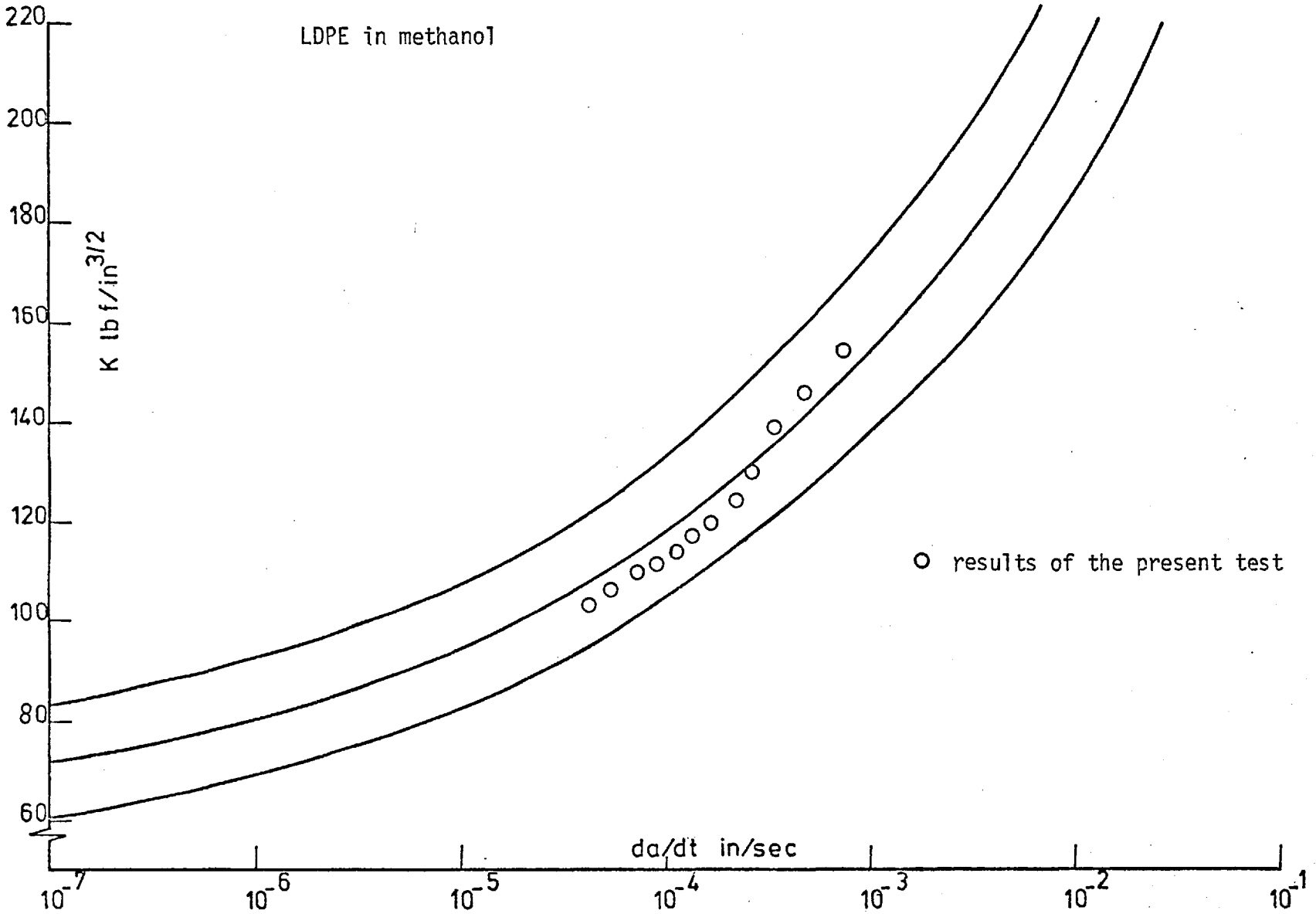

Figure 77: Fracture toughness vs. crack speed for LDPE in methanol - constant load test (after Marshall et al, 1969b)

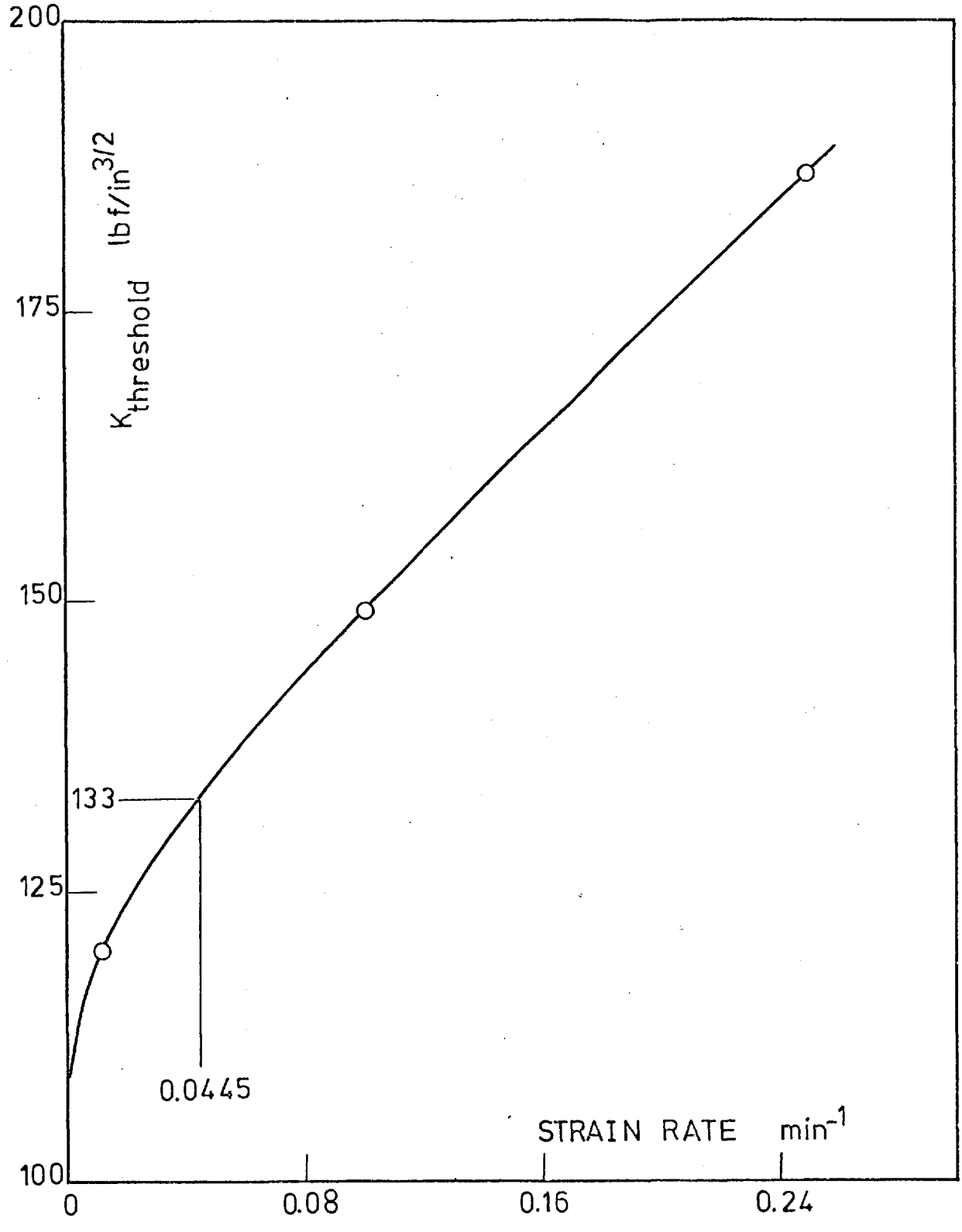

Figure 78: Effect of strain rate on the threshold value of K - LDPE in methanol

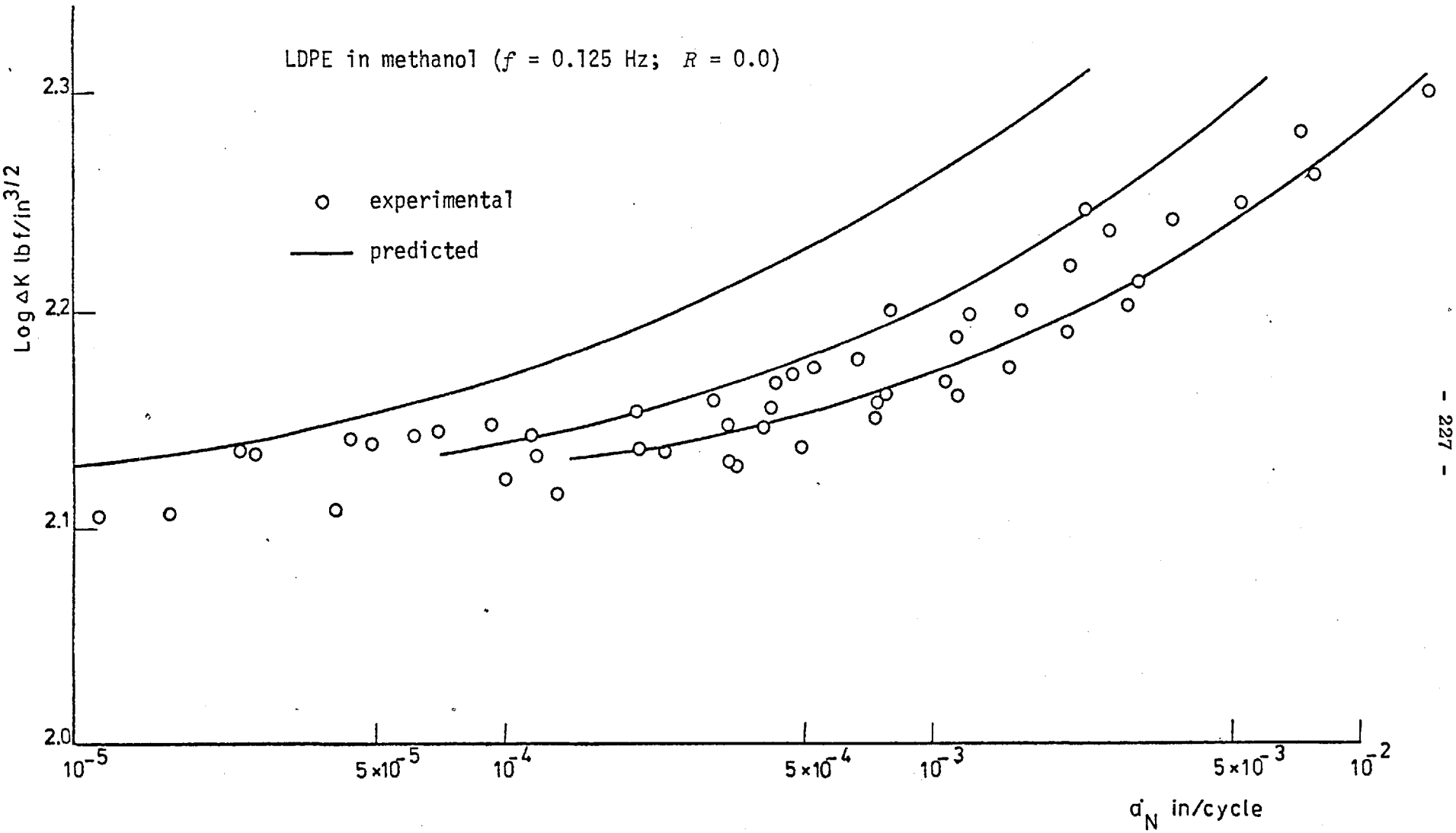

Figure 79: Comparison of the experimental results and the predicted ones by the superposition method considering the rate sensitivity of K_{th}

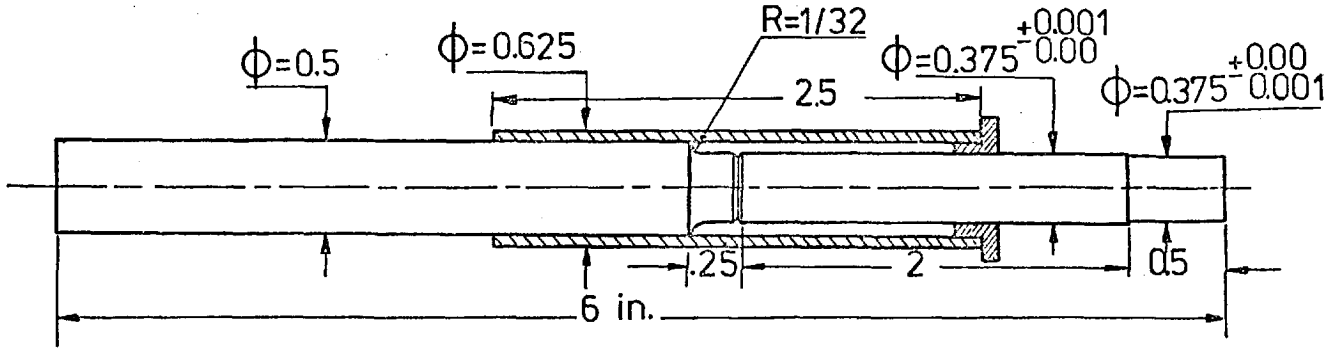

(a)

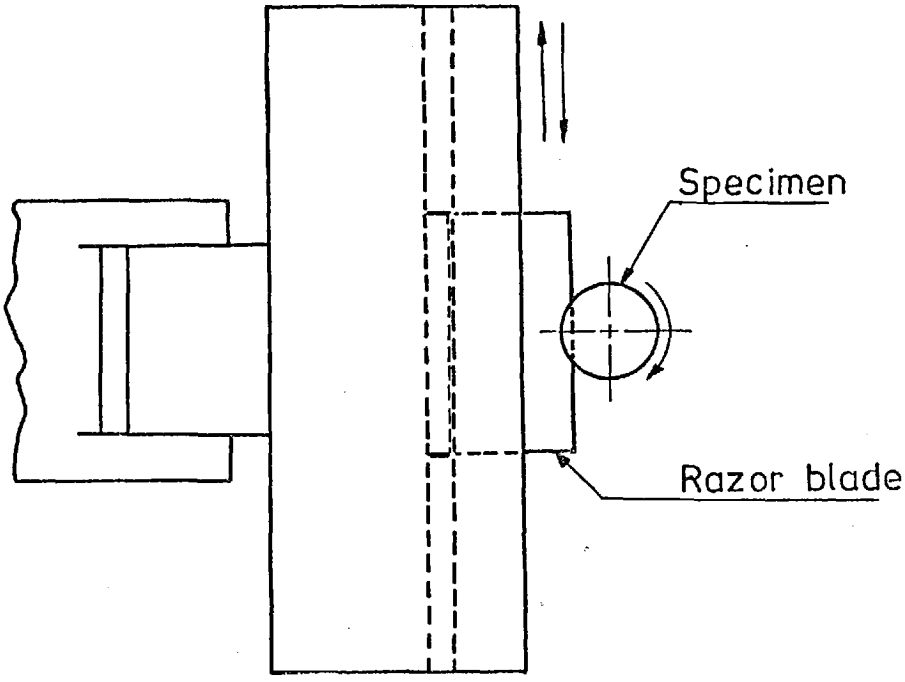

(b)

Figure 80: (a) Test specimen in a rubber sleeve

(b) Notching special attachment

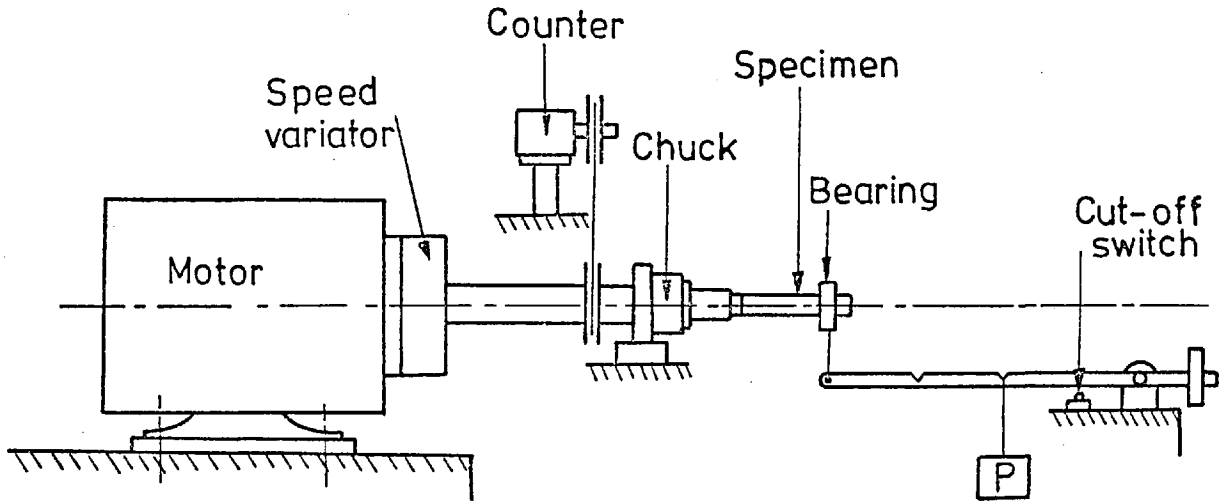

Figure 81: Rotating bending rig

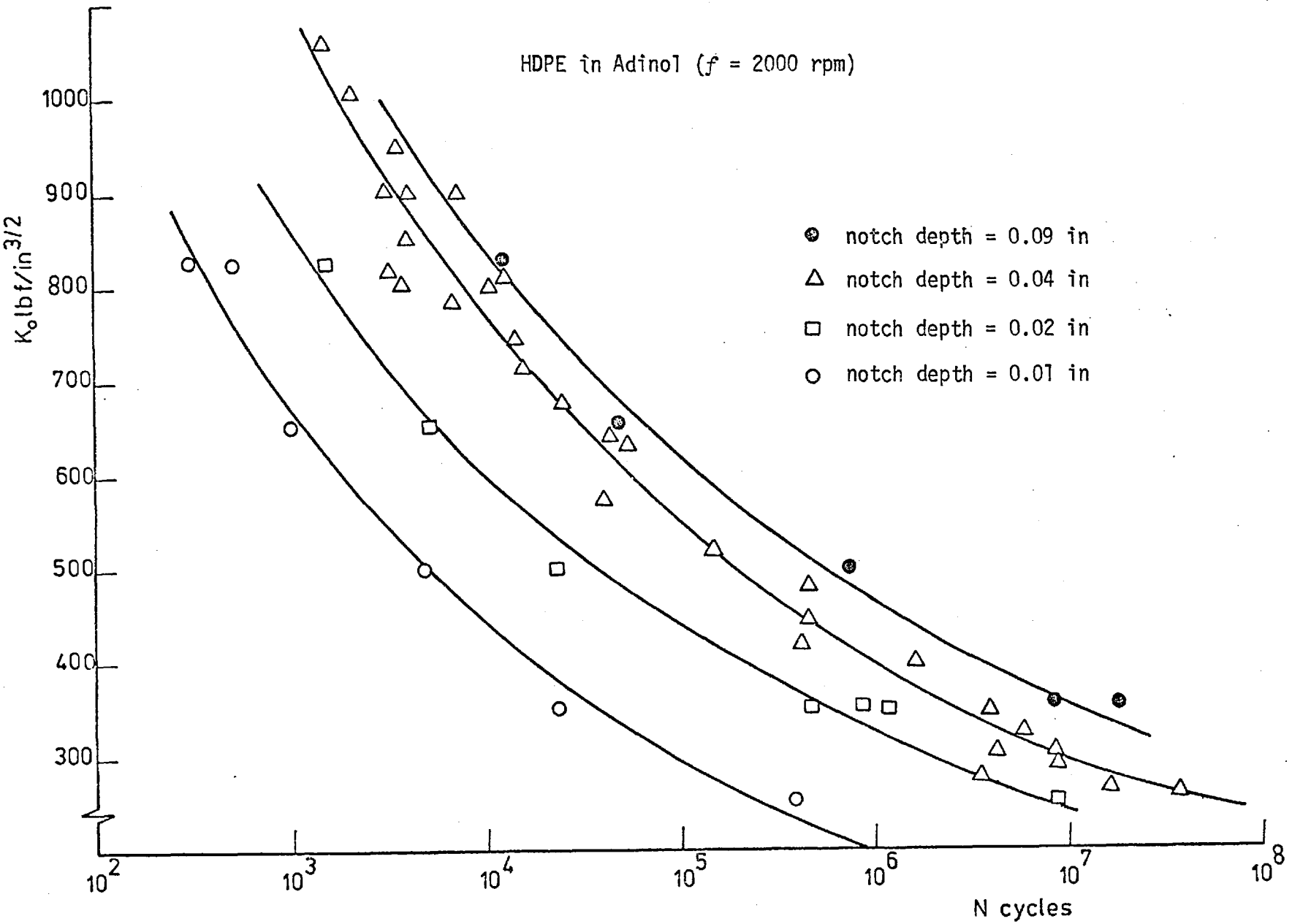

Figure 82: Effect of notch depth on the K_o-log N relationship for HDPE in Adinol at f = 2000 rpm

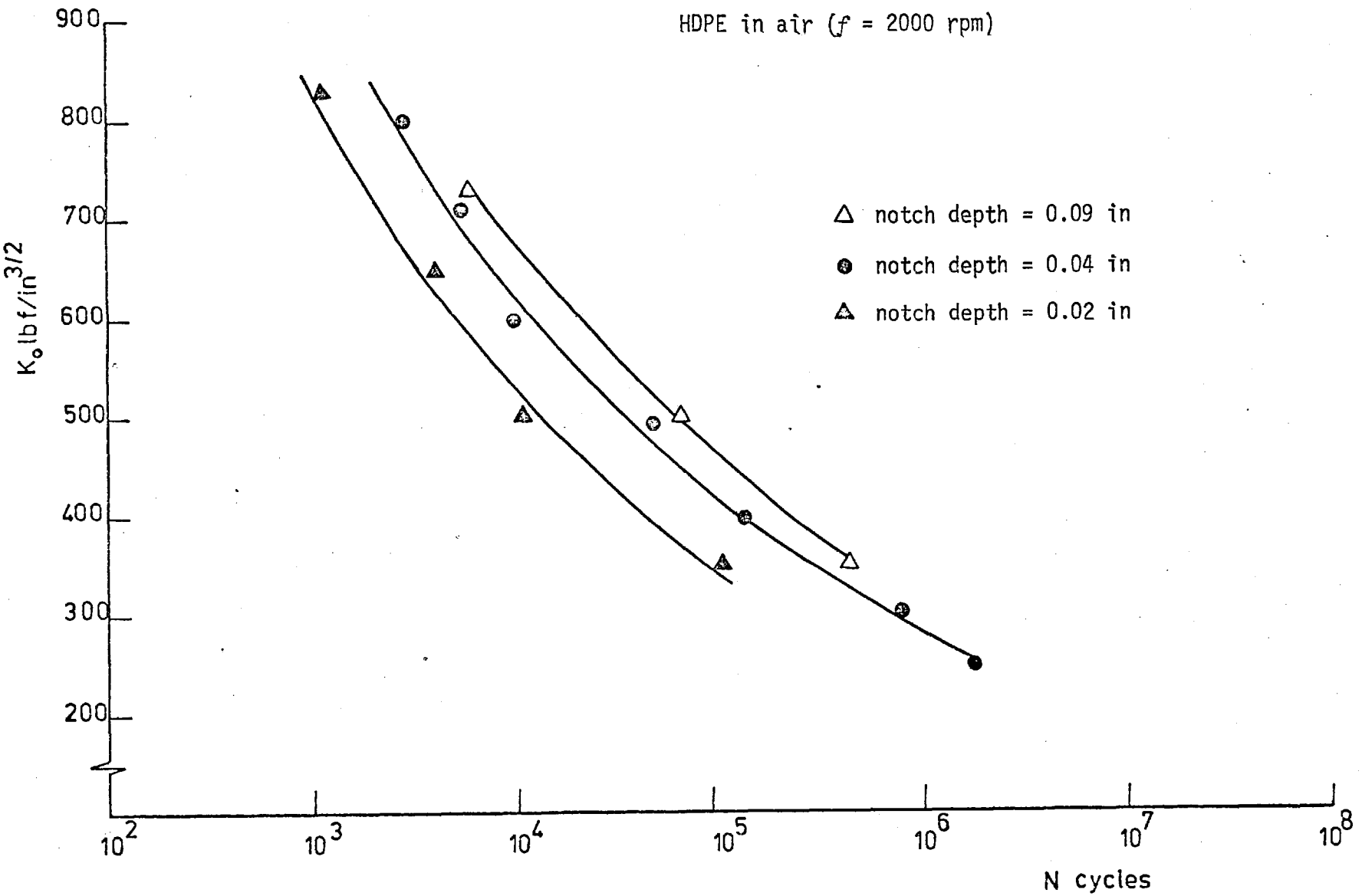

Figure 83: Effect of notch depth on the K_o-log N relationship for HDPE in air at f = 2000 rpm

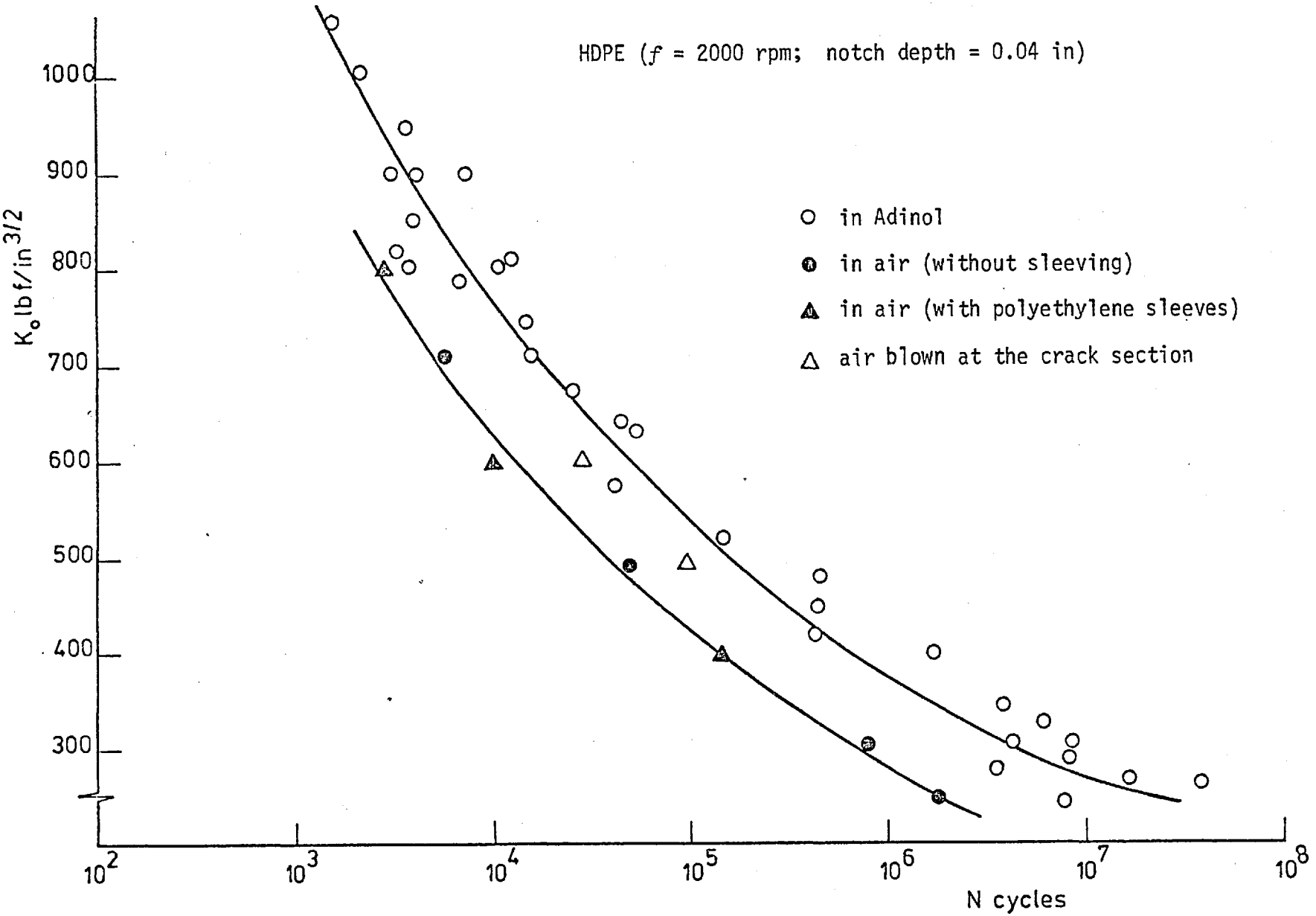

Figure 84: Effect of sleeving and blowing air at the crack tip on the results of HDPE in air and comparison with the results in Adinol

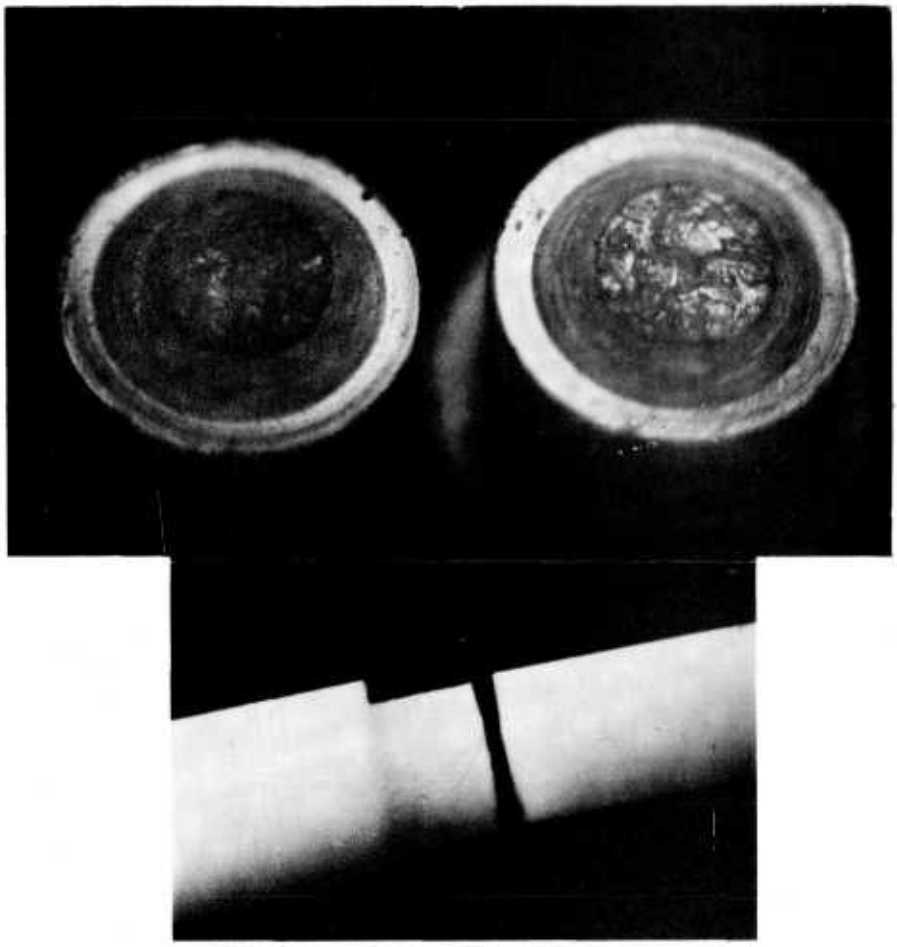

(a)

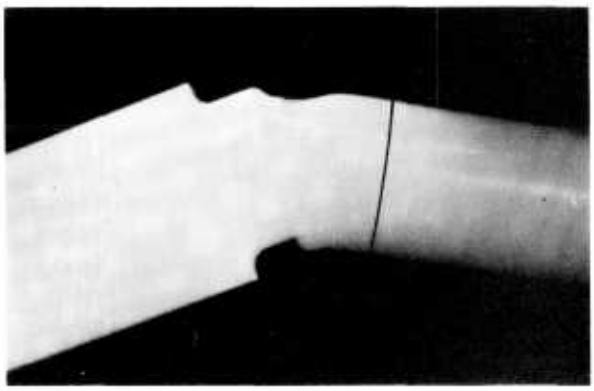

(b)

Figure 85: Cyclic fatigue failure of HDPE

(a) Failure by crack propagation

(b) Failure by thermal softening

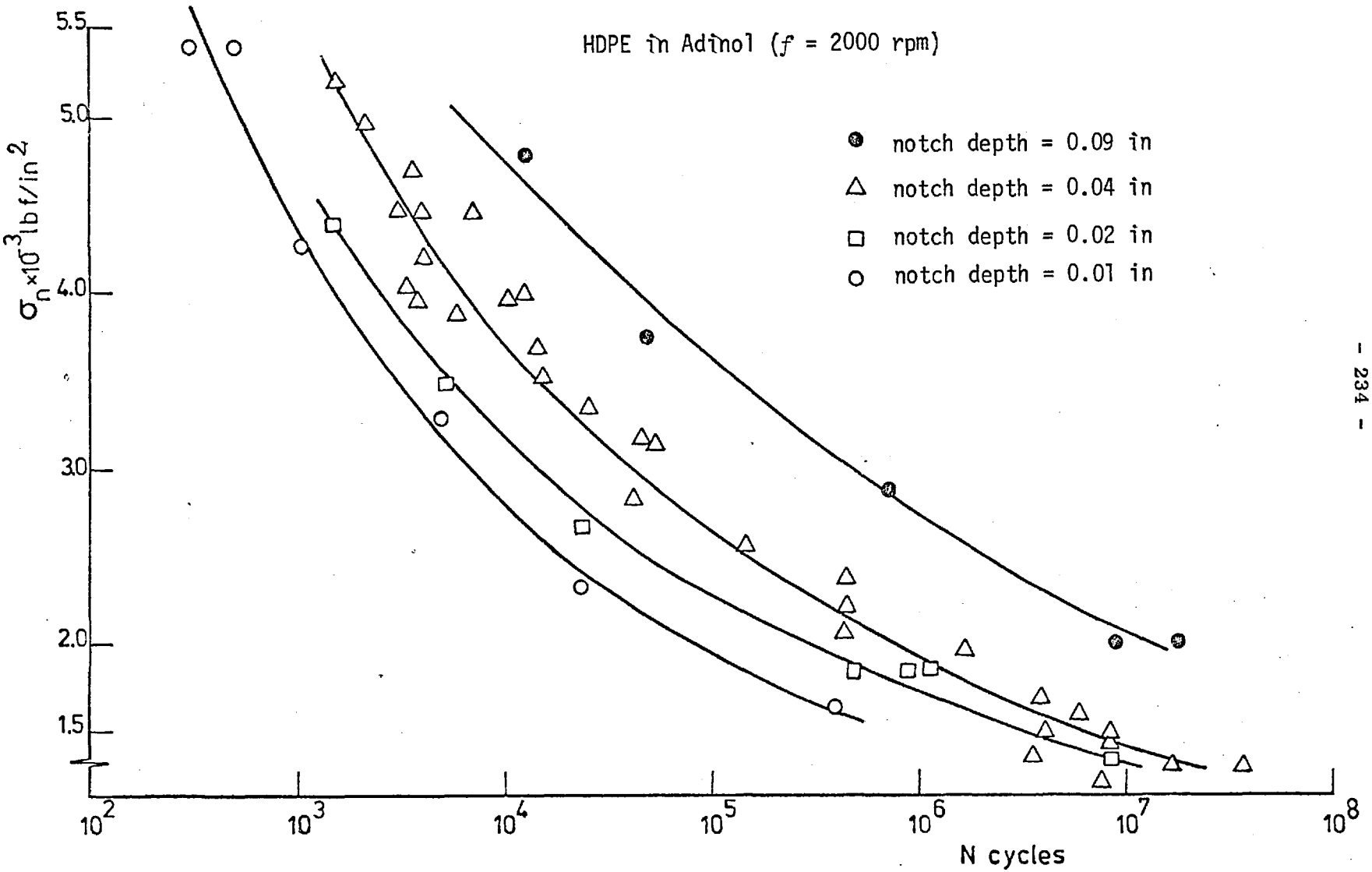

Figure 86: Effect of notch depth on the σ_n-log N relationship for HDPE in Adinol at f = 2000 rpm

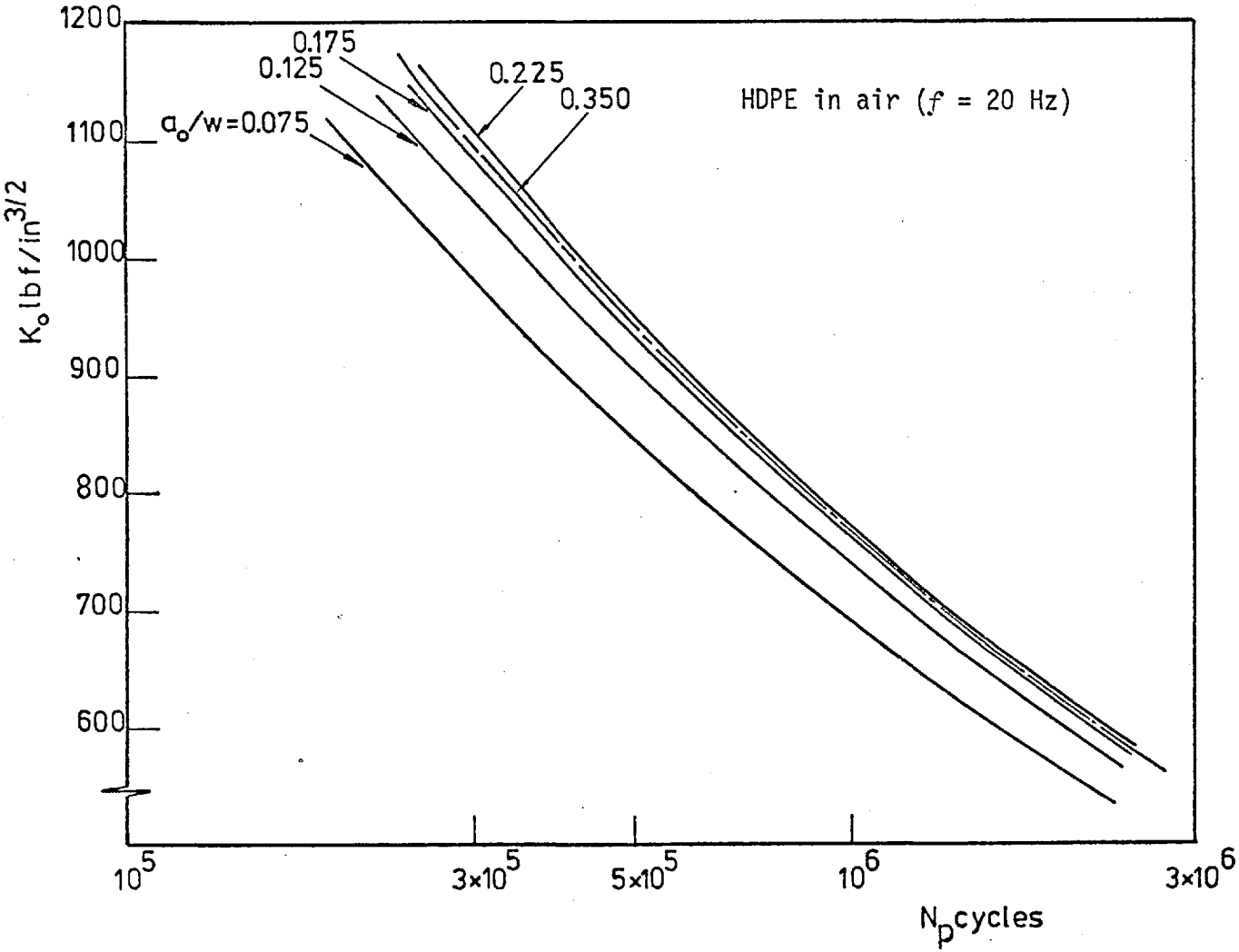

Figure 87: Predicted effect of initial notch depth on the K_o-log N_p relationship for tensile fatigue SEN specimens of HDPE in air

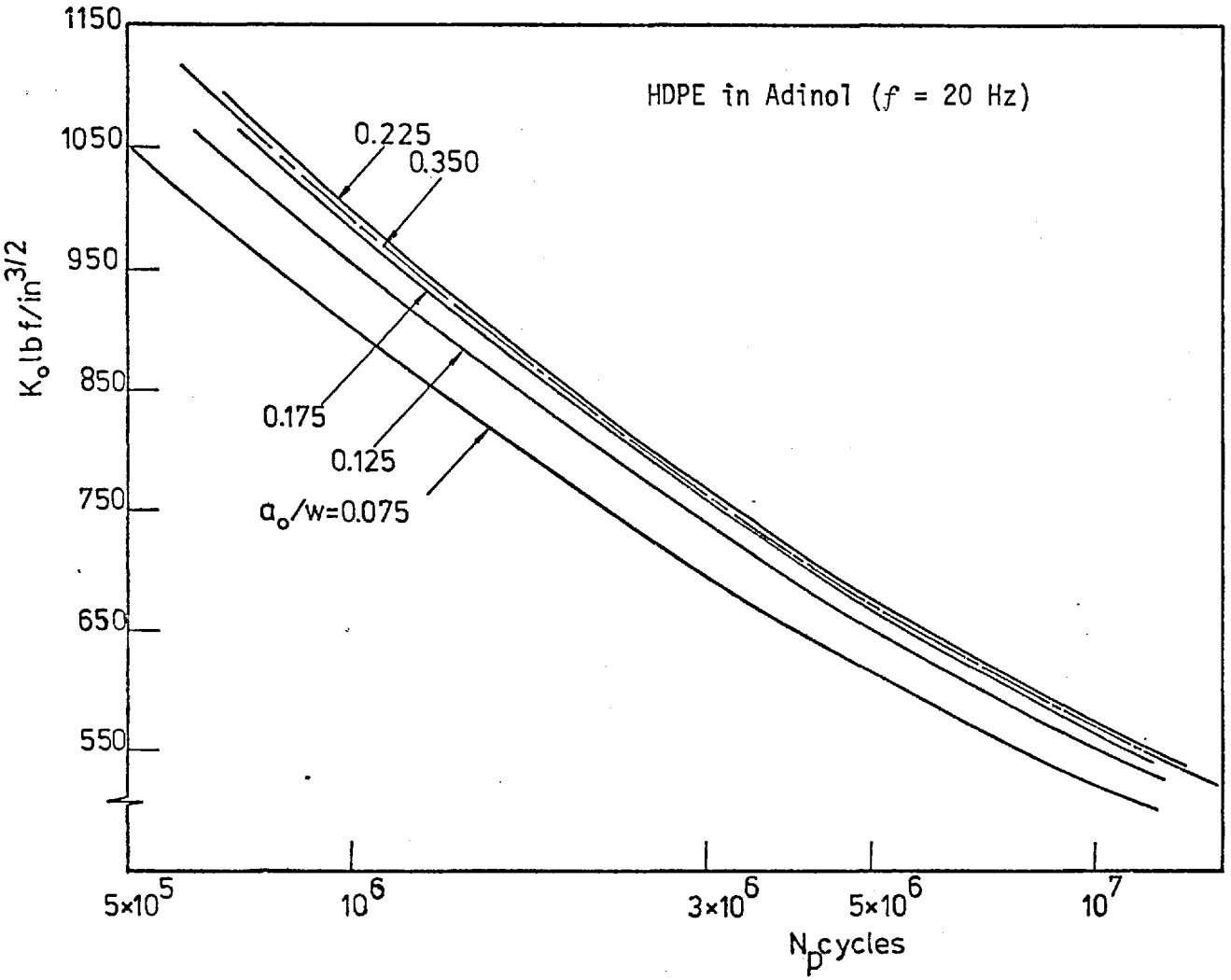

Figure 88: Predicted effect of initial notch depth on the K_o-log N_p relationship for tensile fatigue SEN specimens of HDPE in Adinol

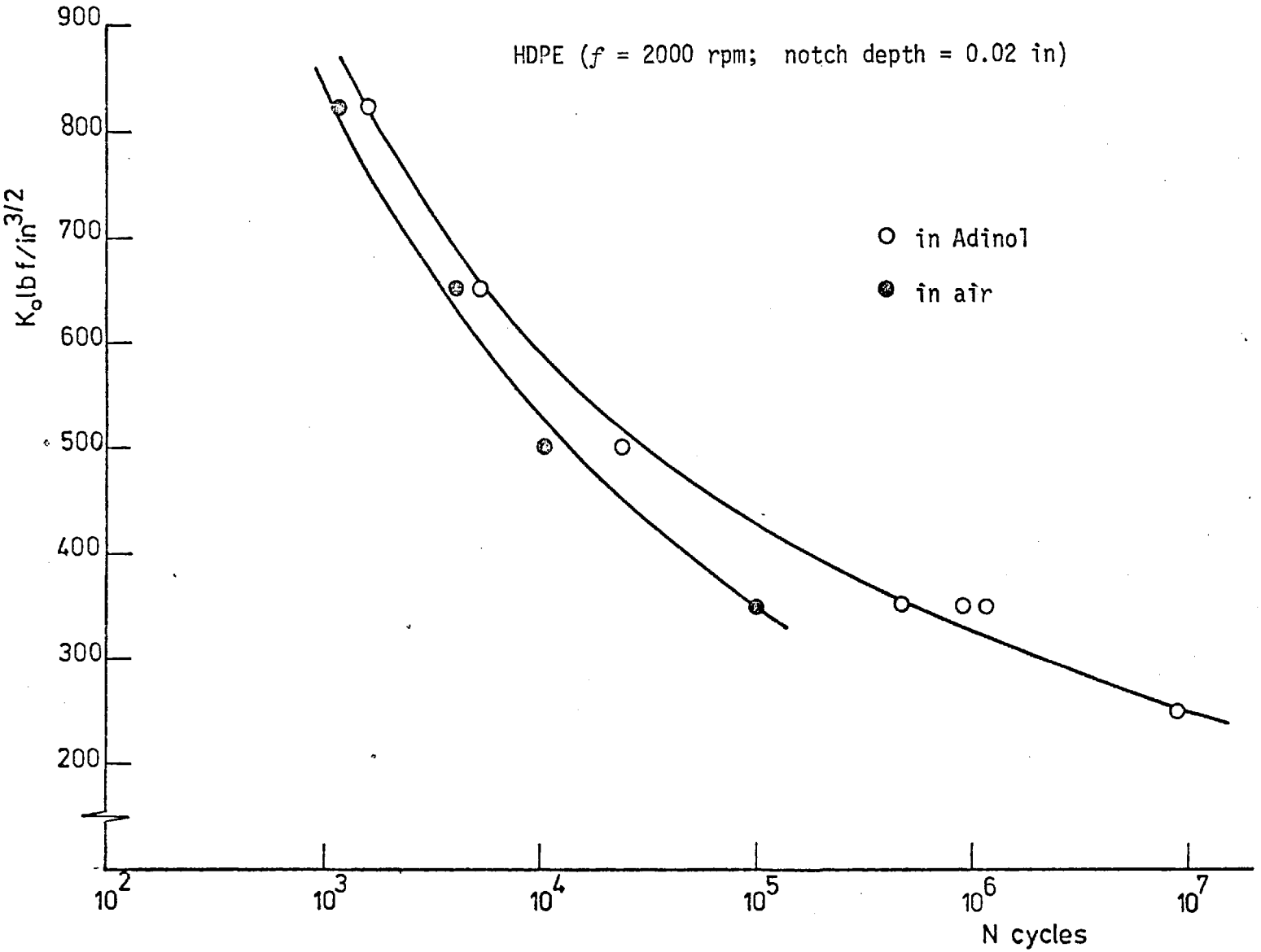

Figure 89: Comparison of air and Adinol results of HDPE round specimens of initial notch depth of 0.02 in at f = 2000 rpm

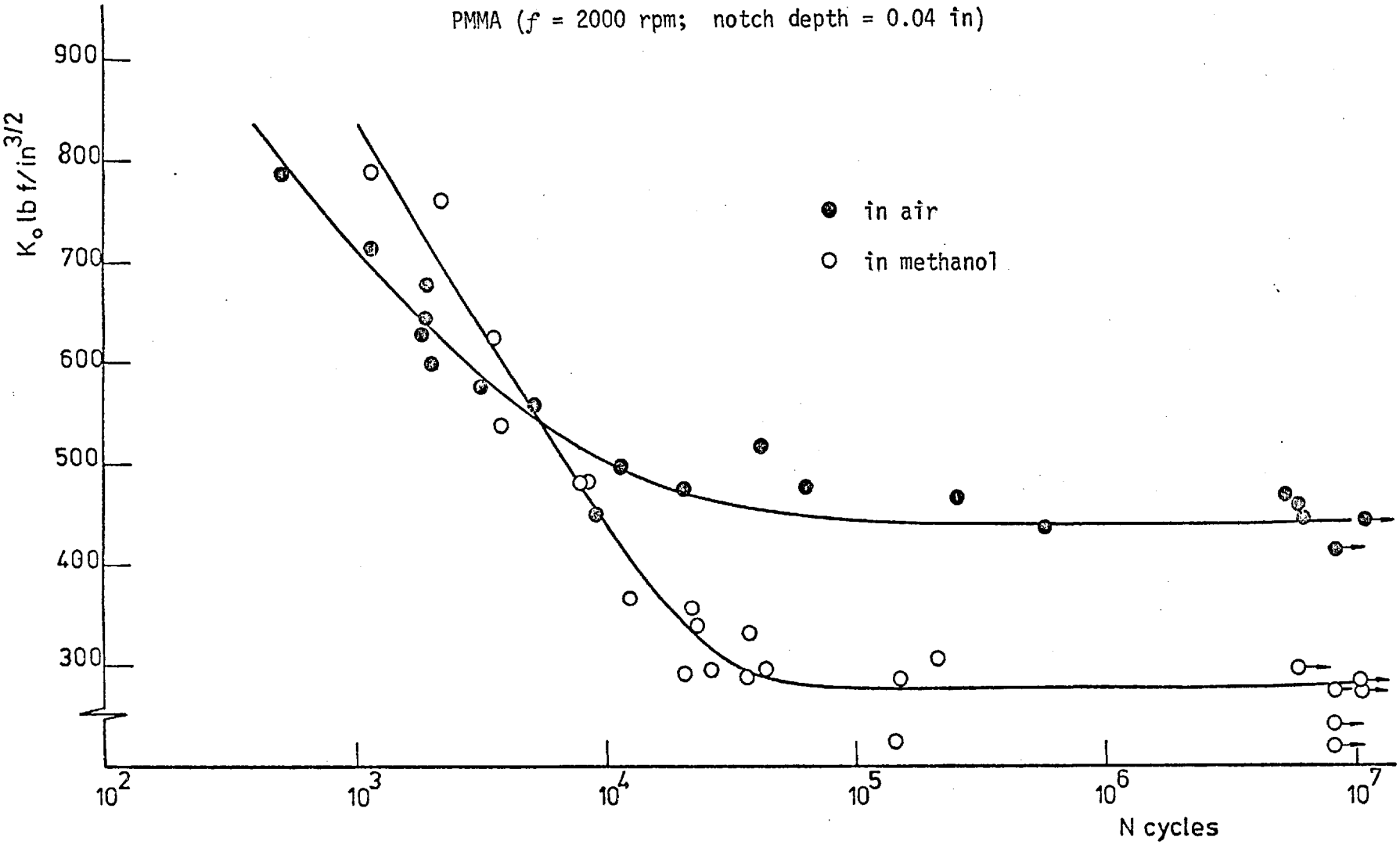

Figure 90: Comparison of air and methanol results of PMMA round specimens of initial notch depth of 0.04 in at f = 2000 rpm

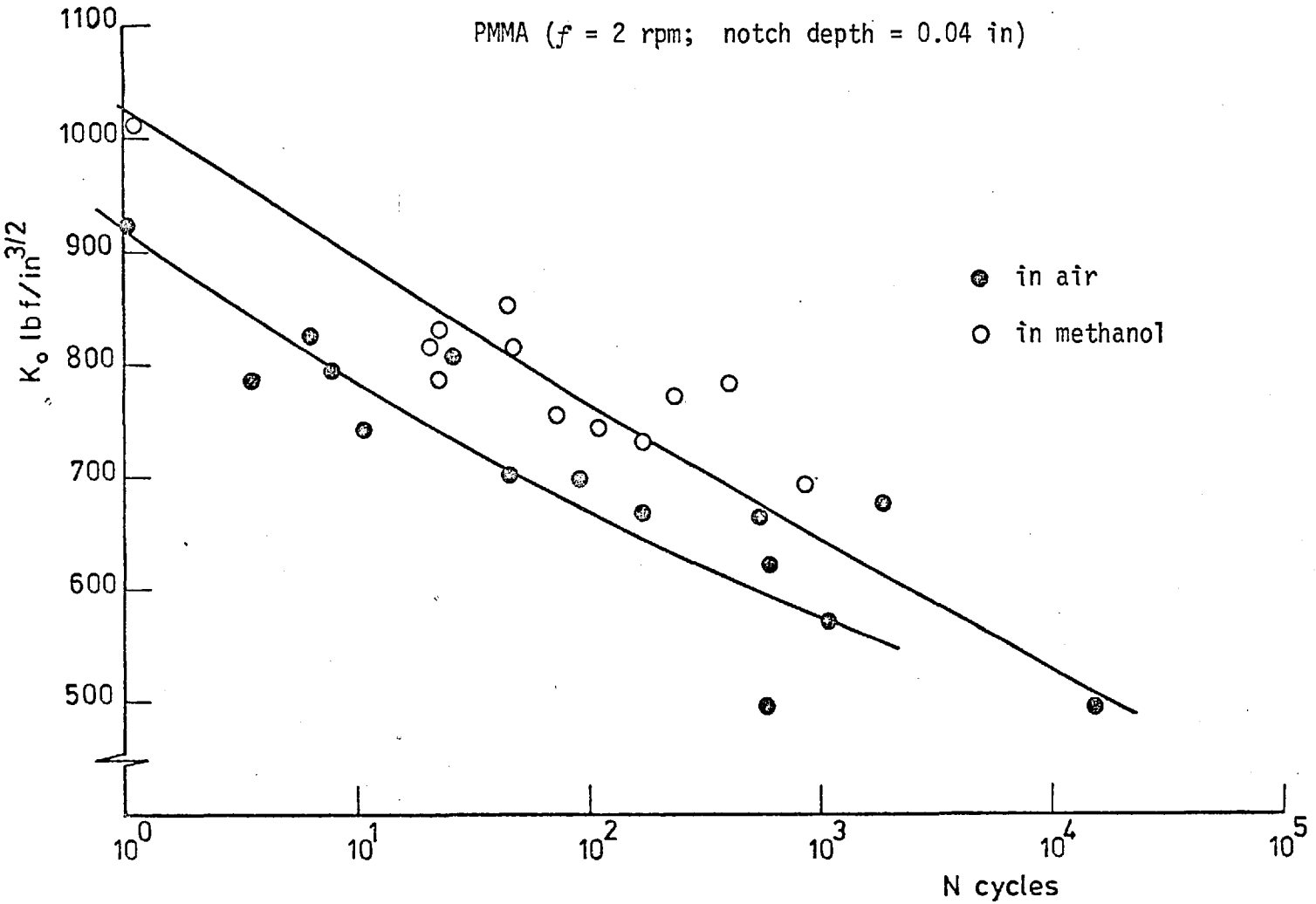

Figure 91: Comparison of air and methanol results of PMMA round specimens of initial notch depth of 0.04 in at f = 2 rpm

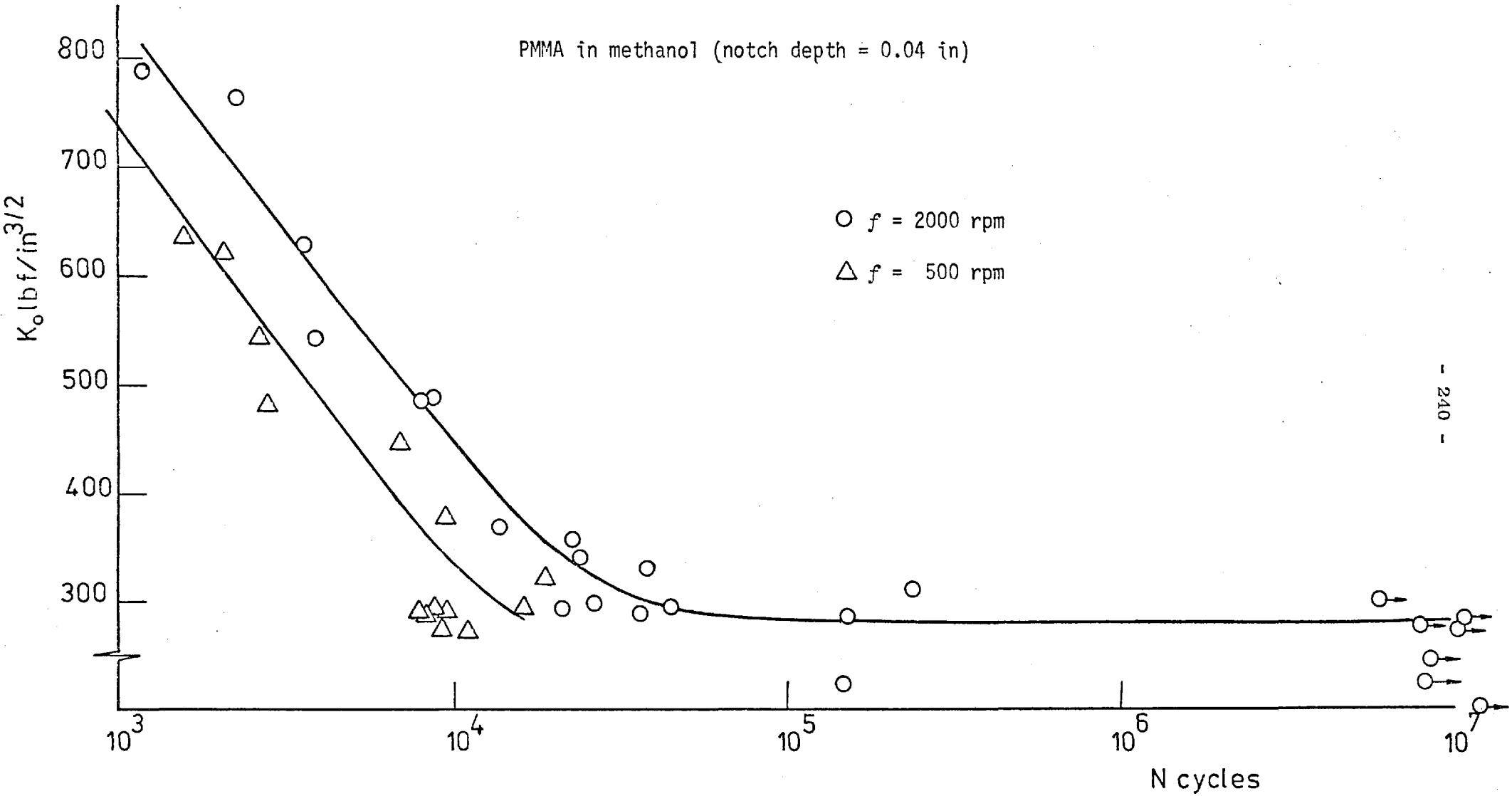

Figure 92: Effect of test frequency on the K_o-log N relationship of PMMA in methanol

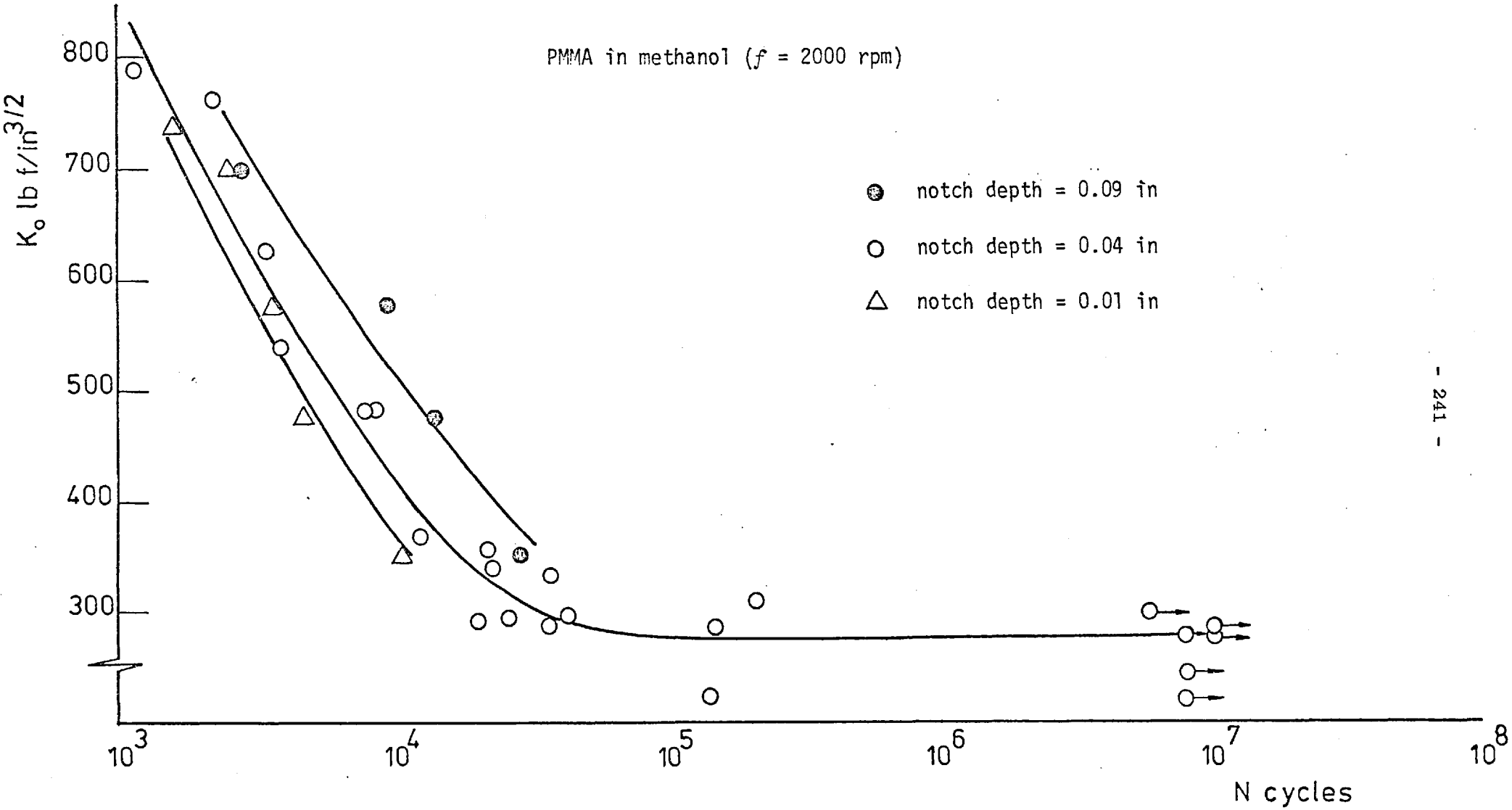

Figure 93: Effect of notch depth on the K_o-log N relationship of PMMA in methanol at f = 2000 rpm

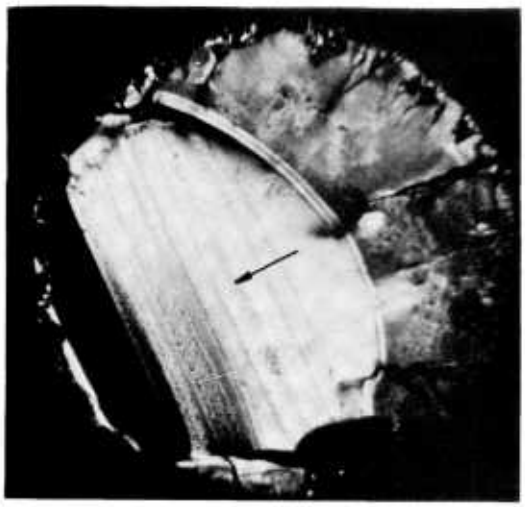

(a)

Arrow indicates direction
of fast crack growth

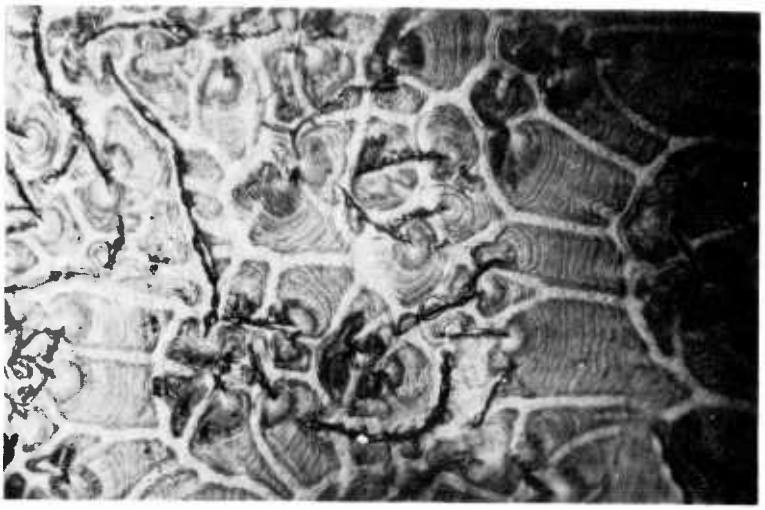

(b)

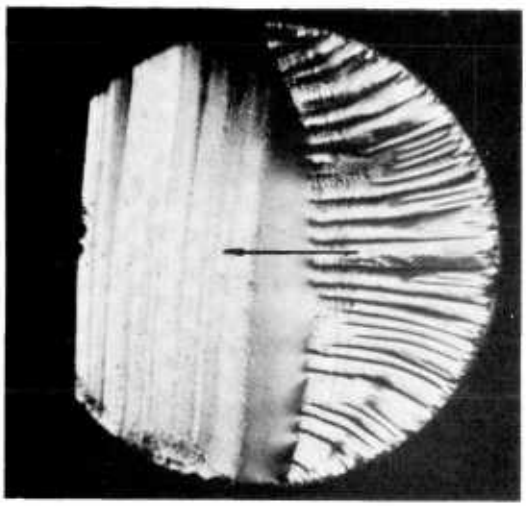

(c)

(d)

Arrows indicate direction of fast and slow crack growth

Figure 94: Fractography of failure surfaces in PMMA

(a) Fracture surface of PMMA in methanol

(b) Cyclic void growth in methanol craze

(c) Fracture surface of PMMA in air

(d) Cyclic crack growth in air

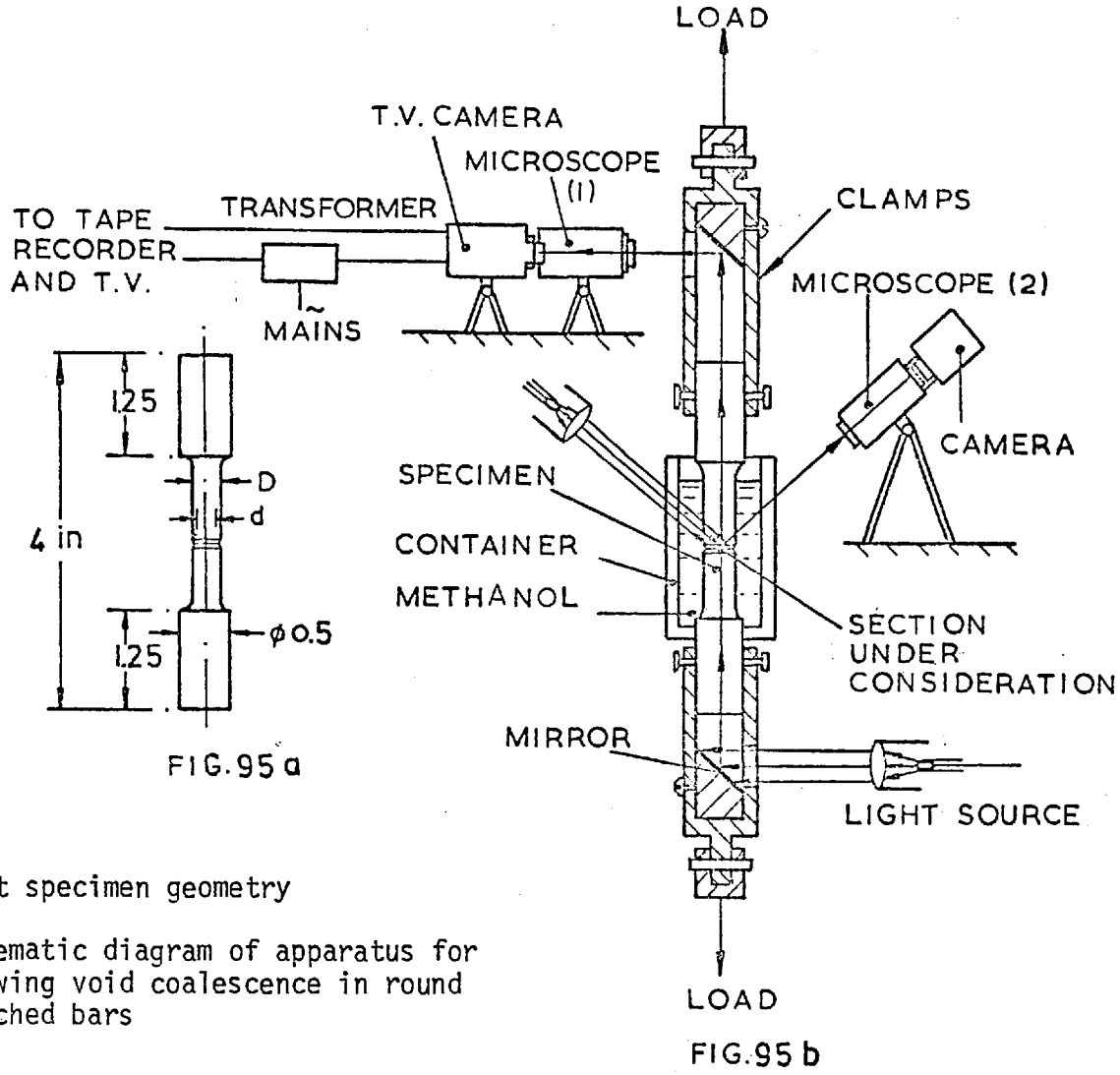

Figure 95: (a) Test specimen geometry

(b) Schematic diagram of apparatus for viewing void coalescence in round notched bars

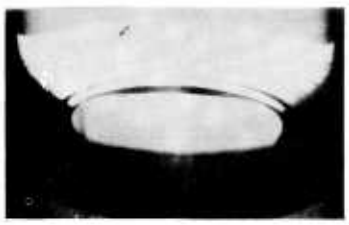

x = 0, t = 0

x = 0.026, t = 70

x = 0.0346, t = 120

x = 0.0398, t = 180

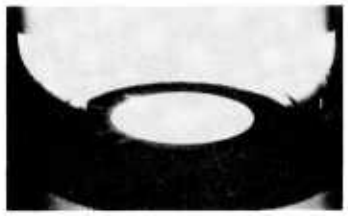

x = 0.048, t = 300

x = 0.0541, t = 360

x = 0.0571, t = 427

x = 0.0642, t = 480

x = 0.0687, t = 570

x = 0.0756, t = 660

x = 0.0819, t = 750

x = 0.0878, t = 840

x = 0.0947, t = 960

x = 0.1035, t = 1080

x = 0.1126, t = 1200

x = 0.1232, t = 1380

x = 0.1453, t = 1560

x = 0.1472, t = 1590

(x in inches, t in seconds)

Figure 96a

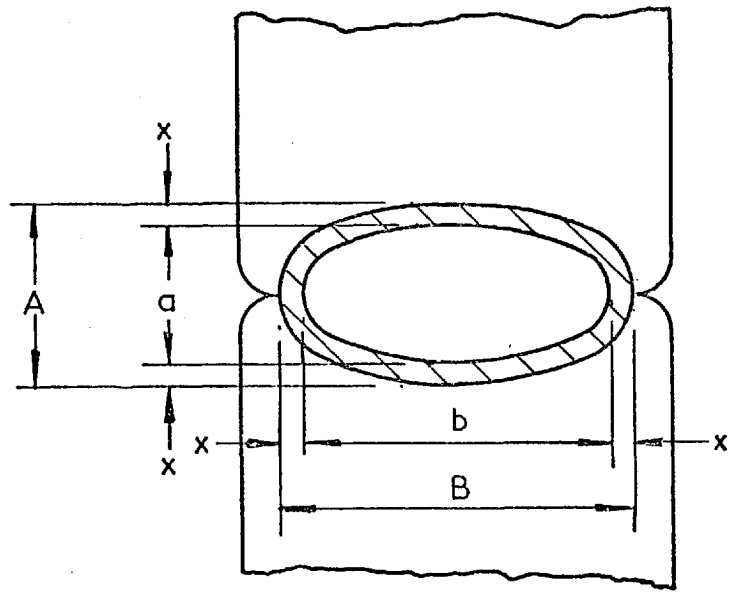

FIG. 96 b

Figure 96: (a) Radial craze growth in PMMA round notched bars (K_o = 325 lbf/in$^{3/2}$)

(b) Schematic representation of craze measurements

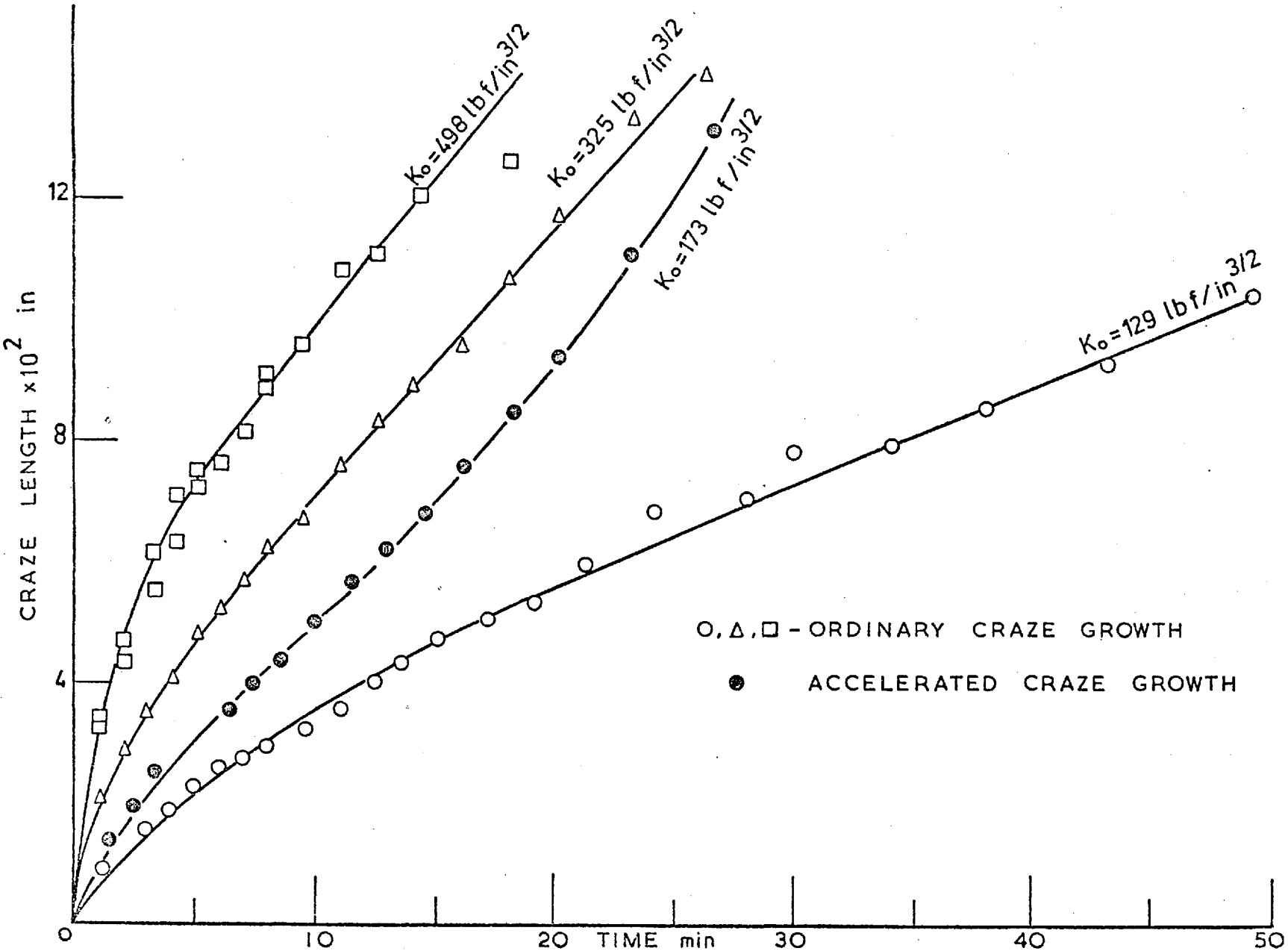

Figure 97: Variation of craze length with time for different values of K_o

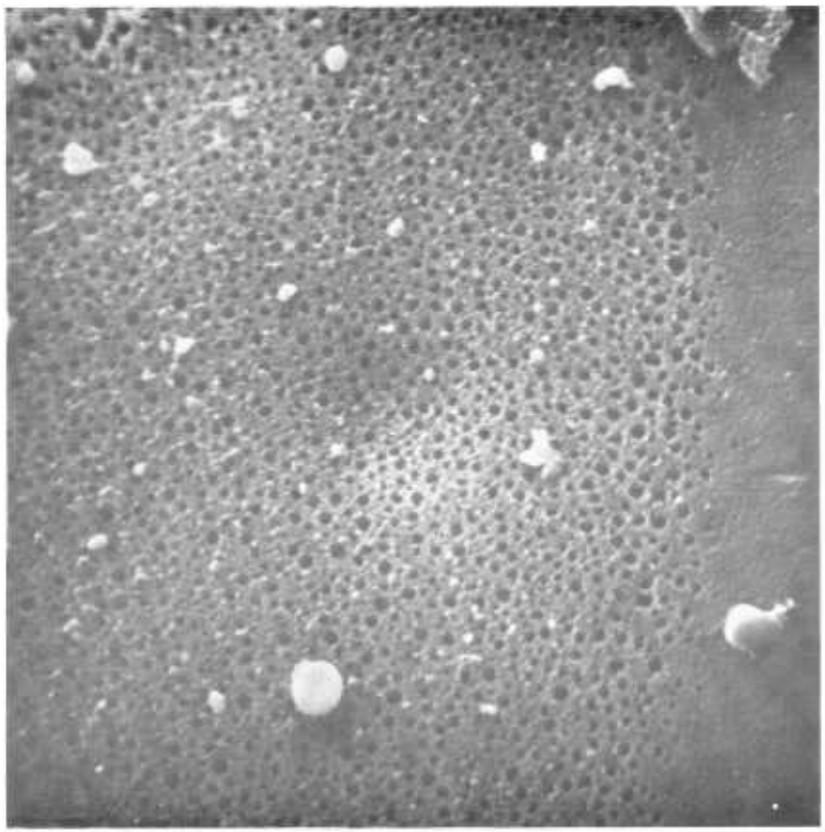

5 µm

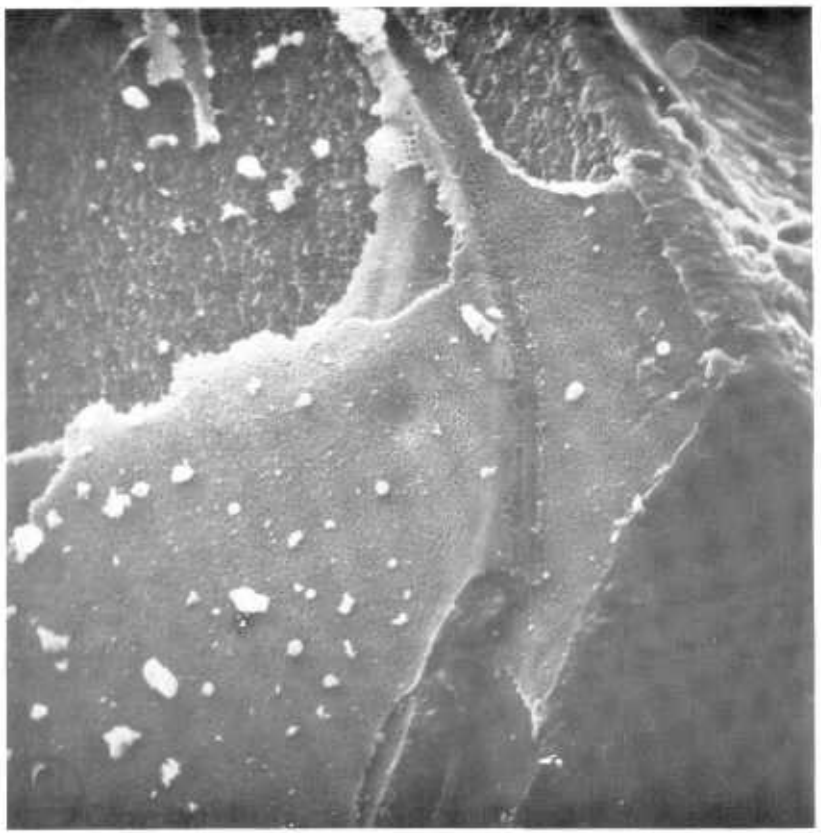

20 µm

Figure 98: The cluster of small voids as they appear on the fracture surface

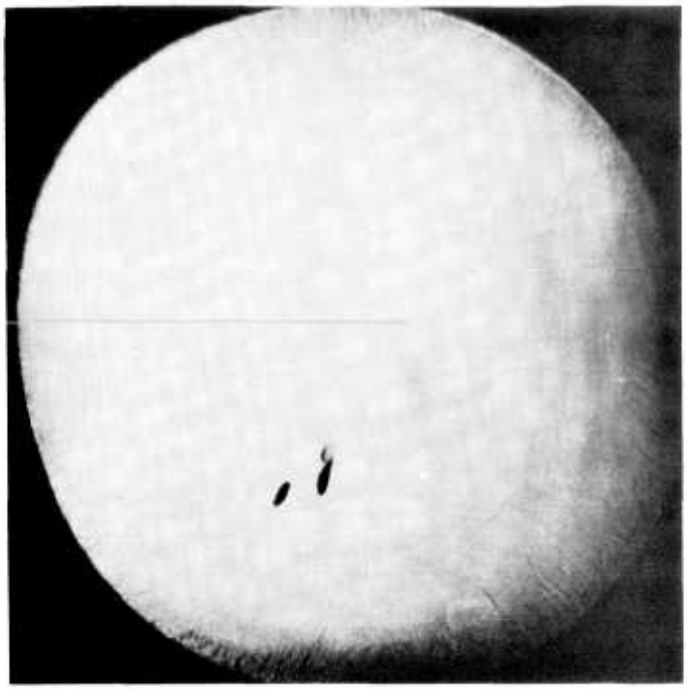

(a) 22 minutes*

Start of void coalescence in the crazed section

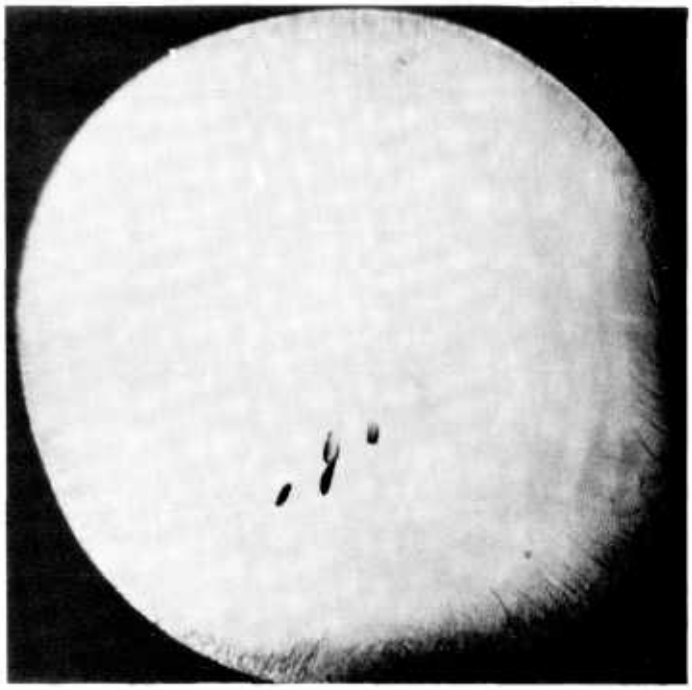

(b) 23 minutes

Type (1) clusters of very small voids

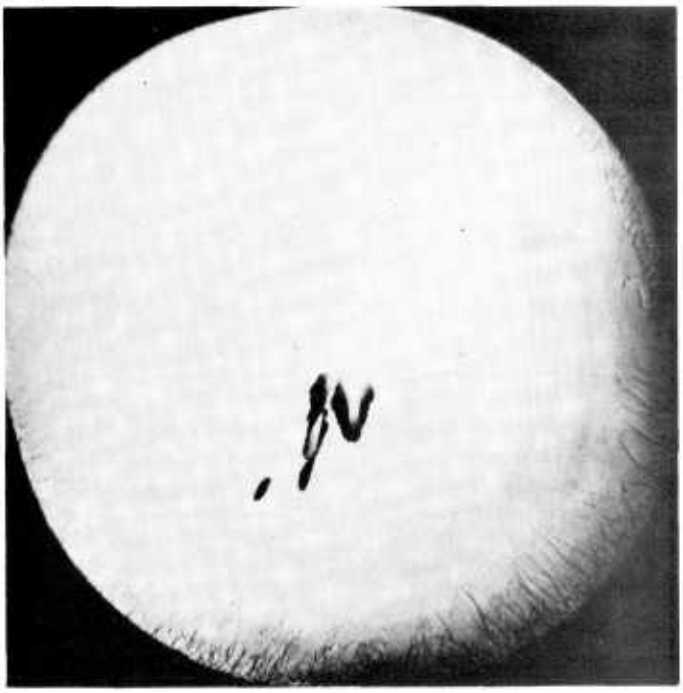

(c) 24 minutes

Spreading of type (1) voids

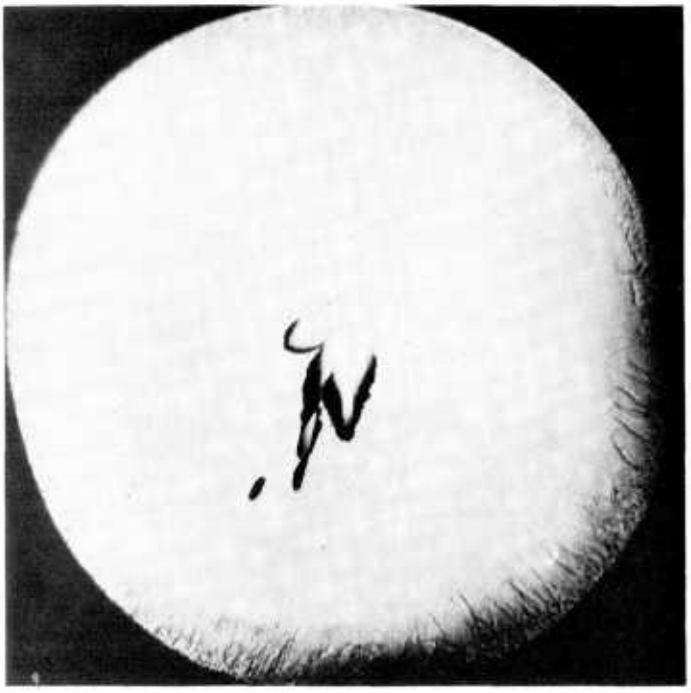

(d) 25 minutes 30 seconds

Continuous spreading of type (1) voids

* Time was considered from the beginning of the test

Figure 99

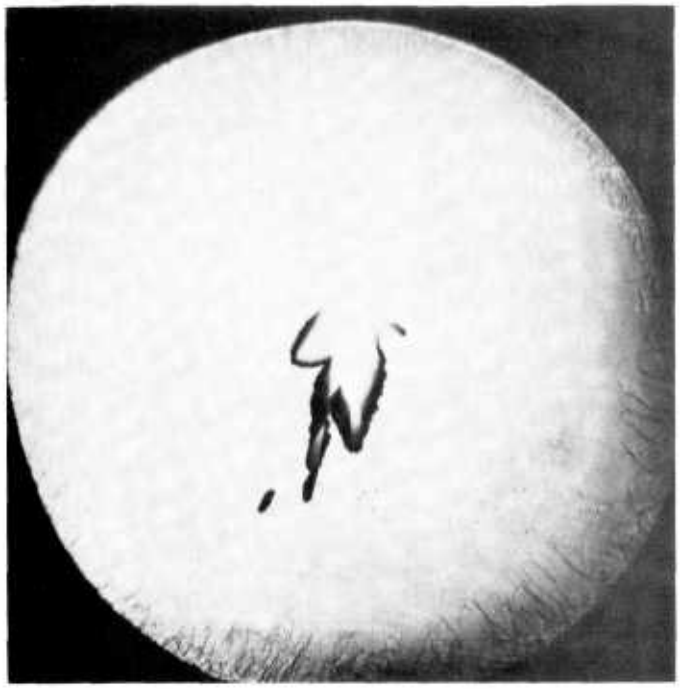

(e) 26 minutes 30 seconds

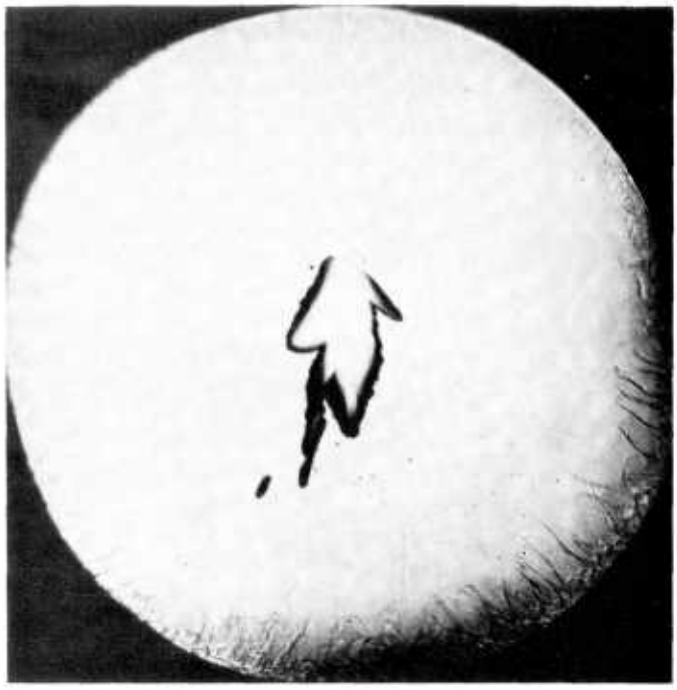

(f) 27 minutes 30 seconds

The appearance of type (2) (separate voids)

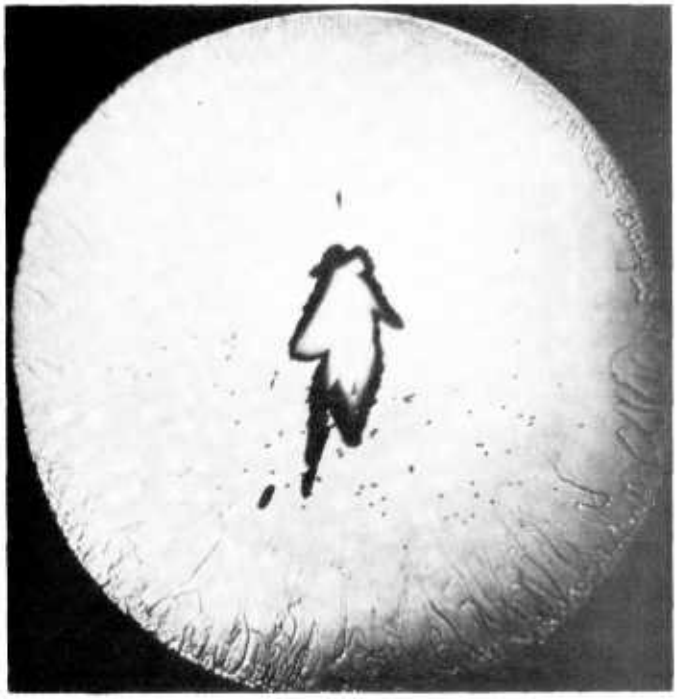

(g) 29 minutes

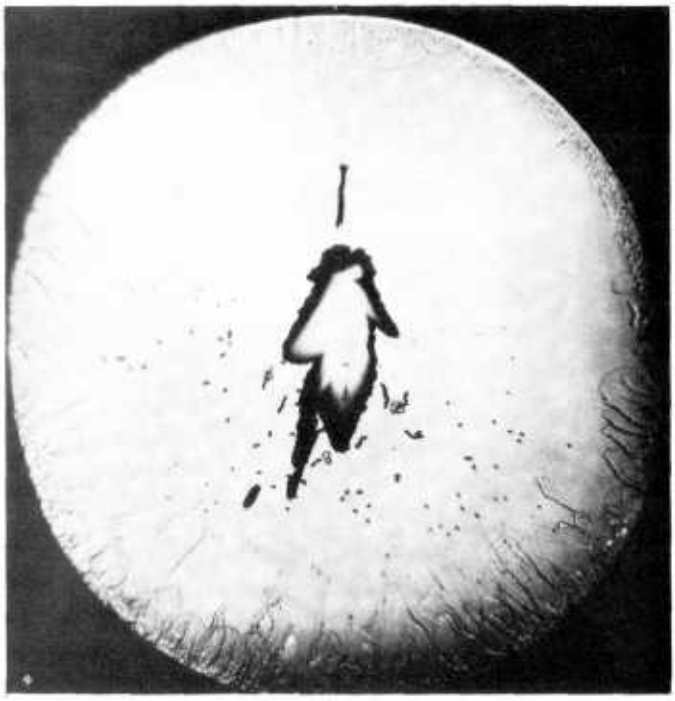

(h) 30 minutes

Growth of type (2) voids

Figure 99

(i) 32 minutes

(j) 32 minutes 30 seconds

Continuous spreading of type (1) and growth of type (2)

(k) 33 minutes 15 seconds

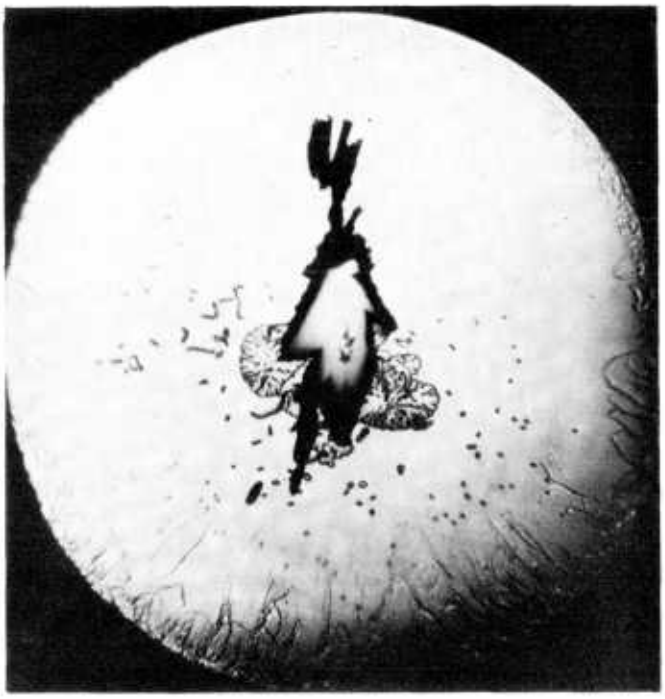

(l) 34 minutes

Figure 99

(m) 34 minutes 15 seconds

(n) 34 minutes 30 seconds

(o) 34 minutes 50 seconds

(p) 35 minutes

Coalescence of type (2) voids

Figure 99

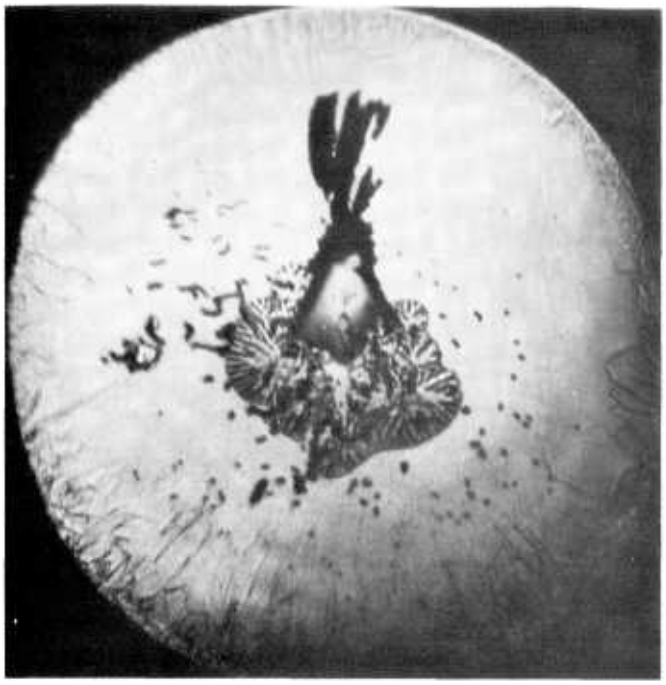

(q) 35 minutes 20 seconds

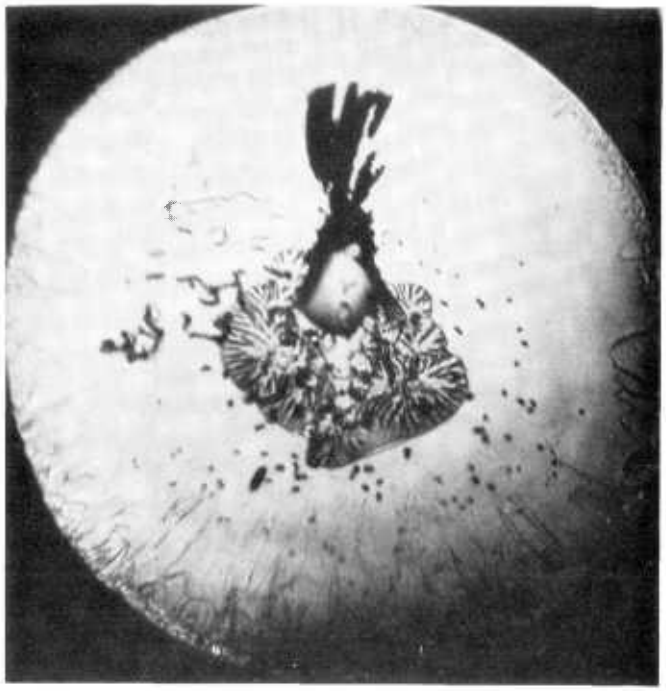

(r) 35 minutes 35 seconds

Continuous growth and coalescence of type (2) voids

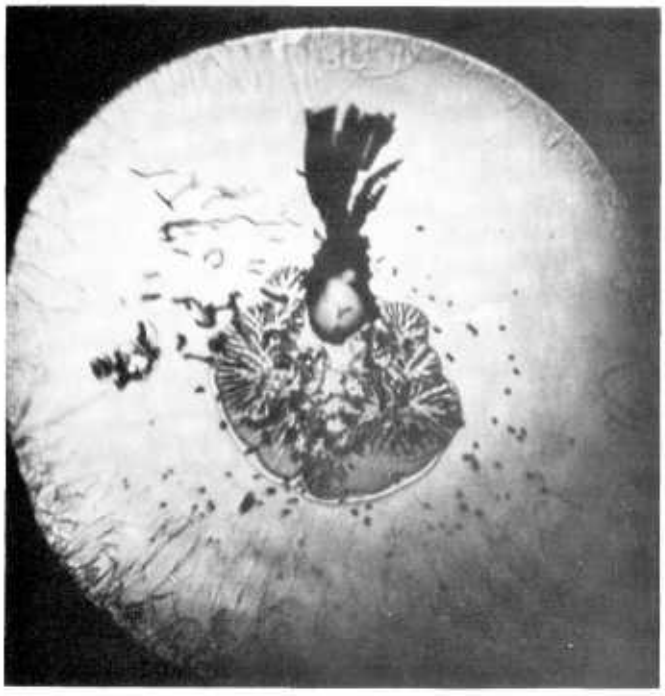

(s) 35 minutes 45 seconds

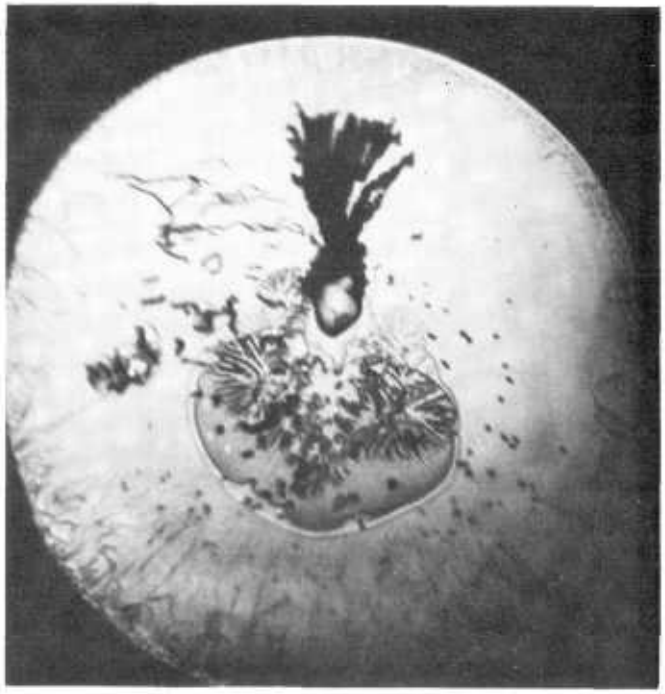

(t) 35 minutes 55 seconds

Big bubble of methanol vapour inside coalesced voids

Figure 99

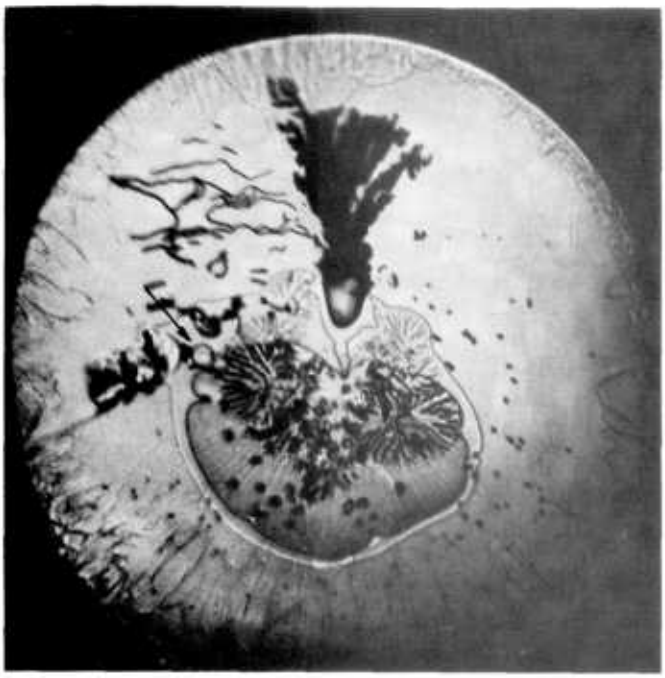

(u) 36 minutes 10 seconds

Small bubble of methanol vapour joining the main bubble

(v) 36 minutes 15 seconds

Immediately prior to fracture

(w) Fracture surface

Figure 99: Void growth and coalescence in the crazed section and fracture surface features after complete separation (K_o = 325 lbf/in$^{3/2}$)

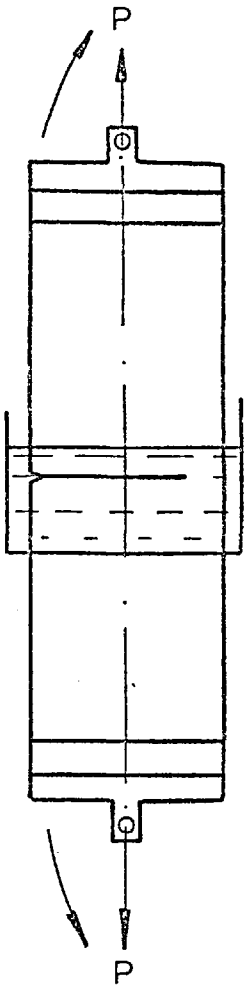

FIG.100 a

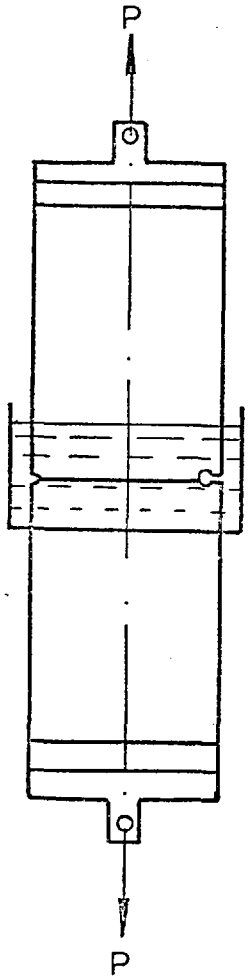

FIG.100 b

Figure 100: (a) Craze growth in SEN specimen

(b) Symmetrical loading of crazed SEN specimen

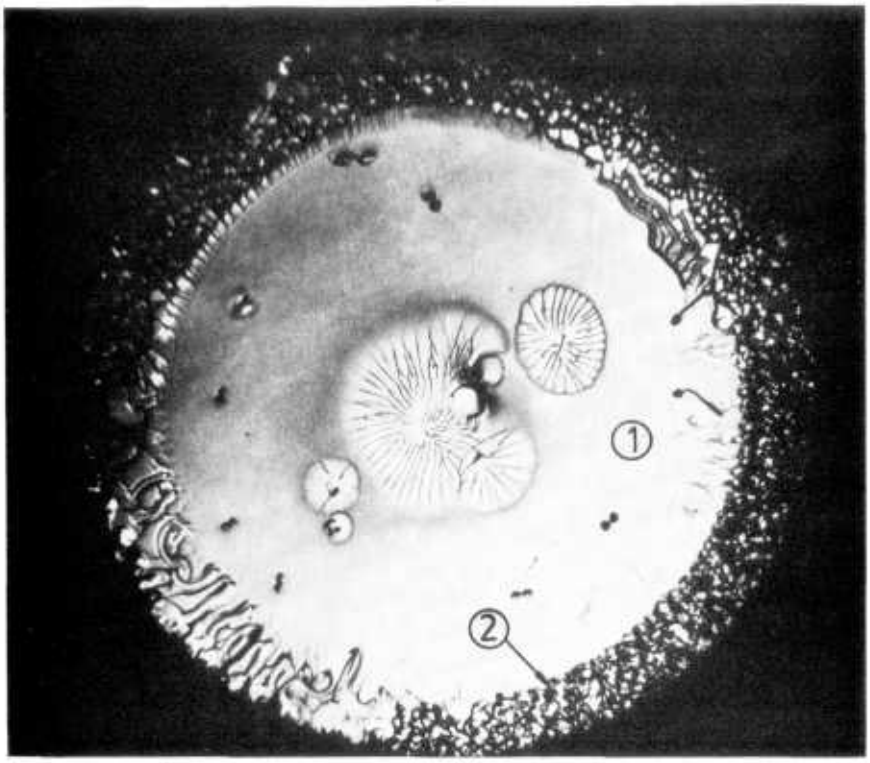

Figure 101: The two main zones of the fracture surface

(1) The featureless zone in which rosette puddles appear

(2) The island and crater zone

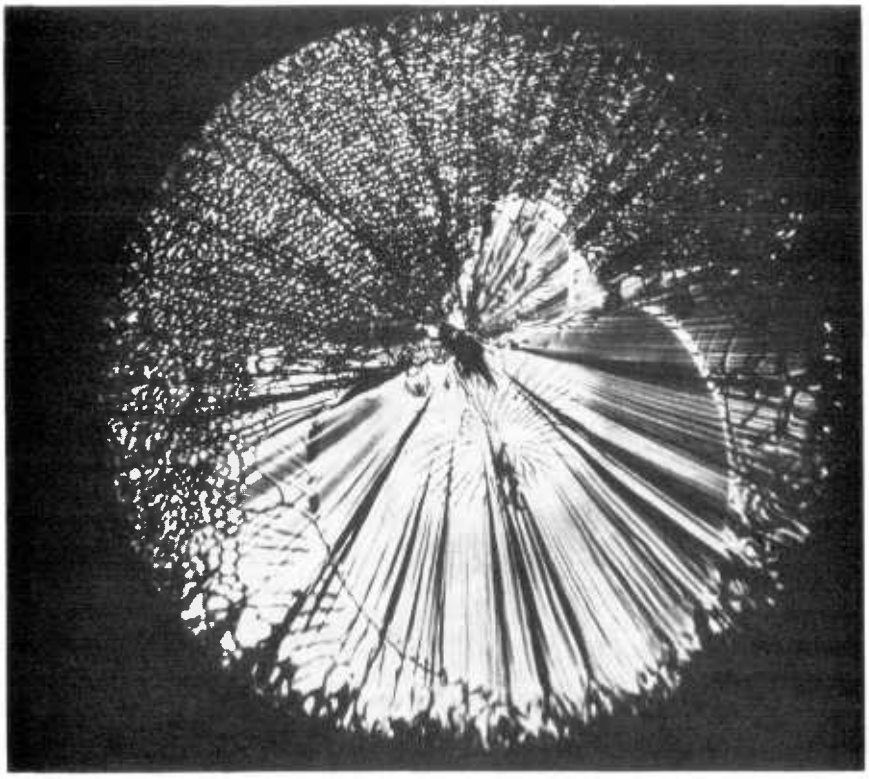

Figure 102: The fracture surface with its radial marks

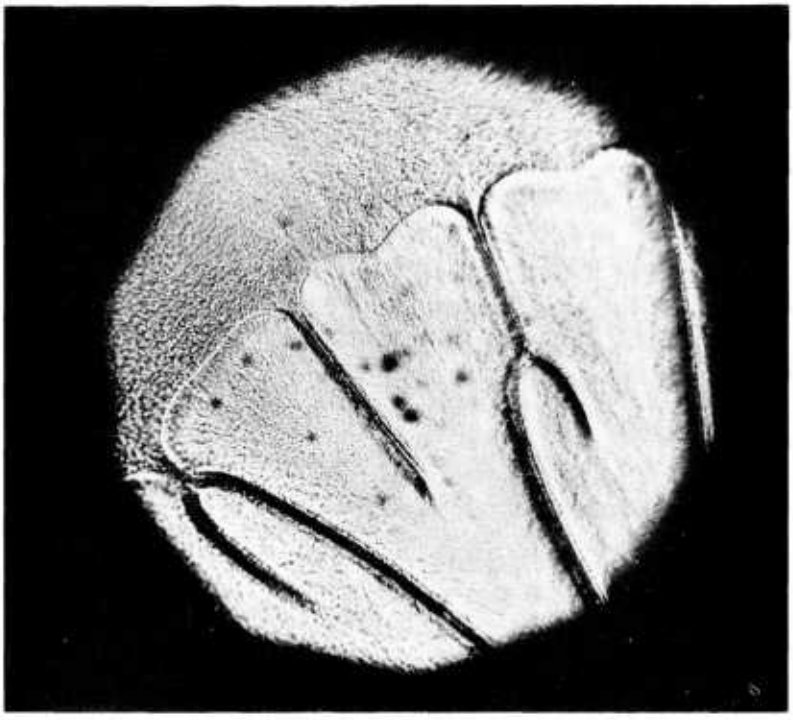

Figure 103: The definitive boundary of a rosette puddle

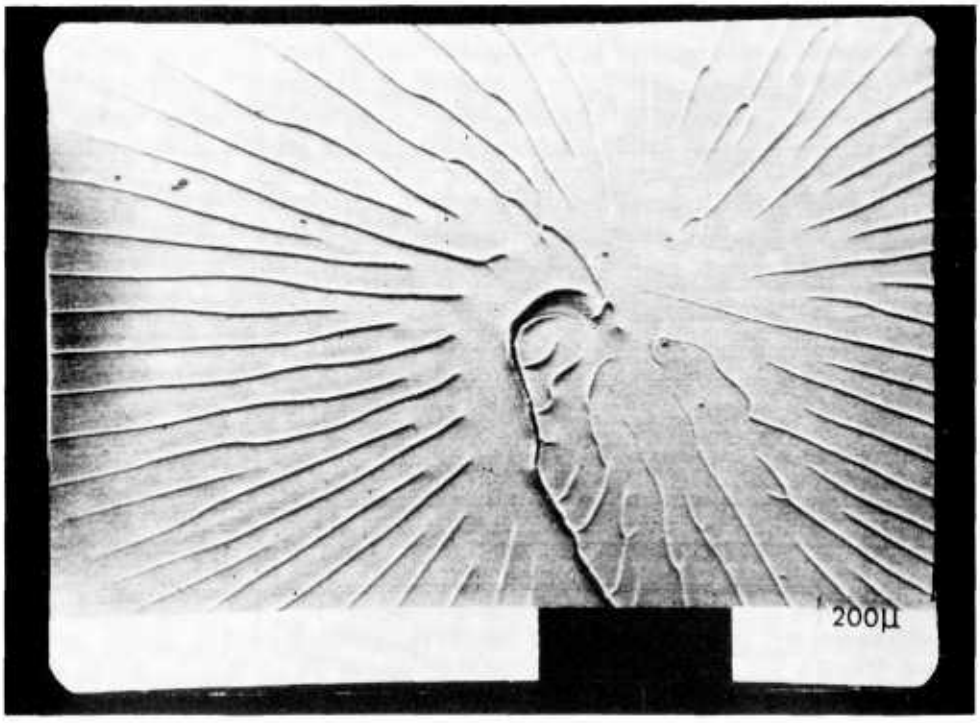

Figure 104: The central area of a rosette puddle

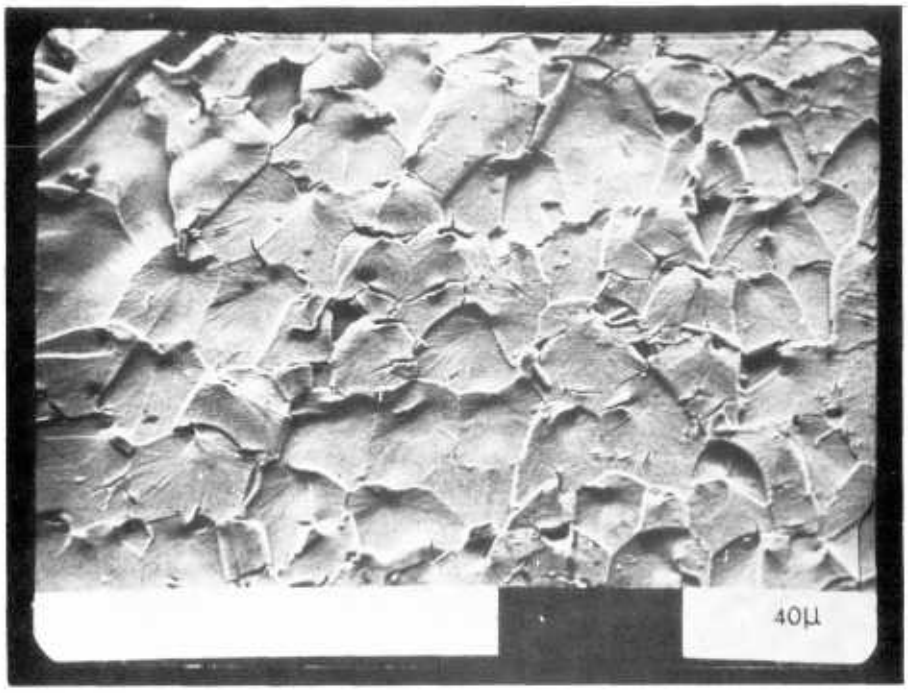

Figure 105: The island and crater structure

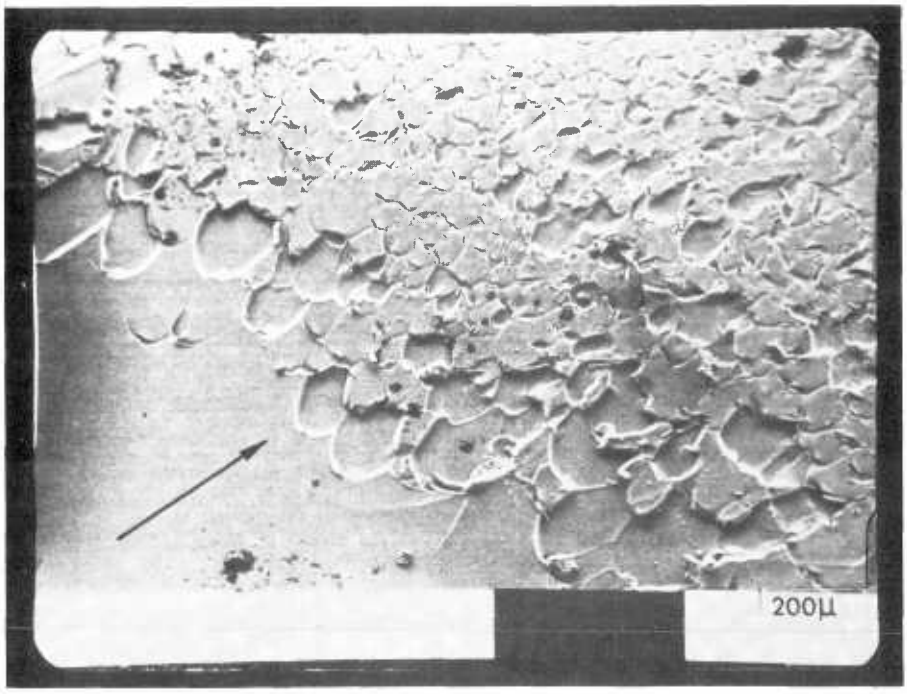

Figure 106: The transition region between the two zones of the fracture surface (The arrow indicates the direction of radial crack growth)

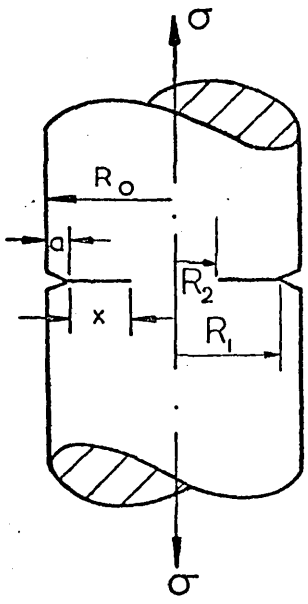

FIG.107 a

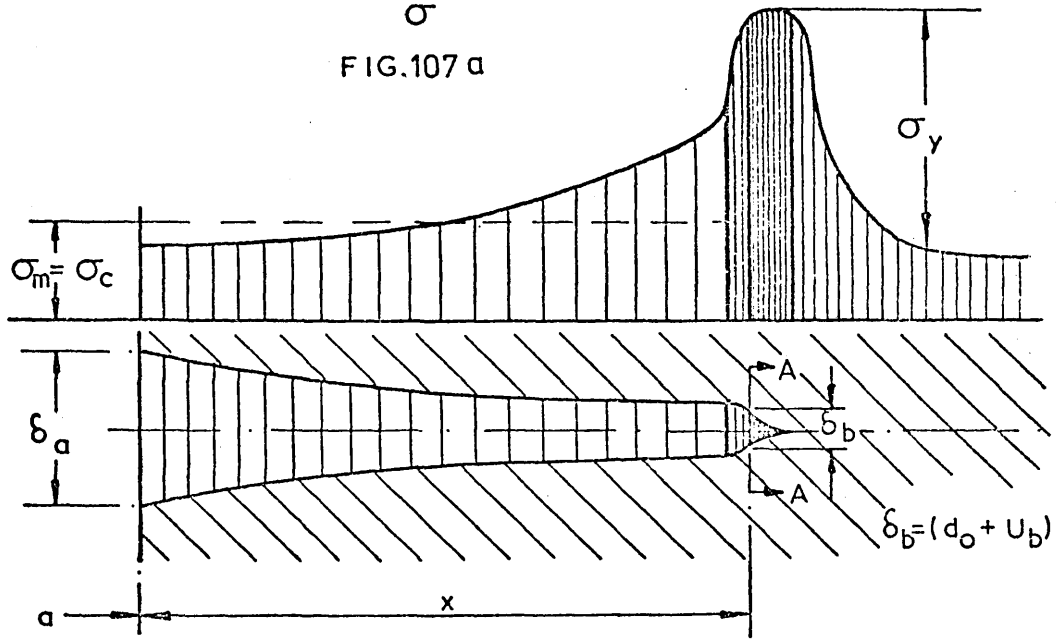

FIG.107 b COLLINEAR ZONES ASSOCIATED WITH CRAZE GROWTH.

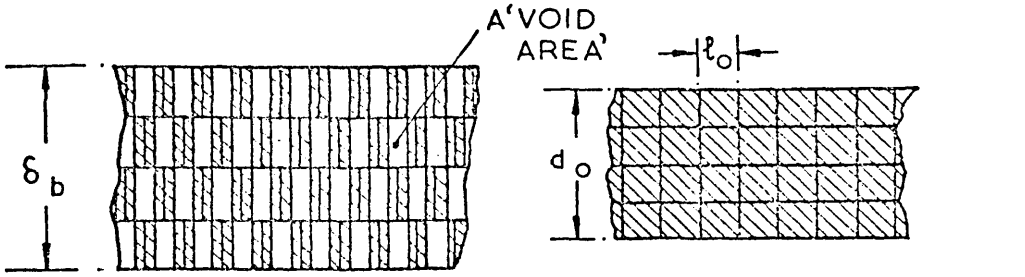

FIG.107 c

Figure 107: Schematic representation of environmental craze in a round notched bar

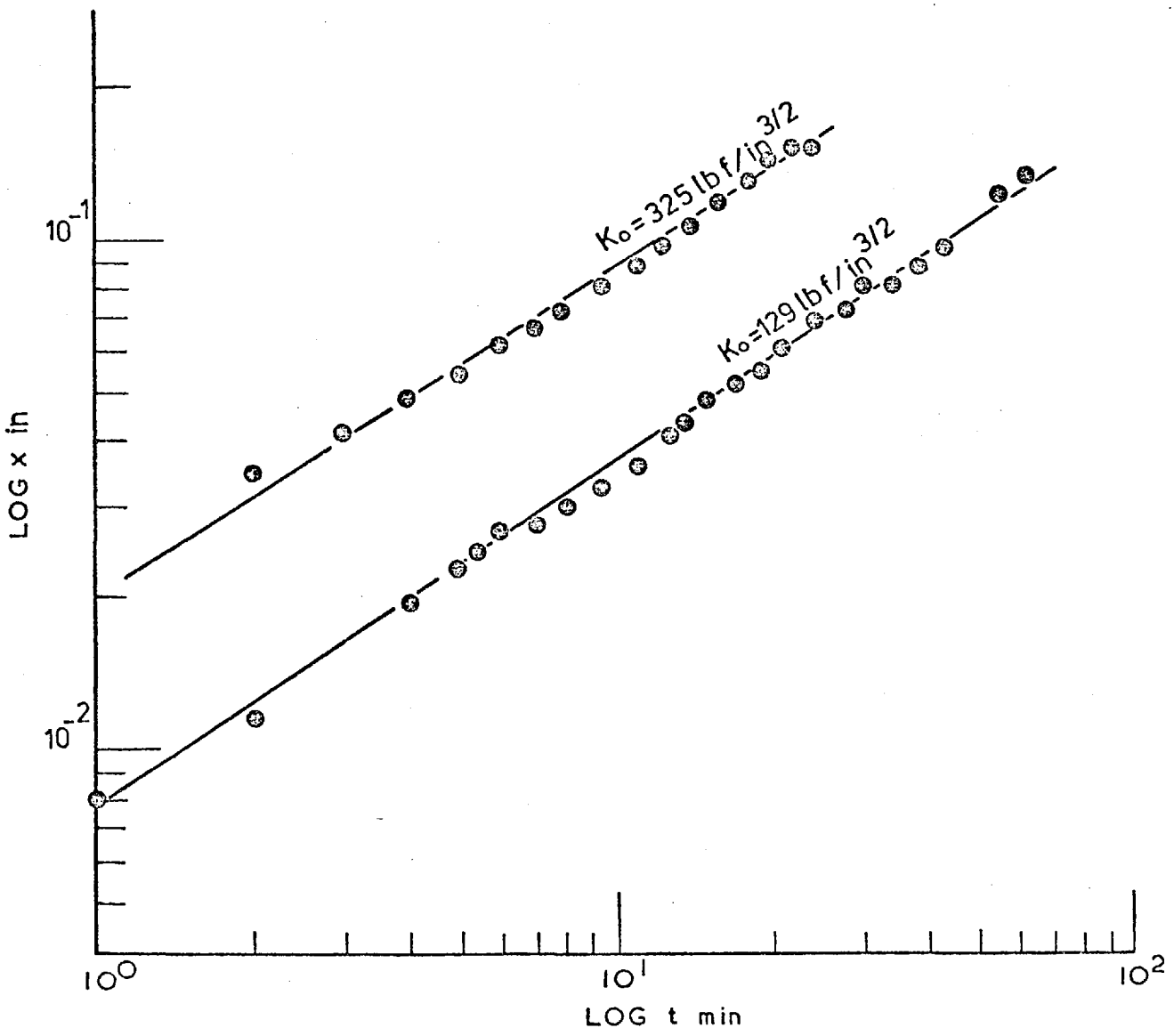

Figure 108: Log-log representation of craze length vs. time

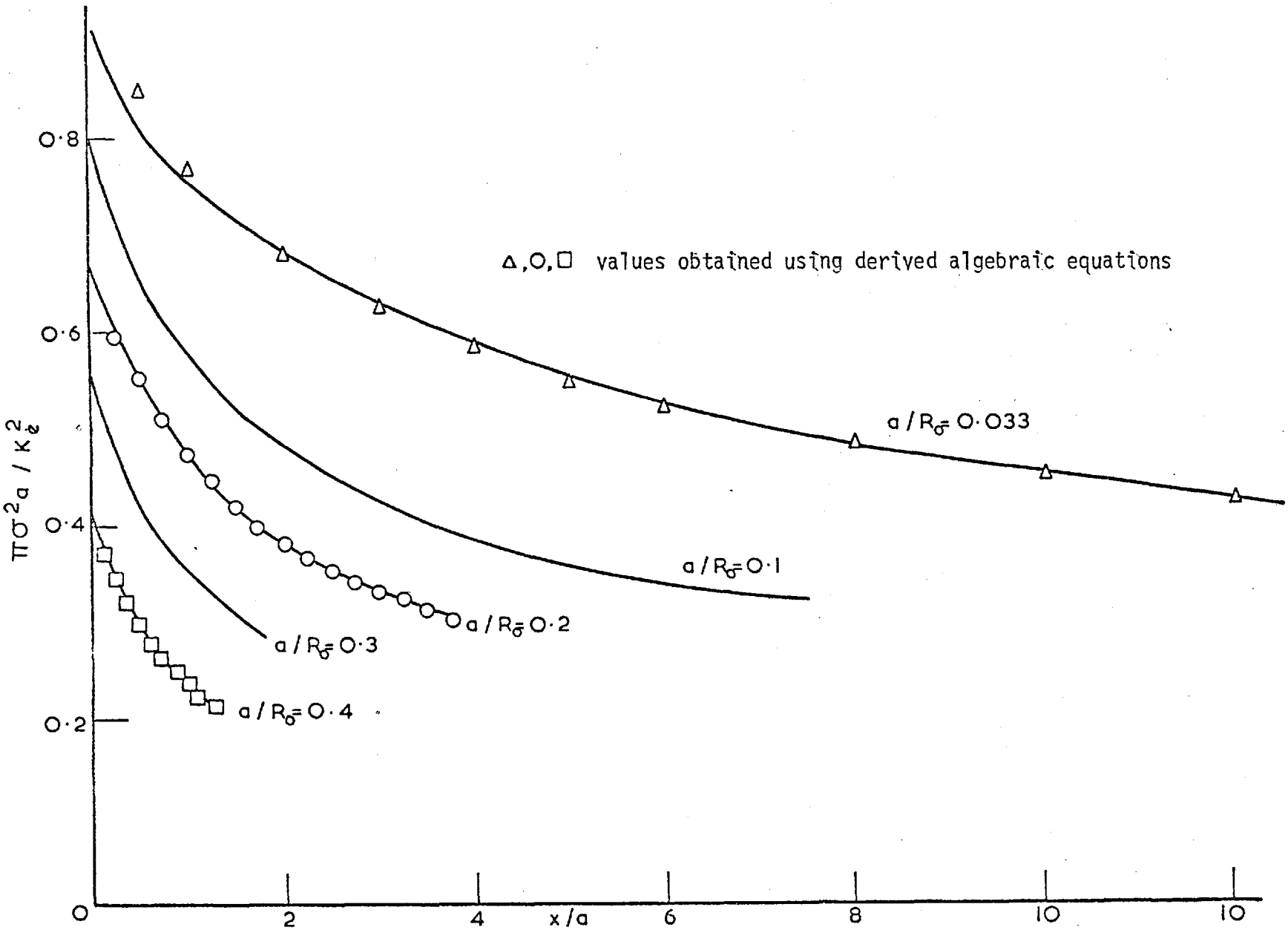

Figure 109: Equivalent stress intensity factor as a function of craze length

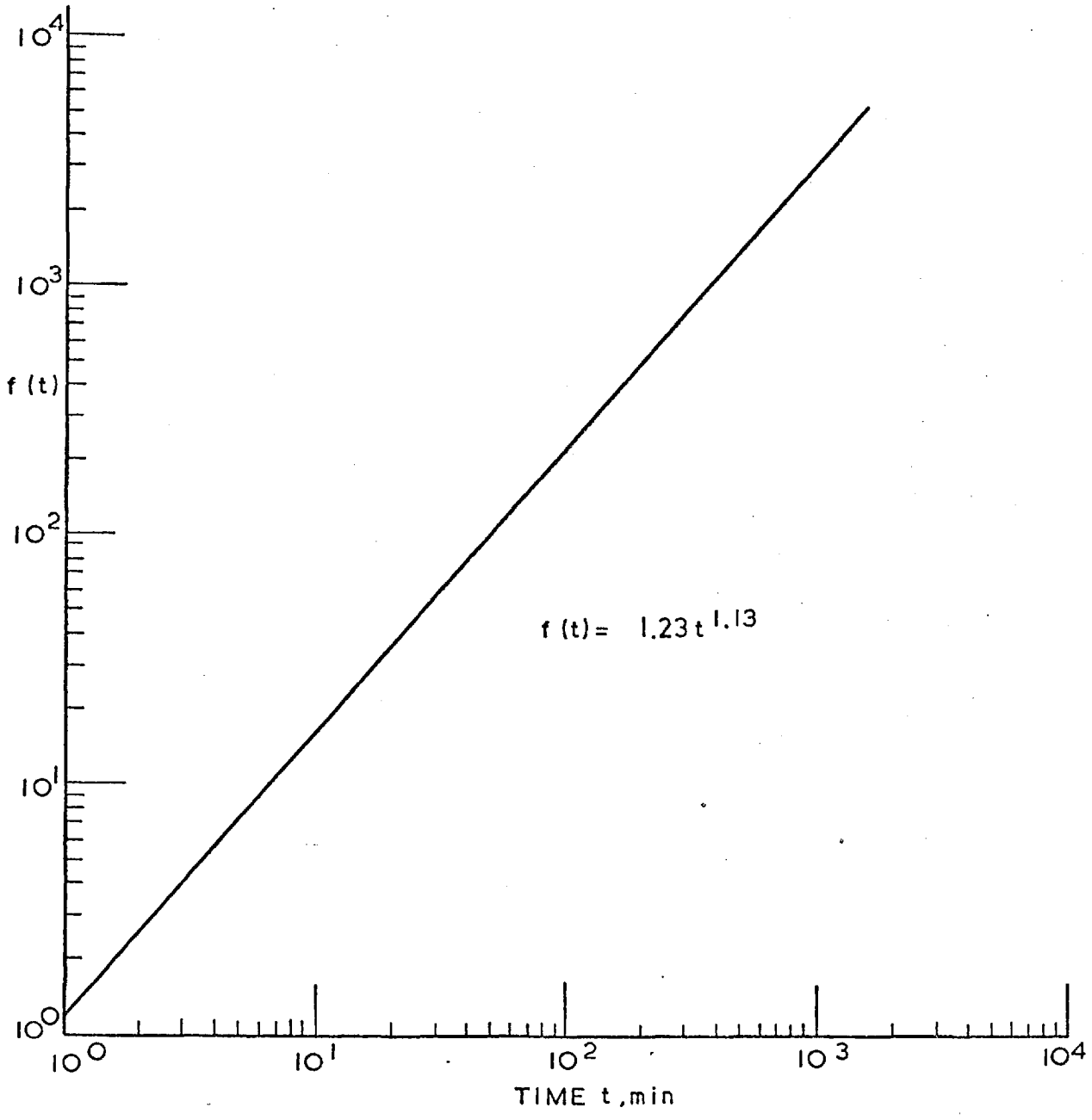

Figure 110: Log-log representation of $f(t)$ versus t

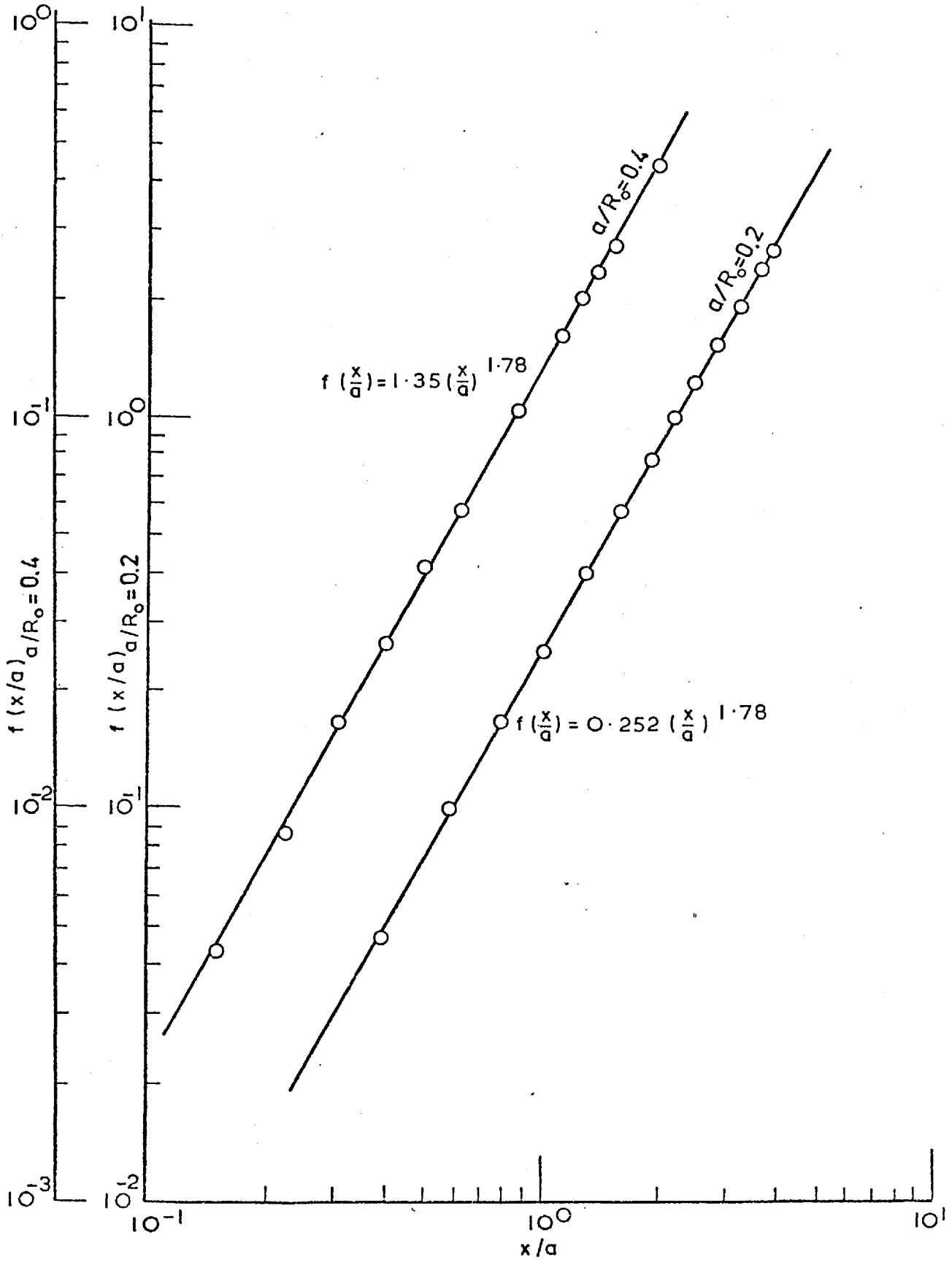

Figure 111: $f(\frac{x}{a})$ as a function of $\frac{x}{a}$

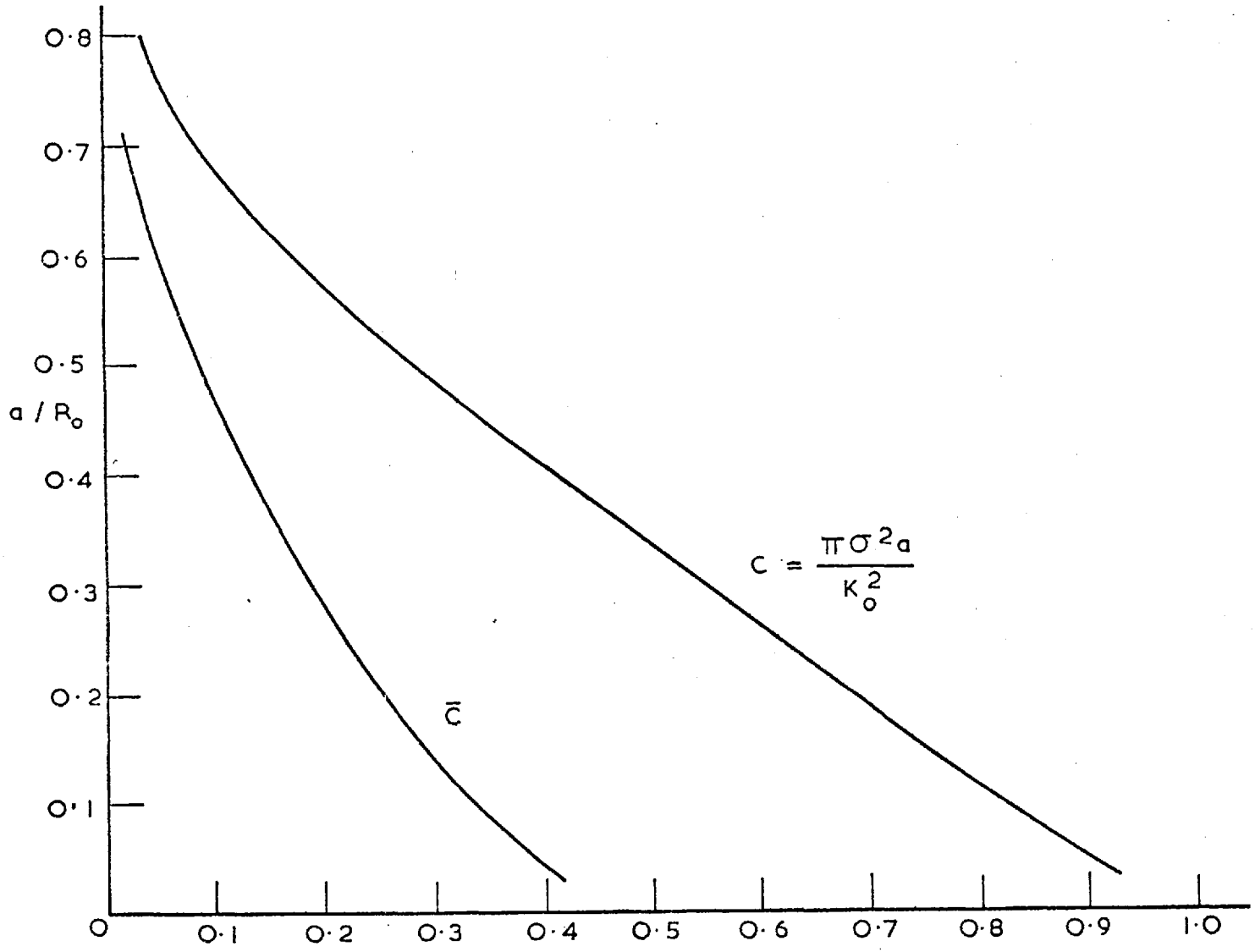

Figure 112: Variation of c and $\bar{c}$ with different values of a/R_o

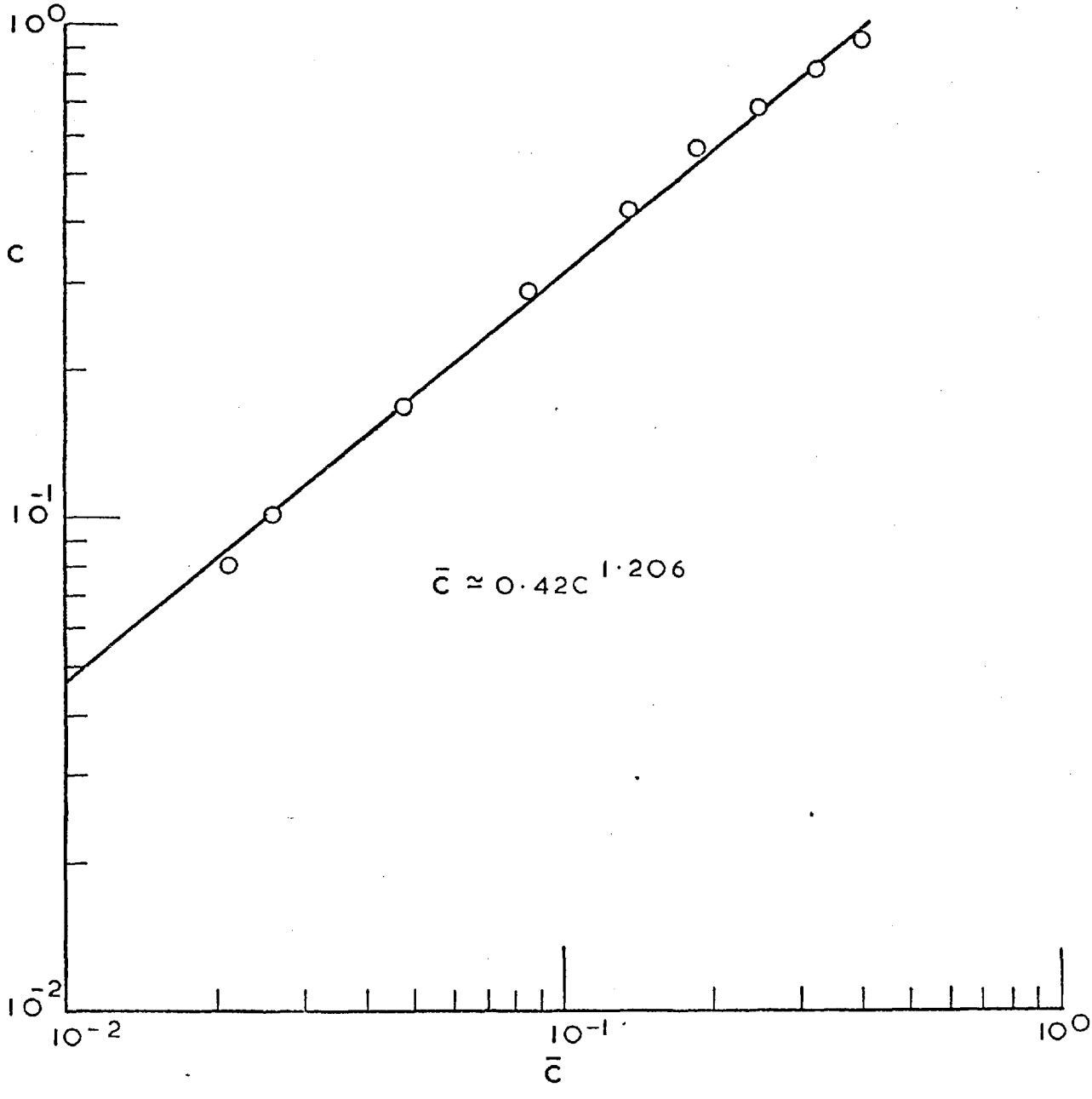

Figure 113: The relationship between c and $\bar{c}$

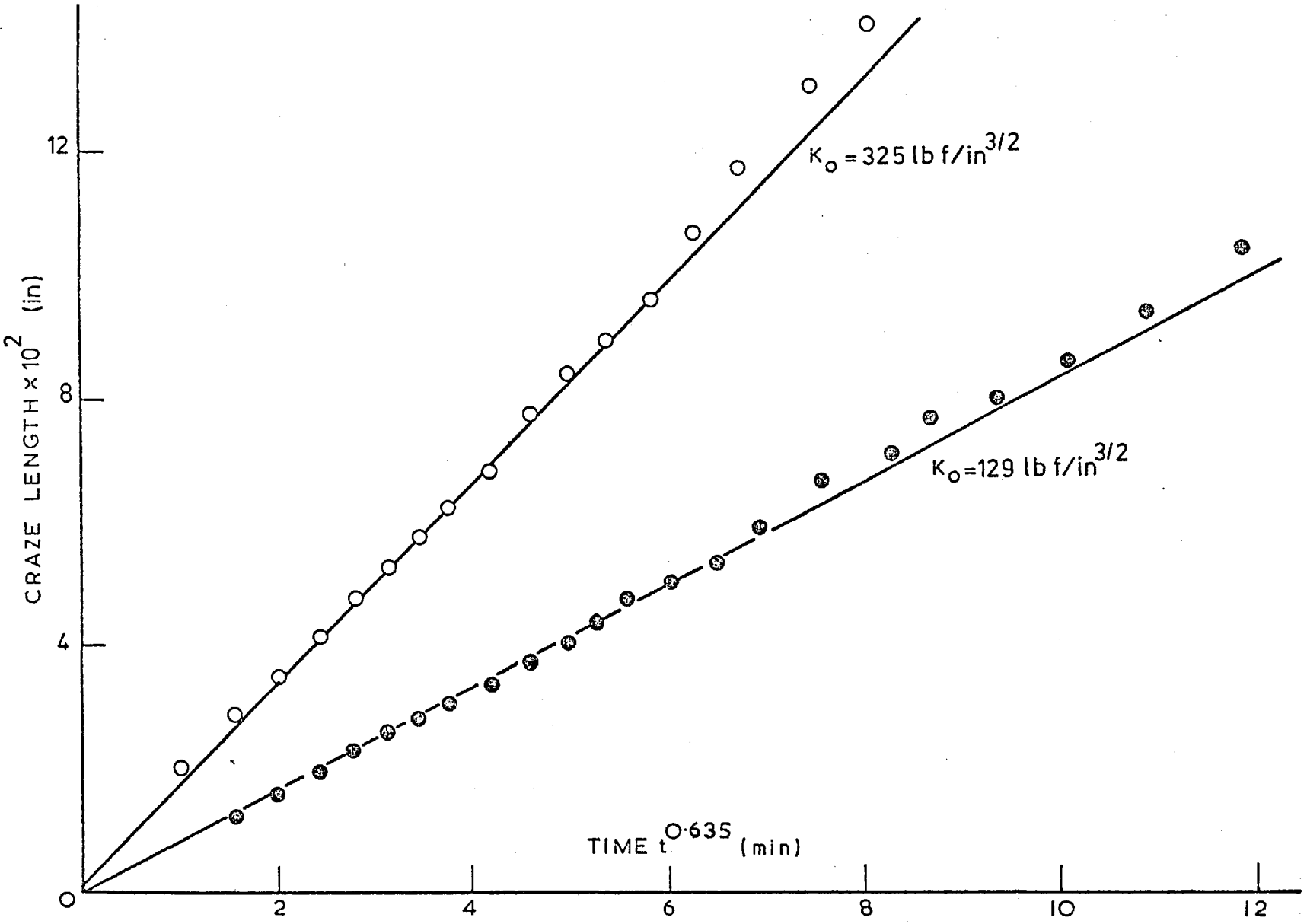

Figure 114: Variation of craze length with $(time)^{0.635}$

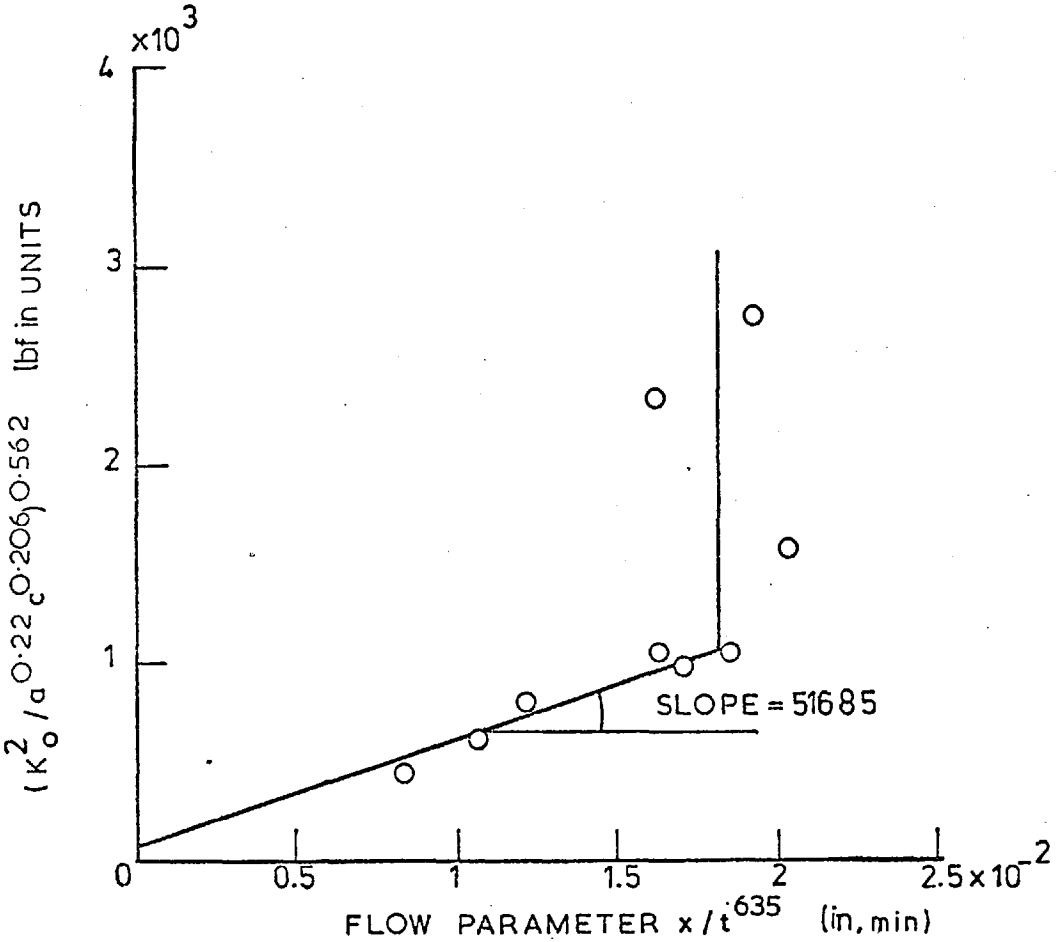

Figure 115: Variation of flow parameter with initial stress intensity factor and initial crack length

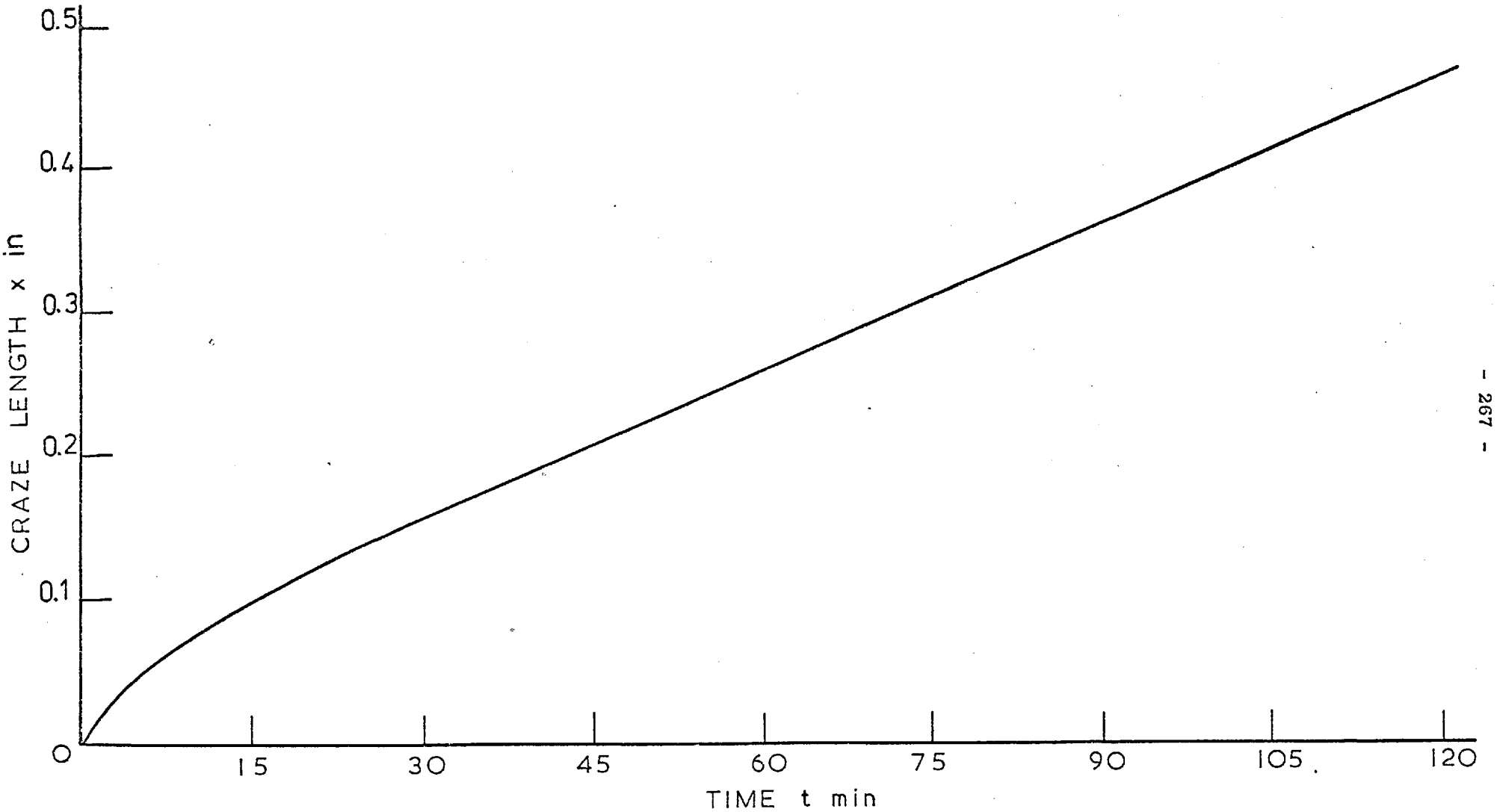

Figure 116: Craze growth history of SEN specimen (after Marshall, 1972)

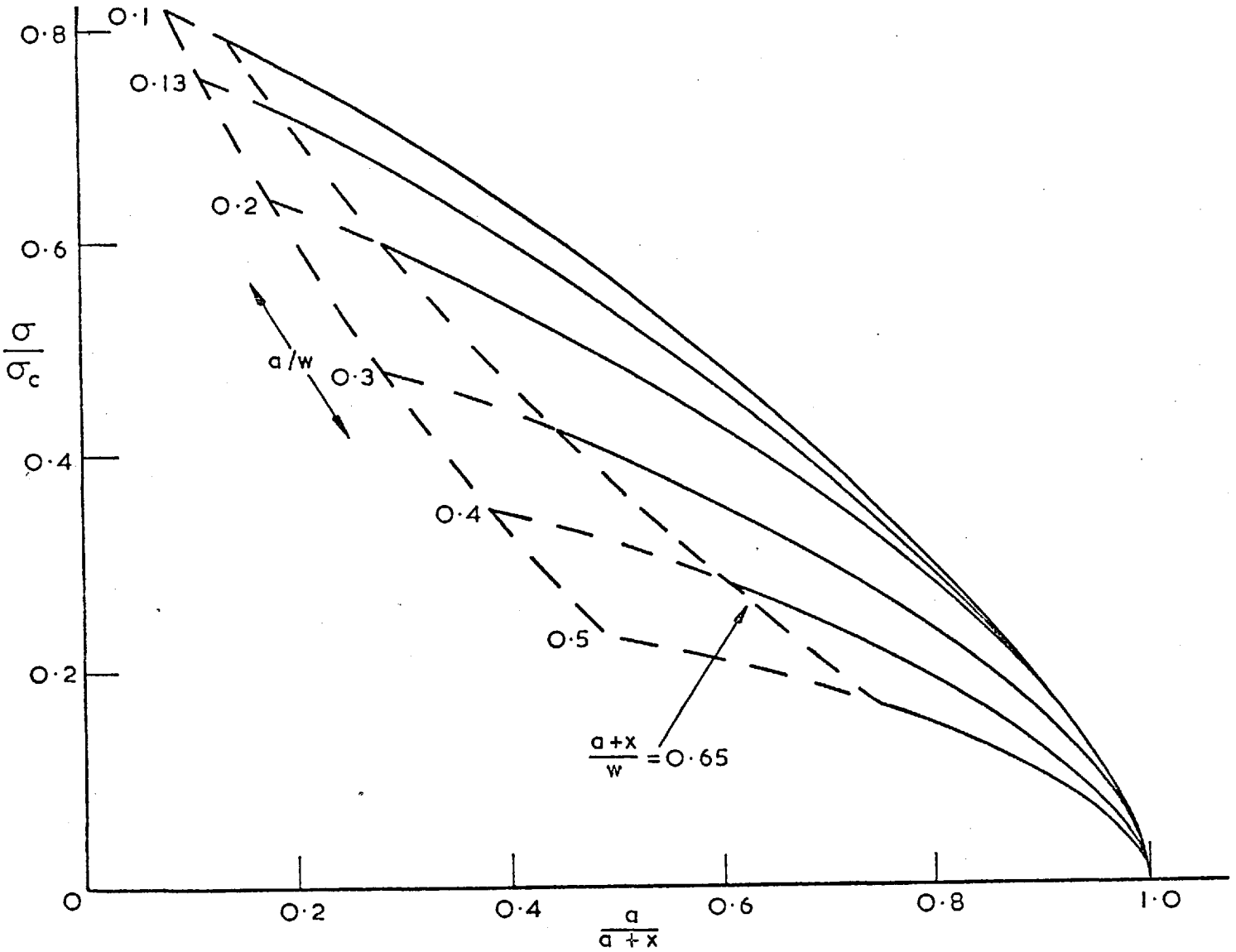

Figure 117: Plastic zone length for finite SEN cracked plate (after Hayes, 1970)

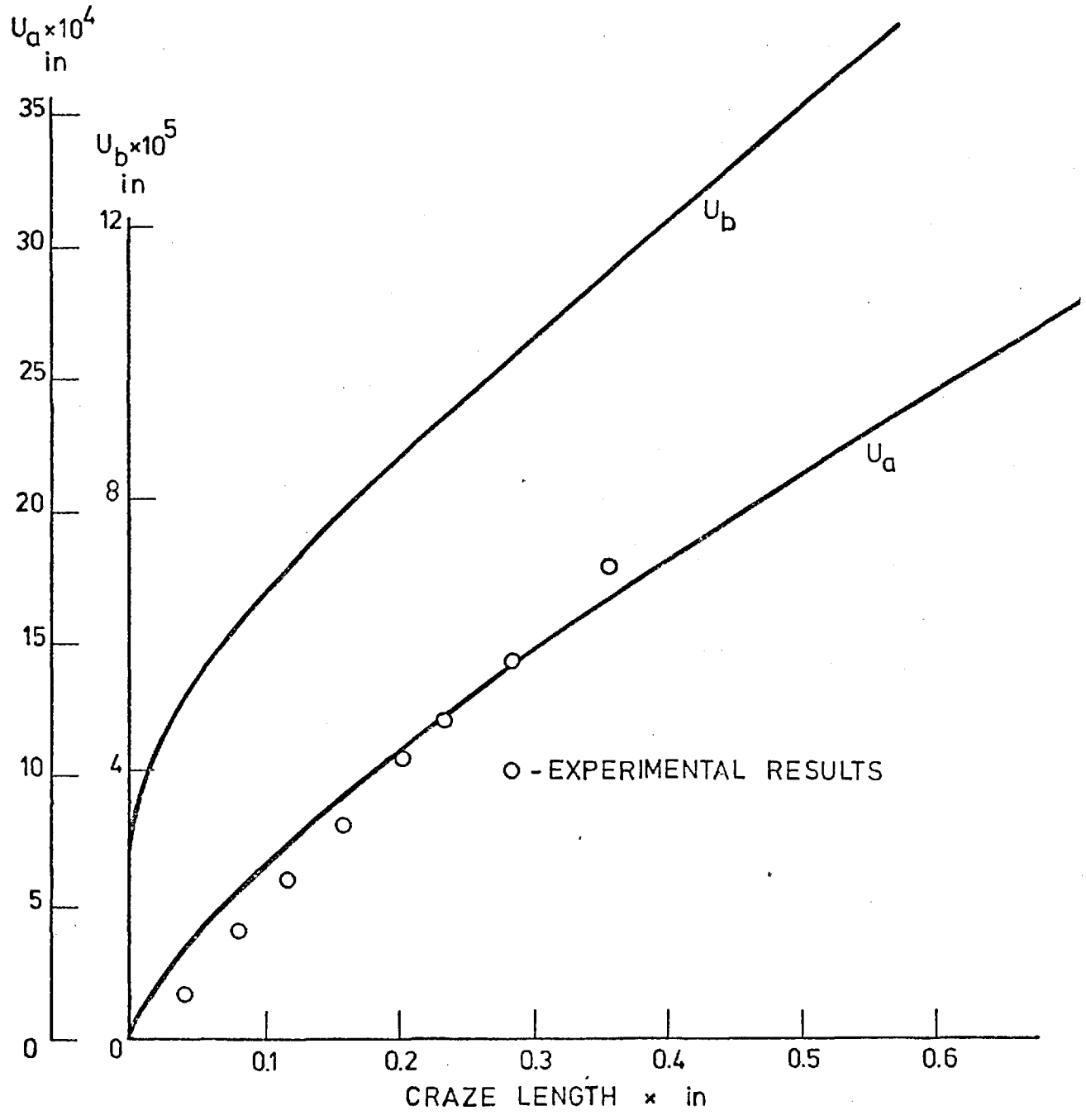

Figure 118: Variation of U_a and U_b with craze length

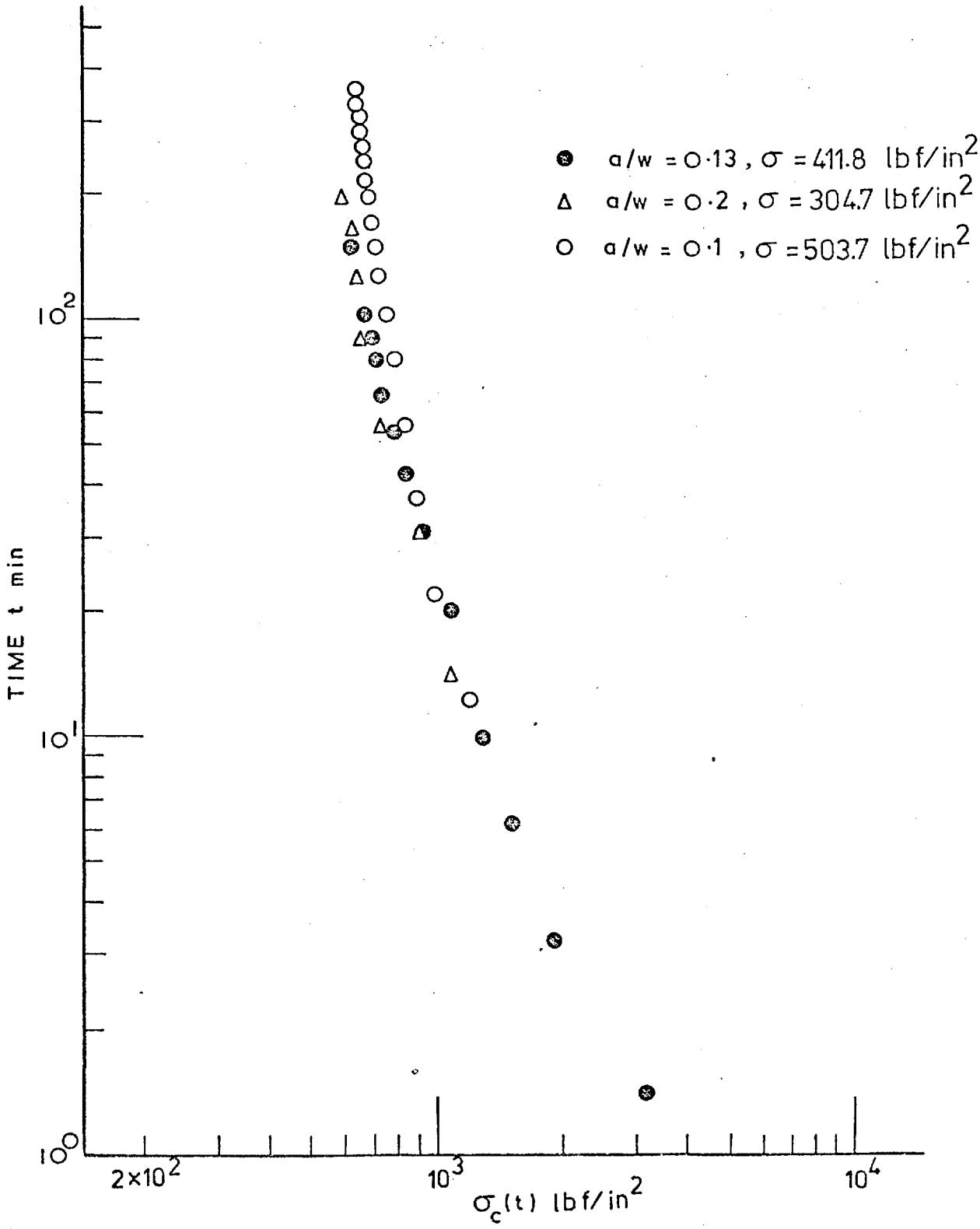

Figure 119: Variation of craze stress with time

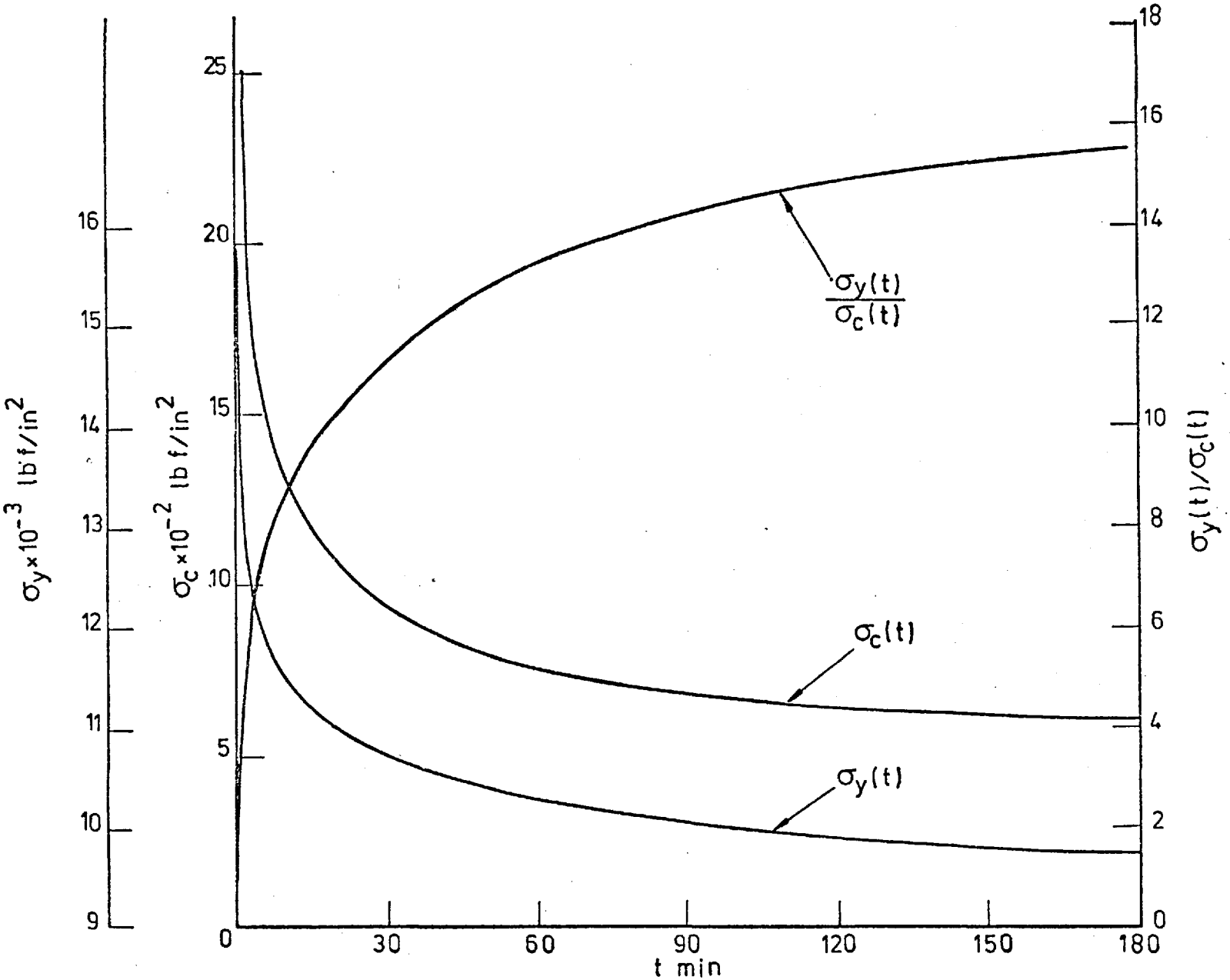

Figure 120: Variation of $\sigma_y(t)$, $\sigma_c(t)$ and $\sigma_y(t)/\sigma_c(t)$ with time t

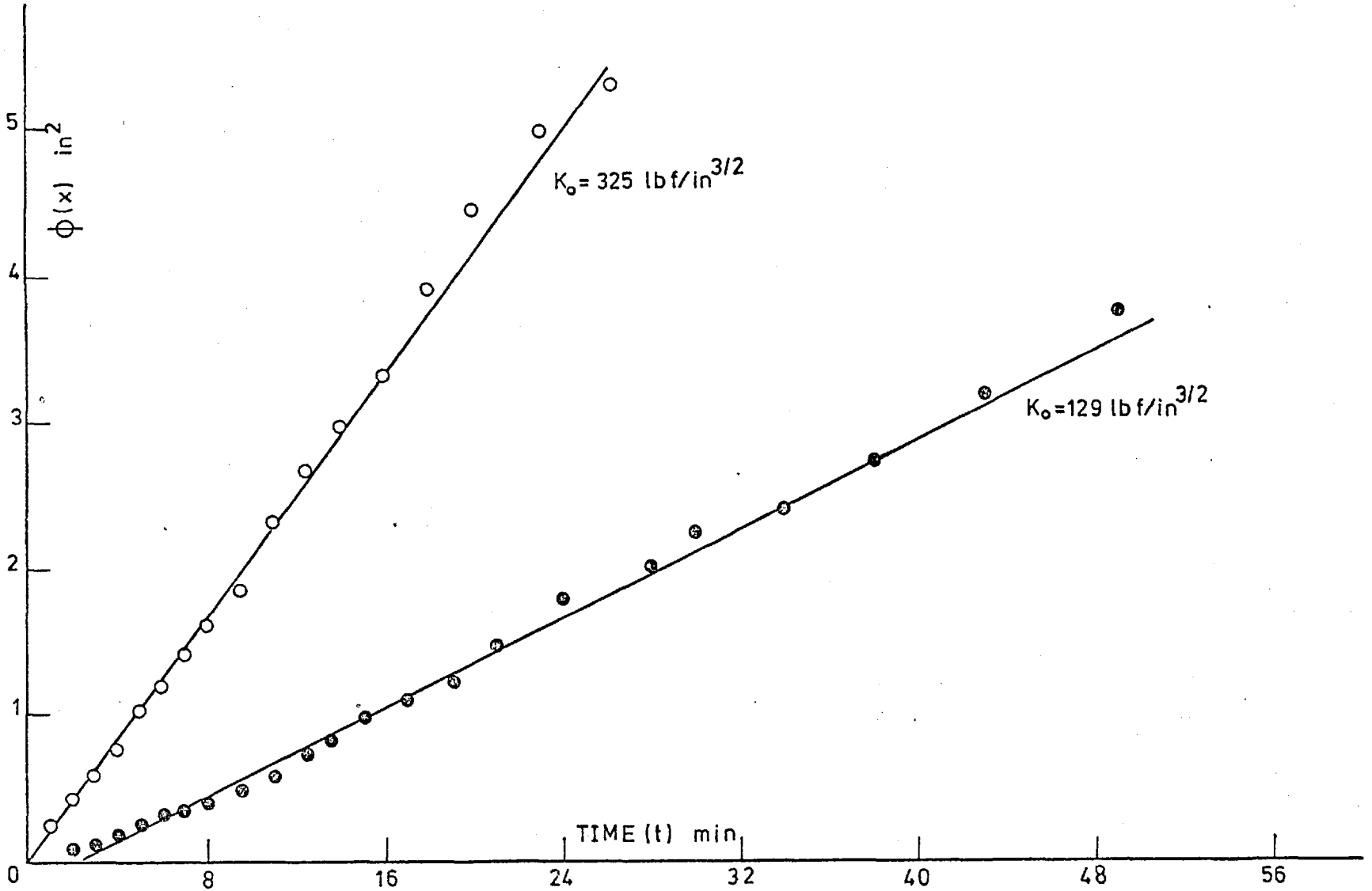

Figure 121: Variation of craze length function ($\phi(x)$) with time

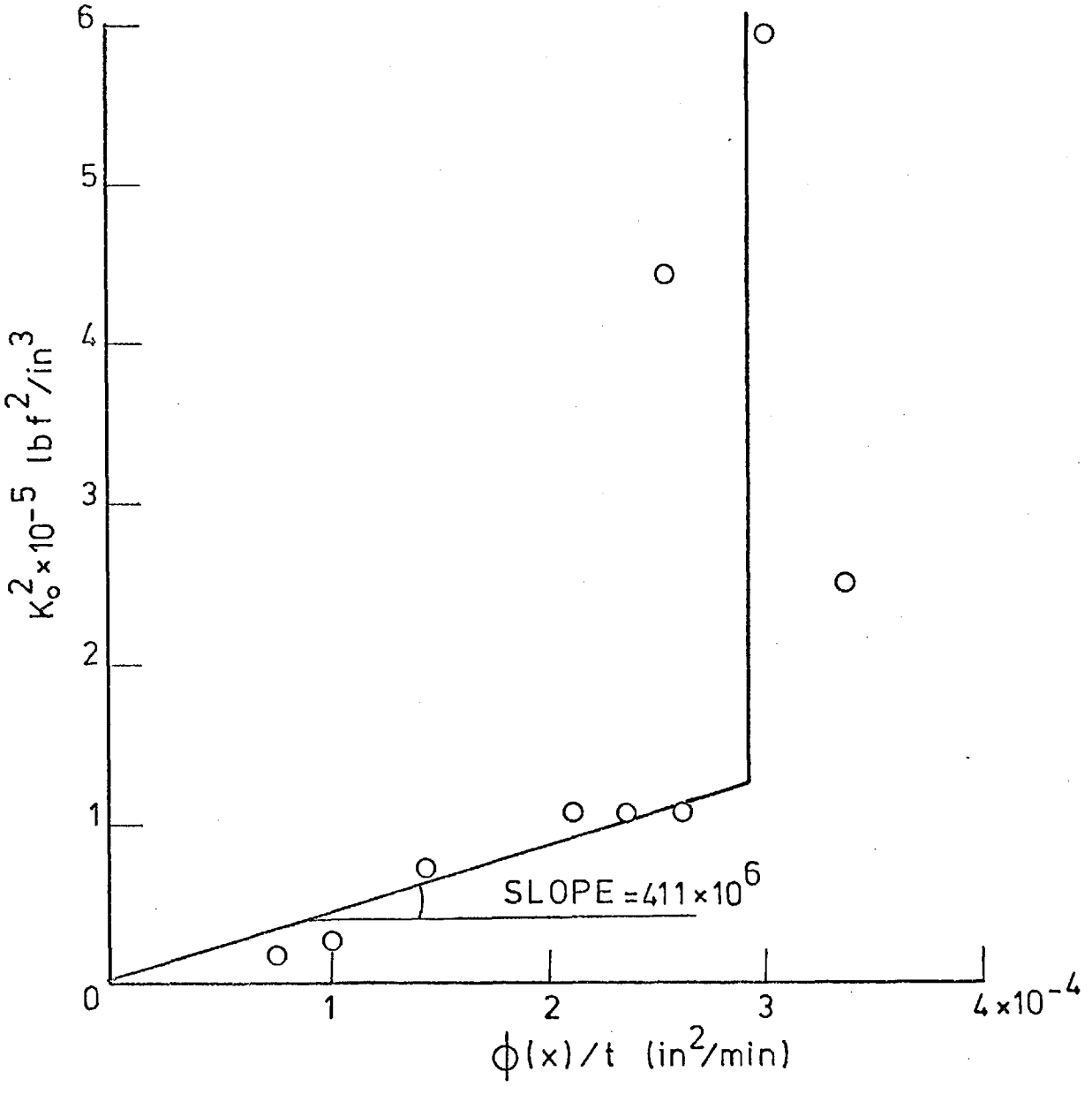

Figure 122: Variation of flow parameter with initial stress intensity factor

APPENDIX A

A BRIEF REVIEW OF FRACTURE MECHANICS CONCEPTS

(a) The Griffith Theory

As a result of his work on glass, Griffith (1921) noticed that the calculated theoretical value of the strength is much higher than that obtained in an actual test. To explain this, he suggested that all real materials contain small crack-like flaws which act as stress raisers, so that the remote stress could be raised at the flaw tip to values reaching the material theoretical strength. Griffith formulated the problem in energy terms and considered the crack propagation as an energy controlled process. He considered the energy absorbed by the process occurring at the crack tip as the work done against molecular cohesion, and that the energy absorbed per unit area of newly created surface as a material constant. The fracture condition was given by:

$$\frac{\partial U}{\partial a} \geqslant 2\gamma \qquad \text{(A.1)}$$

where U is the elastic strain energy, γ is the surface energy and a is the characteristic crack length. The factor 2 arises because of the creation of two surfaces as the crack extends.

Taking Inglis's (1913) results of a single elliptical crack in an infinite plate, Griffith (1924) computed the difference in U between an uncracked and a cracked plate. Differentiating with respect to a led to an expression for the critical failure stress σ_c

$$\sigma_c = \left(\frac{2E\gamma}{\pi a}\right)^{\frac{1}{2}} \qquad \text{(A.2)}$$

where E is the Young's modulus.

However, Griffiths theory describes situations of pure brittle fracture with a complete absence of any plastic deformation at the crack tip. Therefore, development is needed to account for the plastic

behaviour which inevitably occurs at the crack tip in most engineering materials before and during crack propagation.

(b) The Development of Griffith's Theory for Real Materials

Both Irwin (1948) and Orowan (1949) suggested a modification to Griffith's theory to allow for limited plastics behaviour at the crack tip. Their main idea was to replace the surface energy term γ in equations (A.1) and (A.2) by another term γ_p which takes into account the irreversible work absorbed in the plastic deformation at the crack tip per unit area of crack extension. The term γ_p varies widely for different material but it is always much higher than γ, hence, the plastic energy would dominate the fracture behaviour. Orowan (1955) noticed that γ_p was approximately three orders of magnitude greater than γ. Later, Cherepanov (1967) suggested that the ratio γ_p/γ in many cases is of the order of E/σ_y. Both Irwin and Orowan argued that provided the plastically deformed zone at the crack tip is small in comparison with crack length and material thickness, the energy released by crack extension could still, with sufficient accuracy, be calculated from elastic analysis. Irwin emphasised that the strain energy release rate $(\partial U/\partial a)$ is equal to the work absorbed by the fracturing process and the fracture event would occur at the same critical value of energy release rate. He denoted the energy release rate by G and its critical value by G_c. The relation between G_c and γ_p was given by:

$$G_c = 2\,\gamma_p \qquad \text{(A.3)}$$

It should be noted that the magnitude of G_c is theoretically independent of changes in geometry or loading conditions, but it is dependent on some other parameters such as temperature, crack speed and environment. For example, for metals G_c increases rapidly with increasing temperature while in the case of PMMA material it increases with decreasing temperature (Pratt, 1968). In both metals and polymers the energy of fracture increases with increasing crack speed (Goodier and Field, 1963; Berry, 1964; Williams, 1972). However, it may be concluded that variations in G_c are due to changes in conditions which

affect the plastic zone ahead of the crack tip and the material properties. The smaller the G_c the less stable will be the crack growth. In the case of monotonic or dynamic loading there are two zones of crack propagation: the zone of slow or stable crack growth and the zone of fast crack propagation. The value of G_c is considered as the value at the onset of fast crack propagation. The extent of slow crack growth will be less the more favourable the conditions are for the material to behave in a more brittle manner. In the limit, the stable propagation zone will be suppressed and only the fast propagation will be observed (Cherepanov, 1968). The factors which affect the slow growth region are the same as those affecting the energy release rate.

The parameter G can be determined experimentally (Irwin and Kies, 1952) through the relation:

$$G = \frac{\partial U}{\partial a} = \frac{P^2}{2} \frac{\partial C}{\partial a} \qquad \text{(A.4)}$$

where P is the applied load and C is the compliance of the body (the change in displacement due to unit load). By measuring the compliance of a test specimen with various crack lengths, a graphical differentiation gives the value of $\partial C/\partial a$ as a function of crack length, then a fracture test would give the value of G_c by substituting the fracture load and the value of $\partial C/\partial a$ for a given crack length in equation (A.4). The term G could be defined as a force (Irwin, 1957a), since it is the driving force for the fracture process and this force would have the value of G_c at the point of instability.

(c) The Stress Intensity Factor and the Fracture Modes

From the concept of crack driving force, Irwin (1957a,b) demonstrated that G could be associated with the elastic stress distribution near a crack tip. By considering the analysis due to Westergaard (1939) for an elastic cracked sheet subjected to loading at infinity (Figure A.1) he noted that the stress near the crack tip could be expressed in the form:

$$\sigma_{ij} = K (2 \pi r)^{-\frac{1}{2}} f_{ij} (\theta) + 0 r^{0} \qquad \text{(A.5)}$$

where σ_{ij} is the component, parallel to the j direction, of the stress at the point of interest acting on the face of a cubical element which is perpendicular to the i direction; r and θ are polar co-ordinates of the point of interest with the origin at the crack tip; $f_{ij}(\theta)$ is a function of θ dependent upon the particular stress component; Or^0 are terms of the order r^0 bounded at the crack tip. K is a parameter depending only on geometry and loading and is called "the stress intensity factor".

Irwin (1957a,b) went on to show that G could be related to K through the relationship:

$$G = K^2 \frac{1 + \xi}{8 \mu} \qquad \text{(A.6)}$$

where ξ* is a function of Poisson's ratio (ν) and μ** is the elastic shear modulus. This shows that, for elastic situations with limited plastic flow, if fracture occurs when a critical value of G is reached this is equivalent to the attainment of a critical value of K.

In subsequent work (Williams, 1957; Erdogan, 1962; Irwin, 1962; Sih, 1962; Paris and Sih, 1965) it was demonstrated that the characteristic elastic field distribution around a crack is always of the same form independent of the boundary conditions. Generally, the elastic stress field may be given as:

$$\sigma_{ij} = K_I(2\pi r)^{\frac{1}{2}}(f_{ij}(\theta))_I + K_{II}(2\pi r)^{\frac{1}{2}}(f_{ij}(\theta))_{II} + K_{III}(2\pi r)^{\frac{1}{2}}(f_{ij}(\theta))_{III} + Or^0$$

(A.7)

The subscripts I, II and III refer to the modes of fracture according to the relative motion between crack faces (Figure A.2) which could be described by the three basic stress environments acting in the crack

---

* $\xi = 3-4\nu$ for plane strain and equal to $(3-\nu)/(1+\nu)$ for plane stress.

** $\mu = E/2(1+\nu)$.

plane. The subscript I refers to the case where the in-plane (x-y plane) loading is symmetric with respect to the crack plane, i.e. normal separation of the crack faces (cleavage); subscript II refers to the case where the in-plane loading is skew-symmetric with respect to the crack plane, i.e. relative shear motion of the faces perpendicular to the leading edge of the crack (sliding mode), and subscript III refers to the case where loading is anti-plane shear (normal to the x-y plane), i.e. relative shear motion of the faces parallel to the leading edge (screw sliding mode).

The relationship of equation (A.6) may be generalised as:

$$G_I = K_I^2 \frac{(1+\xi)}{8\,\mu} \quad , \quad G_{II} = K_{II}^2 \frac{(1+\xi)}{8\,\mu} \quad \text{and} \quad G_{III} = K_{III}^2/2\mu \qquad \text{(A.8)}$$

However, since the crack extension force is defined in terms of planar crack extension and generally speaking, cracks extend out of their plane except when subjected to symmetric loading, it becomes difficult to justify the attainment of critical values of G_{II} and G_{III} as a fracture criterion. Irwin (1957a) predicted the path of the extending crack to be normal to the direction of maximum tension so that, the component of shear stress on the line of expected crack extension is zero.

By testing suitably shaped and loaded specimens it was possible to determine K_{IC} (G_{IC}) as a material property, but it was found to be strongly dependent on plate thickness (Irwin, 1960a) and only after a certain thickness had been exceeded could K_{IC} be considered as a material constant.

Examination of fracture surfaces demonstrated that K_{IC} becomes constant when the fracture surface was predominantly cleavage. The variations in K_{IC} were attributed to changes in the degree of through-thickness constraint at the crack tip. For thin specimens the plastic zone developed prior to fracture at the crack tip is considered to be unconstrained in the direction normal to the plate surface. With increasing specimen thickness, the surrounding elastic material will inhibit plastic zone growth. Thus, the through-thickness plastic behaviour is essentially three dimensional. The region near the plate surface is in a condition of plane stress whilst that near the centre

approaches plane strain. With sufficient thickness the condition is described as plane strain and cleavage failure predominates (mode I failure). If the plate is not sufficiently thick the crack will exhibit shear lips, failing by a combination of modes I and III.

There are various available methods for determining the stress intensity factor for different specimen configurations and loading conditions. Comprehensive reviews of these methods and their fundamental aspects are given elsewhere, for example Hayes (1970), and here only brief reference is made to those methods.

1. The direct application of Muskhelishvili's (1963) analysis of the elastic stress field: This method provides the exact solutions for cases with reasonable simplicity (for example, an infinite plate with a crack length $2a$ and remote loading σ (Figure A.1); the solution is $K_I = \sigma \sqrt{\pi a}$ and $K_{II} = 0$). This method also could be used as a check for other less accurate methods.
2. The boundary collocation method: It is relatively easy to apply provided that boundary conditions are not complicated. This method was used to determine the stress intensity factor for standard specimens recommended by ASTM (Brown and Srawley, 1966). The solution for K is usually given by $K = \sigma Y a^{\frac{1}{2}}$, where Y is the finite width correction factor.
3. The approximate method by Williams and Isherwood (1968): This method is generally accurate within 20%, however, improved results have been obtained over certain ranges of crack length. The general solution for K is given as $K = F \sigma \sqrt{\pi a}$, where F is the correction factor.
4. The finite element method: This method is useful in dealing with different configurations and loading conditions. It has been developed by Hayes (1970) to overcome the difficulties and the inaccuracy of the previous solutions at certain regions near the crack tip.

(d) The Plastic Zone at the Crack Tip

Irwin (1960b) suggested a modification to take into account the effect of the plastic zone developed ahead of the crack tip before fracture. He

estimated the size of the plastic zone as $2r_p$ where:

$$r_p = \frac{1}{2\pi}\left(\frac{K_c}{\sigma_y}\right)^2 \quad \text{for plane stress} \qquad \text{(A.9)}$$

and $$r_p \quad \frac{1}{4\sqrt{2\pi}}\left(\frac{K_{IC}}{\sigma_y}\right)^2 \quad \text{for plane strain} \qquad \text{(A.10)}$$

where σ_y is the yield stress. He then suggested the crack length to be adjusted to include the effect of the plastic zone and the modified characterising crack length (a) is given by:

$$a = a_o + r_p \qquad \text{(A.11)}$$

where a_o is the physical characterising crack length.

Liu (1965) discussed the effect of the plastic zone on the elastic field at the crack tip. He pointed out that the elastic field remains undisturbed within a certain radius (about 10% of the crack length) provided the plastic zone is small compared with this radius. Thus, the developed plastic zone should be less than 10% of the crack length; under this condition the attainment of a critical K_{IC} will guarantee the same near tip stress environment for different cases.

The attainment of plane strain conditions requires the plastic zone to be small compared with the thickness (t). Brown and Srawley (1966) suggested that:

$$t/\left(\frac{K_{IC}}{\sigma_y}\right)^2 \geq 2.5 \qquad \text{(A.12)}$$

is sufficient to give plane strain conditions.

Following the above estimation of the plastic zone by Irwin and the restrictions on its size by Liu and Brown and Srawley allows the evaluation of crack behaviour in a material in terms of linear elastic fracture mechanics.

1. The Dugdale model

This model was originally suggested by Dugdale (1960) for thin plastic zones which may be identified with a line of yielding ahead of the crack tip. In his model he considered an isolated straight crack of length $2a$ in an infinite sheet with remotely applied stress σ normal to the crack plane (Figure A.3) and yielding is confined to a narrow band along the line of the crack to a distance x from the crack tip. He assumed that the yield stress (σ_y) is constant over that distance x and all the stresses throughout the plate were to remain finite. He obtained the following relation for the plastic zone of length x:

$$\frac{a}{a + x} = \cos \frac{\pi \sigma}{2\sigma_y} \qquad \text{(A.13)}$$

The Dugdale model has been developed by different investigators (e.g. Goodier and Field, 1962; Bilby et al, 1963; Hayes, 1970 and 1972). As a result of their work the solution of the Dugdale model has been extended to cracked bodies of different shapes and loading conditions (Hayes, 1970). Expressions were derived for the opening of the crack (U) at its tip, which is a parameter of interest in fracture mechanics, e.g. U was given by Hayes (1970) for the case considered above in the original Dugdale model as:

$$U = \frac{(\xi + 1)}{\pi \mu} a \sigma_y \ln \left(\frac{a + x}{a}\right) \qquad \text{(A.14)}$$

The restriction of constant σ_y could be removed to allow variations in yield stress, e.g. the case of strain hardening materials (Hayes, 1970).

The experimental investigations of the Dugdale model have proved its ability to give good correlation of the results from different materials, e.g. Hahn and Rosenfield (1965) tests on silicone steel; Kobayashi et al (1968) tests on aluminium and magnesium alloys; Wiederhorn (1969) tests on glass; Brinson (1969) tests on

polycarbonate and Graham et al (1972) tests on PMMA. Therefore, the Dugdale model is regarded as a practical tool in fracture tests where the conditions are suitable for its application.

2. Rice's contour integral

Rice (1968) has developed a relationship for the change in the energy of the body due to the growth of a crack. This relationship was represented in terms of a line contour integral J which has the property of being path independent. The parameter J could be used in cases where large scale plasticity takes place as well as in the elastic case; it may be considered as the most general parameter associated with the stress environment near the crack tip. Rice derived the rate of change of potential energy with respect to crack length for a growing crack in a two dimensional body as:

$$J = -\frac{\partial P}{\partial a} = \int_{\Gamma} \left[W\, dy - T_i \frac{\partial u_i}{\partial x}\, ds \right] \qquad \text{(A.15)}$$

where $\partial P/\partial a$ is the rate of change of potential energy with respect to crack length, W is the strain energy density, T_i and u_i are traction stress and displacement vectors normal to Γ and Γ is any continuous contour surrounding the crack tip starting from the lower crack face and terminating in the upper crack face.

For a linearly elastic body J is identical to G by definition. Rice (1968) evaluated equation (A.15) for the case of linearly elastic body and found that $J = (\xi+1)/8\mu . K_I^2$ which is similar to equation (A.6).

In the case of the Dugdale line plastic zone, J was evaluated (Hayes, 1970) by considering a path of integration around the line of plasticity, Figure A.3, the integration became:

$$J = \sigma_y U \qquad \text{(A.16)}$$

3. The crack opening displacement (COD)

The presence of the plastic zone at the crack tip enables the crack faces to move apart without extending the crack length. This relative movement is called the crack opening displacement (COD). The COD may be used as a failure criterion in materials which exhibit plastic deformation at the crack tip, i.e. failure happens when COD reaches a critical value. This was originally proposed by Wells (1963).

Measuring the COD represents a practical difficulty. However, it has been mentioned by Kobayashi et al (1969) that any portion along the crack surface may be used for COD measurement except a small portion 0.1 a from the crack tip.

The COD has been related to G (Wells, 1963) by the relation:

$$G = \frac{\pi}{4} \sigma_y U \qquad \text{(A.17)}$$

Burdekin and Stone (1966) used the Dugdale model for calculating the COD, and by expanding the expression of U (equation (A.14)) and neglecting the high order terms U was given as:

$$U = \frac{(1 + \xi)}{8 \mu} \frac{K_I^2}{\sigma_y} \qquad \text{(A.18)}$$

It should be noted that the above expression is suitable when the applied stress σ is small enough when compared with σ_y to allow neglecting terms of the order $(\pi\sigma/2\sigma_y)^4$ and higher (i.e. limited plastic zone size). Therefore, for small sizes of plastic zone U may be related to J and G by:

$$U = \frac{G}{\sigma_y} = \frac{J}{\sigma_y} = \frac{(1 + \xi)}{8 \mu} \frac{K_I^2}{\sigma_y} \qquad \text{(A.19)}$$

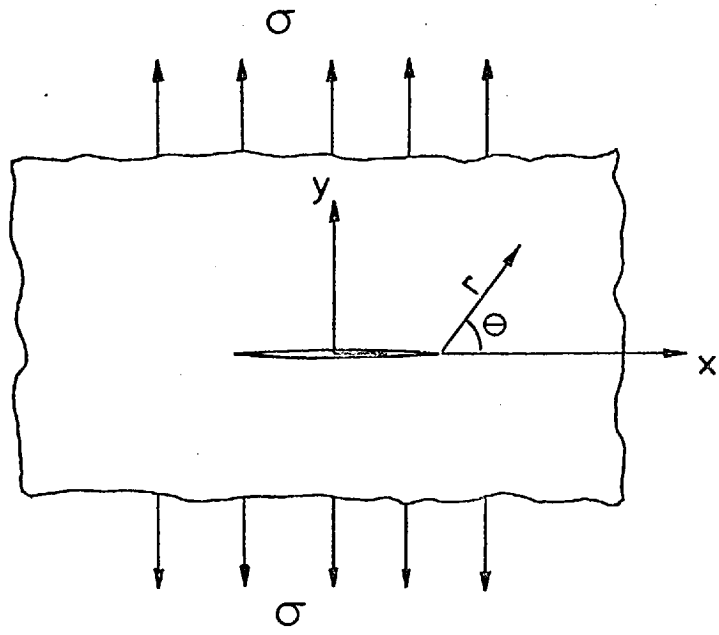

Figure A.1: Centrally notched plate subjected to remote uniform stress

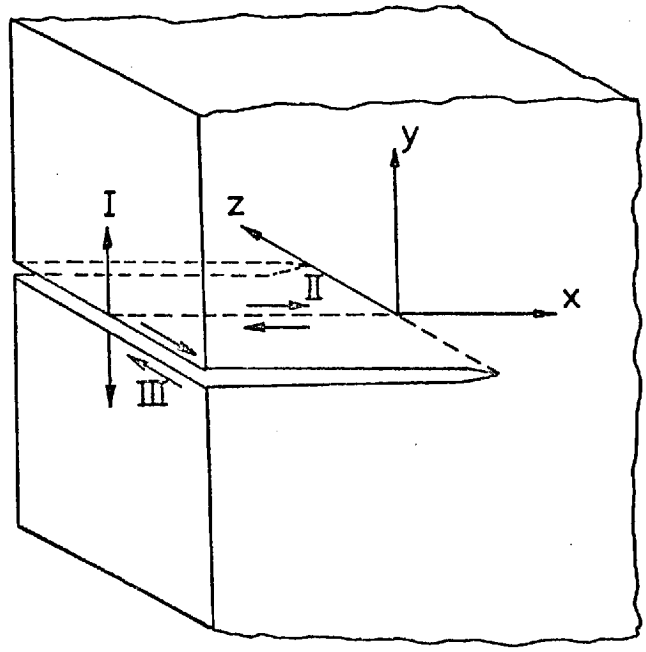

Figure A.2: The modes of fracture

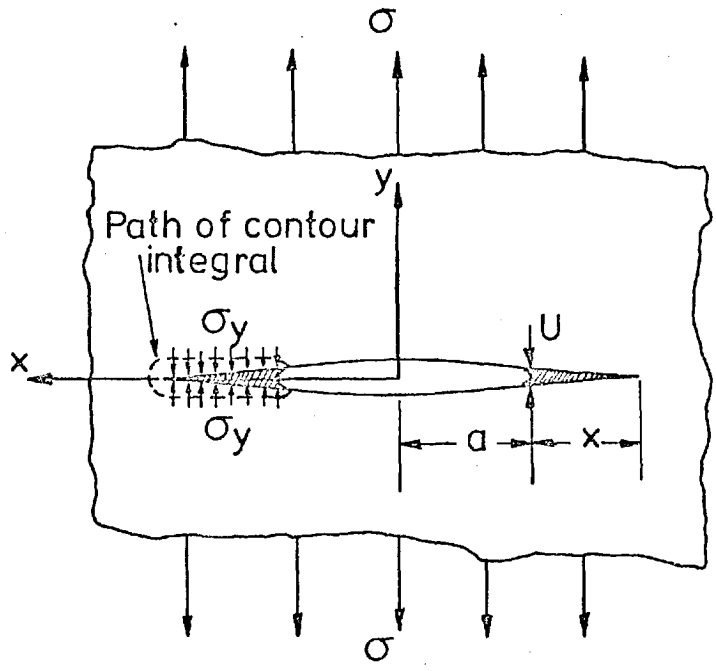

Figure A.3: The Dugdale model and the path of Rice contour integral

APPENDIX B

A NOTE ON CRAZING IN GLASSY POLYMERS

Crazes generally initiate in the surface at the sites of stress concentrations such as voids, inclusions or scratches. However, in some cases, they have been observed internally, for example, in polystyrene (Howard and Mann, 1964). The sites of stress concentrations in this case may be inclusions or internal voids formed during material production.

(a) Craze Structure

Until a few years ago, crazes had been treated as though they were true cracks in which complete separation of the material occurs. However, there is some evidence that this is not the case. For example, Sauer et al (1949) had noted that specimens which had been crazed across the whole section still carried loads without breaking. Warburton et al (1953) had found that crazes in PMMA had been healed and disappeared when specimens were heated above T_g. The work of Kambour (1964a,b), however, has shown that crazes are not true cracks but contain material inside the craze. Kambour treated the craze, from the optical point of view, as a thin layer of material of low refractive index between two pieces of material of high refractive index and measured the critical angle of light reflection at the craze/polymer interface. He then calculated the refractive index and the density of the craze. He found that the volume fraction of polymer in the craze is typically 40 to 60% and that the craze density seemed independent of either the polymer or the way in which the craze had been formed. Kambour suggested that the voids in the craze are interconnected to form continuous channels as evidenced by the ease with which one liquid in a craze can be exchanged for another (Kambour, 1964a).

Kambour and Holik (1969a,b) were able to estimate the size of the voids in the craze by filling the craze with a substance which could show up the voids in the electron microscope, as in the case of infusing sulphur in polyarylene oxide crazes. They showed that at the tip of the craze the voids were smaller, of the order of 20 Å, and that as the craze thickened behind the tip the size increased to reach approximately 200 Å; more material was drawn in, and the structure became fibrillar in nature.

Crazes, even the dry ones in the absence of environments, are much

more compliant than the original polymer. Kambour and Kopp (1967, 1969) showed that the constituent material of the craze undergoes considerable deformation under the effect of loading. Deformations of the already mature craze of 50 to 70% were possible and its modulus lay between 3 and 25% of that of the normal polymers.

(b) Craze Initiation and Growth

As previously mentioned, crazes initiate at the sites of stress concentrations (e.g. at the tip of flaws where the the hydrostatic tensile stress system exists). When these stresses are sufficient to overcome the secondary forces holding the molecular chains together, separation occurs and the craze initiates. Therefore, if the stresses initiating the craze are in the direction of orientation, initiation of the craze will be more difficult than in the condition where these stresses are perpendicular to the direction of orientation (Murphy, 1969).

Crazes initiate more rapidly at high stresses than at low ones so the level of stress below which the crazes do not initiate even for long periods of stress application is termed as the critical stress for craze initiation. Analogous to the critical stress is the critical strain criterion which may be applied to the materials in which homogeneous creep is very limited at low stresses (e.g. polystyrene). However, neither of these parameters is wholly satisfactory because they neglect the effect of flaw size at which the craze initiates and this may lead to fluctuations in the critical value obtained (Stuart et al, 1964).

The existence of triaxial stresses at the craze tip, as at the crack tip, allows the craze to grow when the stress values are sufficient for void formation. The growth direction is perpendicular to the direction of maximum principal stress (Sternstein et al, 1968) and the growth rate under constant stress decelerates with time, which indicates that creep effects make the matrix more resistant to craze growth (Regel, 1956).

(c) Crazing and Fracture

Berry's (1965) proposal that failure takes place within the craze by void coalescence has been verified by direct visual observations of Murray and Hull (1970) on crazes in polystyrene. They observed that fracture initiation involves the appearance and slow enlargement of a very small hole inside the craze. When the hole becomes large enough the remainder

of the craze ruptures suddenly.

Crack propagation energy in glassy polymers was first calculated by Berry (1961) based on the Griffith theory (see Appendix A). The measured surface work γ_p was found to be approximately 1000 times greater than that to break a single layer of chain bonds. That discrepancy was attributed to the dissipation of energy in plastic flow at the crack tip. Kambour (1964c) measured the refractive index of the fracture surface layer of PMMA and found that its value is comparable to that obtained for a craze of 40% void contents. He concluded that the material is not only oriented by plastic deformation but also voided with optical characteristics of a normal craze. In another series of tests Kambour (1966) observed the optical interference fringes at the crack tip during crack propagation in glassy polymers, and this allowed him to deduce the configurations of the crack tip and the craze that precedes it. The craze extended 25 μ beyond the crack tip in PMMA and 550 μ beyond the tip in polystyrene.

According to the above mentioned observations, crack propagation occurs by the formation and breakdown of crazed material at the tip of the crack. The energy of crack propagation is used in forming, distorting and breaking the craze at the tip of the crack (Kambour, 1966, 1968). Most of this energy goes into the plastic work of craze formation and the viscoelastic work of extending the craze to the breaking point. Only a small amount (1 to 10% of the total crack propagation energy) is associated with the production of the surface area required to create the voids in the craze (Kambour, 1968).

The process of craze formation and breakdown by void coalescence ahead of the crack tip is not restricted to slow crack growth. There is evidence that the same process occurs in fast crack propagation, e.g. the hyperbolic markings on the fast fracture surface of PMMA are due to the intersection of the main crack front and a radial expanding void at the crack front (Berry, 1962).

(d) The Environmental Role in Stress Crazing

The presence of organic liquid environment causes the crazes in the glassy polymers to initiate and propagate at lower stresses than in air. This leads to a drastic reduction in the failure stress which is at present a serious problem in the use of glassy plastics. The effects of the liquid environment are mainly plasticisation and surface stabilisation

(Not chemical as in metals). Of these, the former dominates (Kambour, 1971).

Plasticisation means the diffusion of the agent into the polymer structure causing the material to swell, and its action as a plasticiser in making flow easier by lowering the T_g. Bernier and Kambour (1968) have made a detailed examination of the plasticisation effect of organic agents on polyarylene oxide. They used the degree of swelling of the polymer caused by the agent as a measure of the plasticisation effect and considered the difference between the solubility parameter of the liquid (δ_{liquid}), and that of the polymer as a sufficiently accurate measure of the degree of swelling. They measured the critical strain for craze or crack initiation in different liquids and found a good correlation between critical strain ε_c and δ_{liquid}. The minimum in ε_c occurred at δ_{liquid} identical to $\delta_{polymer}$. Liquids having δ_{liquid} near $\delta_{polymer}$ were found to be cracking agents and this was attributed to the degree of swelling being great enough to lower T_g to the ambient temperature or lower. Under these conditions the craze has negligible strength and is unobservable as a steady structure. Increasing the difference between δ_{liquid} and $\delta_{polymer}$ causes the craze to initiate at ε_c less than its value in air.

The role of surface stabilisation is that the organic liquid can reduce the surface energy of the polymer and thus facilitate the formation of a new surface area (Stuart et al, 1964). Therefore, the liquid must be able to wet the plastic (spreads easily on the material surface with zero contact angle). This agrees well with the observation that all the crazing agents wet the polymer surface (Kambour, 1971). However, it has been mentioned above that the energy of surface formation represents only 1 to 10% of the total crack propagation energy which suggests that this factor is of secondary effect to plasticisation.

APPENDIX C

CRAZE GROWTH EQUATION IN ROUND NOTCHED BARS AS BASED ON SIMPLE LIQUID FLOW IN A DISC

(a) Flow in a Disc to a Sink (Cogswell, 1974)*

Consider a fluid of viscosity η flowing through a disc of dimensions shown in Figure C.1 at constant pressure drop P. There are two components of flow:

1. due to shear flow; and,
2. due to elongation or hoop stresses.

For a simple liquid this latter component of flow is only significant for a disc having a radius (r) comparable to the gap (h). In the case of $r >> h$, this hoop component may be neglected and the flow is considered as shear flow.

Shear flow:

For the element δr shown in Figure C.2:

$$\delta P \times 2\pi r \times h = 2\sigma_s \times 2\pi r \times \delta r$$

i.e.
$$\delta P = \frac{2\sigma_s \delta r}{h} \qquad (C.1)$$

where σ_s is the shear stress at the walls.

The shear rate at walls $(\dot{\gamma}) = 6Q/2\pi r h^2$, where Q is the volume flow rate through the element δr, thus σ_s is given by:

$$\sigma_s = \eta \dot{\gamma} \qquad (C.2)$$

---

* F.N. Cogswell, private communication.

From equations (C.1) and (C.2) and integrating for $R_2 < r < R_1$:

$$P = \frac{6\eta Q}{\pi h^3} \ln \frac{R_1}{R_2} \qquad \text{(C.3)}$$

Whence, for a constant head of pressure:

$$Q = \frac{\pi h^3 P}{6\eta \ln \frac{R_1}{R_2}} \qquad \text{(C.4)}$$

Then, if V is the average velocity of the liquid at the front:

$$V = \frac{dx}{dt} = \frac{Q}{2 \pi R_2 h}$$

i.e. $$\frac{dx}{dt} = h^2 P/12 \eta (R_1 - x) \ln \left(\frac{R_1}{R_1 - x}\right) \qquad \text{(C.5)}$$

(b) Craze Growth Equation

The radial craze velocity may be considered as equal to that of the liquid (Marshall et al, 1970 - see page 118), thus, integrating equation (C.5) between $x = 0$ to x and $t = 0$ to t, gives the following relation between radial craze length and time:

$$\frac{R_1^2}{4} - \frac{R_1^2}{2}\left(1 - \frac{x}{R_1}\right)\left(\tfrac{1}{2} - \ln\left(1 - \frac{x}{R_1}\right)\right) = \frac{Ph^2}{12\eta} t \qquad \text{(C.6)}$$

where h^2 may be looked upon as the mean effective voiding area A (Figure 107c). The value of A at craze initiation (see Section 6.3.1) may be given as:

$$A = \frac{\ell_o^2}{2d_o} U_a \qquad (C.7)$$

where ℓ_o and d_o are material constants (see Section 6.3.1) and U_a is the displacement at the original crack tip (i.e. at the radius R_1). U_a for plane strain conditions (see Appendix A) may be given as:

$$U_a = \frac{K_o^2 (1 - \nu)}{E_o \sigma_o} \qquad (C.8)$$

where K_o is the initial stress intensity factor and E_o and σ_o are the modulus and yield stress appropriate to short loading times.

Thus, from equations (C.6), (C.7) and (C.8) the craze growth equation may be given as:

$$\phi(x) = \frac{P(1 - \nu^2)\ \ell_o^2\ K_o^2\ t}{24\ E_o\ \sigma_o\ d_o} \qquad (C.9)$$

where $\phi(x) = \frac{R_1^2}{4} - \frac{R_1^2}{2}(1 - \frac{x}{R_1})(\frac{1}{2} - ln\ (1 - \frac{x}{R_1}))$.

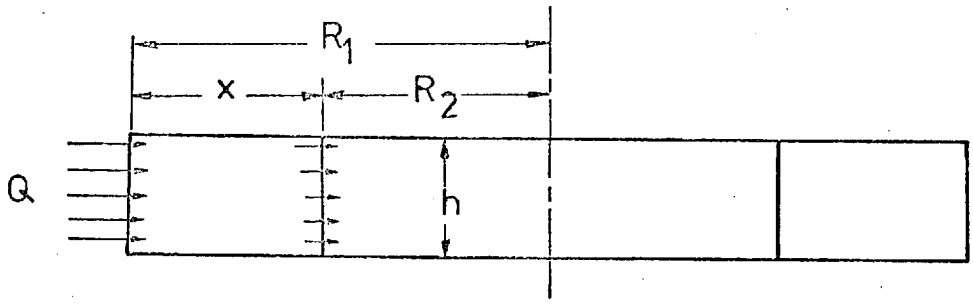

Figure C.1: Flow in a disc to a sink

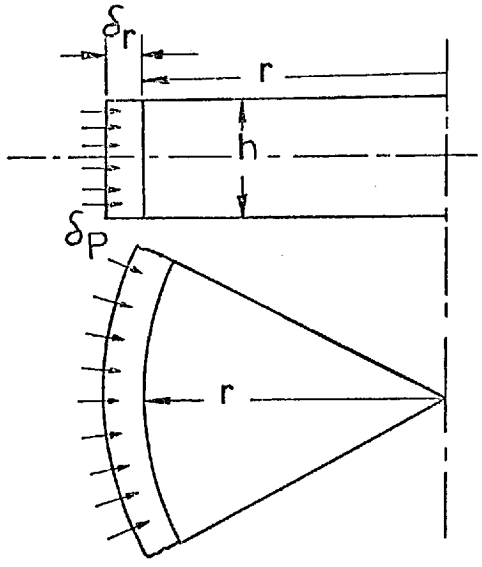

Figure C.2: Shear flow element

REFERENCES

ANDREWS, E.H., and WALKER, B.J.
Proc. R. Soc. London, A.325, (1971), p. 57.

ANON.
ASTM, STP, 381, (1965).

ARAD, S., RADON, J.C., and CULVER, L.E.
J. Mech. Engng Sci., 13, (1971), p. 75.

ARAD, S., RADON, J.C., and CULVER, L.E.
Polym. Engng Sci., 12, (1972a), p. 193.

ARAD, S., RADON, J.C., and CULVER, L.E.
J. Mech. Engng Sci., 14, (1972b), p. 328.

ARAD, S., RADON, J.C., and CULVER, L.E.
J. Engng Fracture Mechs., 4, (1972c), p. 511.

ARAD, S., RADON, J.C., and CULVER, L.E.
3rd International Conference on Fracture, Munich, 7, 8-13 April (1973a), p. VI-323.

ARAD, S., RADON, J.C., and CULVER, L.E.
Canadian Applied Mechanics Conference (CANCAM 73), (1973b), Paper 196.

BARSOM, J.M.
International Conference on Corrosion Fatigue, University of Connecticut, 14-18 June (1971), p. 424.

BASQUIN, O.H.
Proc. ASTM, 10, (1910), p. 625.

BAUSCHINGER, J.
J. Inst. Civil Engrs., 2, (1886-1887), p. 463.

BERNIER, G.A., and KAMBOUR, R.P.
Macromolecules, 1, (1968), p. 393.

BERRY, J.P.
J. Polym. Sci., 50, (1961), p. 107.

BERRY, J.P.
J. Appl. Phys., 33, (1962), p. 1741.

BERRY, J.P.
In: "Fracture Processes In Polymeric Solids", ed. Rosen, B., Interscience Publishers, New York, (1964), p. 195.

BERRY, J.P.
J. Polym. Sci., A.3, (1965), p. 2027.

BILBY, B.A., COTTRELL, A.H., and SWINDEN, K.H.
Proc. R. Soc. London, A.272, (1963), p. 304.

BONNER, R.M., and others
"Properties of Molded Nylons" In: "Nylon Plastics", ed. Kohan, M.I., John Wiley and Sons, (1973), p. 329.

BORDUAS, H.F., CULVER, L.E., and BURNS, D.J.
J. Strain Analysis, 3, (1968), p.193.

BRINSON, H.F.
SESA Spring Meeting, Philadelphia, (1969).
Also in: Exp. Mechs., 10, February (1970), p. 72.

BROWN, H.F., and SRAWLEY, J.E.
ASTM, STP, 410, (1966).

BURDEKIN, F.M., and STONE, D.E.W.
J. Strain Analysis, 1, (1966), p. 145.

BURKE, J.J., and OROFINO, J.A.
J. Polym. Sci., A.2, 7, (1969), p. 1.

CHEREPANOV, G.P.
PMM, 31, (1967), p. 476.
See English Translation in PMM: J. Appl. Math. Mechs., 31, (3), (1967), p. 503.

CHEREPANOV, G.P.
Int. J. Solids Struct., 4, (1968), p. 811.

CHEREPANOV, G.P., and HALMANOV, H.
Engng Fracture Mechs., 4, (1972), p. 219.

COFFIN, L.F.
Appl. Maters Res., 1, (1962), p. 129.

CONSTABLE, I., WILLIAMS, J.G., and BURNS, D.J.
J. Mech. Engng Sci., 12, (1970a), p. 20.

CONSTABLE, I., CULVER, L.E., and WILLIAMS, J.G.
Int. J. Fracture Mechs., 6, (1970b), p. 279.

CROOKER, T.W., and LANGE, E.A.
NRL Report 6805, Naval Research Laboratory, Washington D.C., (1968).

DONAHUE, R.J., ATANMO, P., KUMBLE, R., and McEVILY, A.J.
Int. J. Fracture Mechs., 8, (1972), p. 209.

DUGDALE, D.S.
J. Mech. Phys. Solids, 8, (1960), p. 100.

DUNN, P., and SANSOM, G.F.

J. Appl. Polym. Sci., 13, (1969), pp. 1641, 1657, 1673.

ERDOGAN, F.

Proceedings of the 4th US National Congress on Applied Mechanics, University of California, Berkeley, (1962).

ERDOGAN, F.

"Fatigue Crack Propagation" In: "Fracture", ed. Liebowitz, Vol. 2, Academic Press, New York, (1968), p. 497.

ERDOGAN, F., and RATWANI, M.

Int. J. Fracture Mechs., 6, (1970), p. 379.

EWING, J.A., and HUMFREY, J.G.W.

Phil. Trans. R. Soc. London, A.200, (1903), p. 241.

FEENEY, J.A., McMILLAN, J.C., and WEI, R.P.

Met. Trans., 1, (1970), p. 1741.

FELTNER, C.E., and MORROW, J.D.

TAM Report 576, University of Illinois, (1959).

Also in: ASME. Trans. J. Basic Engng, 83, Series D, (1961), p. 15.

FERRY, D.J.

In: "Viscoelastic Properties of Polymers", 2nd Edition, Wiley, New York, (1970).

FORMAN, R.G., KEARNEY, V.E., and ENGLE, R.M.

Trans. ASME. J. Basic Engng, 89, Series D, (1967), p. 459.

FORSYTH, P.J.E.

Proceedings of Symposium on Crack Propagation, Cranfield, (1961).

FROST, N.E.

Proceedings of 1st International Conference on Fracture, Sendai, (1966), p. 1433.

FROST, N.E., and DUGDALE, D.S.

J. Mech. Phys. Solids, 6, (1958), p. 62.

FROST, N.E., and GREENAN, A.F.

J. Mech. Engng Sci., 12, (1970), p. 159.

GENT, A.N., LINDLEY, P.B., and THOMAS, A.G.

J. Appl. Polym. Sci., 8, (1964), p. 455.

GERBERICH, W.W., BIRAT, J.P., and ZACKAY, V.F.

International Conference on Corrosion Fatigue, University of Connecticut, 14-18 June (1971), p. 396.

GOODIER, J.N., and FIELD, F.A.

"Plastic Energy Dissipation in Crack Propagation" In: "Fracture of Solids", ed. Drucker, D.C., and Gilman, J.J., Interscience Publishers, New York, (1962), p. 103.

GOTHAM, K.V.

Plastics and Polymers, 37, (1969), p. 309.

GOUGH, H.J.

J. Inst. Metals, 49, (1932), p. 17.

GRAHAM, I.D., MARSHALL, G.P., and WILLIAMS, J.G.

Proceedings of International Conference on Dynamic Crack Propagation, Lehigh University, Bethlehem, Pennsylvania, USA, 10-12 July (1972), p. 261.

GRIFFITH, A.A.

Proc. R. Soc. London, A.221, (1921), p. 163.

GRIFFITH, A.A.

Proceedings of the 1st International Congress on Applied Mechanics, Delft, (1924), p. 55A.

HAHN, G.T., and ROSENFIELD, A.R.

Acta. Metallurgica, 13, (1965), p. 293.

HAIGH, B.P.

J. Inst. Metals, 18, (1917), p. 55.

HALL, L.R., and SHAH, R.C.

Engng Fracture Mechs., 3, (1971), p. 169.

HAM, R.K.

Canad. Met. Quart., 5, (1966), p. 161.

HAYES, D.J.

Ph.D. Thesis, Imperial College, University of London, (1970).

HAYES, D.J., and WILLIAMS, J.G.

Int. J. Fracture Mechs., 8, (1972), p. 239.

HEAD, A.K.

The Philosophical Magazine, 44, Series 7, (1953), p. 925.

HERTZBERG, R.W., MANSON, J.A., and WU, W.C.

ASTM, STP, 536, (1973), p. 391.

HERTZBERG, R.W., NORDBERG, H., and MANSON, J.A.

J. Maters Sci., 5, (1970), p. 521.

HINTON, T., and KELLER, A.

J. Appl. Polym. Sci., 13, (1969), p. 745.

HOWARD, J.B.

"Stress Cracking (in Thermoplastics)" In: "Engineering Design for Plastics", ed. Baer, E., Reinhold, New York, (1964).

HOWARD, R.N., and MANN, J.

Proc. R. Soc. London, A.282, (1964), p. 120.

HUDSON, C.M.

NASA Report, TND-5390, Langley Research Center, (1969).

INGLIS, C.E.

Trans. Inst. Nav. Archit., 55, (1913), p. 219.

IRWIN, G.R.

"Fracture Dynamics" In: "Fracture of Metals", ASM, Cleveland, (1948).

IRWIN, G.R.

J. Appl. Mechs., 24, (1957a), p. 361.

IRWIN, G.R.

9th International Congress on Applied Mechanics, Brussels, (1957b).

IRWIN, G.R.

J. Basic Engng, 82, Series D, (1960a), p. 417.

IRWIN, G.R.

Nav. Res. Memo., Report 5486, (1960b).

IRWIN, G.R.

J. Appl. Mechs., 29, (1962), p. 651.

IRWIN, G.R., and KIES, J.A.

Weld. J. Res. Suppl., 17, (1952), p. 95-S.

ISAKSEN, R.A., NEWMAN, S., and CLARK, R.J.

J. Appl. Polym. Sci., 7, (1963), p. 515.

JACK, A.R., and PRICE, A.T.

CEGB (Midland Region) Technical Report, (1970).

Also in: Int. J. Fracture Mechs., 6, (1970), p. 401.

JOHNSON, H.H., and PARIS, P.C.

Engng Fracture Mechs., 1, (1968), p. 3.

KAMBOUR, R.P.

Polymer, 5, (1964a), p. 143.

KAMBOUR, R.P.

J. Polym. Sci., A.2, (1964b), p. 4159.

KAMBOUR, R.P.

J. Polym. Sci., A.2, (1964c), p. 4165.

KAMBOUR, R.P.

J. Polym. Sci., A.2, (1966), p. 349.

KAMBOUR, R.P.

Polym. Engng Sci., 8, (1968), p. 281.

KAMBOUR, R.P.

International Conference on Corrosion Fatigue, University of Connecticut, 14-18 June (1971), p. 679.

KAMBOUR, R.P.

Ind. Engng Chem. Prod. Res. Develop., 11, (1972), p. 140.

KAMBOUR, R.P., and HOLIK, A.S.

J. Polym. Sci., A.2, (1969a), p. 1393.

KAMBOUR, R.P., and HOLIK, A.S.

Polym. Prepr., Am. Chem. Soc., 10, (1969b), p. 1182.

KAMBOUR, R.P., and KOPP, R.W.

J. Polym. Sci., A.2, (1967), p. 211.

KAMBOUR, R.P., and KOPP, R.W.

J. Polym. Sci., A.2, (1969), p. 183.

KEITH, H.D.

J. Polym. Sci., A.2, (1964), p. 4339.

KEITH, H.D., and PADDEN, F.J.

J. Polym. Sci., 41, (1959), p. 525.

KLENSIL, M., and LUKAS, P.

Maters Sci. Engng, 9, (1972), p. 231.

KNAUSS, W.G.

Int. J. Fracture Mechs., 6, (1970), p. 7.

KNAUSS, W.G.

Californian Institute of Technology, Report GALCIT SM 72-5, August (1972).

Also in: Appl. Mech. Review, 26, January (1973), p. 1.

KNAUSS, W.G., and DIETMANN, H.

Int. J. Engng Sci., 8, (1970), p. 643.

KOBAYASHI, A.S., ENGSTROM, W.L., and SIMON, B.J.

Expt. Mech., 9, (1969), p. 163.

KOPPELMANN, J.

Rheol. Acta., 1, (1958), p. 20.

LANDER, L.L.

SPE Journal, 16, (1960), p. 1329.

LIU, H.W.

J. Basic Engng, Trans. ASME, 85, Series D, (1963), p. 116.

LIU, H.W.

ASTM, STP, 381, (1965), p. 23.

MANSON, S.S.

Proc. Soc. Exp. Stress Analysis, 22, (1965), p. 193.

Also in: Exp. Mechs., 5, (1965), p. 193.

MARSHALL, G.P.

Ph.D. Thesis, Imperial College, University of London, (1972).

MARSHALL, G.P., COUTTS, L.H., and WILLIAMS, J.G.

J. Maters Sci., 9, (1974), p. 1409.

MARSHALL, G.P., CULVER, L.E., and WILLIAMS, J.G.

Plastics and Polymers, (1969a), p. 75.

MARSHALL, G.P., CULVER, L.E., and WILLIAMS, J.G.

Conference on Research on Engineering Properties of Plastics, Cranfield, 6-8 January (1969b), p. 95.

MARSHALL, G.P., CULVER, L.E., and WILLIAMS, J.G.

Proc. R. Soc. London, A.319, (1970), p. 165.

MARSHALL, G.P., CULVER, L.E., and WILLIAMS, J.G.

Int. J. Fracture Mechs., 9, (1973), p. 295.

MARSHALL, G.P., LINKINS, N.H., CULVER, L.E., and WILLIAMS, J.G.

SPE Journal, 28, (1972), p. 26.

MARSHALL, G.P., and WILLIAMS, J.G.

J. Appl. Polym. Sci., 17, (1973), p. 987.

MILLER, G.A.

Trans. ASME, 61, (1968), p. 442.

MINER, M.A.

J. Appl. Mech., 12, (1945), p. A159.

MUKHERJEE, B.

3rd International Conference on Fracture, Munich, 6, (1973), p. V-423.

MUKHERJEE, B., CULVER, L.E., and BURNS, D.J.

Expt. Mechs., 9, (1969), p. 90.

MUKHERJEE, B., and BURNS, D.J.

Expt. Mechs., 11, (1971), p. 433.

MURPHY, B.M.

Chem. Ind., 10, 8 March (1969), p. 289.

MURRAY, J., and HULL, D.

J. Polym. Sci., B.8, (3), (1970), p. 159.

MUSKHLISHVILI, N.I.

In: "Some Basic Problems of the Mathematical Theory of Elasticity", 4th Edition, Translated by Radok, J.R.M., Noordhof, Groningen, (1963).

McADAM, D.J., Jnr.

Proc. American Soc. Testing Mat., Part II, 26, (1926), p. 224.

McEVILY, A.J., BOETNER, R.C., and JOHNSON, T.L.

Proceedings of 10th Sagamore Army Materials Research Conference, Syracuse University, New York, (1963), p. 95.

McEVILY, A.J., and ILLG, W.

NACA Technical Note 4394, September (1958).

McEVILY, A.J., KUMBLE, R., and DONAHUE, R.J.

3rd International Conference on Fracture, Munich, 6, (1973), p. V-424.

McEVILY, A.J., and WEI, R.P.

International Conference on Corrosion Fatigue, Univeristy of Connecticut, 14-18 June (1971), p. 381.

NIELSEN, L.E.

In: "Mechanical Properties of Polymers", Reinhold, New York, (1962), p. 178.

OGORKIEWICZ, R.M.

In: "Engineering Properties of Thermoplastics", Interscience Publishers, London, (1970).

OPP, D.A., SKINNER, D.W., and WIKTOREK,

Polym. Engng Sci., 9, (1969), p. 121.

OROWAN, E.

Proc. R. Soc. London, A.171, (1939), p. 79.

OROWAN, E.

Rep. Prog. Phys., 12, (1949), p. 185.

OROWAN, E.

Weld. J. Res. Suppl., 20, (1955), p. 157.

PADDEN, F.J., and KEITH, H.D.

J. Appl. Phys., 30, (1959), p. 1479.

PARIS, P.C.

The Boeing Company, Document Number D.17867, Addendum N, 12 September (1957).

PARIS, P.C.

Proceedings of 10th Sagamore Army Materials Research Conference, Syracuse University, New York, (1963), p. 107.

PARIS, P.C., and ERDOGAN, F.

Trans. ASME, J. Basic Engng, 85, Series D, (1963), p. 528.

PARIS, P.C., and SIH, G.C.

In: "Stress Analysis of Cracks", ASTM, STP, 381, Philadelphia, (1965).

PARVIN, M.

M.Sc. Thesis, Imperial College, University of London, (1972).

PEARSON, S.

Nature, 211, (1966), p. 1077.

PEARSON, S.

Royal Aircraft Establishment Technical Report 68297, December (1968).

PELAGATTI, U., and BARETTA, G.

Mod. Plastics, 36, June (1959), p. 140.

PRATT, P.L.

"Non-Metallic and Composite Materials" In: "Fracture Toughness", The Iron and Steel Institute Publication, ISI 121, (1968), p. 83.

PRINGLE, O.A.

Expt. Mechs., 9, (1969), p. 171.

RANKINE, W.

Proc. Inst. Civil Engrs, 2, (1843), p. 105.

REGEL, V.R.

J. Tech. Phys. (USSR), 26, (1956), p. 359.

See English Translation in Soviet Phys. Tech. Phys., 1, Part 1, (1956), p. 353.

REGEL, V.R., LEKSOVSKII, A.M., BOLIBEKOV, U., and MUCHINA, M.V.

3rd International Conference on Fracture, Munich, 7, (1973), p. VI-324.

RICE, J.R.

"Mathematical Analysis in the Mechanics of Fracture" In: "Fracture - An Advanced Treatise - II", ed. Liebowitz, H., Academic Press, New York, (1968).

RIDDEL, M.N., KOO, G.P., and O'TOOLE, J.L.

Polym. Engng Sci., 6, (1966), p. 363.

RIVLIN, P.C., and THOMAS, A.G.

J. Polym. Sci., 10, (1953), p. 291.

SAUER, J.A., MARIN, J., and HSIAO, C.C.

J. Appl. Phys., 20, (1949), p. 507.

SCHAPERY, R.A.

Report MM 72-3, Texas A & M University, August (1972).

SCHAPERY, R.A.

Report MM 2764-73-1, Texas A & M University, March (1973).

SIH, G.C.

J. Appl. Mechs., 29, (1962), p. 587.

SPEIDEL, M.O., BLACKBURN, M.J., BECK, T.R., and FEENEY, J.A.

International Conference on Corrosion Fatigue, University of Connecticut, 14-18 June (1971), p. 324.

STARKWEATHER, H.W., Jnr.

"Transition and Relaxation in Nylons" In: "Nylon Plastics", ed. Kohan, M.I., John Wiley and Sons, (1973), p. 307.

STERNSTEIN, S.S., ONGCHIN, L., and SILVERMAN, A.

Appl. Polym. Sci., 7, (1968), p. 175.

STUART, H.A., MARKOWSKI, G., and JESCHIKE, H.

Kunstoffe, 54, 10, Ocotber (1964). p. 618.

SULLIVAN, B.

Technical Memorandum Number T210, BP Chem. Industrial Limited, (1972).

TAKAYANAGI, M.

Pure and Appl. Chem., 15, (1967), p. 555.

TOMKINS, B., and BIGGS, W.D.

J. Maters Sci., 4, (1969), p. 532.

TYZACK, C.

International Conference on Corrosion Fatigue, University of Connecticut, 14-18 June (1971), p. 319.

VADIMSKY, R.G., KEITH, H.D., and PADDEN, F.J.

J. Polym. Sci., A.2, (1969), p. 1367.

WADA, Y., and others

J. Polym. Sci., C.15, (1966), p. 101.

WARBURTONHALL, H., and RUSSELL, E.W.

A.R.C. Technical Report, R & M Number 2764, (1953).

WATTS, N.H., and BURNS, D.J.

Polym. Engng Sci., 7, (1967), p. 90.

WELLS, A.A.

Brit. Weld. J., November (1963), p. 563.

WEI, R.P.

Engng Fracture Mechs., 1, (1970), p. 633.

WEI, R.P., and LANDES, J.D.

Maters Res. Standards, ASTM, 9, July (1969), p. 25.

WESTERGAARD, H.M.

J. Appl. Mechs., 61, (1939), p. A49.

WEYLAND, H.G., HOFTYZER, P.J., and VAN KREVELEN, D.W.

Polymer, 11, (1970), p. 79.

WIEDERHORN, S.M.

J. Am. Ceram. Soc., 52, (1969), p. 99.

WILLIAMS, J.G.

Int. J. Fracture Mechs., 8, (1972), p. 393.

WILLIAMS, J.G., and CONSTABLE, I.

Int. J. Fracture Mechs., 5, (1969), p. 113.

WILLIAMS, J.G., and ISHERWOOD, D.P.

J. Strain Analysis, 3, (1968), p. 17.

WILLIAMS, J.G., and MARSHALL, G.P.

Proc. R. Soc. London, A.342, (1975), p. 55.

WILLIAMS, M.L.

J. Appl. Mechs., 24, (1957), p. 109.

WILLIAMS, M.L.

J. Appl. Phys., 38, (1967), p. 4476.

WNUK, M.P.

Int. J. Fracture, 10, (1974), p. 223.

WNUK, M.P., and KNAUSS, W.G.

Int. J. Solids Structs., 6, (1970), p. 995.

WOHLER, A.

English Abstract Engineering, 11, (1871), p. 199.

YOKOBORI, T.

Rep. Res. Inst. Strength and Fracture of Materials, Tohoku University, 5, (1969), p. 19.

ZHURKOV, S.N., KUKSENKO, V.S., and SLUTSKEV, A.I.

Proceedings of 2nd International Conference on Fracture, Brighton, (1969), p. 531.

Craze Growth and Void Coalescence in PMMA Round Notched Bars

by

H. El-Hakeem, G.P. Marshall, E.L. Zichy and L.E. Culver

To be published in: Journal of Applied Polymer Science

October 1974

CRAZE GROWTH AND VOID COALESCENCE IN P.M.M.A. ROUND NOTCHED BARS

H. El-Hakeem, G.P. Marshall, E. L. Zichy and L. E. Culver

INTRODUCTION

The nature of fracture processes in plastics has become of considerable importance in recent years as these materials are used in increasingly demanding situations. The environmental resistance of many plastics is often good under situations where the loadings are low but can change if the materials are required to sustain high stresses.

There are two main categories into which the invironmental attack of polymers may be divided. The first of these, "stress cracking", can occur in polymers subjected to low stresses with or without chemical reactions, for example, the behaviour of polyamides in some metallic salts (1) dissolved either in water or in organic media, and the behaviour of polyethylene in detergents (2). The second category is known as "solvent crazing", and mainly occurs in amorphous polymers such as polycarbonate (3), polystyrene (4), and polymethylmethacrylate (PMMA)(5). The problems of environmental stress cracking and crazing have been studied and a considerable amount of data is available for assessing the environmental crack growth characteristics of plastics (e.g. Reference 2).

Crazes usually initiate at inherent surface flaws, then grow perpendicularly to the direction of maximum stress and they are normally planar and highly reflective like true cracks grown in uniaxial tensile stress in transparent

specimens. The study of crazes has received great attention because they initiate and propagate at low stresses and may cause failure by subsequent void coalescence within the craze.

The concepts of fracture mechanics have been used to describe the craze growth behaviour in single edge notched (S.E.N.) specimens of PMMA subjected to stress in a methanol environment (5). A model for craze formation and propagation for that type of craze was proposed based on simple flow equations and a crack opening displacement "C.O.D." approach assuming the craze to be a porous system and craze propagation to be governed by liquid movements within the craze. That study has been extended to craze growth under cyclic loads (6) in an effort to outline the differences in behaviour which might be expected in practice.

The present work is part of a programme designed to extend the study of a range of materials, environments and frequencies using various fatigue test methods. One of the most common test techniques in fatigue is the use of a rotating bend test to provide S-N data for the prediction of long term behaviour. There already exists a body of knowledge on the fatigue of plastics in air using this technique (e.g. Reference 7) and it therefore seemed logical to extend these data by including environmental attack.

The present paper represents a study of the failure mechanisms and craze growth mechanics for environmental attack in PMMA using notched circular bar specimens (such as those used in the rotating bend tests) in an effort to provide a model background for the explanation of environmental crazing phenomena with this particular geometry.

Material and Specimen Preparations

The circular cross section notched specimen used in these tests is shown in Fig.(1a). The specimens were prepared from 12.7 mm diameter rods machined from PMMA cast sheets, and machine notched with a sharp lathe tool to give a root radius of approximately 00.01 mm. All the specimen surfaces were polished to allow the transmission of light through them, Fig(1b). Similar specimens having different notch depths and diameters were also prepared.

Test Procedure

The specimens were pin loaded in single lever rigs which maintained the load constant throughout the test. As illustrated in Fig(1b), each clamp contained a plane mirror inclined at 45^{o} to the axis of the specimen to reflect the light transmitted through the specimen and microscope (1) was used to observe the surface of the craze formed at the notched section. A closed circuit television camera was attached to the microscope and the process of void coalescence within the craze was recorded on video tape. A transparent container was used to maintain the methanol around the notched section and to allow the light from a second source to be reflected at the craze. This light was received by microscope (2) to which an ordinary camera was attached for the purpose of taking photographs at intervals. Craze growth measurements were taken from these photographs.

Specimens with different notch depths and diameters were subjected to various constant loads to give different initial stress intensity factors K_o (evaluated using the gross stress

and initial crack length).

Results and Discussion

(a) Craze Growth

For craze growth measurements only tests which gave a symmetrical radial craze growth with respect to the specimen axis as shown in Fig.(2a) were considered. Measurements of the radial craze growth with time were taken from these photographs (which were enlarged using a projector and the average radial craze length x was determined from

$x = \frac{d}{2}\left[1 - \frac{1}{2}\left(\frac{b}{B} + \frac{a}{A}\right)\right]$ Fig.(2b), where d is the notch diameter).

Typical curves obtained for radial craze growth with time for specimens subjected to different initial stress intensity factors K_o, are shown in Fig.(3). In some cases there was a tendency for the craze to accelerate as it approached the centre of the specimen Fig.(3), possibly due to early void coalescence in the craze which may cause a further increase in the K value.

(b) Void Coalescence

It is now known that crazes are a network of small voids interconnected by ligaments. The failure of these links allows the small voids to coalesce and hence grow larger. The stresses carried by the material within the craze increase with time due to two factors:

1) The craze growth itself which reduces the material at the crazed section carrying the original load on the specimen and

2) The softening action caused by the diffusion of liquid

in the craze. Such softening causes unequal stresses in the ligaments of the material in the craze i.e. the less softened ligaments in the newly formed part of the craze carry more load and thus become more likely to fail than the more softened ones in the older part of the craze.

The process of void coalescence in the present tests was clearly shown on the T.V. screen. There are two distinct features of void coalescence, the first is the clusters of very small voids (of the order of 3 - 4 x $10^3 A^o$ as measured from the fracture surface Fig.(4)), appearing as dark areas in the craze, Fig.(5b), and the second is the separate voids which grow much larger than the first type and appear in the craze at different points, Fig.(5c). Once the local failure process started it continued to give either one of the previously mentioned void forms, or resulted in both void features in one craze, Fig.(5d and e). Voids usually started to form ,Fig(5a), when the craze had almost completely covered the whole cross section of the specimen, but when the loading was high, early void coalescence started. Final failure was caused by void growth and coalescence eventually leading to complete separation, Fig.(5j). It was usually observed that the large voids grew faster and caused final failure before coalescence occurred between the clusters of small voids if the two patterns were found in one craze.

The pressure inside the voids is low which allows part of the methanol to evaporate and voids are thus full of methanol and methanol vapour Fig.(5h). The movement of methanol vapour bubbles was clear, when the large voids grew in size and coalesced, the bubbles of methanol vapour moving to join each other, Fig.(5h), forming one larger bubble

filling the space above the methanol in the void.

Some tests of unloading and reloading the crazed specimens which contained the larger voids with the bubbles inside, have emphasized the existence of the two phases of methanol in the void. When the specimen was unloaded the craze relaxed, the two surfaces of the void approached each other, the pressure increased and the bubbles became progressively smaller until they disappeared. When the specimen was reloaded the pressure in the void decreased and there was a delay of approximately five minutes and then the bubbles suddenly reappeared.

It has been noticed that void coalescence starts inside the craze away from the original crack or notch and near to the centre of the specimen. This means that failure in the craze starts internally and grows towards the notch in a radial direction. It is thought that this rather surprising event occurs because the material within the craze is plasticized by the methanol, and the effect increases with time, so that the material is more plasticized in the craze near the notch than near the centre. Thus, most of the load is carried by the central section and if a fault or weak link is present there it will cause void coalescence to start and lead to the final failure.

It seems that this type of failure is different from that observed in crazed S.E.N. specimens in which the original crack propagates in the craze causing the final failure (8). However, in the S.E.N. case, the crack may be forced to propagate in that way because the specimen is not completely symmetrical with respect to the loading axis as shown in Fig.(6a). This causes bending which forces the

original crack to propagate in the craze. As evidence of this, additional tests were made on S.E.N. specimens. The load in these tests was controlled to allow the craze to propagate to more than three-quarters of the specimen width and to leave a length of uncrazed material ahead of the craze approximately equal to the original crack length, then the material ahead of the craze was removed and the specimen quickly reloaded in methanol but with a smaller load, Fig. (6b). Complete failure of all these specimens was caused by void coalescence in the newly formed part of the craze at the far end from the original crack and the crack started and propagated from this end while the original crack remained stationary.

(c) Fracture Surface

The fracture surface patterns produced by void coalescence and crack propagation through the wet craze distinguish that sort of failure from others e.g. fracture in air.

The first distinct zone is the featureless part in which "puddles" appear, Fig.(7). However, in some cases radial marks appear in this zone pointing to the centre of the specimen as shown in Fig.(8). The puddles represent the maximum size of the voids before fracture starts and the radial marks represent the direction of craze propagation. In some cases these puddles had very definitive boundaries, Fig.(9) and usually had radial marks pointing to the origin of the start of void coalescence, Fig.(10) and showing the direction of void growth. However, these marks have no relation to those showing the direction of craze propagation, they may intersect each other at any angle, Fig.(8).

In the featureless region, Fig.(7), mating surfaces are identical. It is thought that the crack was propagating slowly through the centre of the craze which would give two identical surfaces with hills and valleys of the order of 300 A^{o}, the average spacing between the sites of inhomogeneities in the material. This feature would be difficult to see however, even with a powerful microscope. Alternatively it is thought that any micro-features which might have been formed in this region were masked by the relaxation of the highly stressed craze.

It was noticed that the clusters of small voids which appear as dark areas in the craze before failure did not usually leave any feature on the fractured surface. However, in some cases when these clusters were formed in that part of the craze where fast crack propagation occured, the features were seen on the fracture surface, e.g. Fig.(5j), and when compared with Fig.(5e) and Fig.(5i) this shows that some of these clusters have disappeared on the fracture surface where there was slow crack propagation while some are still visible where there was fast crack propagation.

The second distinct zone is the island structure, Fig. (11), with its definitive type of island and crater features which may give an indication of the discontinuous propagation along the craze/matrix interface, i.e. the crack transferring across the craze thickness in an irregular manner. The transition to this type of feature, Fig.(12), may be the result of the crack within the craze reaching its instability condition causing a transition from slow to fast crack propagation. The parabolic markings at the zone boundary are similar to those found for fast crack propagation in a

craze in air in PMMA (9) and are thought to represent the intersection of an expanding void in the craze and a radial crack moving at high speed.

Analysis of the Craze Growth

In all the tests measurements had been made of the rate of craze growth across the specimens, a typical example of craze length vs time curve having been shown previously as Fig.(3). Such data had been obtained at different loading levels and an analysis was made of the data to provide a basis for predicting growth rates.

A previous model for craze formation and growth(5) in PMMA had shown that the K_o dependence of growth rates was due to variations in the displacements in the craze. At high K_o values large deflections occur since the crack opening displacement (COD) U_a is given by $U_a = K_o^2/\sigma_y.E$ (where σ_y is the yield stress and E the modulus) and the void area is increased. Basing an analysis in terms of fluid flow rates within the pores of the craze had given an equation of the form:

$$\Delta = A K_o t^{\frac{1}{2}}$$

where Δ is the craze length, t is time and A is a constant based on void dimensions and fluid properties.

A refinement of this analysis (10) has been proposed to account for viscoelastic effects since both the yield stress and modulus of PMMA are time dependent and the COD (U_a) changes with time (as shown in Fig.(13)).

Assuming a power law dependence of the form:

$$\sigma_y = \sigma_o t^{-m} \text{ and } E = E_o t^{-n}$$

gave: $\Delta\alpha K_o t^{\frac{1}{2} + (\frac{m+n}{2})}$ (10)

Such an assumption is not a perfect fit to modulus and yield data for PMMA (11) and if an equation is fitted to the data a more-precise solution can be obtained. Also the solution evaluates an equivalent K value for the case of a crack with long extended zone instead of K_o. The analysis has been conducted* but because of the complexity of the mathematics only the general result is given viz:

$$\Delta\alpha K_o t^{0.635}$$

(The approximate solution above gives an exponent of 0.6).

The craze growth data from the present tests were plotted on such a power law basis and as can be seen from the examples shown in Fig.(14) the results are well-represented by a straight line. It would thus appear that the same fluid flow controls considered in other geometries are applicable to the circular notched specimen and provide an excellent basis for future prediction of growth rates and failure times in fatigue tests.

REFERENCES

1. Dunn, P. and Sansom, G.F.,J.Applied Polymer Sci., Vol.13, p 1641,(1969).
2. Marshall, G.P., Linkins, N.H., Culver, L.E. and Williams, J.G., SPE Journal, Vol. 28, p 26,(Sept.1972).
3. Miller, G.W., Visser, S.A.D. and Morecroft, A.S., Polymer Engineering and Science, Vol. 11, No. 2, (March,1971).
4. Hall, D., J. of Materials Science 5, 357-363,(1970).

*Available on request.

5. Marshall, G.P., Culver, L.E. and Williams, J.G., Proc. Roy. Soc. Lond.A. 319, p165 (1970).

6. Marshall, G.P., Williams, J.G., Journal of Applied Polymer Science, Vol.17, pp 987-1005,(1973).

7. Constable, I., Culver, L.E. and Williams, J.G., International Journal of Fracture Mechanics, Vol. 6, No. 3, (Sept.1970).

8. Graham, I.D., Marshall, G.P. and Williams, J.G., Proc. Int. Conf. on Dynamic Crack Propagation, Lehigh University, Bethlehem, Pennsylvania, USA, p 261, (July 10-12, 1972).

9. Berry, J.P., J.Applied Physics, Vol. 33, No. 5, p 1741, (May, 1962).

10. Williams, J.G. and Marshall, G.P. (to be published) (1974).

11. Williams, J.G., Int. J. Fract. Mech. (8), p 393, (1972).

LEGEND

Figure 1 (b) Schematic diagram of apparatus for viewing void coalescence and craze growth in round bar in tension.

(a) Test specimen geometry.

Figure 2 (a) Radial craze growth in PMMA round notched bar.

(b) Chematic representation of craze measurements.

Figure 3 Variation of craze length with time for different K_o.

Figure 4 The clusters of small voids as they appear on the fracture surface.

Figure 5 Void growth and coalescence in the crazed section and fracture surface features after complete separation.

Figure 6 (a) Craze growth in S.E.N. specimen.

(b) Symetrical loading of crazed S.E.N. specimen.

Figure 7 The two main zones of the fracture surface.
1 - The featuresless zone in which rosette puddles appear.
2 - The island and crater zone.

Figure 8 The fracture surface with its radial marks.

Figure 9 The definitive boundary of a rosette puddle.

Figure 10 The central area of a rosette puddle.

Figure 11 The island and crater structure.

Figure 12 The transition region between the two zones of the fracture surface.

Figure 13 Variation of crack opening displacement (U_a) with time in SEN specimen "K_o = 15.4 N/mm$^{3/2}$".

Figure 14 Variation of craze length with (time)$^{0.635}$.

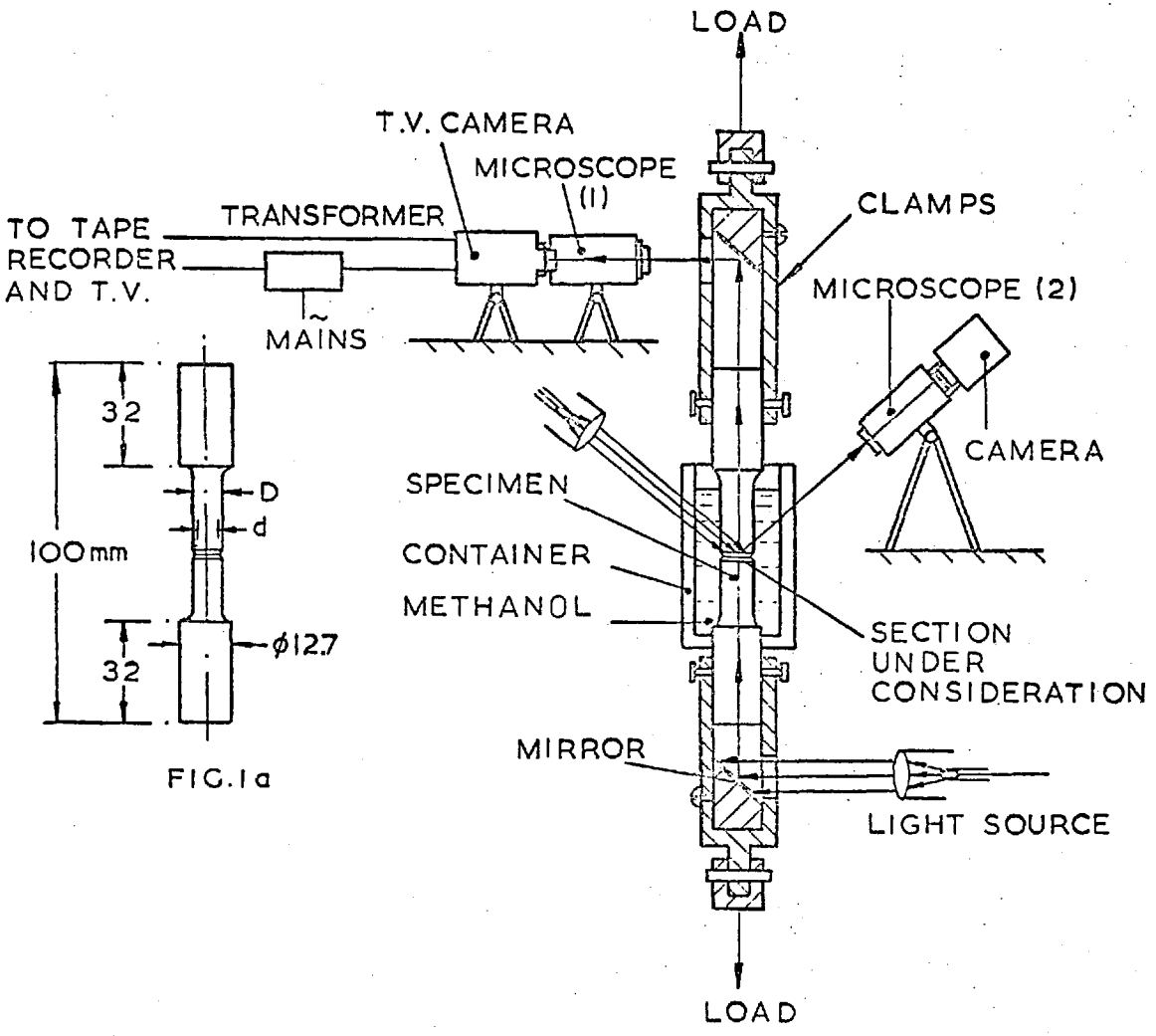

FIG. 1a

FIG. 1b

FIG. 1 a & b H. EL-HAKEEM, P. MARSHALL, L.E. CULVER

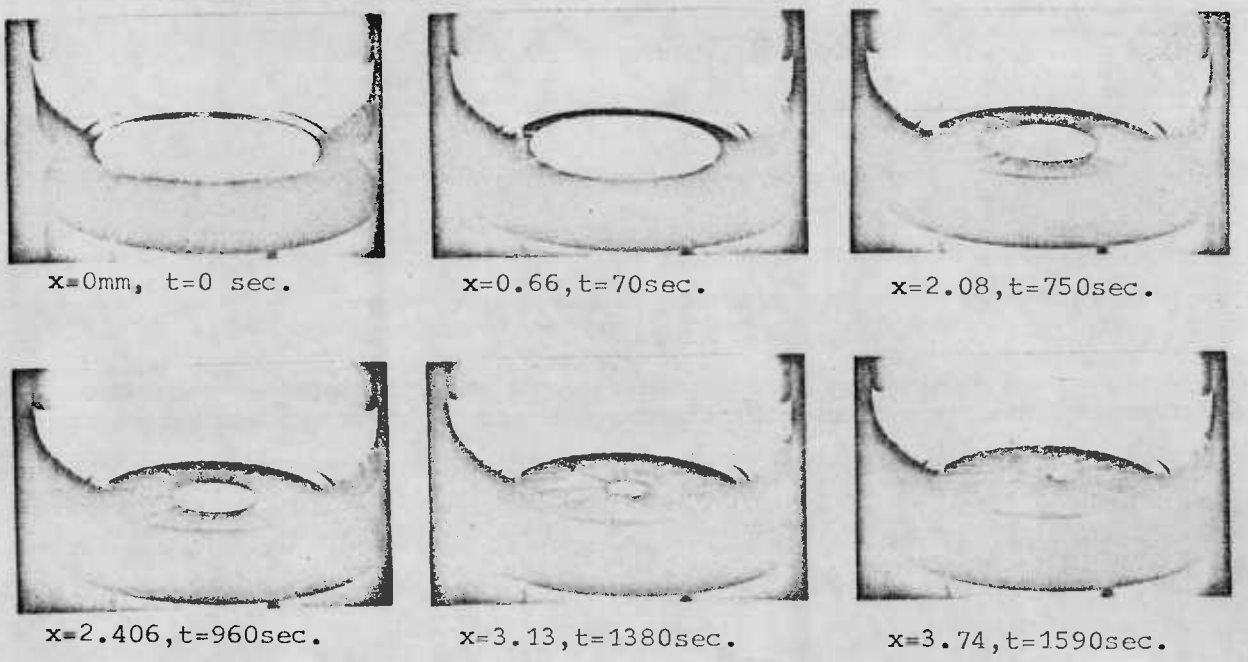

FIG. 2a

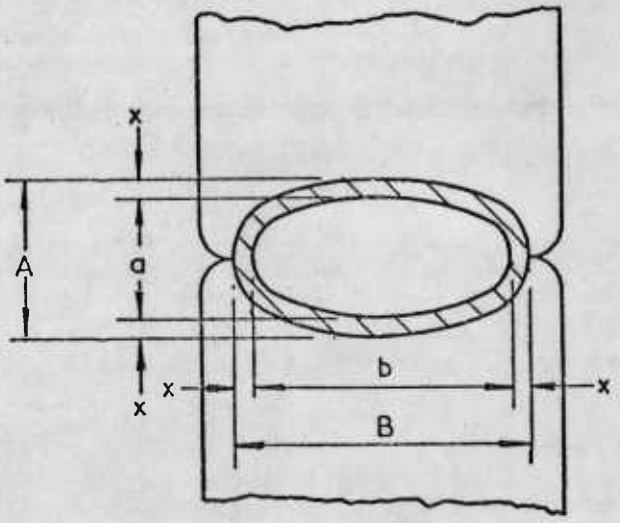

FIG. 2b

FIG. 2 a&b. H.EL-HAKEEM, P. MARSHALL, L.E.CULVER

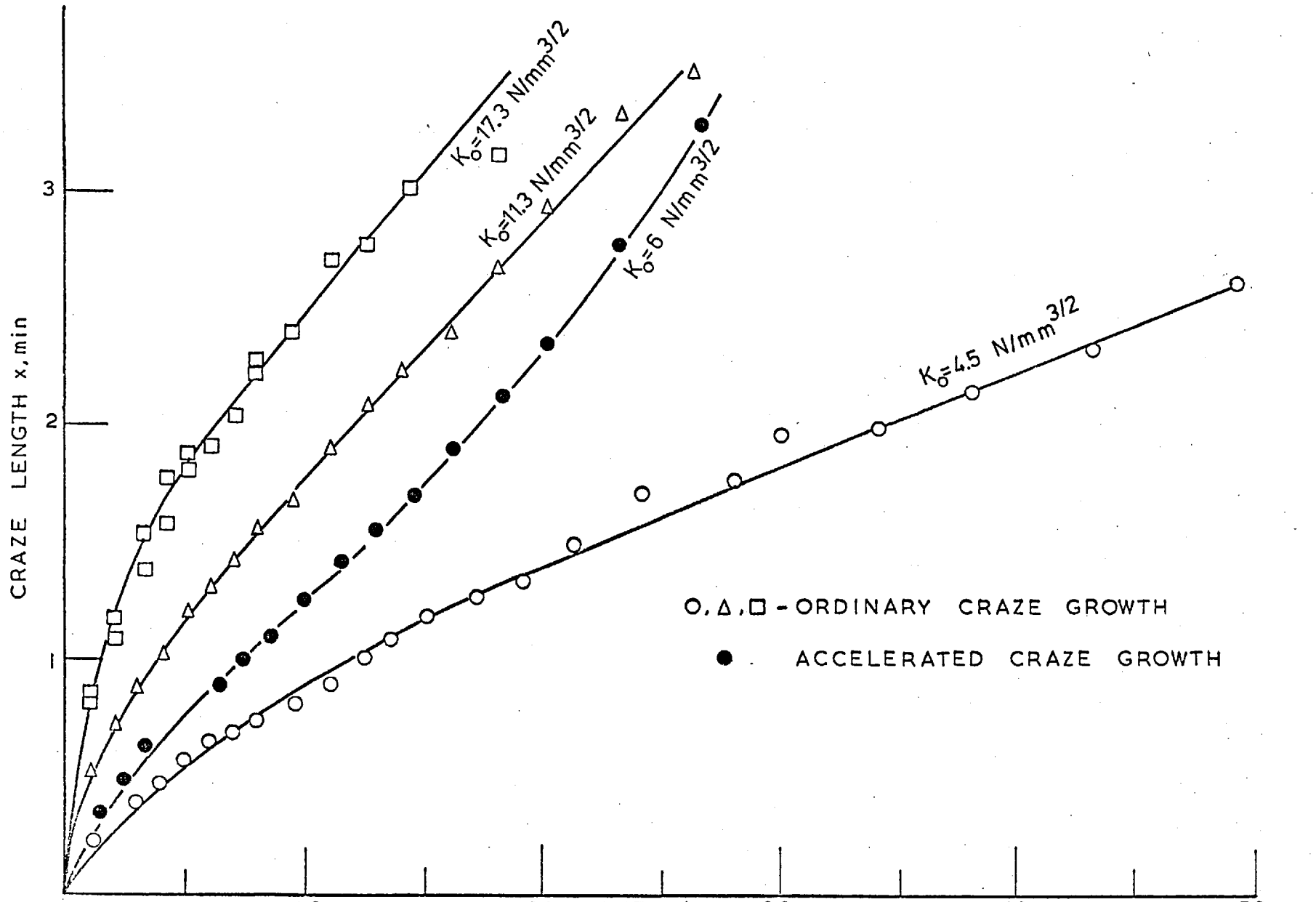

FIG. 3. H. EL-HAKEEM, P. MARSHALL, L.E. CULVER

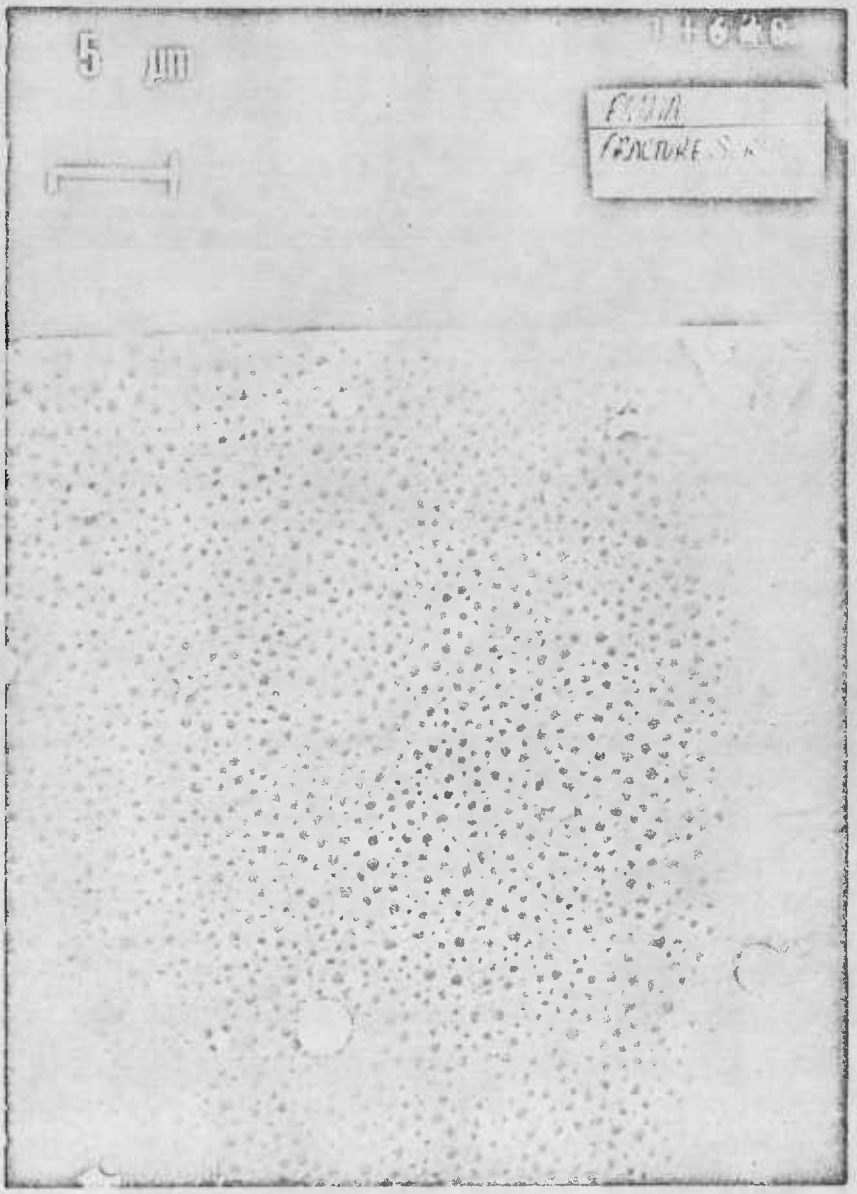

FIG. 4

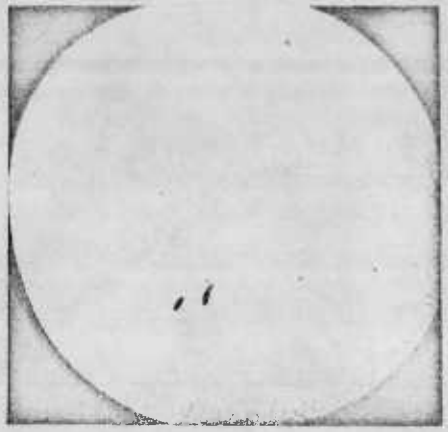

(a) 22 min.*

Start of void coalescence

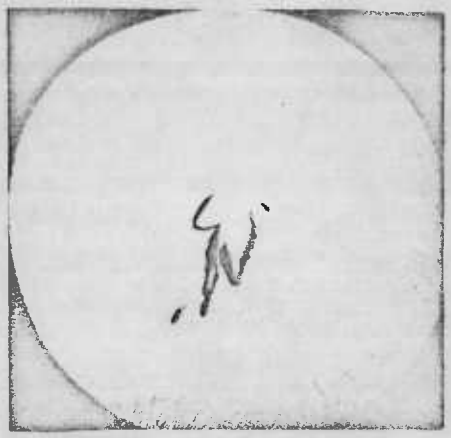

(b) 26 min. 30 sec.

Type (1), clusters of very small voids

(c) 30 min.

Type (1) voids spreading

Type (2) "Separate voids" appearing

(d) 32 min.

Growth of type (2) voids

(e) 34 min. 50 sec.

Continuous spreading of type (1), growth of type (2)

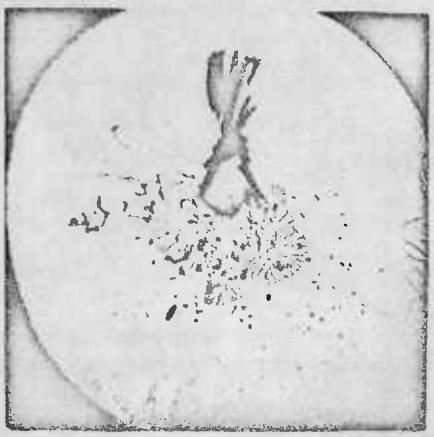

(f) 35 min. 35 sec.

Coalescence of type (2) voids

FIG. 5

(g) 35 min. 55 sec.

Bubble of methanol vapour inside coalesced voids

(h) 36 min. 10 sec.

Small bubble of methanol vapour joining main bubble

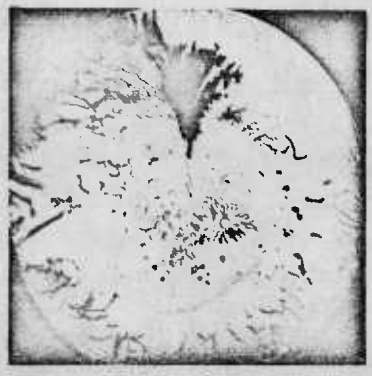

(i) 36 min. 15 sec.

Immediately prior to fracture

(j) Fracture Surface

*"Time was considered from the beginning of the test".

FIG. 5

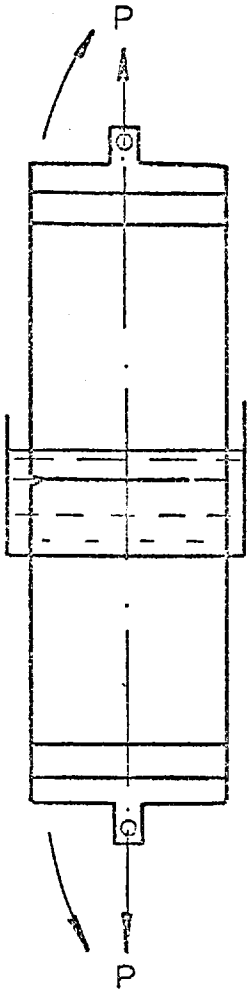

FIG. 6 a

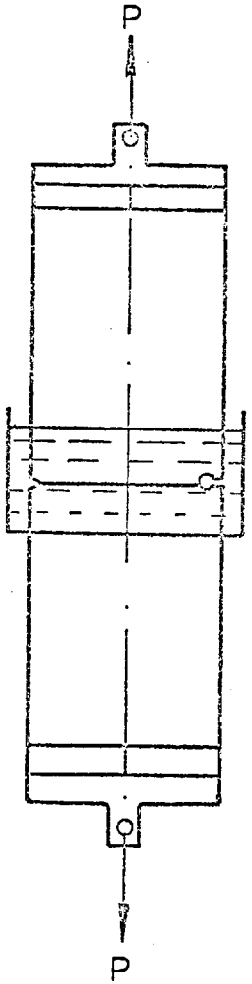

FIG. 6 b

FIG. 6 a & b H.EL-HAKEEM, P. MARSHALL, L.E.CULVER

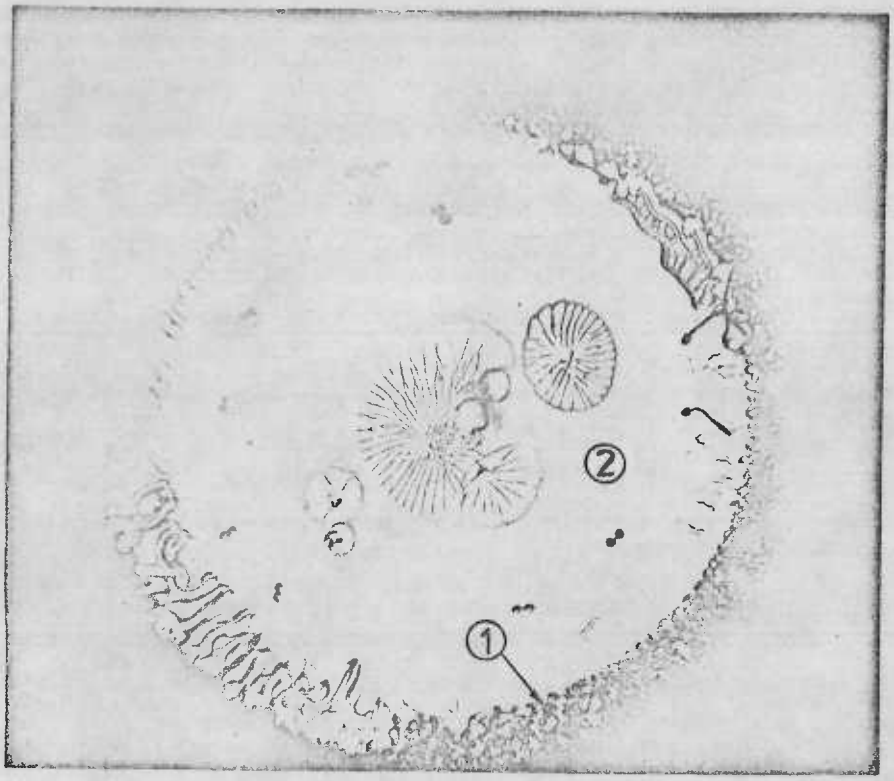

FIG. 7

1 The island and crater zone

2 The featureless zone

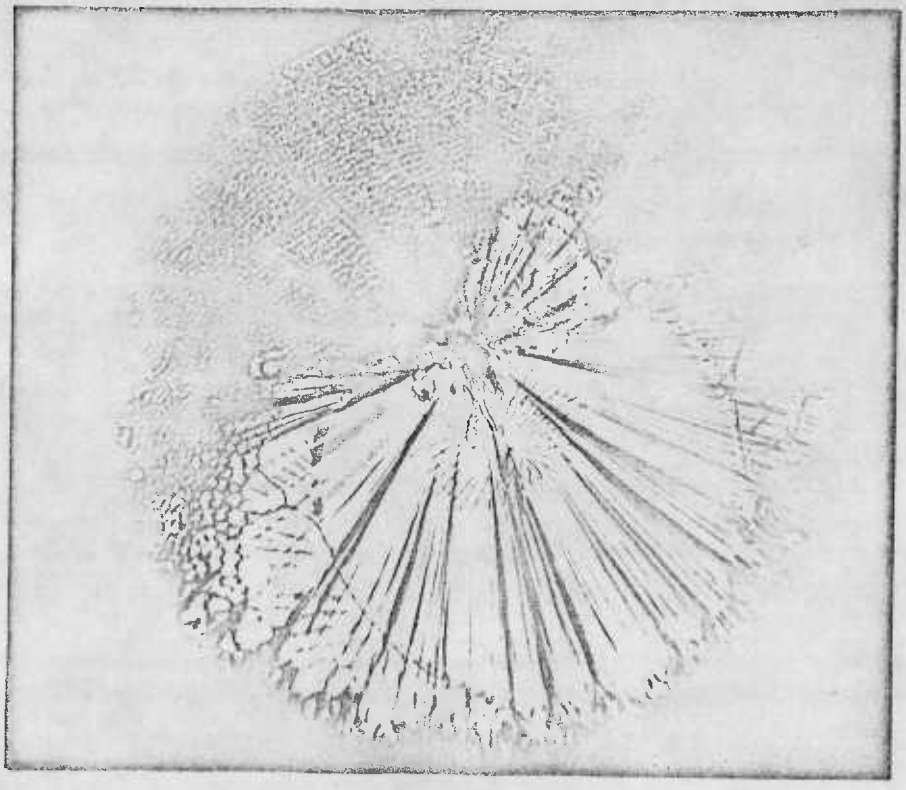

FIG. 8

FIG. 9

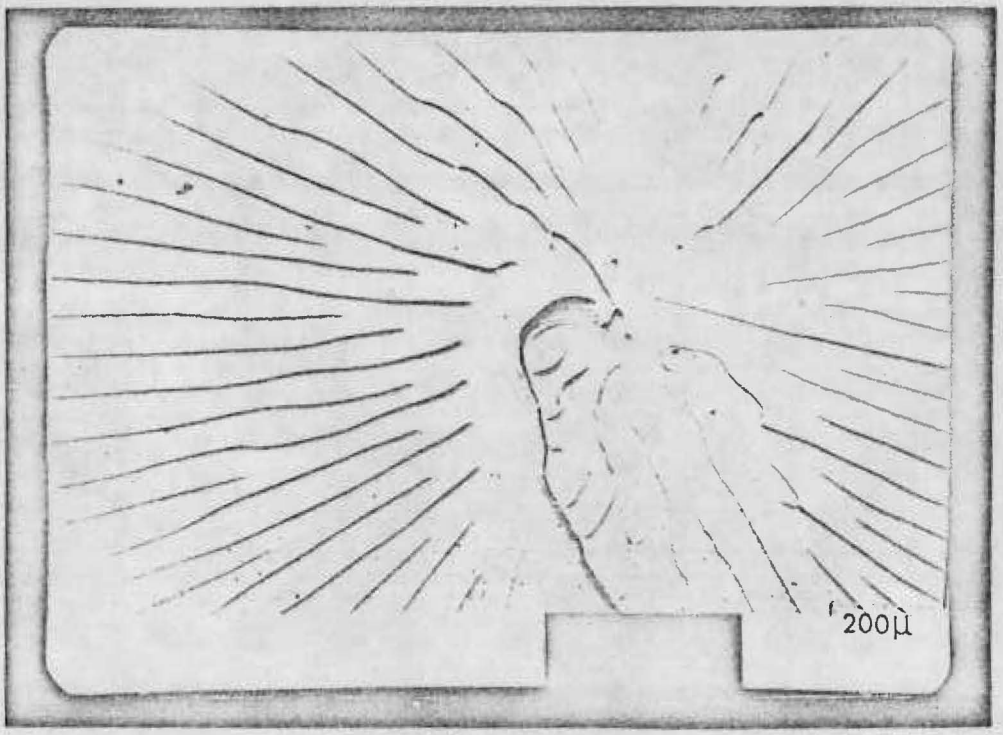

FIG. 10

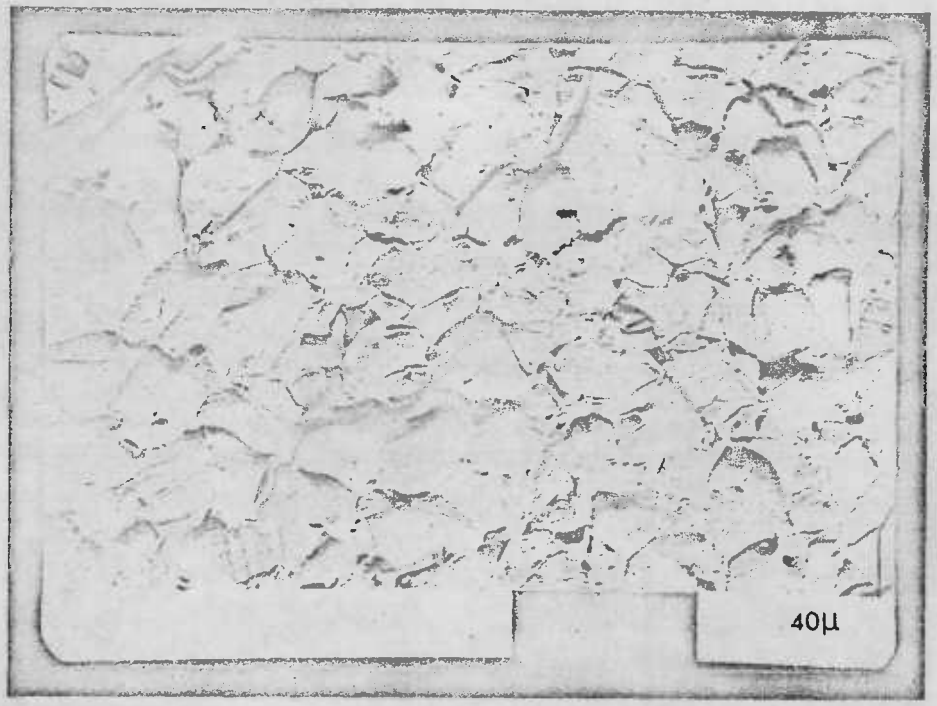

FIG. 11

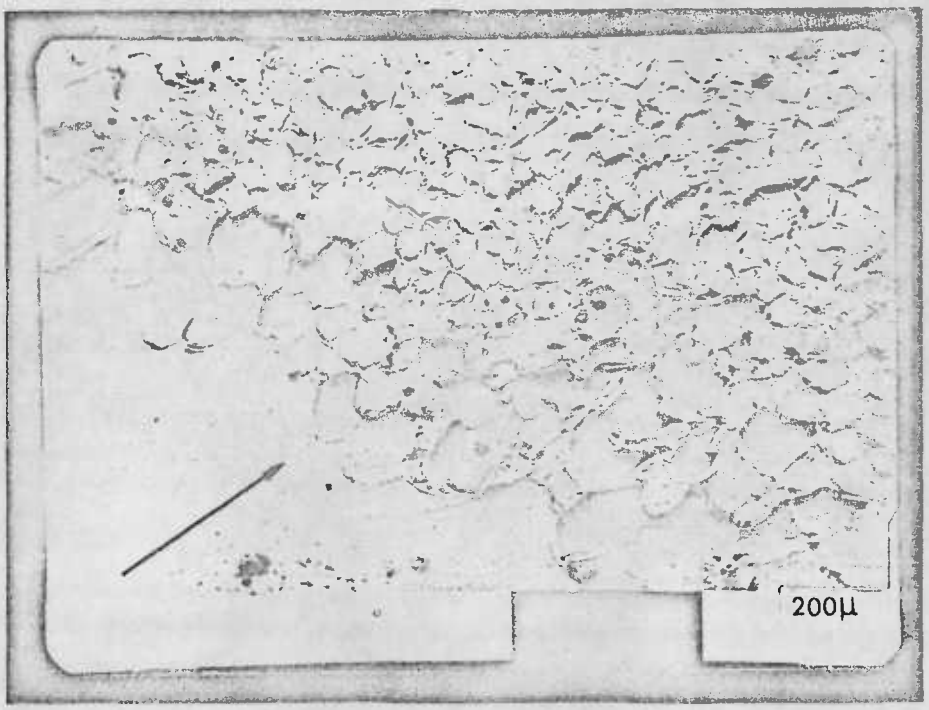

FIG. 12

Direction of radial crack propagation

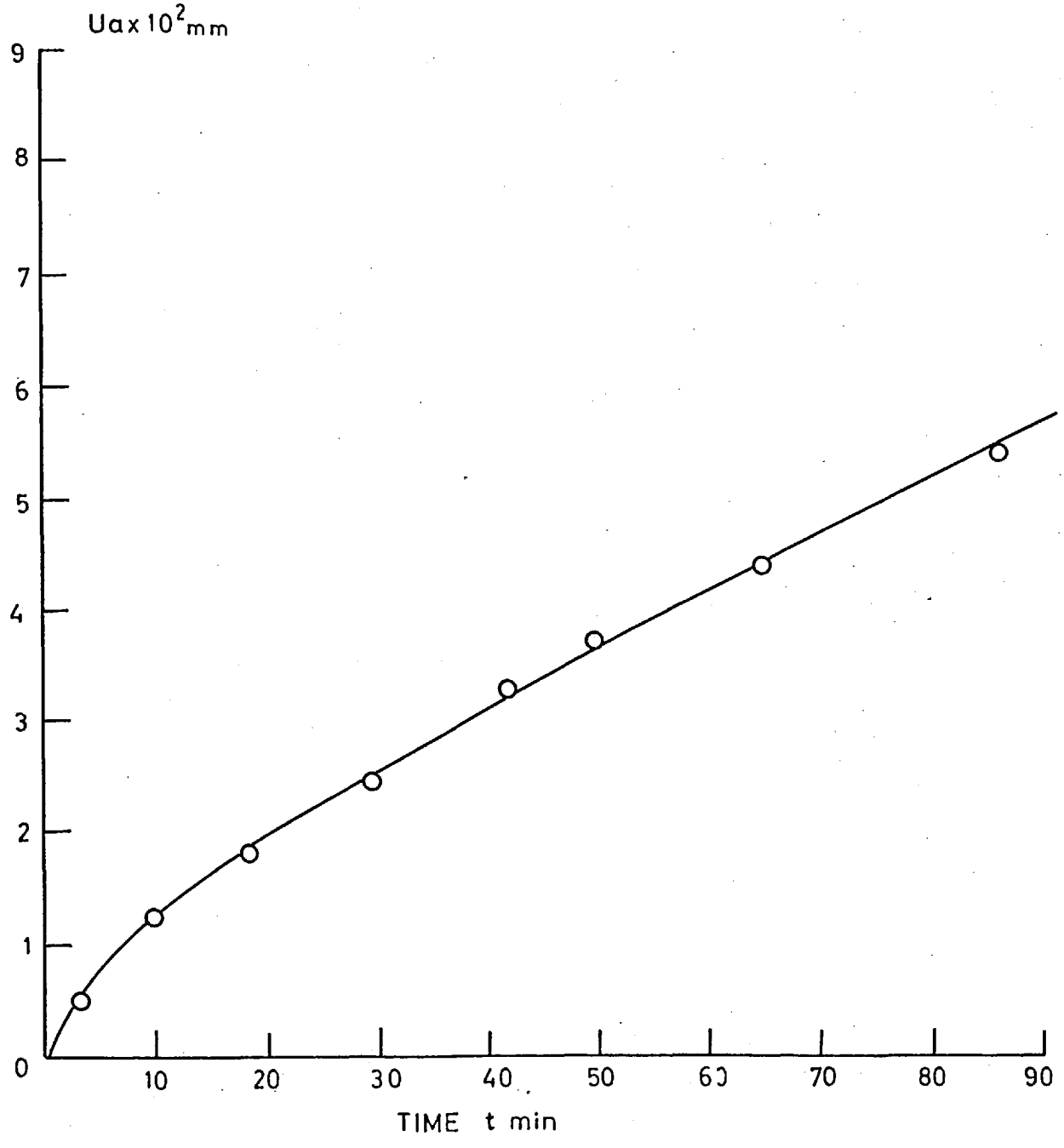

FIG. 13 H.EL-HAKEEM, P.MARSHALL, L.E.CULVER

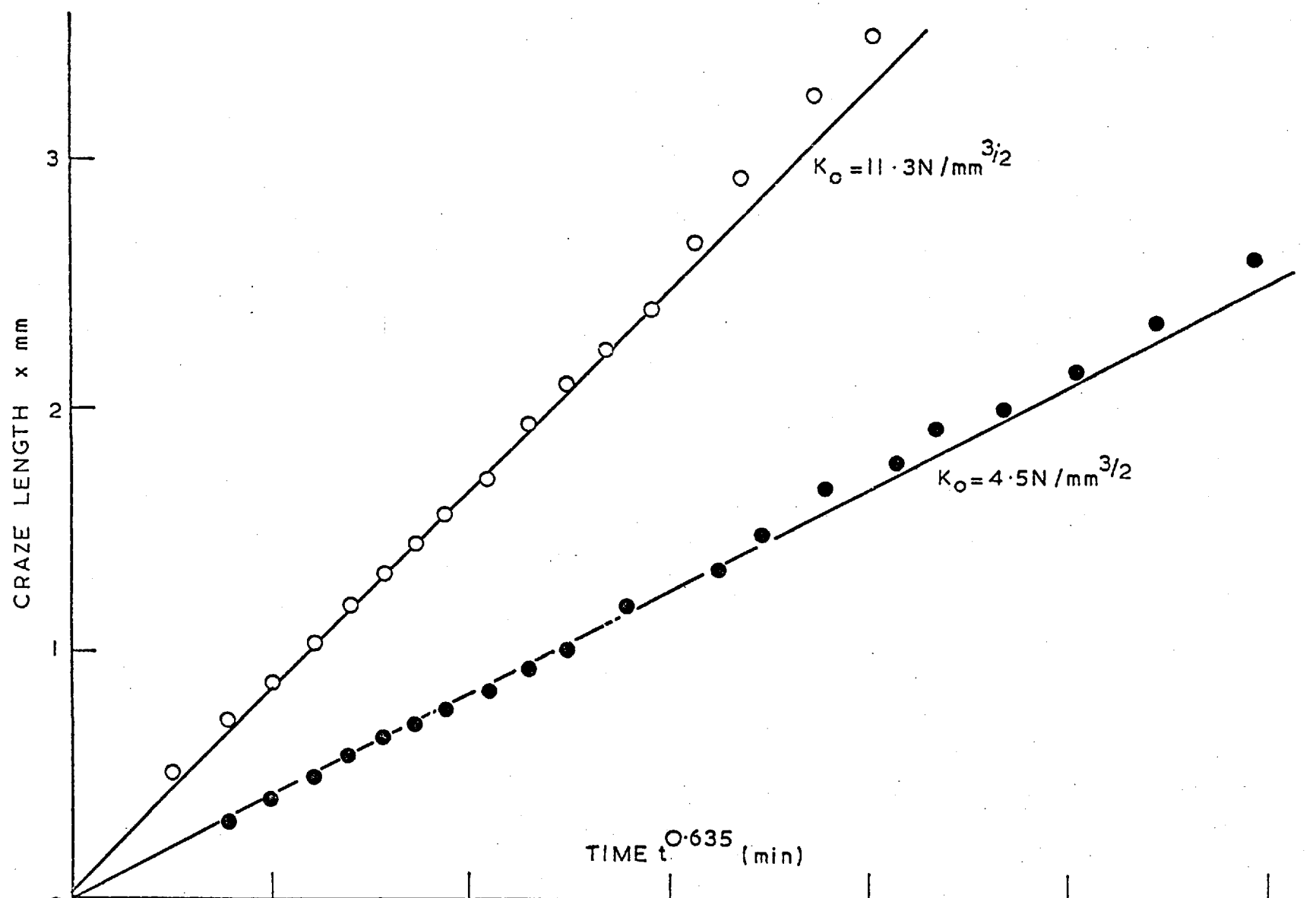

FIG. 14. H.EL-HAKEEM, P. MARSHALL, L.E. CULVER